SKB

Glacial ripping as a significant erosion mechanism in eastern Sweden – Field evidence and modelling

Maarten Krabbendam

Adrian M Hall

Romesh Palamakumbura

Andrew Finlayson

Fabio Diogardi

Christian Arnhardt

SVENSK KÄRNBRÄNSLEHANTERING

Glacial ripping as a significant erosion mechanism in eastern Sweden – Field evidence and modelling

Maarten Krabbendam[1], Adrian M Hall[2,3], Romesh Palamakumbura[1], Andrew Finlayson[1], Fabio Diogardi[1], Christian Arnhardt[4]

1 British Geological Survey, The Lyell Centre
2 Department of Physical Geography, Stockholm University
3 Institute of Geography, University of Edinburgh
4 British Geological Survey, Keyworth

Preface

The following report describes a study on the process of glacial ripping, a glacial erosional process that links three sequential processes: i) hydraulic jacking, ii) rock mass disintegration, and iii) boulder transport; all operating subglacially. The study reviews and presents a wide range of field evidence in eastern Sweden for this process sequence, as well as presenting modelling results to test the physical plausibility of some of the aspects of glacial ripping. In areas where glacial ripping has been operating, including over parts of the Forsmark site, this erosional process has been effective. The study complements the comprehensive study on denudation and glacial erosion in Forsmark and Uppland reported in TR-19-07.

The study was initiated by Jens-Ove Näslund (SKB) and it was jointly designed by Jens-Ove Näslund, Maarten Krabbendam (British Geological Survey) and Adrian Hall (Stockholm University). Maarten Krabbendam led the writing of the report. All authors contributed to the final version of the report.

The results will be used, together with other scientific information, for constructing future scenarios of climate and climate-related processes in SKB's work on assessing long-term safety of nuclear waste repositories in Sweden. The safety assessments performed for the planned repository for spent nuclear fuel in Forsmark, Sweden, cover a total time span of one million years. Since this time span covers the timescales relevant for glacial cycles, the effect of future glacial erosion needs to be analysed in the safety assessments.

The report was scientifically reviewed by Nicholas Eyles, University of Toronto, and Jens-Ove Näslund, SKB. Parts of the study have also been reviewed earlier on, since certain aspects of the work have been published in peer-review journals.

Stockholm, December 2022

Jens-Ove Näslund
Coordinator Climate Research Programme SKB

Summary

The effects of future glacial erosion need to be included in assessments of post-closure safety for the planned repository for spent nuclear fuel at Forsmark, Uppland. Traditionally, two main processes of glacial erosion are recognised: abrasion and plucking. Recently, a third effective erosion process, termed *glacial ripping* has been documented to have affected parts of the low relief basement gneiss terrain in eastern Sweden, beneath the retreating margin of the last Fennoscandian Ice Sheet, including near the planned nuclear waste repository at Forsmark. Glacial ripping differs from plucking (quarrying) in that it involves extensive disintegration of rock hills and rock surfaces, with 100s to 1 000s of boulders generated in broadly the same place at the same time. Glacial ripping is seen as an erosion mechanism that links three sequential processes: (i) hydraulic jacking, (ii) rock mass disintegration, and (iii) boulder transport; all operating subglacially.

In this report we review and present a wide range of field evidence in eastern Sweden for this process. We also present modelling to test the physical plausibility of some aspects of glacial ripping.

Evidence for glacial ripping in eastern Sweden comes from three types of features: (1) open, dilated fractures, locally filled with sediment, and disruption or brecciation of the uppermost (top 1–13 m) rock mass indicating hydraulic jacking by subglacial groundwater; (2) disrupted roches moutonnées, locally with fracture caves, that show further disintegration of the upper rock mass below the ice sheet, as well as variable damage on low-relief rock surfaces; and (3) boulder spreads of large, angular boulders, with limited transport distances (usually less than 100 m, and not more than a few kilometres) that occur widely in eastern Sweden, and represent the final stage of transport and deposition by ice. Detailed analyses of fracture patterns, disrupted bedrock and boulder spreads are presented, as well as transitional cases.

Excavations during construction of the nuclear plants and the cooling water inlet canal have shown evidence for hydraulic jacking and associated rock brecciation mainly to depths of 5 m but locally reaching 13 m along exceptionally hydraulically transmissive subhorizontal fractures. Available evidence for adjacent areas indicates that hydraulic jacking was shallow (< 3 m) or absent. Dilated fractures with fracture fills are described for a further 7 quarries in eastern Sweden.

Patterns of further glacitectonic disintegration were analysed on seven large roches moutonnées in eastern Sweden, including Bodagrottorna. Spatially variable patterns of damage from the combined impacts of hydraulic jacking and glaciotectonic disintegration on different hills are also identified at Forsmark. Evidence for glacial transport and deposition is described with displacement of rock blocks in a down-ice direction, including the formation of lee side boulder trains.

Boulder spreads and underlying rubble till represent the final stage of glacial ripping. Boulder spreads locally overlie esker deposits and are locally reworked in terminal moraines, consistent with boulder spread generation close to the retreating ice margin. These observations suggest that boulder spreads, boulder-rich tills and moraines were formed by basal ice movement after glaciotectonic disintegration.

We present transitional cases between hydraulic jacking, disintegration by glaciotectonics, and boulder transport that support the continuity of the ripping process sequence and note that ripping was often arrested before completion of the full sequence.

Asymmetric disintegration of roches moutonnées, transport of boulders, piling up of boulders into moraines, as well as previous compression tests on sediment fills, indicate that these processes operated subglacially. However, limited edge rounding and short transport distances of the boulders, suggest the processes operated during final deglaciation. This in turn suggest that ripping was particularly effective close to the retreating ice margin. It is possible that glacial ripping also occurred earlier during a glaciation, however, evidence for this is likely to have been obliterated by continuing ice sliding.

The impact of glacial ripping during the last glaciation in lowland eastern Sweden was spatially variable. Boulder concentrations mapped by SGU in these settings predominantly comprise boulder spreads, cover 1 000s of km^2 and are distributed in patches or kilometre-wide ice-flow parallel belts. Some boulder spread belts lie adjacent to eskers and in interpreted meltwater corridors.

Near Forsmark, disrupted rock surfaces and roches moutonnées occur within boulder spreads which are mainly confined to two belts, one west of the nuclear power plant and another to the east which follows the Börstil esker. Distribution of boulder spreads at the regional and local scales may thus be partially controlled by subglacial meltwater distribution. The distribution of hydraulic jacking and ripping at Forsmark appears to have been influenced by similar factors to elsewhere in Uppland: distribution of water at overpressure (potentially in large volumes), fracture patterns, local topography and till cover. Similar patterns and depths of ripping can be predicted at Forsmark in future glaciations.

The subglacial groundwater overpressure required for hydraulic jacking is provisionally linked to strong water pressure fluctuations occurring at the ice-bed beneath the rapidly deglaciating Fennoscandian Ice Sheet, similar to those documented beneath the present-day Greenland Ice Sheet. The presented modelling suggests that overpressures as measured beneath the Greenland Ice Sheet are sufficient to cause hydraulic jacking in the shallow rock mass, provided suitable fractures (in particular, subhorizontal fractures) are present to allow overpressured water to enter the rock mass. The maximum depth of hydraulic jacking is limited to c. 3 % of ice thickness. Over pressurised water, when entering and opening fractures in the uppermost rock mass, dilates the rock mass. Dilation reduces friction along the fractures, and/or lowers the rock-mass strength. One component of modelling shows it is feasible for new subvertical fractures to form following jacking of underlying subhorizontal fractures, by beam failure. This process can add to further lowering of the rock-mass strength.

Further disintegration occurs if ice drag forces exerted by sliding ice exceed the rock-mass strength. Mathematical models of forces beneath sliding glacier ice indicate that overall sliding velocity and the sizes and shapes of 1–10 m high rock steps, bumps and hills at the glacier bed strongly influence drag forces. Threshold conditions for potential failure of rock surfaces are identified under different fracture water-pressure scenarios. Factors that favour hydraulic jacking thus include high subglacial meltwater pressures, high fracture connectivity and aperture, and limited till cover. Factors that favour subsequent glaciotectonic disintegration include high ice velocity and blunt shapes of obstacles.

Glacial ripping has evidently contributed to the total glacial erosion in eastern Sweden, relevant for safety assessments for the planned deep repository for spent nuclear fuel at Forsmark, Uppland. The depths of rock mobilised or disintegrated by glacial ripping (1–4 m) are of the same order or higher as the 0.6–1.6 m (interquartile range) depth of erosion during the Late Weichselian glaciation as derived from cosmogenic nuclide inventories measured on abraded surfaces. Glacial ripping is thus a potent, if localised, erosion process, likely operating as a distinct temporal pulse during final deglaciation. The mechanical impact by hydraulic jacking, if not followed by further disintegration, also prepares the near-surface rock for removal in subsequent glacial stage. The potential impact of ripping needs to be considered together with abrasion and plucking when modelling erosion depths and rates in similar glaciated terrains.

Furthermore, the process of glacial ripping implies that disintegrated roches moutonnées and fracture caves are formed by subglacial processes. These features cannot be used to constrain the magnitude, extent and timing of post-glacial earthquakes.

Sammanfattning

Effekten av framtida glacial erosion behöver inkluderas i analysen av säkerhet efter förslutning för det planerade kärnbränsleförvaret i Forsmark. Traditionellt räknas två processer till glacial erosion: abrasion (slipning) och plockning. Nyligen har en tredje process identifierats, kallad *glacial ripping* (ungefär *glacial uppslitning* på svenska), vilken varit effektiv inom vissa områden inom den relativt flacka kristallina berggrunden i östra Sverige. Processen var aktiv under den retirerande iskanten vid den senaste deglaciationen av den Fennoskandiska inlandsisen, inklusive inom vissa delar av platsen för det planerade kärnbränsleförvaret i Forsmark. *Glacial ripping* skiljer sig från glacial plockning i det att den inbegriper omfattande desintegration av bergkullar och bergytor, med hundratals till tusentals block bildade vid ungefär samma plats och tidpunkt. *Glacial ripping* beskrivs som en process som länkar tre sekventiella händelser: i) hydraulisk upplyftning (eng. hydraulic jacking), ii) uppspräckning av den upplyfta bergmassan, och iii) transport av de resulterande blocken. Alla tre processerna sker subglacialt.

I den här rapporten granskar och presenterar vi omfattande fältbevis från östra Sverige för denna erosionsprocess. Vi presenterar även modellering som genomförts för att testa den fysikaliska rimligheten hos vissa aspekter av *glacial ripping*.

Bevis för glacial ripping i östra Sverige kommer från tre typer av observationer: i) öppna sprickor, ibland fyllda med sediment, och uppsprickning av den översta delen (1–13 m) av berggrunden, indikativt för hydraulisk upplyftning genom subglacialt vatten, ii) uppspräckta rundhällar, ibland med lokalt förekommande blockgrottor, vilket visar på fortsatt desintegrering av den övre delen av bergvolymen under inlandsisen, samt förekomst av flackare bergytor med olika grad av uppsprickning, och iii) blockfält bestående grova kantiga block som transporterats kort sträcka (ofta kortare än 100 m och inte mer än några få km). Blockfälten är vanligt förekommande i östra Sverige, och representerar det sista steget av isens transport och deposition av blocken. Detaljerade sprickanalyser, observationer av uppspräckt berggrund och blockfält presenteras, samt övergångsfaser däremellan.

Vid konstruktionen av kärnkraftverket och dess kylkanal i Forsmark framkom bevis för hydraulisk upplyftning och associerad uppsprickning av berggrunden, oftast ner till ett djup på runt 5 m, men lokalt ner till 13 m (längs subhorisontella sprickor med hög hydrauliskt transmissivitet). Data från intilliggande områden indikerar hydraulisk upplyftning till grundare djup (< 3 m) eller ingen hydraulisk upplyftning alls. I föreliggande rapport redovisas även öppna sedimentfyllda sprickor för ytterligare sju lokaler (stenbrott) i östra Sverige.

Ytterligare glaciotektonisk desintegration av sju större rundhällar i östra Sverige, inklusive Bodagrottorna, analyserades i detalj. Även i Forsmark beskrivs rumsligt varierande mönster av sönderdelning av berggrunden genom kombinationen av glacial upplyftning och glaciotektonisk desintegration. Bevis för glacial transport och deposition beskrivs genom kartering och tolkning av blocktransport i den forna isrörelseriktningen, inklusive bildandet av läsides blockansamlingar.

Blockfält och underliggande morän representerar det sista steget av *glacial ripping*. På vissa platser överlagrar blockfälten glacifluviala åsavlagringar och på andra platser är de lokalt omarbetade i ändmoräner, i linje med att blockfälten är bildade subglacialt nära den retirerande iskanten. Dessa observationer indikerar att blockfälten och de blockrika moränerna bildades av den basala isrörelsen efter glaciotektonisk desintegration.

Vi presenterar även övergångsformer mellan hydraulisk upplyftning, glaciotektonisk uppspräckning och blocktransport, vilket stöder den sekventiella processen *glacial ripping.* Vi noterar att processen i flera fall avslutats innan hela sekvensen skett.

En asymmetrisk desintegration av rundhällar, blocktransport, block ansamlade till ändmoräner, samt tidigare kompressionstester på sedimentsprickfyllnader, indikerar att processerna skett subglacialt. Eftersom blocken ofta inte har rundade kanter och eftersom de är korttransporterade visar detta att processen sannolikt skett under den senaste deglaciationen samt att *glacial ripping* varit speciellt effektiv nära den retirerande iskanten. Det är möjligt att *glacial ripping* också förekommit tidigare under nedisningen, men att spåren av denna blivit förstörda genom den fortsatta basala isrörelsen.

Förekomsten och effekten av *glacial ripping* under den senaste nedisningsperioden i östra Sverige var rumsligt variabel. Blockansamlingar karterade av SGU i dessa områden, vilka utgörs i huvudsak av blockfält, täcker 1000-tals km^2 och är fördelade fläckvis eller i km-breda stråk parallella med den tidigare isrörelseriktningen. Vissa blockfältstråk ligger intill åsar och inom tolkade smältvattenkorridorer.

Nära Forsmark förekommer uppspräckt berg och uppspräckta rundhällar inom blockfält i två huvudsakliga stråk, ett väster om kärnkraftverket och ett längre österut vilket följer Börstilåsen. Förekomsten av blockfält på regional och lokal skala kan därför delvis vara kontrollerad av fördelningen av subglacialt smältvatten. Förekomsten av hydraulisk upplyftning och *glacial ripping* i Forsmark förefaller vara påverkad av samma faktorer som i övriga Uppland nämligen i) fördelningen av subglacialt smältvatten vid övertryck (potentiellt i stora volymer), ii) berggrundens sprickmönster, iii) den lokala topografin, samt iv) förekomst av moräntäcke. Motsvarande fördelning och djup hos *glacial ripping* kan förväntas i Forsmark under framtida nedisningar.

Det subglaciala grundvattnet vid övertryck som krävs för hydraulisk upplyftning är preliminärt kopplat till kraftiga variationer i vattentryck vid bottnen hos den snabbt retirerande inlandsisen under deglaciationen, liknande de tryckvariationer som dokumenterats från dagens Grönländska inlandsis. Den modellering som presenteras indikerar att de övertryck som uppmätts under den Grönländska isen är tillräckliga för att inducera hydraulisk upplyftning av det ytnära berget, givet en lämplig sprickighet hos berget (speciellt subhorisontella sprickor) som tillåter vattnet att infiltrera bergmassan. Det maximala djupet hos den hydrauliska upplyftningen är ca 3 % av den ovanliggande istjockleken. När vattnet vid övertryck infiltrerar och öppnar sprickor i den övre delen av bergmassan reduceras friktionen längs sprickorna och bergets hållfasthet minskar. En del av modelleringen visar att det är möjligt för nya subvertikala sprickor att bildas efter upplyftning av underliggande subhorisontella sprickor. Detta skulle i så fall kunna minska bergets hållfasthet ytterligare.

Ytterligare desintegration sker om dragkraften som utövas av den mot underlaget glidande isen överskrider bergets hållfasthet. Numerisk modellering indikerar att den basala glidhastigheten hos inlandsisen samt storleken och formen hos 1–10 m höga hinder i form av block, steg och höjder under isen har en stor påverkan på dragkrafterna vid bottnen av isen. Gränsvärden för när bergets hållfasthet överskrids identifieras för olika scenarier för vattentryck i sprickor. Faktorer som gynnar hydraulisk upplyftning inkluderar därför högt tryck hos det subglaciala smältvattnet, hög sprickkonnektivitet och stor sprickapertur, och ett begränsat moräntäcke. Faktorer som gynnar efterföljande desintegration av den upplyfta bergmassan inkluderar hög isrörelsehastighet (basal glidning) och trubbig form på hindren vid bottnen.

Glacial ripping har bidragit till den totala glaciala erosionen som förekommit historiskt i östra Sveriges kristallina berggrund, och är därmed relevant för säkerhetsanalyserna för det planerade kärnbränsleförvaret i Forsmark. Djupet hos berget som påverkas av desintegration genom glacial ripping (1–4 m) är i samma storleksordning eller större än erosionsdjupet på 0,6–1,6 m (interkvartilintervallet) under sen Weichsel som erhållits från studier av kosmogena nuklider från hällar påverkade av glacial abration (slipning). Glacial ripping är därför en potent, om än lokalt fokuserad, glacial erosionsprocess, som förmodligen är aktiv under en distinkt tidsmässig avslutningsfas under deglaciationen. Den mekaniska påverkan från hydraulisk upplyftning, om den inte efterföljs av ytterligare desintegration, förbereder även det ytnära berget för erosion av block under efterföljande nedisade perioder. Den potentiella effekten av glacial ripping behöver beaktas, tillsammans med glacial abrasion och plockning, vid modellering av erosionsdjup och erosionshastigheter vid liknande tidigare nedisade områden.

Därutöver visar processen *glacial ripping* att desintegrerade rundhällar och blockgrottor formas genom subglaciala erosionsprocesser. Uppspräckta rundhällar och blockgrottor kan därför inte användas för att dra slutsatser kring magnituder, omfattningar eller tidpunkter för post-glaciala skalv.

Contents

1 Introduction

One important question that is addressed in the assessments of long-term safety of spent nuclear fuel repositories, such as the planned repository at Forsmark, is the depth of glacial erosion by future ice sheets (e.g. SKB 2020, Iverson and Person 2012, Hallet 2011). Understanding past glacial erosion over lowland Sweden can inform modelling of future erosion that may affect the Forsmark site. Glacial erosion rates can vary from near zero (Fabel et al. 2002) to rates that surpass fluvial erosion rates (Koppes and Montgomery 2009). Many aspects of glacial erosion remain uncertain or enigmatic, mainly because the processes occur below ice and cannot be directly observed. Thus, the understanding of the mechanisms of glacial erosion is strongly grounded on geomorphological studies of deglaciated areas, where analysis of the shape of the remaining bedrock and resultant deposits provides clues as to the processes of glacial erosion (e.g. Chamberlin 1888, Rastas and Seppälä 1981, Glasser and Warren 1990, Alley et al. 2019).

Recent studies managed by SKB have addressed aspects of glacial erosion over the last 100 ka and 1 Ma in eastern Sweden (e.g. Hall et al. 2019a, b, 2020, Heyman et al. 2019, Goodfellow et al. 2019). Hall et al. (2019a, b) examined the potential of using the sub-Cambrian unconformity as a reference surface to estimate past erosion of hard basement gneisses. Terrestrial cosmogenic nuclide inventories in samples from bedrock surfaces can also constrain past glacial erosion; in the Uppland region results from such studies suggest typical total depth of glacial erosion on abraded surfaces was c. 1.6–3.5 m over the last 100 ka, and 0.6–1.6 m over the Late Weichselian (MIS2) glaciation (Hall et al. 2019a, Heyman et al. 2019). Goodfellow et al. (2019) studied the role of subhorizontal fractures and sheet jointing in subglacial erosion below the Fennoscandian Ice Sheet for the formation of "conspicuously flat surfaces".

Over the last hundred years, abrasion and plucking (quarrying) have been recognised as the main mechanisms by which glaciers erode rock (e.g. Boulton 1979, Benn and Evans 2010, Hallet 2011, Alley et al. 2019). The relative contribution of direct meltwater erosion has been vigorously debated (Sharpe and Shaw 1989, Benn and Evans 2006, Ó Cofaigh et al. 2010, Shaw 2010), but meltwater erosion of bedrock appears to be substantial only in very localised areas, such as tunnel valleys, meltwater channels and areas subjected to large lake-drainage events (e.g. Bretz 1969).

In eastern Sweden a number of geological and geomorphological features occur that cannot be easily explained by abrasion or plucking, or indeed any other well-understood and documented glacial process:

1. Dilated subhorizontal or gently dipping factures, filled with water lain silt-sand, suggesting some form of subglacial hydraulic jacking of bedrock fractures (Carlsson 1979, Carlsson and Christansson 1987, Pusch et al. 1990, Leijon 2005, Forssberg et al. 2007),

2. Disrupted and partially disintegrated roches moutonnées, including fracture caves (Sjöberg 1986, 1994, Mörner et al. 2000, Mörner and Sjöberg 2018),

3. Extensive fields of large, angular boulders (Sohlenius et al. 2004, Lagerbäck et al. 2005; and wider mapping by SGU, the Swedish Geological Survey), termed here *boulder spreads*. Given their setting, commonly on flat ground and previously submerged beneath the Baltic Sea, they can be formed neither by periglacial nor by slope processes, nor can be explained by classic abrasion or plucking. Associated with these are isolated megaclasts (or 'giant blocks') that are locally obvious features in the lowland landscape of Sweden.

1.1 Previous hypotheses

The three types of features described above have been documented individually before, but their origins have been contentious, and different hypotheses have been forwarded as to their explanations.

The dilated fratures were initially attributed to dilation by freezing ice, followed by later sediment infilling (Stephanson and Erickson 1975). Pusch et al. (1990) assumed dilation was caused by hydraulic jacking, but in the proglacial foreland, with overpressure envisaged to be caused by the

pressure difference between the englacial water table and the proglacial foreland (see also Talbot 1999). To maintain high water pressure between the ice sheet and the foreland and prevent leakage, a 10–30 m thick layer of proglacial permafrost was envisaged. No link between hydraulic jacking and disintegrated roches moutonnées or boulder spreads was discussed.

The disintegrated roches moutonnées and fracture caves have received much attention. One hypothesis is that the caves were formed by large magnitude (> M7) earthquakes caused by postglacial isostatic uplift during and following deglaciation of the Fennoscandian ice sheet (De Geer 1940, Mörner 1978, Sjöberg 1986, 1994, Ekman 1988, Mörner et al. 2000, Mörner and Sjöberg 2018). Mörner et al. (2000) specifically linked the disintegrated roche moutonne at Bodagrottorna to a potential 9663 BP seismic event in the Iggesund area (Gävleborg county), that was dated on the basis of disturbed varves, in part interpreted as paleo-tsunami deposits.

Talbot (1999) linked the occurrence of fracture caves and boulder spreads and further suggested explosive methane venting as a possible explanation, without providing an exact mechanism or origin. Explosive methane venting, possibly triggered by earthquakes, was proposed as mechanism by Mörner (2017) and Björklund (1990), commonly for the same roches moutonnées that were previously attributed to earthquakes.

In those studies that proposed a seismic or a methane-venting origin, a subglacial origin was negated on the basis that the disintegration must have occurred proglacially, since the fracture surfaces and blocks were not striated afterwards (e.g. Sjöberg 1986, 1994, Mörner et al. 2000, Mörner 2017, Mörner and Sjöberg 2018).

Concerning the isolated megaclasts, Sandegren et al. (1939) noted that "giant blocks often lie close together in groups, all of the same rock"; that locally "block movement be so insignificant that they are practically in their own original position"; and that block rotation can be seen on boulders with vertical striated surfaces. All these features were interpreted as formed by action of ice. A glacial origin for disruption of large bedrock hills was also suggested by Lundqvist (1987), who envisaged an ice-marginal process, linked to the Younger Dryas ice sheet advance. Lagerbäck et al. (2005) first suggested that these three different phenomena are related and of subglacial origin. However, none of these studies proposed a detailed mechanism.

1.2   Glacial ripping hypothesis

Hall et al. (2020) and Krabbendam et al. (2022a, b) proposed an hitherto unrecognised subglacial erosion mechanism, *glacial ripping*, that operated over lowland Sweden and explains the features described in Section 1.1. Glacial ripping is proposed to be caused by a sequence of three consecutive processes: (1) hydraulic jacking and bedrock disruption caused by overpressured subglacial melt-water, (2) glaciotectonic disintegration of the shallow rock mass into blocks and then boulders and (3) transport and final deposition of boulders. Glacial ripping has also been proposed to have operated in NW Scotland (Hall et al. 2021a), and in Ontario (Bukhari et al. 2021), albeit termed 'large-scale quarrying' in the latter study.

1.3   Relevance of glacial ripping hypotheses

The recognition of glacial ripping as an effective erosion mechanism is important for several reasons.

Firstly, in order to constrain total erosion rates of a previously glaciated terrain, a parameter used in SKB safety assessments, it is necessary to integrate the contributions of different erosion processes acting across variable geology and topography at the ice sheet bed. The recognition of glacial ripping as a locally effective and extensive erosion mechanism is important for the estimation of integrated total glacial erosion depths over lowland Sweden in the last glacial cycle. For instance, if erosion depths determined from terrestrial cosmogenic nuclide inventories rely solely on samples taken from abraded upper surfaces on roches moutonnées, then such erosion depths give an incomplete estimate on the overall erosion depth in lowland Sweden, as they only constrain the depth of erosion on these upper surfaces. The total erosion depth integrated over a larger area (such as in the GIS analysis of

Hall et al. 2019a) includes contributions from erosion processes other than abrasion, including plucking and glacial ripping, and from rock surfaces in lower positions on the former glacier bed, including valleys, trenches and rock basins (see also Hall et al. 2022). Thus, a good understanding of the mechanisms, patterns and depths of glacial erosion must include glacial ripping, its distribution and its controlling and rate-limiting factors.

A second issue relevant for the safety assessments performed for the planned spent nuclear fuel repository is the potential for large earthquakes. Although Sweden is nowadays situated far from active plate boundaries, with limited seismic activity, earthquakes may be triggered by differential movement of the Earth's crust and excess horizontal stresses due to rapid deglaciation (e.g. Bödvarsson et al. 2006, Lund et al. 2009). Typically, the evidence for such isostatically triggered, late-glacial seismic activity relies on (i) deformation of late-glacial sediments such as glaciomarine or glaciolacustrine sediments, (ii) the displacement of surface features or (iii) the identification of postglacial fault scarps (e.g. Lagerbäck 1990, Lagerbäck et al. 2005, Mikko et al. 2015). Whilst in northern Scandinavia there appears to be good evidence for such features (e.g. Mikko et al. 2015, Mattila et al. 2019), in eastern Sweden this is more ambiguous (Öhrling et al. 2018). In eastern Sweden it has been suggested that the above-mentioned fracture caves, such as Bodagrottorna, attest to large magnitude (> M7) earthquakes related to postglacial isostatic uplift (De Geer 1940, Mörner 1978, Sjöberg 1994, Mörner et al. 2000, Mörner and Sjöberg 2018). However, this interpretation is not universally accepted (e.g. Smith and Öhrling 2022) and a glacial origin for disruption of these bedrock hills has also been proposed (Lundqvist 1987, Lagerbäck et al. 2005). The interpretation of the disrupted roches moutonnées and their fracture caves therefore has a bearing on the assessment of post-glacial seismic events during deglaciation in lowland Sweden.

Lastly, entry of subglacial water at overpressure along bedrock fractures, and related hydraulic jacking or hydro-fracturing, is also of interest in SKB safety assessments. This issue has been studied and discussed for deep (> 100 m) fractures (Talbot 1999, Hökmark et al. 2010, Lönnqvist and Hökmark 2013). The mechanism for this overpressure is generally seen as a result of the relatively static hydraulic pressure difference between the ice sheet and the glacial foreland. The sediment-filled subhorizontal fractures, however, mainly occur at shallow depths, and the question whether they developed subglacially or proglacially is an important constraint as to their formation. Results from the Greenland Ice Sheet has shown significant subglacial water-pressure fluctuations, commonly resulting in overpressure, in the englacial and subglacial hydraulic system (e.g. Wright et al. 2016, Andrews et al. 2014, Harper et al. 2016, 2019), and associated with the drainage of supraglacial lakes (Das et al. 2008, Doyle et al. 2013). The potential for transient overpressurization of subglacial meltwater during deglaciation is increasingly recognised also beneath the former Laurentide and Fennoscandian ice sheets (e.g. Ahokangas et al. 2021, Dewald et al. 2021).

1.4 Presented evidence and modelling

In this report, we test the hypothesis that glacial ripping is a potentially significant subglacial erosion mechanism, in addition to the two widely recognised mechanisms of abrasion and plucking (quarrying). We present field data to characterise and analyse:

1. shallow (< 5–10 m depth) fracture systems in terms of fracture spacing, dilation and sediment-fill,

2. disrupted roches moutonnées and associated fracture caves, and

3. boulder spreads.

In order to test whether glacial ripping is a physically plausible mechanism we also report some theoretical calculations and modelling, focussing on

a) the maximum depth of hydraulic jacking,

b) the possibility that some fractures are newly generated by beam failure, during and following the process of hydraulic jacking, and,

c) an analysis of the balance of drag forces and resisting forces acting on rock hills and subjected to water overpressure conditions at the base of an ice sheet.

2 Setting

The main study area is the Uppland county in eastern Sweden, with special importance to sites close to Forsmark. Some additional study sites are in Gävleborg county further north (Figure 2-1).
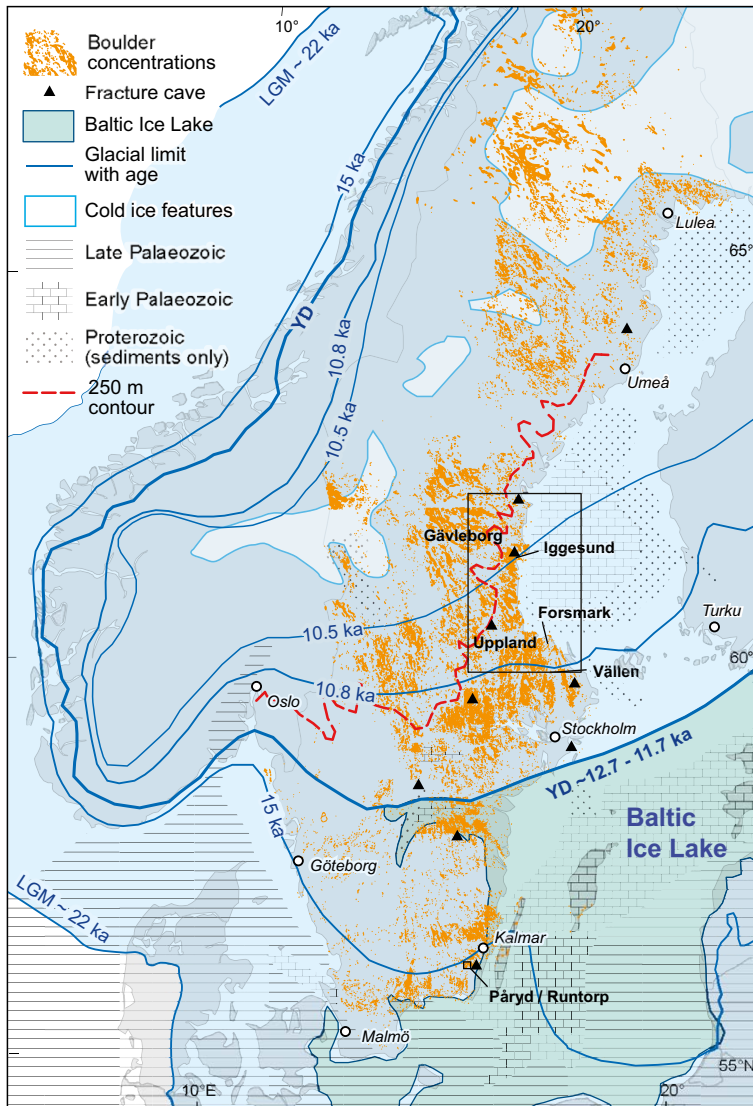
Figure 2-1. *Overview map of the Fennoscandian Ice Sheet with selected margin positions, Baltic Ice Lake (Stroeven et al. 2016), boulder concentrations (SGU data), fracture caves (Sjöberg 1987, 1994); schematic bedrock geology after Asch (2005). YD = Younger Dryas limit. Only Proterozoic sedimentary rocks are shown ('Jotnian' and 'Riphean' sandstone); Proterozoic metamorphic and igneous rocks are not shown.*

2.1　Bedrock geology

Eastern Sweden is underlain by basement gneisses that formed c. 1 900–1 800 Ma ago as part of the Svecokarelian orogen (e.g. Stephens 2010). Rock types include a variety of mainly felsic gneisses (granitic gneiss, tonalitic gneiss etc), as well as more mafic rocks, such as amphibolite gneiss (Figure 2-2). Grain-size is highly variable, ranging from coarse grained, porphyritic meta-granites, to fine grained aplitic and meta-rhyolitic rocks. Mesoproterozoic 'Jotnian' sandstones and Cambrian sandstones and Ordovician limestones, exposed in the Bothnian Sea floor (Figure 2-2), unconformably overly the basement.

Depending on the amount and localisation of early ductile shearing, the basement rocks can vary from nearly undeformed (e.g. 'massive granite'), to strongly foliated. Near Forsmark, the older ductile structure of the gneisses shows several NW-SE orientated, steeply dipping shear zones, with well-developed ductile shear fabrics including mylonitic zones, separated by km-scale lenses of less deformed rocks (e.g. Stephens 2010).

The basement gneisses first cooled into the brittle regime at c. 1 800–1 750 Ma (Hermansson et al. 2008, Söderlund et al. 2009) and later remained in the brittle regime. The basement was first exhumed to the near-surface in the Mesoproterozoic, and subsequently subjected to several cycles of burial and exhumation associated with deposition and erosion of foreland and shelf basins (e.g. Larson et al. 1999, Huigen and Andriessen 2004).

2.1.1　Fractures networks in the shallow basement rock

The basement in Uppland is divided into a mosaic of fault blocks along regional and local brittle deformation zones with lengths of > 10–40 km and spacing of 2–15 km (Tirén and Beckholmen 1989, Grigull et al. 2019). The major vertical fracture zones extend to great depth but are narrow (mainly < 100 m wide). Fracture densities are high, forming long corridors along linear fracture zones from which small rock block sizes have been eroded beneath the Fennoscandian Ice Sheet to form rock trenches.

Around Forsmark, different rock domains (RFMxxx) and fracture domains (FFMxxx) have been established and described (e.g. Olofsson et al. 2007). A number of steeply dipping, anastomosing NW-SE striking shear zones occur that separate kilometre-wide lenses of less deformed rocks (e.g. Follin et al. 2007, Nordgulen and Saintot 2008, Stephens 2010). These are connected by subsidiary deformation zones that strike NE-SW (ZFMENE).

The fracture domains close to the surface (FFM02 and FFM03) show a high frequency of gently dipping and sub-horizontal, open fractures. In domain FFM02, the dominant fracture system is formed by large subhorizontal fractures, connected with smaller, subvertical fractures. In the SE, distinctive features are gently inclined 'deformation zones' (including ZFMA2 and ZFMF1), possibly initiated as minor thrust faults during the later stages of the Svecokarelian orogeny and later reactivated (Juhlin and Stephens 2006).

The fracture domains at depth (e.g. FFM01 and FFM06 on Figure 2-3) show fewer open fractures and few subhorizontal fractures. There is a general upward increase in fracture density towards the surface (Follin et al. 2007, SKB 2013), in particular in the top 10 m (Carlsson 1979, Brojerdi et al. 2014). Near Forsmark (that is in the area where detailed SKB studies have been carried out) there is a general upward increase in frequency of open fractures and fracture transmissivity (Olofsson et al. 2007, Min and Stephansson 2011). However, widely-spaced, open fractures near Forsmark occur down to considerable (> 100 m) depth (Follin et al. 2007, SKB 2013). In excavated sections, sub-horizontal fractures had much larger aperture (10–100 mm) than steep fractures (typically < 1–2 mm; Carlsson 1979, Carlsson and Olsson 1982a, b). This compares with much smaller apertures of 0.5–5 mm below 15 m (Carlsson and Olsson 1978, SKB 2013).
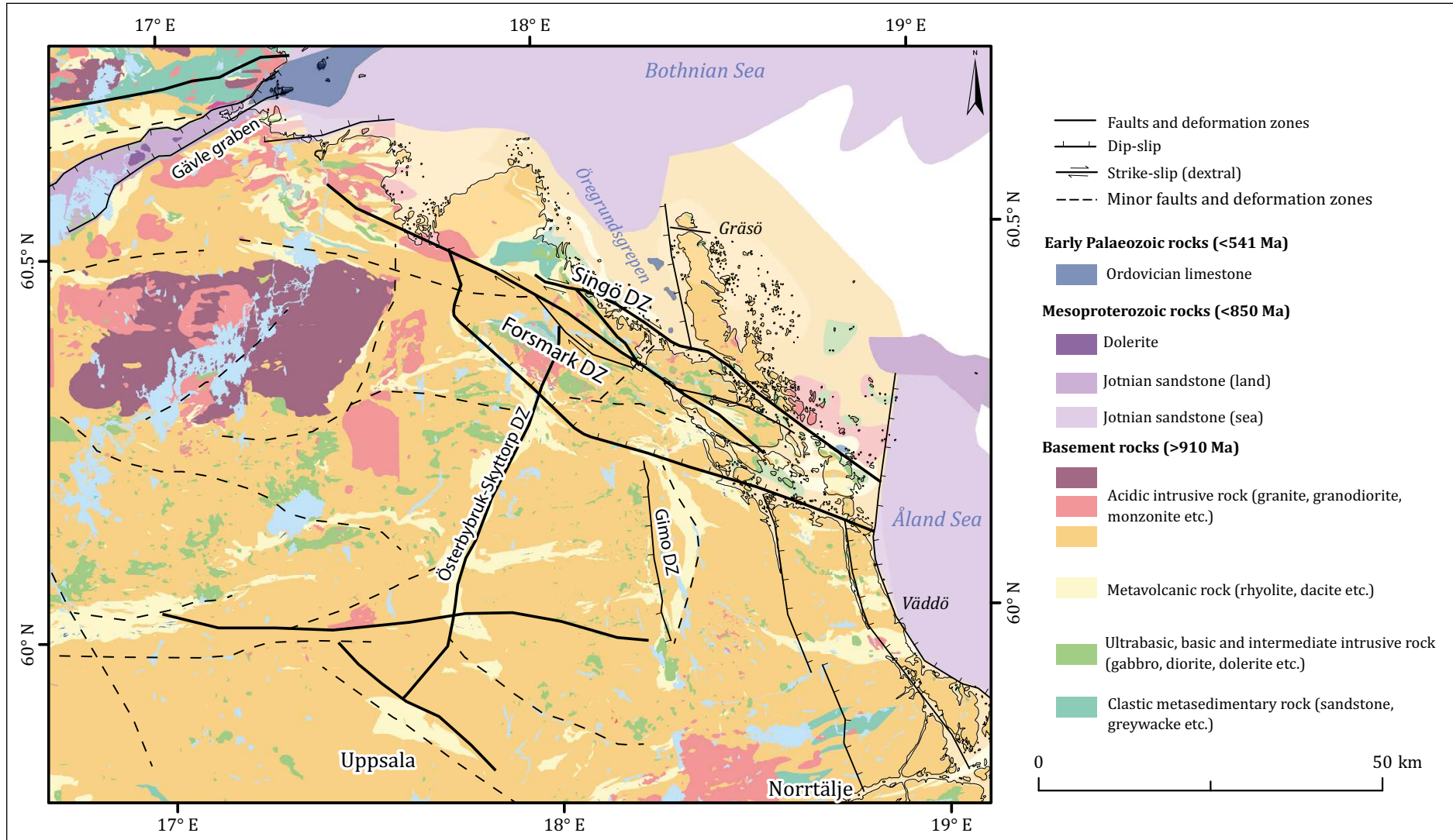
Figure 2-2. *Geology of NE Uppland from Hall et al. (2019a; Figure 2.1); mapping by SGU.*
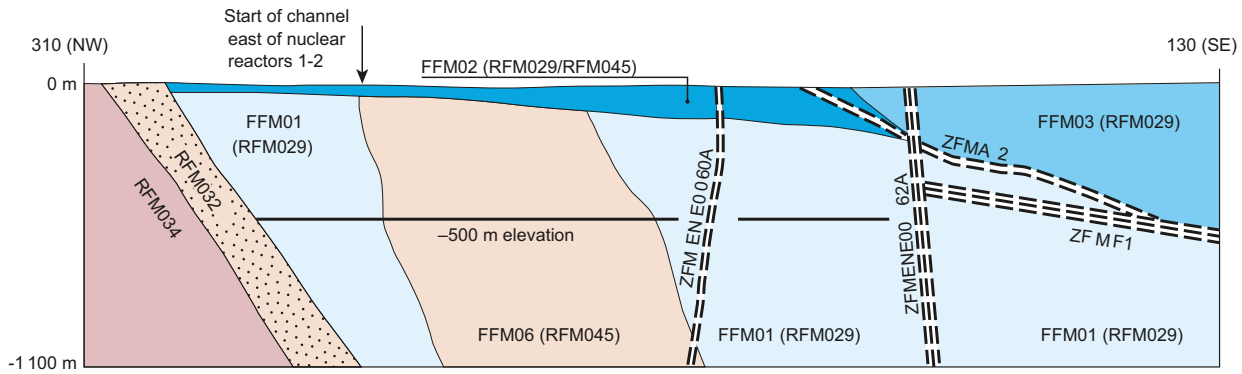
Figure 2-3. *Simplified profile showing different rock domains and fracture domains for the Forsmark area. After Olofsson et al. (2007).*

The hydrological transmissivity in the shallower fracture domains is highly variable, and include high transmissivity values (1×10^{-10}–1×10^{-3} m^2 s^{-1}). Deeper fracture domains (FFM01 and FFM03-5) have lower transmissivity (1×10^{-10}–1×10^{-7} m^2 s^{-1}), although some gently dipping deformation zones show high transmissivity (1×10^{-5}–1×10^{-3} m^2 s^{-1}) to considerable depth. The bedrock in between the horizontal fractures/sheet joints, however, shows low hydraulic conductivity (c. 1×10^{-11}–1×10^{-8} m s^{-1}) except where it is intersected by transmissive steeply-dipping or gently-dipping deformation zones (Johansson 2008). Fracture transmissivities of horizontal and gently dipping fractures is generally higher than for steeply dipping fractures (Olofsson et al. 2007). Little information is available, however, on near-surface hydraulic transmissivity in fracture domains that lie outside the repository target area.

2.1.2 Fracture coatings and age of fractures

Basement fractures are commonly coated with minerals such as chlorite, epidote, corrensite, laumontite, adularia, quartz, calcite and hematite. Detailed analysis at Forsmark has shown that these can be attributed to at least four generations: the first two are Proterozoic, the third Palaeozoic and a fourth Palaeozoic to Pleistocene; most fractures were thus formed well before Quaternary glaciation (Sandström et al. 2008, 2009, 2010). Fractures were re-opened to depths of 500 m under the presently prevailing stress regime (Moon et al. 2020).

Carlsson (1979) provided detailed counts on the number of coated versus uncoated fractures for different fracture sets at shallow depths near Forsmark. Most fractures (75–90 %) are coated with chlorite. Uncoated fractures account for 10–25 %, with the E-W trending subvertical fracture set being most commonly (25 %) uncoated (Carlsson 1979). Other temporary, shallow excavations in the Forsmark area also record uncoated vertical fractures (Hermanson et al. 2003, Leijon 2005, Lagerbäck et al. 2005). These reports interpret uncoated vertical fractures as new fractures. At depths of > 100 m in bedrock, borehole logs assessment show that only very few (< 5 %) of the fractures are uncoated (Claesson Liljedahl et al. 2011). Elsewhere in Sweden, coated fractures are also common (Viola et al. 2009, Löfgren and Sidborn 2016).

2.1.3 Sediment-fill of fractures

Near the Forsmark nuclear power plant, large canal and construction excavations in domain FFM02 previously revealed subhorizontal fractures (< 10° dip), up to 170 m long, that are dilated and filled by 1–80 cm of laminated silt and sand (Stephansson and Ericsson 1975, Carlsson 1979) (Figure 4-2A, B). In subsequent test excavations near Forsmark (Drill Site 5, AFM001264 and AFM001265) similar sediment-filled fractures were studied (Leijon 2005, Forssberg et al. 2007, Petersson et al. 2007). Fracture sediment fills are common only in the upper 5 m of the bedrock (Carlsson 1979, Leijon 2005), but rare occurrences have been recorded in boreholes down to depths of 50 m (Follin et al. 2007).

Sediment fill in bedrock fractures consists mainly of silt, with minor sand and diamicton, and some rock fragments (Stephansson and Ericsson 1975, Carlsson 1979, Leijon 2005). The rock fragments are likely from a very local origin (e.g. broken off from the fracture faces), whereas the finer sediment has been transported into the rock mass along open fractures (e.g. Leijon 2005). Laminations in the silt-sand fill (Figure 4-2C) indicate deposition by flowing water (Stephansson and Ericsson 1975, Carlsson 1979, Leijon 2005). Compression tests on the silt-sand sediment fill at Forsmark suggest the sediment fill was subjected to pre-consolidated load of 3.4–3.9 MPa (Carlsson and Olsson 1976, Carlsson 1979). This suggests compaction by effective pressure (ice sheet pressure minus water pressure) of similar amounts (e.g. Iverson and Person 2012), requiring substantial ice sheet thickness, altogether indicating the fill was deposited sub-glacially. It is not known to what extent Carlsson's (1979) measurements are representative for other fracture sediment fills in lowland Sweden.

Microfossil and pollen content of the silt sediment in the fractures is similar to that of overlying, hard calcareous till deposits (Stephansson and Ericsson 1975, Robertsson 2004), consistent with sourcing of the sediment from till at the ice-bed interface. The reworked palynomorphs include those of tree species present in east central Sweden in the last, Eemian interglacial (Leijon 2005), or possibly other, younger warm periods (Helmens et al. 2020). As the Forsmark site probably was glaciated in at least two phases since the Eemian (SKB 2010), the fracture infill potentially predates, in part, the last deglaciation. Alternatively, the sediment was deposited during the last glaciation, but was sourced from erosion of till that was deposited prior to the last glaciation.

2.2   Geomorphological setting

Eastern Uppland comprises a low-relief shield terrain, eroded into hard basement gneisses. By the start of the Palaeozoic, the basement had been eroded to a peneplain (e.g. Lidmar Bergström 1993). The basement gneisses were overlain by Early Palaeozoic sedimentary strata, thus separated by a very flat unconformity surface, the sub-Cambrian unconformity (Nielsen and Schovsbo 2011, Hall et al. 2019b). The unconformity was faulted (typically with faults with 10s of meters of vertical displacement) but has retained a near-horizontal attitude (e.g. Grigull et al. 2019). Early Palaeozoic sedimentary rocks still rest on basement offshore from Forsmark in the Bothnian basin (Figure 2-2) and also occur as outliers in central southern Sweden. Basement surfaces close to present outliers, including in Uppland, retain the general low relief of the original unconformity surface and have been widely referred to as the sub-Cambrian Peneplain (e.g. Lidmar-Bergström 1993). Here, basement was likely re-exposed by removal of cover rocks during Pleistocene glaciations (Hall et al. 2019a). However, even where the sedimentary strata have been removed by erosion, and the present bedrock surface is formed by basement gneisses, the high points of the present bedrock surface in Uppland county are thought to be very close (< 10 m) beneath the original surface of the sub-Cambrian unconformity (Hall et al. 2019a).

The present landscape of eastern Uppland has a rougher bedrock surface than the original unconformity surface (Hall et al. 2019a). Despite a close accordance of summit elevations, the typical relative relief of the present bedrock surface is 5–30 m due to the development of many shallow valleys, trenches and basins below the original unconformity surface, guided by underlying fracture zones (Hall et al. 2022). The numerous low hills have rectilinear outlines and asymmetric long profiles (Hall et al. 2019a). Such terrain is typical of glaciated basement gneiss shields (e.g. Rea and Evans 1996, Johansson et al. 2001, Olvmo and Johansson 2002, Roberts and Long 2005, Krabbendam and Bradwell 2014).

The glacial landscape in Uppland county contains various components developed at different scales by glacial erosion. At the regional scale, three terrain types are recognised (Hall et al. 2019a):

1. **Ice-roughened terrain.** Exposed bedrock is extensive on topographic high points. Rectilinear hills (*box hills*) and smaller roches moutonnées are widespread. Fracture-guided valleys of varying widths and orientations are common. Till cover thickens in depressions and partly infills shallow rock basins with star- and box-shaped outlines. Three sets of fractures are apparent in the regional relief, striking NNE-SSW, WNW-ESE and WSW-ENE. Weak glacial streamlining towards the south or SSE is evident from the orientation of bedrock ridges, hills and valleys.

2. **Weakly streamlined terrain.** Exposed bedrock is more restricted in extent, and till cover is more widespread. Drumlinoid hills are common, mainly of 50–300 m length and aligned parallel with former ice flow. Rock-cored hills show rounded stoss faces and fracture-guided flanks. Small lee side and flank cliffs are seen in LiDAR-based imagery. Many hills (mapped as crag and tails by SGU) have low till tails of 50–250 m length, parallel to former ice-flow direction. Broad trenches, depressions and rock basins occur in fracture zones between hill groups; local bedrock streamlining has exploited NNW-SSE to N-S trending fractures. Here, thicknesses of glacial and marine deposits often exceed 5 m.

3. **Glacially disrupted terrain.** *In situ* bedrock is widely concealed by spreads of large, angular boulders that are mapped by SGU as occurring in 1–2 km wide patches and belts. Surrounding undisrupted terrain, and enclaves within boulder spreads, show typical features of ice-roughening or weak streamlining. Till cover is absent or present only in patches. It is not known whether extensively disrupted bedrock lies concealed beneath post-glacial sediment in topographic lows. It is this terrain that is the main subject of this report.

Large eskers, up to 1 km wide, > 100 km long and 10–30 m high, occur with 5–20 km spacing further west in Uppland and Gästrikland (Lundqvist 1999, Sund and Ericsson 2015, Dewald et al. 2022). SE of Forsmark, the smaller, c. 40 km long Börstil esker trends NNW-SSE (Sohlenius et al. 2004; see also Section 4.3.4; Figure 4-38).

Present day till distribution around Forsmark was mainly influenced by the morphology of the bedrock surface (Sohlenius et al. 2013). Elevated areas of bedrock today have generally thin (< 2 m) or no sediment cover; sediment occurrence is concentrated in topographic lows. At the local scale around the Forsmark site, the sub-till bedrock surface generally has up to 20 m relief and high roughness (Sohlenius et al. 2013, Hall et al. 2019a). Around Forsmark, when areas with bedrock outcrops are excluded, the average modelled sediment thickness (both glacial and post-glacial sediment) is 6.5 m, with a maximum of 42 m. The average regolith depth at Forsmark is 4.0 m but increases to 8.3 m offshore (Hedenström and Risberg 2008); an approximate thickness of more than 4 m of sediment has been redistributed during emergence from the Baltic Sea in the Holocene (Hall et al. 2019a).

In Uppland county, the highest marine limit is located at c. 180 m a.s.l. Any ground lower than this was submerged by the Baltic Ice Lake or Yoldia Sea for some time since the last deglaciation and later emerged, driven by isostatic uplift. Any such ground was thus exposed to a phase of coastal processes including wave action and ice floe erosion (Philip 1990), which may have modified some glacial features, particularly in poorly consolidated sediments (Sohlenius et al. 2004, Sund and Ericsson 2015). Wave-wash has thinned and reworked sediments (Sohlenius et al. 2019). It is thus possible that other sediment occurrences, including boulder spreads, have been modified by coastal erosion, even if presently located tens of km from the coast.

In Gävleborg county, terrain has greater relief, with hills of some 100 m a.s.l. near the coast but reaching 400–500 m a.s.l. near Ramsjö (Figure 2-4C). The terrain has a strong WNW-ESE grain, presumably because of long term glacial erosion, although ice flow appeared to have switched to a more SE to SSE direction during deglaciation (Strömberg 1989). Near Iggesund, boulder concentrations, mapped by SGU, occupy large swaths of ground (Figure 2-4D), and are interspersed with bedrock outcrops. In the lower ground, the main depositional landforms are ribbed and hummocky moraines (Hättestrand 1997) and eskers; deposits of till and glaciofluvial gravel are widespread.
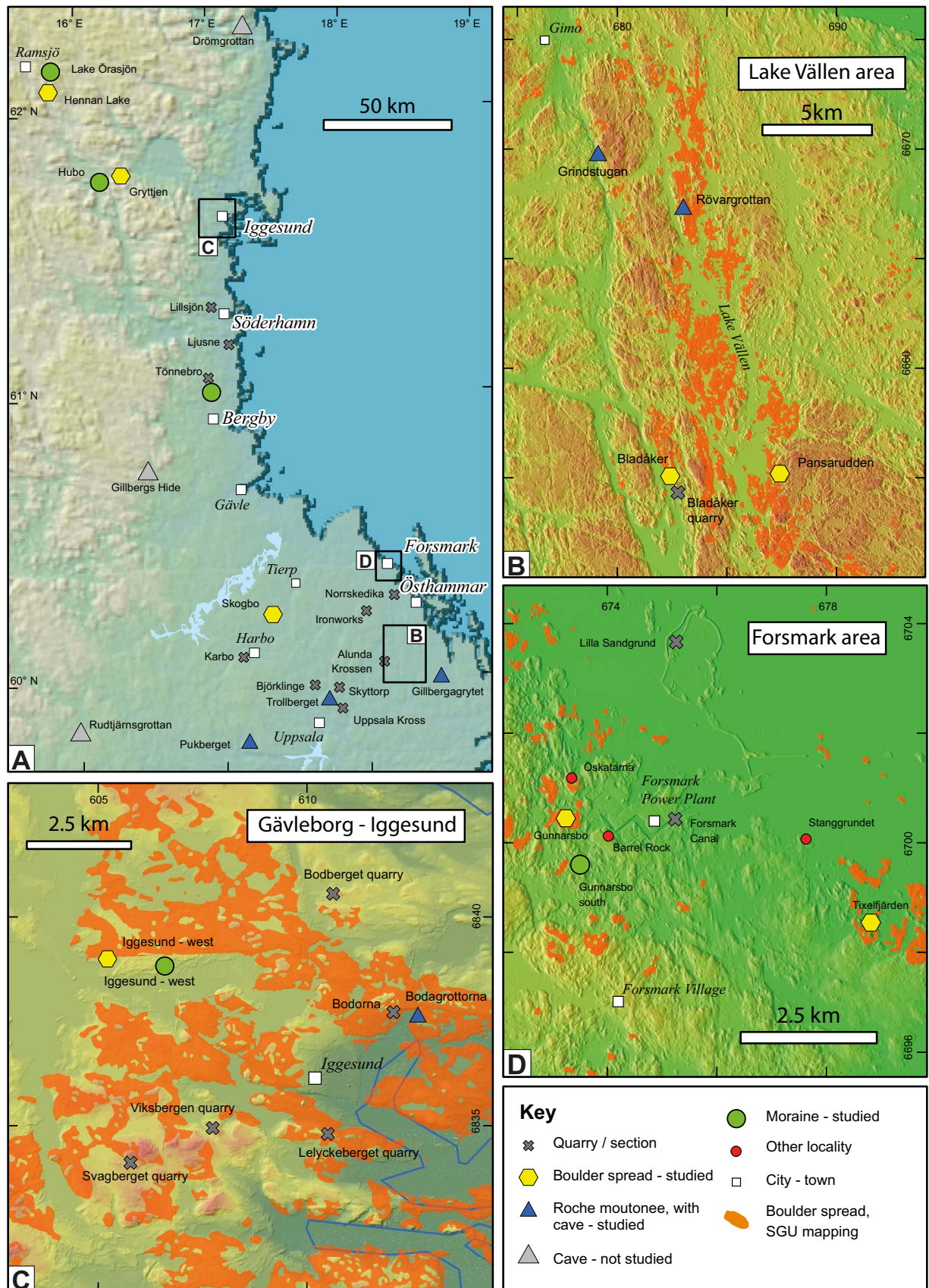
Figure 2-4. *Map with locations and study areas mentioned in this report, separated by feature type; and boulder spread distribution in more detailed areas. Some fracture caves reported by Sjöberg (1986, 1994) but which were not visited are also indicated. A. Locality map, eastern Sweden; Digital Terrain model (DTM) after Aster GTOPO30. B. Lake Vällen area. C. Gävleborg – Iggesund area. D. Forsmark area. For B, C, D: boulder spreads after SGU data; DTM from Lantmäteriet.*

2.3 Ice-sheet setting

Eastern Sweden, and indeed all of Fennoscandia, was repeatedly glaciated during the Pleistocene. The Late Weichselian ice sheet in Fennoscandia reached its maximum extent in its southern sector between 22–19 ka BP (Stroeven et al. 2016), with maximum ice thickness over Uppland county modelled at almost 3 000 m (SKB 2010). During deglaciation the ice margin retreated across SE Sweden after 15 ka BP (Stroeven et al. 2016, Avery et al. 2021) (Figure 2-1). A prolonged stillstand or re-advance occurred during the Younger Dryas stadial ($\sim$ 12.7–11.7 ka), with the ice margin situated south of Stockholm. Subsequent northward retreat after 11.7 ka, constrained by detailed varve chronology, was uninterrupted and rapid at 100s of m yr^{-1} (e.g. Strömberg 1994). Over Uppland county, the ice front retreated at c. 10.7 ka and with fast retreat rates estimated at 300–350 m yr^{-1} (Hedenström and Risberg 2003). High meltwater fluxes are inferred from extensive esker and channel systems beneath the melting ice sheet (Jansen et al. 2014, Greenwood et al. 2017, Shackleton et al. 2018).

Rapid basal ice sliding over what is now the bed of the Bothnian Sea is suggested by mapping of broadly southward-directed megascale glacial lineations (Greenwood et al. 2017). Together with widespread evidence of abrasion (see Section 2.2), this strongly suggests that in lowland eastern Sweden the base of the ice sheet was warm-based throughout much of the Late Weichselian, and especially during the last deglaciation. The same has been suggested from ice sheet modelling (SKB 2010). This is also corroborated by further ice sheet modelling which, in lowland eastern Sweden, predict substantial surface ice velocities (> 50–100 m yr^{-1}, rising to 200–400 m yr^{-1} in the Bothnian Sea; Patton et al. 2017) during deglaciation of the Fennoscandian Ice Sheet and considerable cumulative sliding distances (> 3 000 km) over the entire Weichselian (Näslund et al. 2003). Cold-based conditions, however, occurred further west and north nearer to the centre of the Fennoscandian Ice Sheet (e.g. Kleman and Hättestrand 1999, Stroeven et al. 2016), and it is possible that in Gävleborg county (Figure 2-1) basal conditions changed from cold-based during the last glacial maximum to warm-based during deglaciation. A short period of cold-based conditions was also suggested for Uppland and Forsmark during the initial part of the last (MIS2) phase of the Weichselian (SKB 2010).

Ice margin retreat during deglaciation was by calving in a lacustrine (Baltic Ice Lake) to marine-terminating (Yoldia Sea) setting (Lundqvist 1987, Andrén et al. 2011). Mapping of shorelines, combined with accurate varve chronology, suggests that the level of the Baltic Ice Lake during deglaciation of Uppland was some 150–190 m higher than present sea level (Hedenström and Risberg 2003). This implies significant water depth at the retreating, calving margin; at Forsmark an ice-thickness of c. 300 m at the grounding has been suggested (Hedenström and Risberg 2003). Buoyant ice margins may be unstable and retreat rapidly (Greenwood et al. 2015) and influence ice overburden and subglacial water pressures in grounding zones (Leguy et al. 2014). Above the highest shoreline, the ice margin had a terrestrial termination, and is relevant for the highest study locations herein, e.g. upper parts of Gävleborg county.

3 Methods, datasets and terminology

3.1 Datasets

This report relies on primary observations obtained during fieldwork and interpretations of remote sensing datasets such as air photos and Digital Elevation Models (DEM), augmented by previous work by various authors. Orthorectified air photos and DEM or their hill-shaded relief maps were downloaded from Lantmäteriet (the Swedish Mapping, Cadastral and Land Registration Authority). These downloads provide metre-accurate coordinates, allowing accurate georeferencing and use on a GIS platform. For the Gunnarsbo boulder spread near the Forsmark power plant, a very high resolution (c. 1 cm) orthorectified photo mosaic was captured with a helicopter drone, flying at c. 25 m altitude. For GIS manipulation and analysis, both Arc-GIS and Q-GIS were used, augmented with Python coding for specific operations. Geological mapping data, both bedrock and superficial mapping, comes from the digital mapping dataset from SGU (Geological Survey of Sweden).

3.2 Terminology

We define and describe a number of terms used in this report that are either relatively new in the literature, or have ambiguous or mulpiple meanings; these are clarified below.

The term *glacial ripping* is used herein to describe a process that involves damage to the internal rock mass that can lead to partial or complete disintegration of a rock hill or rock surface. It involves a multitude (100s to 1 000s) of rock blocks at a particular location in broadly a single event. Glacial ripping is thought to involve a three-stage process of hydraulic jacking, glaciotectonic disintegration and transport (Hall et al. 2020, Krabbendam et al. 2022a). Whilst some authors regard any subglacial process that removes a block from bedrock as plucking (e.g. Benn and Evans 2010), the vast majority of studies dealing with plucking describe a process of block removal involving a single (or a few at most) blocks, typically on the lee-side of a roche moutonnée. The difference between plucking and glacial ripping is thus partially one of scale, with glacial ripping involving several orders of magnitude more material in a single event; further differences are discussed in Section 7.4.

The terms *plucking* and *quarrying* are both used for the same subglacial erosion process of individual block removal. As this study uses many observations from man-made quarries, there is potential confusion, for instance in the phrase 'a quarried face'. For that reason, the terms *plucked* and *plucking* is used herein for the subglacial erosion, and *quarried* and *quarrying* for the industrial activity.

Rock fractures at Forsmark are described as *uncoated* and *coated.* Fractures apertures may be described on visual inspection as *closed/tight* (< 0.5 mm aperture), *open* (0.5–10 mm aperture), or *dilated* (> 10 mm aperture), where the aperture has been enlarged, for example, by water at overpressure). Fractures are described as sub-horizontal where dips are < 10°.

We use the term *hydraulic jacking* for the dilation of pre-existing fractures, without formation of new fractures. *Hydraulic fracturing* involves the formation of new fractures, or the propagation of existing fractures, in previous intact rock. The term '*block'* is used in this report for a fracture-bound block that is still in contact with adjacent blocks, and *in situ* or nearly so. Once a block is separated from its neighbours, it becomes a 'clast' (Lane 1947). Most clasts are *boulders* (e.g. 0.25–4 m across); larger clasts (> 4 m across) are termed *megaclasts,* following Terry and Goff (2014). Note these terms are used differently by SGU geologists who refer to clasts of > 200 mm diameter as 'blocks" and > 1 m as 'storblocks' (e.g. Persson 1985).

Dense *boulder concentrations* have been mapped by SGU geologists throughout Sweden (Figure 2-1). In high mountains, these include periglacial blockfields; in upland valleys, these include boulder-strewn ribbed and hummocky moraines. In the lowlands of eastern Sweden, the predominant mapped boulder concentrations are 'blockrik yta' ('boulder-rich surface') and 'storblockig yta' ('surface with large boulders'). Our field observations in lowland Sweden confirm the general accuracy of the mapping and indicate that most boulder concentrations comprise boulder spreads. *Boulder spreads* are deposits of large, angular boulders, with limited transport distances (< 10 m to a few kilometres), and which

are interpreted to represent a late stage of block release from bedrock, transport and deposition by glacier ice. Boulder spread is a morpho-stratigraphic term which refers to surface deposits of boulders at high densities and to boulder-rich near-surface till sheets.

Transitions can be recognised between undisturbed rock, and *breccia* formed after dilation of fractures but with little movement. A further transition can be recognised between virtually *in situ* brecciated rock masses and boulder spreads or *immature rubble till* with high clast angularity, low matrix fines content and short-distance glacial transport (Hall et al. 2021a). The latter equates with the 'Till Area III' of Hedenström and Sohlenius (2008) near Forsmark and is similar to the immature till of Croot and Sims (1996) except it may contain more and larger boulders. In eastern Sweden, much of the surficial till comprises poorly consolidated sandy till (e.g. Persson 1985, 1988), as in the 'Till Area I' of Hedenström and Sohlenius (2008). This contrasts with mature till: a matrix-supported diamicton, relative rich in fines (clay and silt) but relatively depleted in gravel, with a high degree of edge rounding of the cobble and boulder-sized clasts, and is commonly stiff ('over-consolidated'), in particular if rich in silt or clay. Near Forsmark, this is represented by the clayey till of 'Till Area II' of Hedenström and Sohlenius (2008).

3.3 Methods

3.3.1 Fracture characterisation

A wealth of fracture data is available for the immediate Forsmark area, but much of this data concerns the deeper (> 50 m) bedrock and is based on deep boreholes providing 1D data only (e.g. Follin et al. 2007, Curtis et al. 2011). Some 2D data is available on shallow subsurface fracture networks, close to Forsmark (Carlsson 1979, Hermanson et al. 2003. Leijon 2005. Forssberg et al. 2007) and are partially reviewed herein. To gain a wider characterisation of shallow fracture networks in Uppland and Gävleborg, and to compare shallow bedrock with and without sediment-filled fractures, several quarries were visited (Figure 2-4; Table 4-1), and general descriptive characterisations are given. We use epidote, chlorite or hematite (red staining) as indicators of pre-Quaternary fracturing (e.g. Sandström et al. 2009), as these minerals can be readily identified in the field.

For quantitative fracture density analysis, photographs with accurate scales were used. These were either photographs taken during fieldwork or historic (1970s) photographs from the cooling water canal, plant construction and test excavations at Forsmark (see also Carlsson 1979). Many of these photos have an accurate scale (ranging pole) and hence are suitable for analysis.

Photos were imported in a GIS and georeferenced against an artificial, but accurately scaled, grid. Fracture networks were digitised from these images, giving a quantified, 2D dataset of a vertical section of particular fracture sets (full details of the method in Palamakumbura et al. 2020). Once the fracture network is captured as lines in a GIS, various statistical operations can be applied to yield data on fracture density or spacing and fracture dip. Fracture density is reported as fracture length divided by surface area, in m^{-1}, or the number of fractures per unit length, also in m^{-1}; fracture spacing is then simply the reciprocal of fracture density, in m (following Singhal and Gupta 2010). Fracture density as used herein is equivalent to the P10 and P21 linear and areal fracture intensity (e.g. Niven and Deutsch 2010). Fracture dilation was identified visually from the photograph and attributed to the corresponding digital fracture trace.

From the digitised lines, polygons were constructed. These polygons represent blocks (in 2D) in the quarry or section wall, which can be analysed in terms of block size, further explained in Section 3.3.3.

3.3.2 Characterisation of disrupted roches moutonnées

Characterisation of disrupted roches moutonnées involved detailed fieldwork, aided by use of geo-referenced orthorectified air photos from Lantmäteriet. Outlines of blocks were digitised in a GIS. In the field, the same GIS dataset was used on a ruggedized Tablet PC to record additional data, such as thickness (z) of blocks, as well as the orientation of abraded surfaces, to constrain rotation of blocks. With the aid of the orthorectified air photos as well as measuring tape, cross-sections were constructed for some of the disrupted roches moutonnées.

3.3.3 Boulder spread characterisation

Boulder spread facies are described in cross-section from quarries and road cuts and in plan-view for field localities. To characterise the density of boulder spreads, we used orthorectified, georeferenced Lantmäteriet air photos from recently clear-felled areas (most boulder spreads occur in dense forest). To quantify boulder dispersion and boulder size, the air photos were rendered in greyscale in an image processing programme. Brightness, contrast and intensity were manipulated to produce a 2-bit black and white image, in which boulders appear white and the background black. The 2-bit image was imported into a GIS platform, georeferenced, and converted to polygons, with each polygon representing a boulder; resulting polygons that were not boulders (e.g. felled trees or tracks) were removed by hand. By comparing the polygons with the original colour image, the polygons were adjusted by adding a buffer of variable width, so that the polygons represent the true areal extent of the boulders as near as possible. This method did not achieve good results for the Gryttjen boulder spread (too many boulders and too little other ground) and the Gunnarsbo boulder spread (too much moss and vegetation growth on the boulders): for these boulder spreads, the boulders were digitised manually in GIS from the georeferenced colour image (see Section 4.3.4).

From the resulting polygons, the aerial extent ('surface area') and the relative position or aerial frequency can be obtained with standard GIS functionality. Boulder density is defined as the proportion of the aerial extent occupied by boulders (in %), so that if all boulders touch, boulder density is 100 %. This is different from the more qualitative definitions of boulder density applied by SGU to their mapping. Density variations are presented as cluster heat maps, based on the density of boulders per cell on a 10×10 m grid. The ArcGIS Spline tool was used to interpolate between density values of each cell to create a density heat map of across each boulder spread.

The high-resolution photomosaic of the Gunnarsbo boulder spread was used in the field (using a ruggedized tablet PC) to record additional attributes of individual boulders, such as height (z), lithology, and character of surfaces (e.g. abraded and striated or fracture surfaces). Height (z) was used, together with the surface area obtained from polygons from digitised boulders, to calculate the approximate volume of the boulders. In addition, the orientation of the striations and abraded surfaces, and the orientation (dip azimuth and dip) of the gneissic foliation *within* the boulders were measured with a geological compass. Orientation data of striae and the gneissic fabric was compared with a nearby *in situ* outcrop ('Barrel Rock') of the same rock type. The orientation measurements, which are related to clast rotation after dislodgement and transport, are presented as rose diagrams or stereograms, the latter using lower-hemisphere projections.

Slope roughness maps, as used in the Section 4.3, were derived from the Lantmäteriet DTM. Roughness parameter used is the standard deviation (SD) of elevation with a window size of 10×10 or 20×20 m was used. For more details, see Hall et al. (2019a).

3.3.4 Boulder/block size comparison

Boulder or block sizes are reported as 'nominal' B-axes. The true B-axis of a boulder is its intermediate axis, for which all three axes need to be known. We use a proxy approach, in which we define the nominal B-axis as:

$$B \; axis = \sqrt[3]{V} \quad (\text{in m})$$

if all three axes are known (V = volume), but this is only possible for those boulders in which the z axis was measured in the field. If only the aerial extent A of a boulder was available, the following definition is a reasonably proxy:

$$B \; axis = \sqrt{A} \quad (\text{in m})$$

Whilst not as accurate as B-axis based on volume, nominal B-axes based on areal extent A can be derived from air photos only and thus yielded a far larger dataset. As most blocks where all three axes are known proved to be approximately cuboid, this is a valid approach. We focus on boulders with B-axis > 0.8 m or areal extent > 0.65 m^2 as smaller boulders may have been moved by wave or ice-floe action as the area emerged from the Baltic Sea.

4 Results – field data

4.1 Fracture characterisation and analysis

Fracture characterisation and analysis was performed at the metre-scale in rock aggregate quarries, natural sections, and on historic photographs of excavations from the Forsmark power plant construction (Carlsson 1979). We present a general characterisation of the range of fracture patterns of the shallow basement rock and describe quarries and sections with tight, open, and dilated fractures (See Section 3). Our results augment previous studies on the construction excavations and later temporary excavations at Forsmark (Carlsson 1979, Leijon 2005, Forssberg et al. 2007), which is briefly reviewed where relevant.

4.1.1 General characterisation of fracture sets in the shallow subsurface

In the various quarries and sections studied across Uppsala and Gävleborg counties (Figure 2-4; Table 4-1), fracture networks are highly variable in pattern, fracture density and fracture aperture, and can change substantially over short distances. As an example, in the Uppsala Krossen quarry in granitic gneiss, three different sections display three distinct fracture patterns (Figure 4-1A-D). One section shows an orthogonal fracture pattern, with subvertical and subhorizontal fractures (Figure 4-1C). A second section shows subhorizontal fractures with pronounced curvature, connected by steeper fractures (Figure 4-1B). The curved subhorizontal fractures are akin to sheeting joints but do not follow the topographic surface (cf. Martel 2017); rather, they terminate against (abut) gently dipping fracture zones that separate the different sections (this may be regarded as 'pseudo-topography' delineating solid bedrock, which would have the same mechanical effect as true topography in the models of Martel (2017)). A third section is dominated by a 'criss-cross' pattern of gently-dipping fractures (Figure 4-1D). None of the fractures are discernibly dilated or jacked.

An approximate orthogonal fracture pattern, with one set of subhorizontal fractures and two sets of subvertical fractures, occurs in numerous quarries and sections. A good example is seen along the outlet canal on Lilla Sandgrund, near Forsmark (Figure 4-1E). In some quarries and sections, subhorizontal fractures increase in density close to the surface (also documented by Carlsson (1979) for fractures near Forsmark), and likely include sheeting joints (e.g. Martel 2007). More generally, in many quarries and road cuts increased fracture density is observed in the uppermost 1–2 m of the rock mass (see Section 4.1.4).

Other quarries are dominated by long (> 10 m) steep to subvertical fractures, with shorter (< 2 m) interconnecting shallow-dipping fractures, as seen at Alunda Krossen quarry (Figure 4-1F). In quarries where steeply dipping fractures are dominant, these fractures are commonly parallel to an older ductile fabric which comprises mica-rich foliation planes or other gneissic lithology boundaries (e.g. quarry near Karbo (Figure 4-1G). Such foliation-parallel fractures can be recognised by clear discontinuities as well as by various fracture coatings. Other quarries appear dominated by gently-dipping (dip 10–20°) fractures, connected by steeper fractures (e.g. Bladåker quarry). The very long subhorizontal fractures observed in the Forsmark Canal excavations (e.g. Carlsson 1979) are thus not typical.

The majority of fractures are coated with chlorite or are iron-stained, and many show epidote coatings, indicating these fractures developed at depth and are old, likely Precambrian, fractures, unrelated to Quaternary processes (see also Carlsson 1979, Sandström et al. 2008).

Fracture apertures vary in rock faces exposed at shallow depths in quarries and other excavations in locations without evidence of sediment-filled, dilated fractures. Some fractures are tight, even close to rockhead (including parts of Alunda Krossen, Karbo, Norrskedika, Uppsala Krossen quarries). Other fractures at these (Figure 4-1B and E) and other locations (Figure 4-2) are open, some with groundwater seepage, particularly in the in the upper 2 m of the rock mass. Opening of fractures in the near-surface has been linked to removal of crustal loading by the latest Weichselian ice sheet during glacial isostatic rebound (Selroos and Follin 2014).

4.1.2 Dilated fracture networks and sediment-fills

Fracture fills of silt, sand and diamicton indicate movement of sediment-laden, pressurised meltwater at the glacier bed and through open fractures. Where jacked subhorizontal fractures carry only rock fragments derived from bounding fracture surfaces, the meltwater that passed through the open fractures likely lacked sediment load. The combined widths of sediment-filled subhorizontal fractures indicate that the cumulative height of vertical jacking of the rock surface was typically 1–50 cm (Figure 4-2A, B, C), rarely exceeding 1 m (Carlsson 1979).
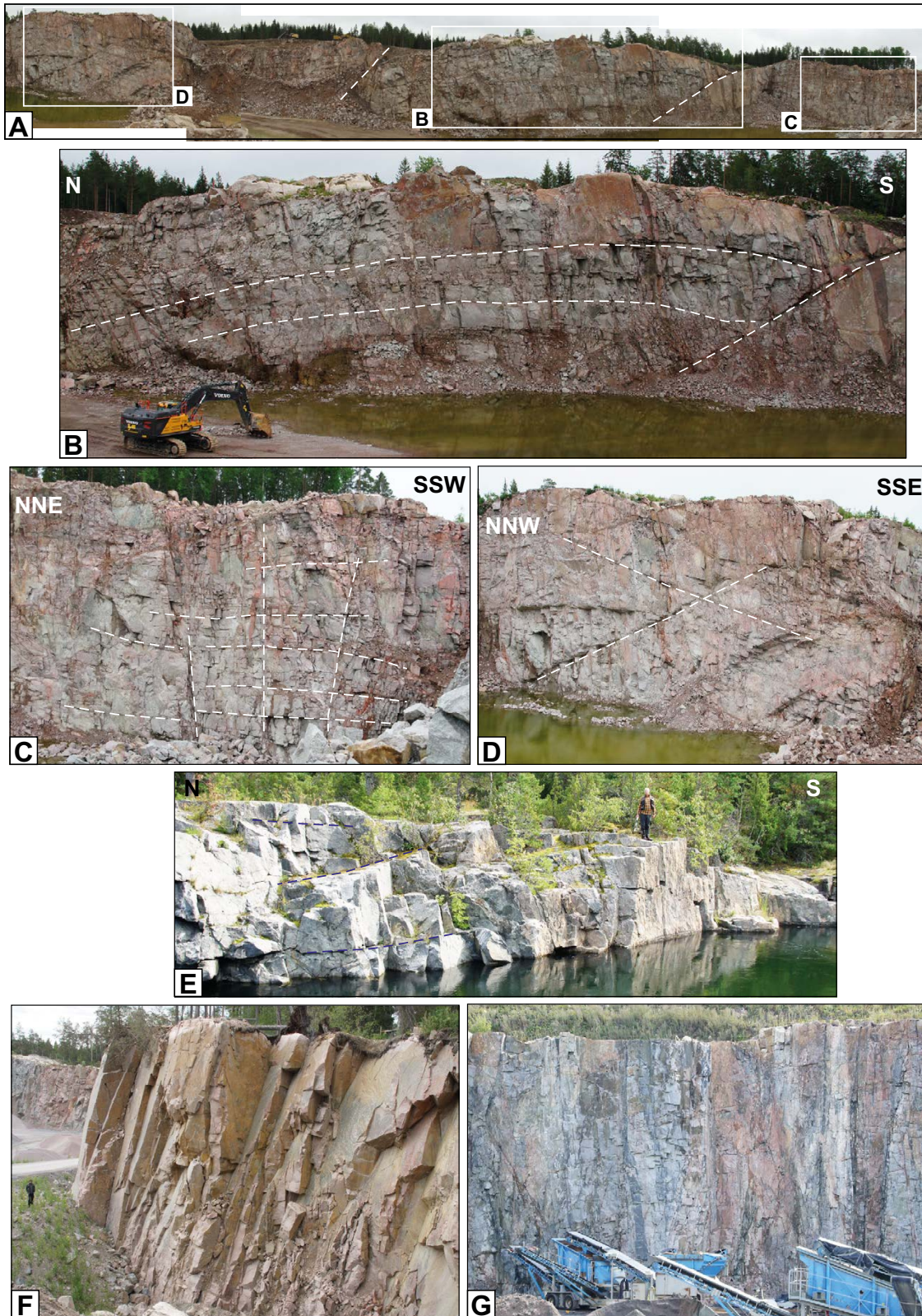
Figure 4-1. *Quarries and sections with different fracture patterns. A. Overview of Uppsala Krossen quarry. B. Section of Uppsala Krossen quarry with curved 'sheeting joints' – 'Sector B'. C. Section of Uppsala Krossen quarry with orthogonal (vertical and horizontal) fractures – 'Sector C'. D. Section of Uppsala Krossen quarry with gently dipping, cross-cutting fractures 'Sector D". E. Sections along cooling water outlet canal on Lilla Sandgrund, near Forsmark: orthogonal fracture pattern – possibly sheeting joints. F. Alunda Krossen quarry: subvertical fractures with chlorite and iron staining. G. Karbo quarry: sub-vertical fractures parallel to gneissic foliation. For grid references to locations: see Table 4-1.*
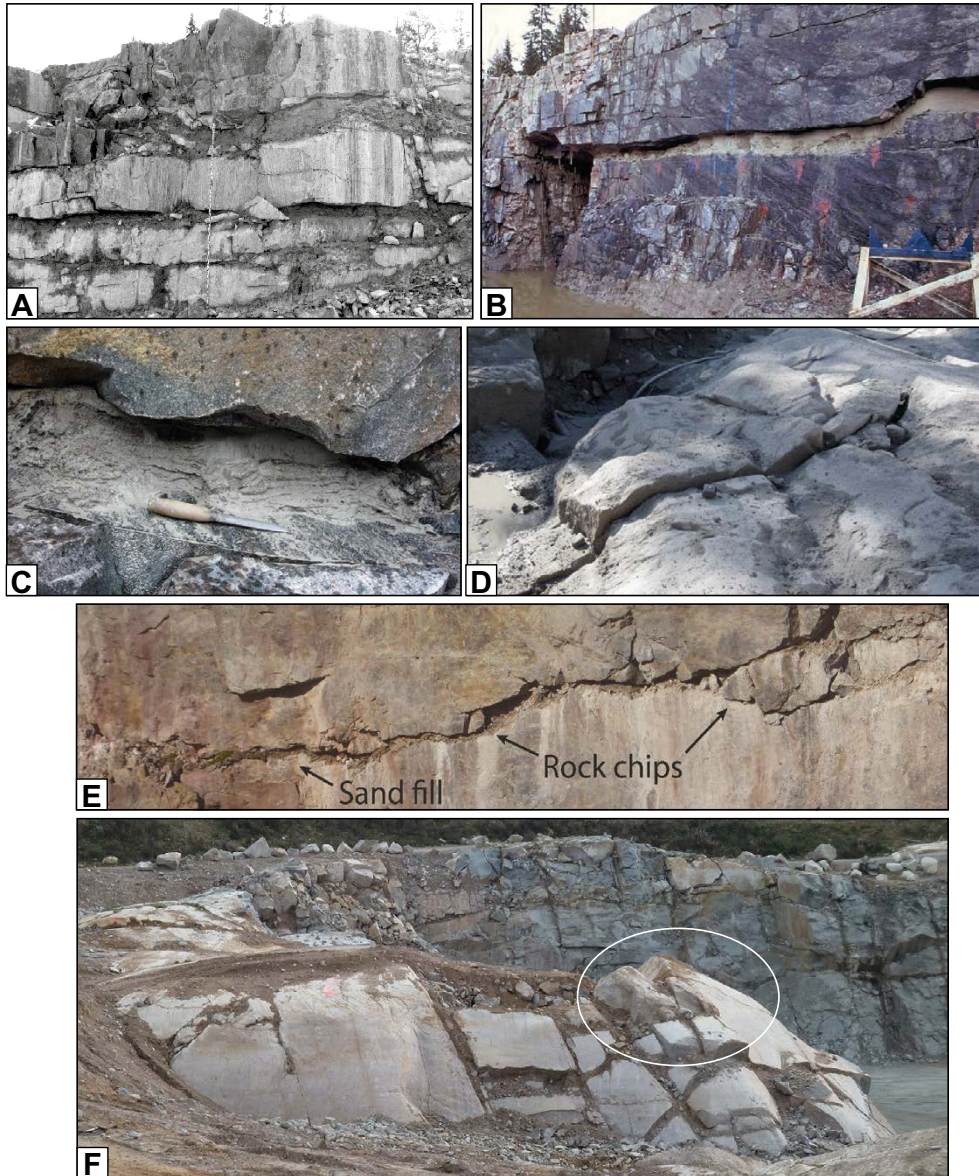
Figure 4-2. *Bedrock with dilated fractures and sediment fill. A. Dilated fractures with sediment-fill in excavation near Forsmark nuclear power station (Carlsson 1979; Fig. 39). The stick is 4 m long. Photo: Göran Hansson. B. Dilated fractures with sediment-fill in construction excavation near Forsmark nuclear power (Leijon 2005; Fig. 5-1). Fracture is c. 50 cm wide. Photo: Göran Hansson. C. Sand and silt fill in open sub-horizontal fracture, temporary excavation, near Forsmark (Forssberg et al. 2007; Fig. B3) Photo: Assen Simeonov. D: Uneven jacking, showing displacement of abraded surface, temporary excavation, Forsmark (Forssberg et al. 2007; Fig B5). E. Dilated fracture with fill of sand and rock chips, c. 2 m below rockhead. Runtorp Quarry, Påryd. F. East face of Runtorp Quarry. Small, disrupted roche moutonnée (white circle) with disrupted abraded surface and diamicton-filled dilated fractures. The main face in the background shows inclined, dilated, sediment-filled fractures below a 2–5 m thick disrupted rock layer. Quarry access courtesy of Nybogrus A.B.*

At site investigation area AFM001264 (Figure 4-2D), a rock block with an abraded surface was displaced upwards by 5–10 cm (Forssberg et al. 2007). At site area AFM001265, 100 m to the N, another rock block has been lifted up and dislocated by approximately 20 cm (Petersson et al. 2007). The resulting edges are still sharp, indicating a lack of glacial abrasion (but note that these bedrock surfaces were covered by till prior to excavation). Displacement was presumably by uneven jacking along fractures. A first-pass interpretation of these features suggests the following order of events: (1) a rock surface was abraded, forming multiple sets of striae (Forssberg et al. 2007); (2) the abraded rock surface was covered in till; (3) some time later, uneven hydraulic jacking lifted up some rock blocks, but not others; (4) any subsequent ice sliding was taken up by deforming till, so that the sharp edges were not rounded by ice sliding.

In addition to the Forsmark sections, as documented by Carlsson 1979) dilated fractures were observed in seven quarries: near Björklinge, Karbo, Lillsjön and Tönnebro (near Söderhamn), Ljusne and Svagberget (near Iggesund) – see Figure 2-4 for locations; and in the Runtorp quarry (in Påryd, south Sweden – see Figure 2-1 for location). Dilated fractures with sand and gravel fills have also been observed in new bedrock exposures after mining of sand and gravel along the Uppsala, Rimbo and Börstil eskers. Three localities with dilated fractures were noted in temporary excavations near the E4 motorway (Arnbom 2005, Lokrantz 2014). Open fractures occur in the top 1–8 m of rock sections.

At the **Runtorp** quarry, dilated fractures are gently southward dipping and show both sand and diamicton fill as well as rock chips (Figure 4-2E). The dilated fractures are not straight, but show distinct steps, suggesting water movement along connected open fractures. The top 4–5 m is much more densely fractured ('disrupted') than the rock below (Figure 4-2F). A whaleback, excavated beneath till, shows a freshly abraded surface, with distinct fracture dilation, with blocks that are uplifted (10s of cm) and with sharp edges (Hall et al. 2020), mirroring the observations from site investigation areas near Forsmark.

At the **Svagberget** quarry, SW of Iggesund, excavated in the lee-side of a large, 3 000 m long, 30–40 m high whaleback-like hill, one quarry face shows numerous dilated fractures with apertures ≥ 5–10 cm in the top 4–7 m of bedrock. Maximum width of individual dilated fractures is c. 20–30 cm. The upper rock mass is strongly disrupted, even brecciated, but is underlain by a relatively sharp base formed by a more or less continuous subhorizontal fracture with coherent bedrock beneath (Figure 4-3). Sediment was observed along the main subhorizontal fracture, although close examination was too risky, given the unstable nature of the quarry face. In another adjacent quarry face, no dilated fractures were seen, suggesting that dilation is localised.
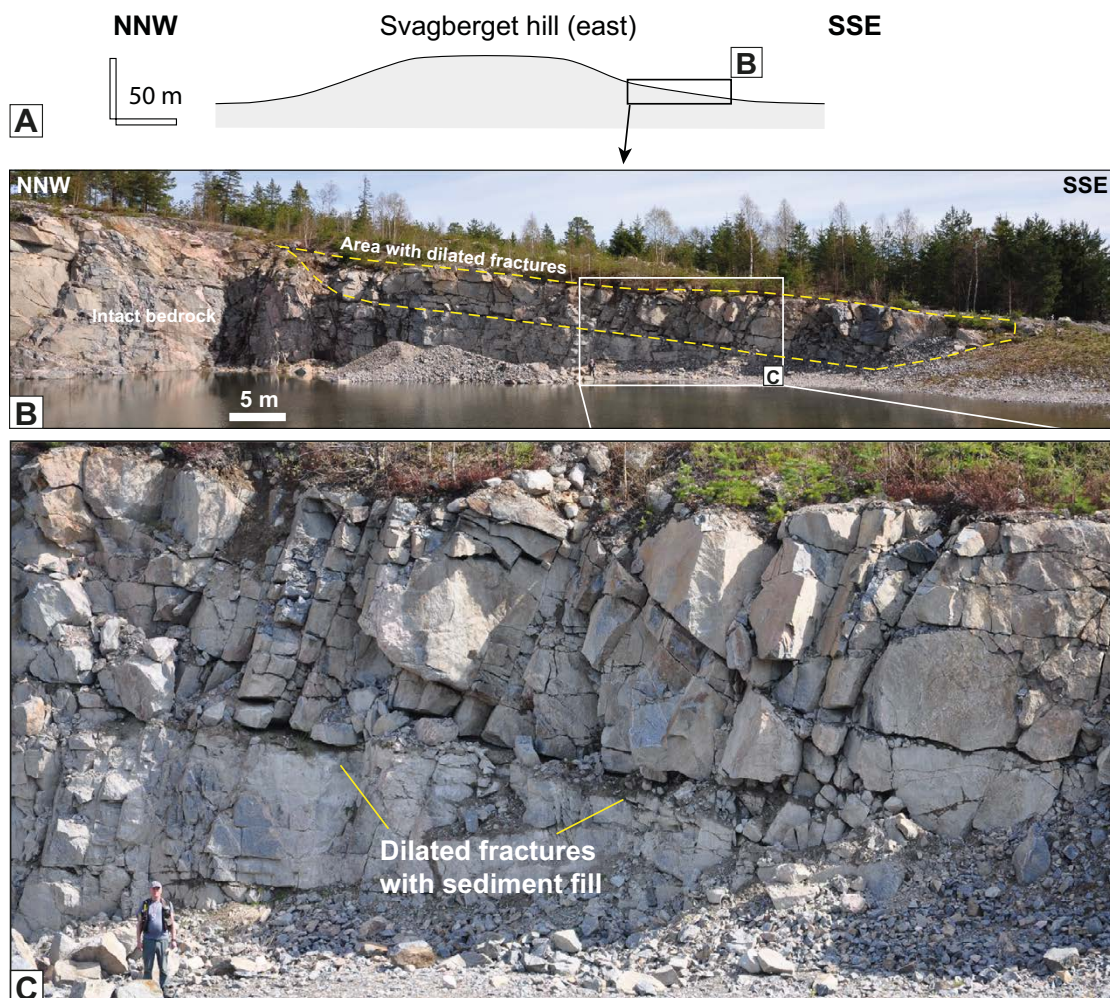
Figure 4-3. *Svagberget rock hill and quarry, SW of Iggesund. A. Cross-section along ice flow. B. Quarry view with both intact rock and region of dilated fractures, on lee-side of rock hill. C. Dilated fractures with sediment fill.*

At **Ljusne** an open fracture was coated (and hence old), but filled with sediment, indicating Pleistocene reactivation and dilation of a pre-existing fracture.

At **Lillsjön** a quarry in the side of a hill stands above ground with extensive ribbed moraine and boulder spreads. Dilated subhorizontal and vertical fractures are found to ~2 m depth beneath till cover in the NW corner of the quarry (Figure 4-4A). The hill surface remains otherwise undisrupted with extensive abraded surfaces.

At **Tönnebro** sub-horizontal fractures on the flank of a 20 m high hill are locally dilated to a depth of 2–6 m. The rock is brecciated along sub-horizontal fractures and fracture are filled by rock fragments and diamicton. Vertical fractures also have diamicton fills. The NE quarry face cuts one of a series of WSW-ENE oriented, boulder strewn ribbed moraines preserved on the lee side of the hill.

Figure 4-4. A. Lillsjön quarry. Gently dipping fractures, with locally dilated fractures in upper 2 m. B. Björklinge quarry with gently dipping and vertical fractures, dilated in the upper part, with fills of diamicton. C. Detail of dilated fractures in upper c. 3 m.

At **Björklinge** a quarry is set in low ground between the Uppsala and Vattholma eskers. Boulder spreads occur around several rock outcrops in the vicinity. In those parts of the quarry with prominent sub-horizontal fractures, dilated fractures occur with fills of diamicton to a depth of 3 m below the rock surface (Figure 4-4B, C). The overlying diamicton is weakly horizontally bedded, with occasional sand lenses and incorporates and is overlain by large angular blocks mainly derived from the local bedrock.

At the **Karbo** quarry, the majority of fractures are tight or open, but one section shows an upper brecciated bedrock mass, c. 2 m thick, underlain by long dilated fracture filled with diamicton. This is further described below in Section 4.4.2.

About one third of the visited quarries possess dilated fractures close to rockhead (top of bedrock), with or without sediment fill, whilst the remaining two thirds of quarries have tight or open fractures (Table 4-1). We note that this sample is non-systematic (systematic analysis of fracture distribution in basement terrain with extensive forest and soil cover is challenging). We further note that it is possible that rock aggregate quarries have a bias for (i) being located in hill flanks in areas of lower than average fracture density and (ii) so being sited in high points whereas the water involved in fracture dilation was likely ponded in low points. However, long, dilated sub-horizontal fractures with thick sediment fills (as shown in Figure 4-5 at Forsmark) are comparatively rare.

4.1.3 Additional observations on fracture fill and fracture networks from historic photos

Observations from the historic photos from Forsmark, in addition to those previously reported (Carlsson 1979, Leijon 2005, Forssberg et al. 2007), include the following. In one section (Figure 4-5A), crackle and mosaic brecciation (terminology following Morrow 1982) occurs 1 m below the top-rock surface in a zone of closely spaced subhorizontal fractures. In this c. 50 cm thick zone, the rock mass has clearly been dilated and disrupted to such a degree that blocks have lost coherence, leaving a loose mass of 10–50 cm blocks, with the creation of substantial void space in between. The rock below appears not to be affected by jacking or dilation. The rock above still shows coherence but has more vertical fractures than the rather massive rock below the zone. In another section (Figure 4-5B), similar forms of brecciation affect the entire top 3–4 m of bedrock.

In a later test excavation (AFM 001264; Forssberg et al. 2007), old vertical fractures, coated with iron oxide are clearly seen ((1) on Figure 4-5C). An uncoated, possibly new fracture (2) is visible on the right, although this could be machine damage during excavation. Other uncoated fractures were interpreted as formed subglacially (Forssberg et al. 2007). Brecciation into angular rock fragments occurs at two levels. At the upper level (3), brecciation is focused where subvertical and subhorizontal fractures interact, with new formation of short fractures. At the lower level (4), the subhorizontal fracture shows in detail (Figure 4-5D) a sediment fill of silt and sand up to 15 cm thick. The sediment is laminated, but the laminations are disturbed and folded (5). The roof of the fracture is uneven, and the soft-sediment deformation was likely caused by uneven vertical compression during fracture closure, following a water-pressure drop. On the right (6), small (1–2 cm) rock fragments are mixed with sediment.

In another test excavation ('Drill Site 5'; Leijon 2005), till cover was cleared from a 20 by 30 m area and the bedrock surface was cleaned to reveal an abraded rock surface with many dilated (1–3 cm) fractures (Figure 4-6). Most dilated fractures belong to the same sets as older fractures, and were regarded by Leijon (2005) as being reactivations of older fractures. However, many short (< 0.5 m) fractures with steep dip but random strikes have no host rock staining or mineral coating and were interpreted as 'new', subglacially formed fractures.

Table 4-1. Fracture characteristics of visited quarries and sections. Some names are informal (*) or refer to the nearest settlement or feature. Grid reference system: Sweref 99.

Name/location	Fracture pattern	Fracture aperture	North	East	Loc
Bodberget quarry, N of Iggesund	Steep, inclined and horizontal fractures	Numerous dilated fractures on lee side of hill	6840553	610619	MK 16
Viksbergen; quarry, SW of Iggesund	Multiple fracture sets of steep, inclined and horizontal fractures	Tight and open; no dilated fractures seen	6834938	607738	MK20
Svagberget Quarry. SW of Iggesund	Orthogonal, dense, long subhorizontal fracture	Numerous dilated fractures; likely sediment-filled; brecciation in top 6 m	6834108	605776	MK22
Kråpelas ("Ironworks") NW of Gimo	Steep fractures dominate (parallel to gneiss foliation), with short connecting fractures	Tight and open; no dilated fractures seen	6681795	666728	MK 88
Bladåker; quarry	Gently and steeply dipping and vertical fractures	Tight; open in the S face; no dilated fractures seen	6654741	682750	MK93
Alunda Krossen	Steep fractures dominate, with short connecting fractures	Tight; no dilated fractures seen	6662145	673853	MK102
Uppsala Krossen, Sector B	Near orthogonal, with curved SHF	Tight; SHF open in the upper 10 m; no dilated fractures seen	6645251	656082	MK121
Uppsala Krossen, Sector C	Orthogonal, dense, long subhorizontal fracture	Tight; open fractures to 3 m depth; no dilated fractures seen	"	"	MK121
Uppsala Krossen Sector D	Diamond pattern of inclined fractures	Tight and open; no dilated fractures seen	"	"	MK121
Norrskedika Quarry	Steep fractures dominate, with short connecting fractures	Tight; no dilated fractures seen	6688550	678830	AMH
'Ballast Quarry*, Skyttorp	Multiple fracture sets of steep fractures (parallel to gneiss foliation, inclined and horizontal fractures	Tight; no dilated fractures seen	6662229	654931	AMH
Tönnebro	Dominant subhorizontal/ gently inclined fractures; shorter vertical fractures	Tight and open in most places; dilated fractures with sediment fill locally.	6770770	604990	MK140
Ljusne	Subhorizontal and gently inclined fractures; shorter vertical fractures	A few open fractures; some brecciation in upper 3 m	6785493	611099	MK143
Karbo quarry	Steep fractures dominate (parallel to gneiss foliation), with short connecting fractures	Mostly tight; open fractures and brecciation in one small sector	6663691	618842	MK237
Lilla Sandgrund, Outfall Canal section	Subhorizontal and gently inclined fractures; shorter vertical fractures	Tight and open SHFs; no dilated fractures seen	6703466	675121	MK332
Lillsjön, Söderhamn	Subhorizontal, inclined and vertical fractures	Dilated subhorizontal and vertical fractures to ~2 m bgl in NW corner	6800379	606391	AMH
Björklinge	Diamond pattern of long inclined fractures with vertical fractures	Locally, dilated sub-horizontal and inclined fractures, with fills of diamicton	6652925	608530	AMH
Forsmark Excavations	Subhorizontal and gently inclined fractures; shorter vertical fractures	Numerous dilated fractures; commonly sediment-filled; brecciation in top 1–5 m	(Carlsson 1979)		
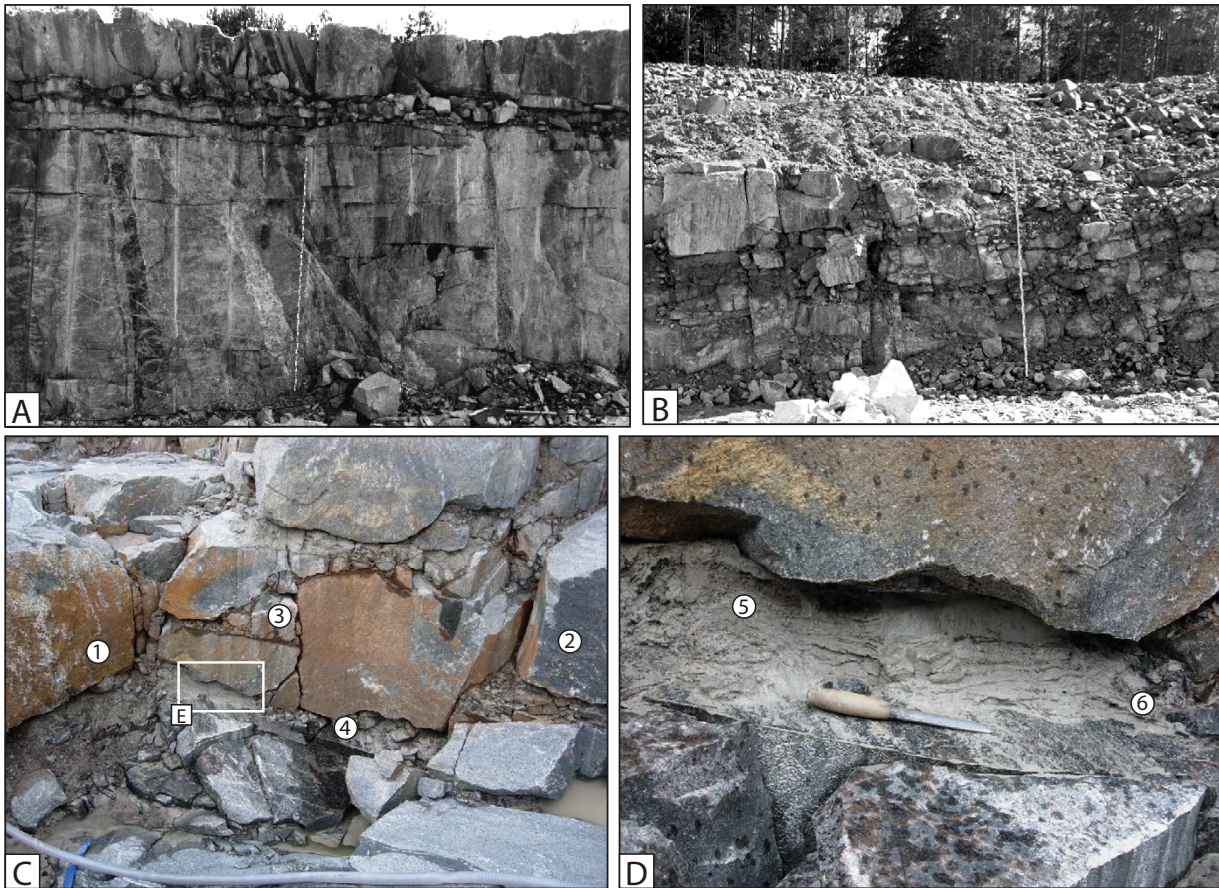
Figure 4-5. *Observations on fracture fill and brecciation. A. Layer of brecciated rock, with closely-spaced vertical fractures along a closely-spaced set of subhorizontal fractures, c. 1.5 m below rock surface. Forsmark excavations. B. Extensive brecciation in upper 4 m of bedrock. For A, B: The stick is 4 m long. (Carlsson 1979; Fig. 39; Photo: Göran Hansson). C. (1) Old, iron-coated fracture; (2) New, uncoated fracture – possibly related to excavation; (3) and (4) brecciation with rock fragments. Test excavation at AFM 001264; Forssberg et al. (2007); Photo: Assen Simeonov. D. Detail of sediment-filled subhorizontal fracture in C., note laminations in sediment; (5) folded lamination; (6) rock fragments mixed with sediment. Test excavation at AFM 001264; Forssberg et al. (2007); Photo: Assen Simeonov.*

The following features can be seen (Figure 4-6A): 1. Uplifted block. 2. Abraded precursor surface. 3. Cover of sandy and mostly matrix-supported diamicton with abundant subrounded bedrock clasts. 4. 'New' vertical fracture. 5. Brecciation of the rock surface by development of new, short fractures along an existing fracture. 6. Uplifted and slightly rotated block above a dilated and filled subhorizontal fracture (Figure 4-4C). 7. Existing fracture with brecciation from development of new branching fractures along its length. 8. Unabraded face. A partly sediment-filled, branching, sub-horizontal fracture (Figure 4-6B) shows angular rock fragments (1–20 cm long) that appear to be broken off from the roof of the fracture. The rock fragments are partly mixed with fine sediment. On the right (yellow arrows), the rock fragments appear little displaced or rotated, whilst to the left (blue arrow) some rock fragments are substantially rotated and displaced.

4.1.4   Fracture density analysis

Fracture analysis from the historic Forsmark cooling water intake canal photos show a general increase in fracture density towards rock head (Figure 4-7), as reported by Carlsson (1979). In our study, we calculated fracture density separately for subvertical and subhorizontal fractures.

In two sections (SKB-003 and SKB-006; Figure 4-7A, B), the subvertical and subhorizontal fracture densities increase in tandem, from < 1–2 m^{-1} at the base of the section to 2–4 m^{-1} at the top of the sections, with the highest fracture density caused by a concentration of subhorizontal fractures, with numerous subvertical fractures, 1–3 m below rockhead. These two sections also show the most pronounced dilation along subhorizontal fractures (blue arrows). A quarry section MK-22 from the Svagberget quarry, SW of Iggesund (Figure 4-7H) shows similar high densities for subvertical and subhorizontal fractures. The top 4–7 metres of the section is clearly dilated and the rock mass disrupted. Sediment was observed (from a distance – unstable quarry face) in the subhorizontal fracture that underlies this disrupted rock mass.

In contrast, sections SKB-037, SKB-064, SKB-031, SKB-036 and SKB-057 (Figure 4-7C–G) show clear upward increases in subhorizontal fracture density, but only modest increases in the density of subvertical fractures (SKB-037, SKB-064, SKB-031) or no increase in subvertical fracture density at all (SKB-036 and SKB-057). Fracture dilation is absent in section SKB-036, and minor in section SKB-057, SKB-037, SKB-064 and SKB-031.

A nominal or proxy length:height ratio of resultant blocks or slabs (Figure 4-8) was calculated by dividing horizontal and vertical fracture spacing (the reciprocal of the horizontal and vertical fracture density). This shows that: (i) for section MK22 and SKB-006 the length:height ratio remains below 5 for their entire thickness, (ii) some sections show a marked decrease in length:height towards the top (e.g. SKB 003), with (iii) sections SKB-036 and SKB-057 – which show no dilation at all along subhorizontal fractures – showing very large length:height ratios.
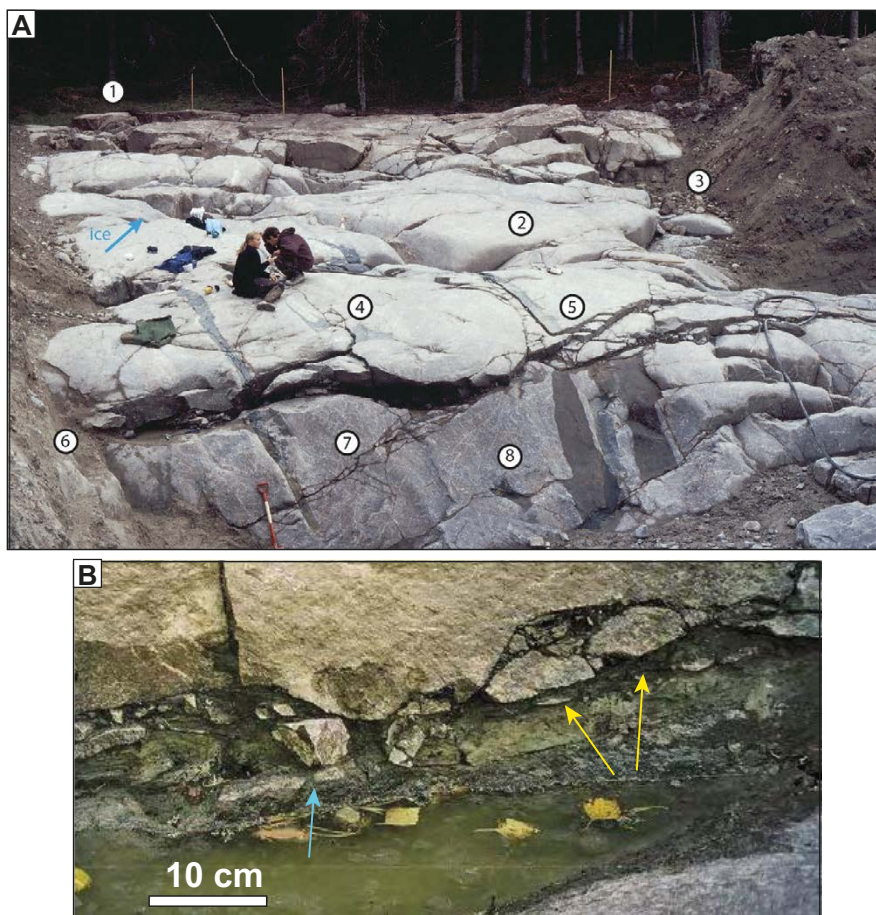
Figure 4-6. Observations on fracture fill and brecciation: excavation at Drill Site 5. A. Overview of excavation: numbers explained in text. B. Rock fragments detached from roof of dilated subhorizontal fracture. Test excavation at Drill Site 5, Leijon (2005); Photo: Assen Simeonov, reproduced from Lagerbäck et al. (2005).
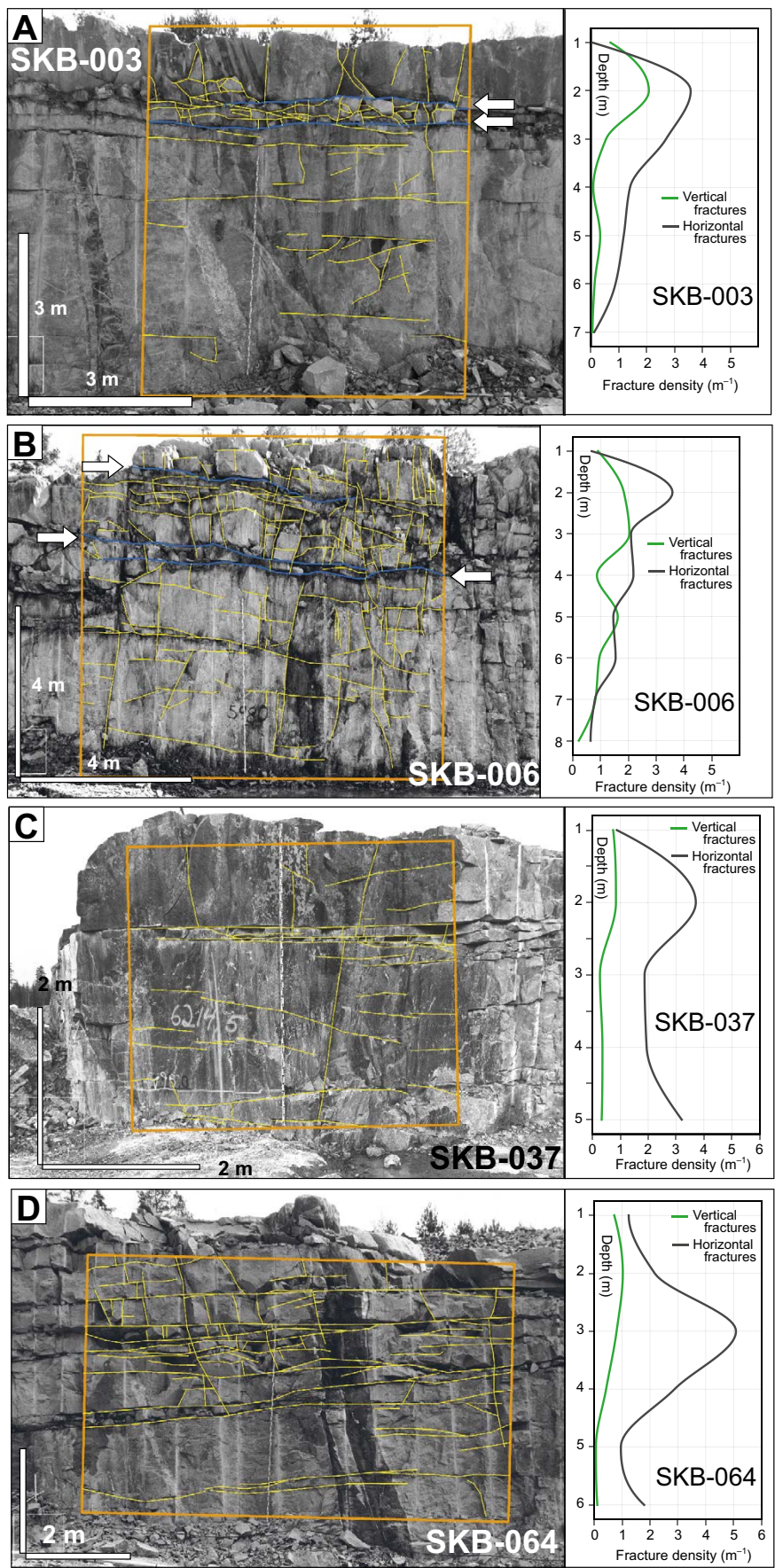
Figure 4-7. *Digitised fracture patterns in the canal excavations at Forsmark (left hand panels). Blue fractures (with white arrows) are dilated. Fracture density for subvertical and subhorizontal fractures, against depth (right hand panels). A–G from Forsmark construction excavations – Photos: Göran Hansson; H: Svagberget quarry, SW of Iggesund.*
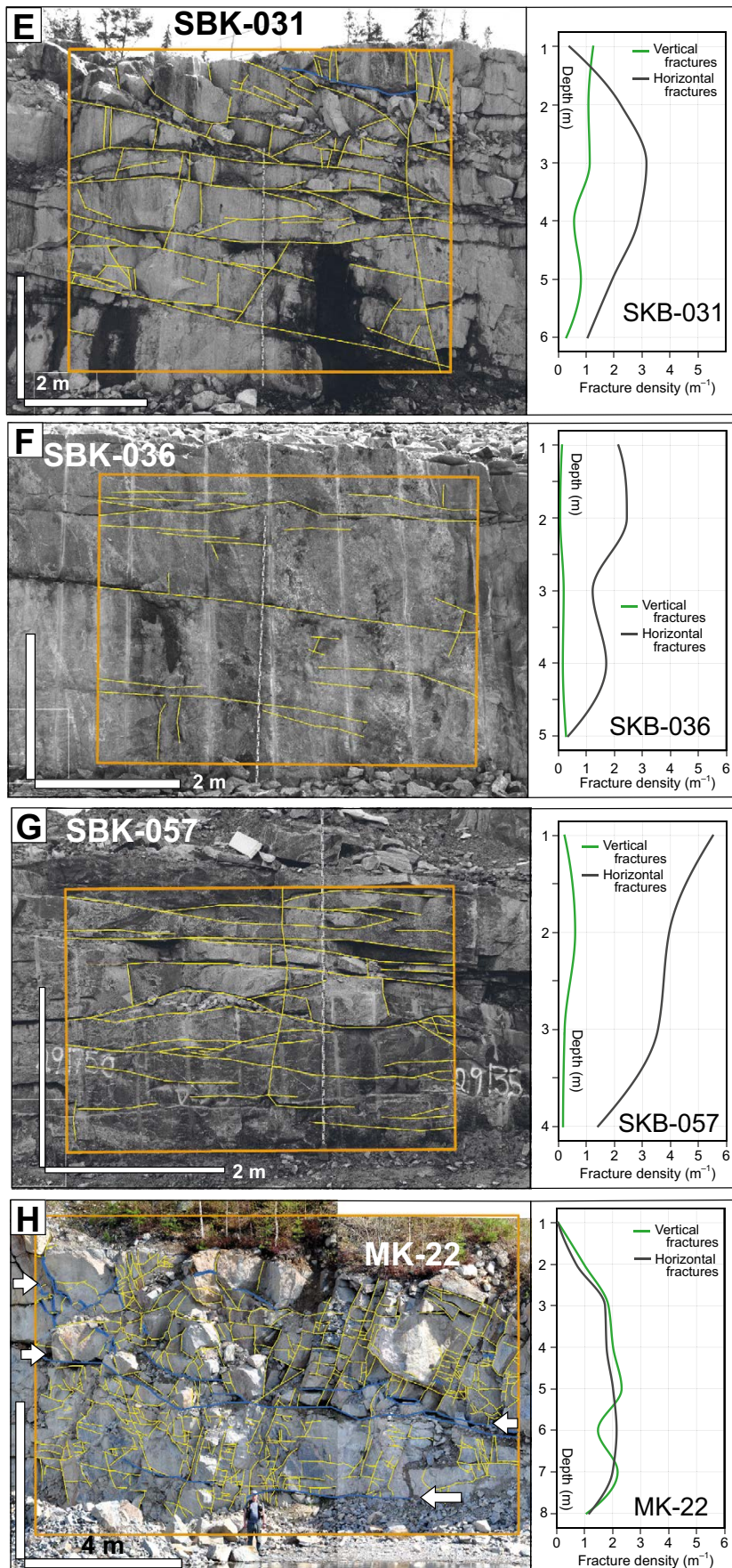
Figure 4-7 continued. Digitised fracture patterns in the canal excavations at Forsmark (left hand panels). Blue fractures (with white arrows) are dilated. Fracture density for subvertical and subhorizontal fractures, against depth (right hand panels). A–G from Forsmark construction excavations – Photos: Göran Hansson; H: Svagberget quarry, SW of Iggesund.
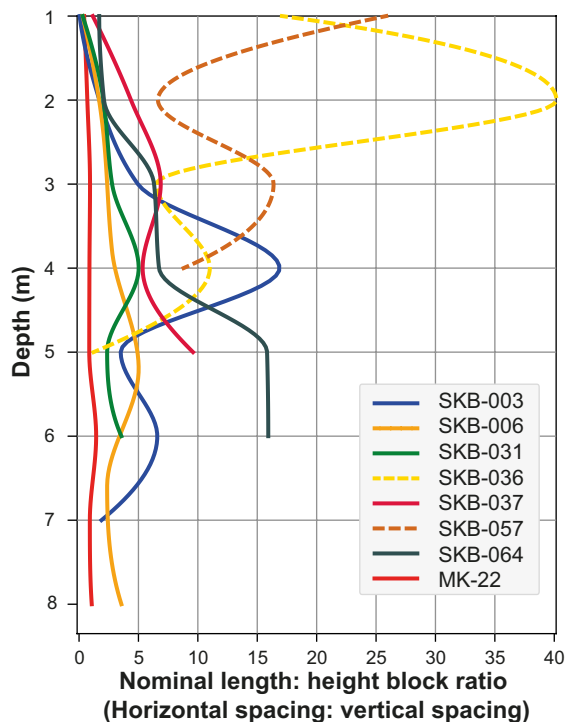
Figure 4-8. *Nominal block length:height ratio, calculated from horizontal fracture spacing: vertical fracture spacing.*

Altogether, it appears that an increase in subvertical fracture density in the top few metres of the rock mass is present above dilated subhorizontal fractures (SKB-003 and SKB-006), but is absent if subhorizontal fractures are not dilated. This suggests that at least some vertical fractures were opened as a result of dilation of the underlying subhorizontal fractures and that new vertical fractures were generated during subglacial hydraulic jacking, representing a form of mechanical weathering. This is further discussed in Section 5.1.

4.1.5   Evidence of formation of new fractures by hydraulic fracturing

Dilation predominantly involved the opening of existing fractures, as evidenced by their mineral coatings (see also Carlsson 1979). However, in a number of places there is evidence of the formation of new, uncoated fractures by subglacial dilation. The brecciation of rock surfaces, such as at Drill Site 5, involved formation of many new fractures with uncoated surfaces during or after formation of the youngest striae (Leijon 2005). At Drill Site 5, branching micro-fractures formed along the roof of a subhorizontal fracture (Figure 4-6B). Detachment of rock chips occurred during dilation and sediment infill of the main fracture rather than at its closure, allowing rock chips to remain intact. Where rock chips are present, lateral displacement is often restricted to mm or cm distances (Figure 4-6), indicating no sustained water flow along the open fracture, suggesting dilation was brief, consistent with fast hydrofracture crack-tip propagating velocities (e.g. Tsai and Rice 2012). Characteristic features of these new fractures are (i) undulating or curved fracture faces, (ii) rough fracture surfaces, (iii) branching micro-fractures along the edges of old fractures and (iv) cracking at fracture intersections (Figures 4-2E; 4-7C). These characteristics are consistent with experimentally-induced hydro-fractures in granite blocks (Cheng and Zhang 2020), numerical modelling (Krzaczek et al. 2020) and of hydro-fractures induced by wave water impacts in ignimbrite sea cliffs (Hall et al. 2008).

New, subvertical fractures at Drill Site 5 and at excavation AFM001264 (Figure 4-5C) are part of the general brecciation of the near-surface rock. Brecciation of closely-fractured rock units in the Cooling Water Canal excavations (Figure 4-5A and B) involved pervasive dilation to depths of 1–13 m of subhorizontal and subvertical fractures. Hydrofractures also appear to have formed at Runtorp where large *in situ* rock blocks are split by dilated, new fractures.

4.1.6 Key features of near-surface fractures relevant for hydraulic jacking

Important characteristic of near-surface fractures in east-central Sweden, relevant for hydraulic jacking and glacial ripping include:

1. Fracture patterns in the Precambrian gneisses are highly variable in fracture connectivity, spacing, length, orientation and aperture, with pronounced spatial heterogeneity.

2. Fracture density generally increases in the upper 5–15 m of the rock mass. Commonly fracture density is highest in the uppermost 1–2 m of the rock mass (Figure 4.7).

3. Open (aperture 0.5–10 mm) subhorizontal fractures are common in the upper 2–5 m of rock masses. At greater depths, open fractures are widely spaced and are mainly sub-horizontal or gently dipping.

4. Dilated fractures (aperture > 10 mm) occur locally in the upper 1–5 m of the rock at Forsmark and in other excavations. The Forsmark power plant and canal excavations revealed sediment-filled, dilated fractures at depths of up to 13 m.

5. Where vertical fractures dominate, subhorizontal fractures are absent, or intermittent in the near surface and hydraulic conductivity is low compared to 3.

6. The majority of fractures are coated and hence pre-existing: any dilation represents a re-activation of older fractures. However, locally, 'new' uncoated fractures occur, formed as a result of hydraulic jacking (see also Section 6.2).

7. About one third of the visited quarries possess dilated fractures close to rockhead, with or without sediment fill, whilst the remaining two thirds of quarries have only tight or open fractures. Hydraulic jacking in rock hills is considered further in Section 4.2.

4.2 Disintegrated roches moutonnées and fracture caves

Large roches moutonnées occur where fracture density is low, and have commonly steep and blunt stoss faces. Rock block sizes are large; larger than for most other rocks in eastern Sweden. In ice-roughened and weakly streamlined terrain, large roches moutonnées remain intact, indicating that these rock kernels have resisted glacial erosion. Locally, some such large roches moutonnées are found partially disintegrated, with fracture caves and lee-side boulder trains. Previously, such disintegrated roches moutonnées have been interpreted as caused by major earthquakes related to isostatic rebound (e.g. Sjöberg 1986, Mörner et al. 2000, Mörner and Sjöberg 2018), an interpretation that is invalidated if the fracture caves are of subglacial origin. A glacial origin was suggested by Lundqvist (1987) and Lagerbäck et al. (2005) but no detailed model was proposed in these studies. We describe in some detail three disintegrated roches moutonnées with fracture caves (Rövargrottan; Gillberga gryt, and Bodagrottorna) and then add short descriptions of other disintegrated roches moutonnées (Trollberget; Grindstugan, and Pukberget; Figure 2-4 for locations). A further example from Trollegater, near Rimforsa, has been described elsewhere (Hall and Krabbendam 2022). Disintegration also affects numerous smaller roche moutonnées and low-relief rock surfaces throughout the region, commonly associated with boulder spreads. We present an analysis of the area surrounding Forsmark to illustrate different damage patterns to such low-relief rock surfaces.

4.2.1 Rövargrottan – description and analysis

Rövargrottan (also named *Tjuvgrottan*) is a c. 50 m long bedrock hill along the east shore of Lake Vällen (Figure 2-2B; 4-9A), set in massive, poorly foliated granitic rock. Extensive boulder spreads occur to the east; to the north is another smaller disintegrated roche moutonnée, suggesting wide-spread disruption. It is not known if boulder spreads occur extensively on the bed of Lake Vällen, although many boulders occur in shallow water near the road bridge at the southern end of the Lake. The long axis of the feature is parallel to the approximately north-to-south former ice-flow direction. Vertical fracture sets occur as a N-S and an E-W set. The largest block (*C*) measures L=16 m; H > 3 m; W = 5 m, with a volume of > 260 m^3 (Figure 4-9B, C). Two vertical metre-wide gaps occur: between blocks *A–B* and between blocks *B–C*. The fracture surfaces bounding gap *A–B* can be matched so

block *B* was displaced c. 1 m with respect to block *A,* and the smaller blocks at the top of the gap have partially fallen in (Figure 4-9D). The top of block *B* is c. 1 m higher than up-ice block *A* and this formed a pronounced stoss face. The fracture surfaces that bound gap *B–C* cannot be matched, and smaller blocks in between larger blocks were more or less *in situ*; nevertheless, blocks *B* and *C* must have moved apart by c. 0.5 m for the smaller blocks to collapse downward. These smaller blocks partially form a roof to the start of the fracture cave.

A triangular fracture cave occurs on the east side of block *C*, with its roof formed by block *E* (Figure 4-9E). The west-facing surfaces of blocks *B* and *C* are in part fracture surfaces: blocks previously present west of blocks *B* and *C* (i.e. on the side facing Lake Vällen) must have been removed, likely by some form of lateral plucking. Block *D* shows an abraded surface, with striae: this is now oriented subvertically, so that block *D* must have been rotated by c. 90°. Overall, the degree of disintegration increases to the south, with larger spacing between blocks.
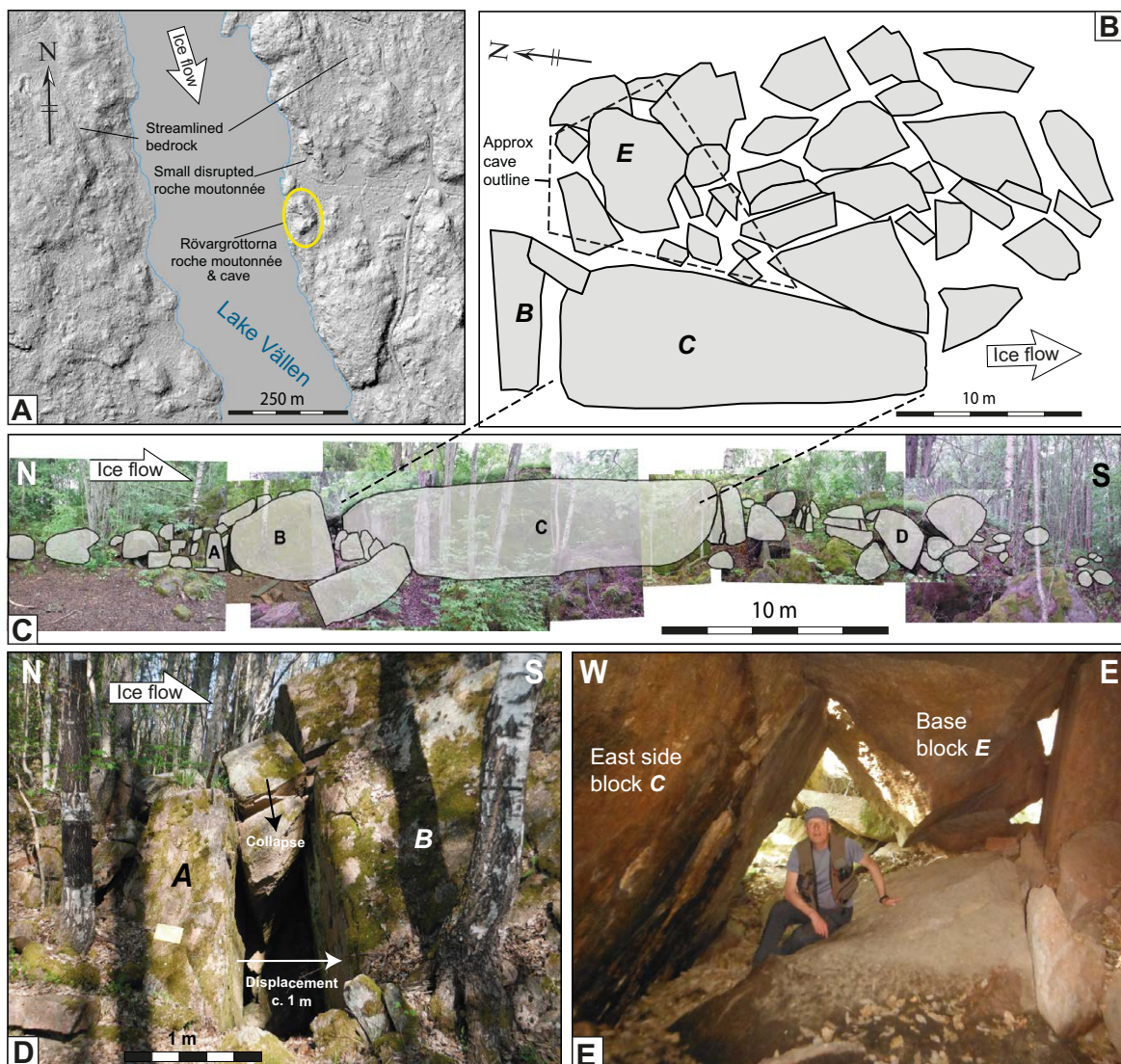
Figure 4-9. *Rövargrottan: disrupted roche moutonnée with fracture cave, east of Lake Vällen. A. Setting of Rövargrottan, shown on a hillshade DTM (from Lantmäteriet). Regional ice flow is indicated. B. Sketch map – map view of disrupted roche moutonnée. Approximate outline of cave indicated. C. N-S section; outlines constructed from stitched panorama. D. Detail of gap between block A and block B. E. Cave to east of block C, view to the north.*

Interpretation of Rövargrottan

Displacements indicates overall N-S extension. The overall disintegration shows a N-S asymmetry, consistent with differential displacement by south-directed ice flow. Some displaced blocks (in particular block *B*) have steep stoss-side faces, allowing for a component of ice-push. Overall, it appears that the blocks show separation in a N-S direction, with ≥ 1 m displacement between blocks, consistent with south-directed ice flow. Thus, even the very large block *C* ($V = 260$ m^3) has moved southward with respect to smaller (and lower) block *B*. The arrangement of the smaller blocks east of block *C* (Figure 4-9B) suggests that they were translated further southwards than block *C*, as well as rotated clockwise along vertical axes, akin to 'dextral strike-slip faulting' in structural geology. This is consistent with the triangular shape of the cave below these blocks. The overall arrangement is consistent with differential translation or push of blocks by a south-directed ice flow.

4.2.2 Gillbergagryt – description and analysis

Gillbergagryt is a disintegrated bedrock hill with a fracture cave, c. 5 km SE of Hallstavik (Figure 2-4; 4-10). The feature occurs on the oblique stoss-side of a larger, flat-topped bedrock hill that rises c. 15 m above a shallow, peat-floored valley to the north; north of that a boulder spread covering 1.5 km^2 occurs. The surrounding bedrock surfaces are mainly intact, with well-developed abraded surfaces in the west and south.

The rock step trends WNW-ESE, oblique to the regional SSW-directed ice flow (Figure 4-10A). The rock type is a coarse-grained, poorly foliated granite gneiss, with wide (> 1–6 m) fracture spacing. Vertical fractures occur predominantly in a WNW-ESE and a NE-SW set (see also Sjöberg 1994).

The area consists of a jumbled mass of disrupted and disintegrated rocks, covering an area of c. 80 by 40 m, and is described in 4 sectors (Figure 4-10B, C, D).

Sector 1, in the WNW part of the area, comprises rock blocks that show minor disintegration, with individual blocks moved apart by 10–50 cm, separated by voids 1–2.5 m deep, and relative vertical displacement of up to 50 cm. Block size in the sector varies from 5–40 m^3. Most blocks show their top surfaces as abraded surfaces. In the WNW, the abraded surfaces are subhorizontal, indicating limited block rotation, but further SE abraded surfaces dip c. 30° to the W, indicating significant block rotation and tilting (e.g. Block *C*). Some blocks show block rotation to the east (Block *D*).

Sector 2, west of the centre, shows a higher degree of disintegration, and is characterised by a jumble of smaller blocks, in the range of 0.5–4 m^3, stacked on top of each other. Some blocks show right-way-up abraded surfaces, but many blocks have rotated significantly (> 90°) showing a higher degree of disintegration. Sector 2 overlies the main cave entrance system; the cave outline (after Sjöberg 1994) is plotted on Figure 4-10C. The cave entrance stretches in a NE-SW direction and is formed by the displacement of block *E* in a SE direction (Figure 4-10D, E). The two coated fracture surfaces that bound this passage (blocks *E* and *G*; Figure 4-10E) match and show c. 2–5 m relative NW-SE displacement. Most cave passages are formed by dilation of the vertical fractures along the two dominant fracture sets, only a few along the horizontal fractures. Cave passages are up to 5 m wide and 6 m high, indicating < 5 m horizontal displacement of the blocks in a SE direction. Block *G* in the cave is substantially larger than the blocks above it that form the surface of Sector 2: a subhorizontal fracture probably separates these: such a fracture is not present in sector 3 (block *E*), indicating discontinuity of subhorizontal fractures.

Sector 3 is dominated by a very large, single block (Block *E*), at least 5 m deep, of > 800 m^3 (Figure 4108C, D). The top surface of Block *E* shows well-preserved rounding and striae (to 160°) typical of subglacial abrasion and indicating limited rotation (Figure 4-10C). The top surface of Block *E* is about 1 m higher than the (jumbled) top surface of Sector 2, suggesting relative subsidence of the Sector 2 (Figure 4-10D, F). Block *E* thus displays a prominent NNW facing step, in effect a steep, oblique stoss-side face. The group of blocks (each 5–10 m^3) directly east of Block *E* show clear relative subsidence with respect to that block. Blocks immediately SE of Block *E* appeared to have been 'cleaved off' that block, showing toppling towards the SE (e.g. Block *H*; Figure 4-10D).
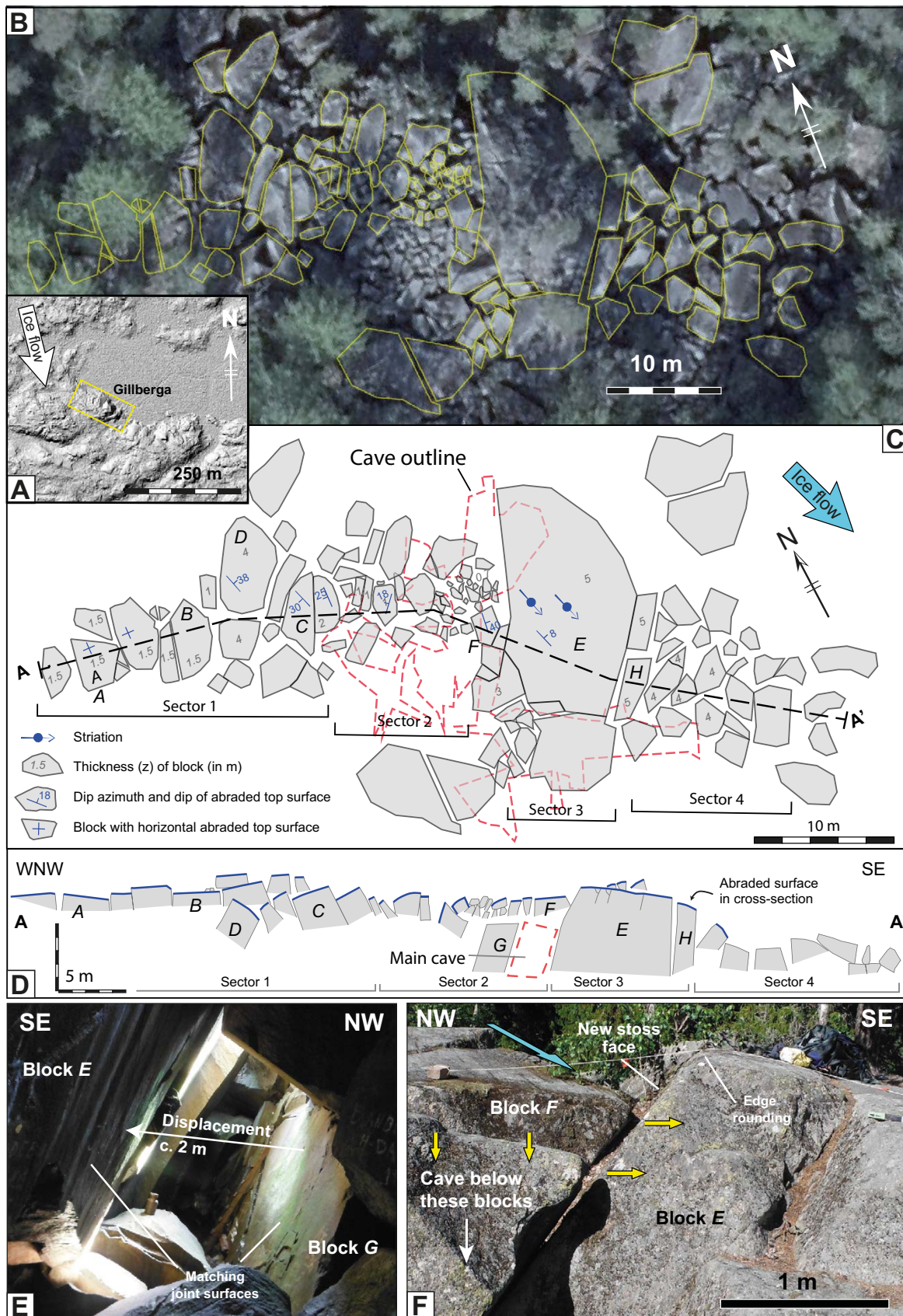
Figure 4-10. *Gillbergagryt: disrupted roche moutonnée with fracture cave. A) Setting of Gillbergagryt hillshade DTM (from Lantmäteriet). B) Orthophoto (from Lantmäteriet), with outline of blocks. C). Map, based on orthophoto and field work. Thickness (in m) of a selection of blocks indicated, dip azimuth and dip of selected blocks shown. Approximate outline of cave indicated. D) WNW-ESE cross-section, with noted abraded surfaces shown. Line of section on B. Some blocks are lettered to allow cross-referencing between section and map view.*

Sector 4 is a jumble of large blocks (5–45 m^3), with strongly tilted abraded surfaces (10° to > 90° tilting). Several blocks only display fractured surfaces, suggesting either that blocks were turned completely upside down, or that blocks were broken up beneath the original abraded surfaces. The rock mass has lost any coherence and is in essence a dense boulder spread: not a single block retains its original orientation. The top surface of Sector 4 is 2–4 m below the top surface of block E, showing clear relative subsidence, but itself shows voids 3–5 m deep, indicating significant collapse and disintegration. The total depth of disruption is thus at least 7–9 m, consistent with the depth of the cave below Sector 2. Further loose boulders occur up to c. 20 m ESE of Sector 4. Minor edge rounding (c. 1–4 cm) occurs in Sectors 1 and 3, as seen on block E (Figure 4-8F).

Interpretation Gillbergagryt

Overall, Gillbergagryt shows a pronounced asymmetry, with limited disruption in the Sector 1, substantial SE movement in Sector 3, leading to extension and collapse of Sector 2, and complete collapse and disintegration in Sector 4. Thus, the extent and magnitude of disruption, as shown by relative subsidence between blocks, rotation of blocks, and width of voids, increases towards the ESE, broadly consistent with SE-directed ice flow. The step-like stoss side of block E, with an abraded top edge, suggests it moved to the SE or ESE, consistent with ice-flow, creating void space in its wake and resulting in collapse, subsidence and formation of voids and the fracture cave beneath Sector 2. Block size is highly variable, (from < 1 m^3 to > 800 m^3) and hence the precursor fracture network was highly irregular. Hydraulic jacking likely caused some or all of the initial disruption and fracture dilation as seen in Sector 1, but further block separation and tilting suggest a component of ice drag.

4.2.3 Bodagrottorna (Boda)

The Bodagrottorna, or Boda, NW of Iggesund (Figure 2-4 for location), consists of a large disintegrated roche moutonnée (~ 5 000 m^2, ~ 20 m high), containing an extensive fracture cave system (Figure 4-11). The area has been studied before, e.g. by Sjöberg (1994), Mörner et al. (2000), Carlsten and Stråhle (2000) and Wänstedt (2000). The Boda roche moutonnée developed in gneissic, poorly foliated granodiorite. Extensive boulder spreads occur around Bodagrottorna (Figure 4-11A) in terrain with prominent W-E orientated rock ridges that carry low roches moutonnées with lee-side cliffs that face SE.

Local ice flow indicators are somewhat ambiguous and it is likely that ice flow direction changed during glaciation: the overall streamlining suggests an eastward ice flow, flow offshore during deglaciation is to the SE (Greenwood et al. 2017), whereas moraines to the south of Iggesund suggest southward ice flow. Local ice-flow indicators, as described below, suggest south to SSE ice flow during deglaciation. To the SW of the Boda roche moutonnée itself, there are two trains of boulder spreads, stretching in a SSE direction (Figure 4-11B). (They did not originate from the main Boda roche moutonnées, but from smaller roches moutonnées to the south: a remnant low rock stump occurs at the northern end of the western boulder train). In addition, c. 120 m to the SSE is a cluster of megaclasts (c. 200 and 90 m^3) that likely originated from the Boda roche moutonnée itself, as no other outcrop occurs nearby. The direction of transport (S to SSE) is consistent with the elongation of the two nearby boulder spreads. The boulders were noted on older, black and white orthophotos from Lantmäteriet, taken when the area was clear felled. The forest has regrown since and the boulders were revisited and measured (see also Lagerbäck et al. 2005).

Dominant fracture sets comprise a horizontal set, and steeply dipping E-W and NW-SE trending sets (Carlsten and Stråhle 2000). Four boreholes were drilled previously in the immediate vicinity of Boda (Figure 4-11B for locations), and fractures were observed with downhole radar and video by Carlsten and Stråhle (2000). Their data (re-plotted as depth against fracture dip, with open fractures highlighted in Figure 4-12A) shows that (i) fracture spacing is large but highly variable between < 1 to > 20 m, and (ii) subhorizontal fractures are few and short, and occur at different depths in different boreholes. The overall fracture pattern must be a complex 'interlocking' fracture pattern, rather than a simple orthogonal pattern, with cross-cutting fractures.
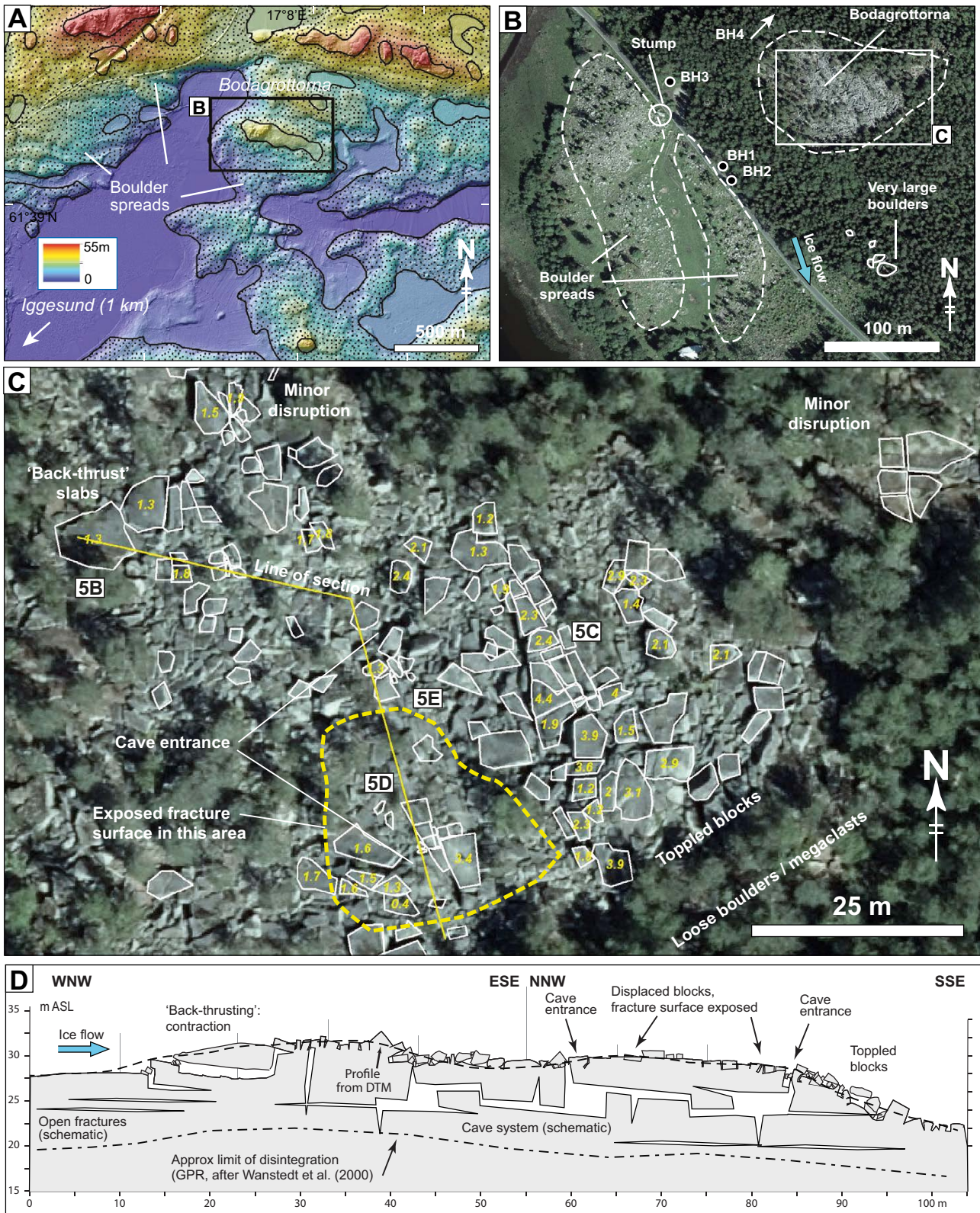
Figure 4-11. Bodagrottorna roche moutonnée. A. Setting of Bodagrottorna roche moutonnée (centre), on hill-shaded relief map from Lantmäteriet. Stippled areas mapped by SGU as boulder deposits. B. Orthorectified air photo of Bodagrottorna roche moutonnée and immediate surroundings. Two linear boulder spreads extend in a NNW-SSE direction. Location of boreholes after Carlsten and Strahle (2000). C. Digitised outlines of blocks on orthorectified air photo (from Lantmäteriet). Yellow numbers indicate thickness (z, in m), measured in the field. Yellow line is the section line for D. Location of photos in Figure 4-13 are indicated. D. Cross-section of the disrupted roche moutonnée. Approximate limit of disintegration at depth after Wänstedt (2000). See also Krabbendam et al. (2022a).
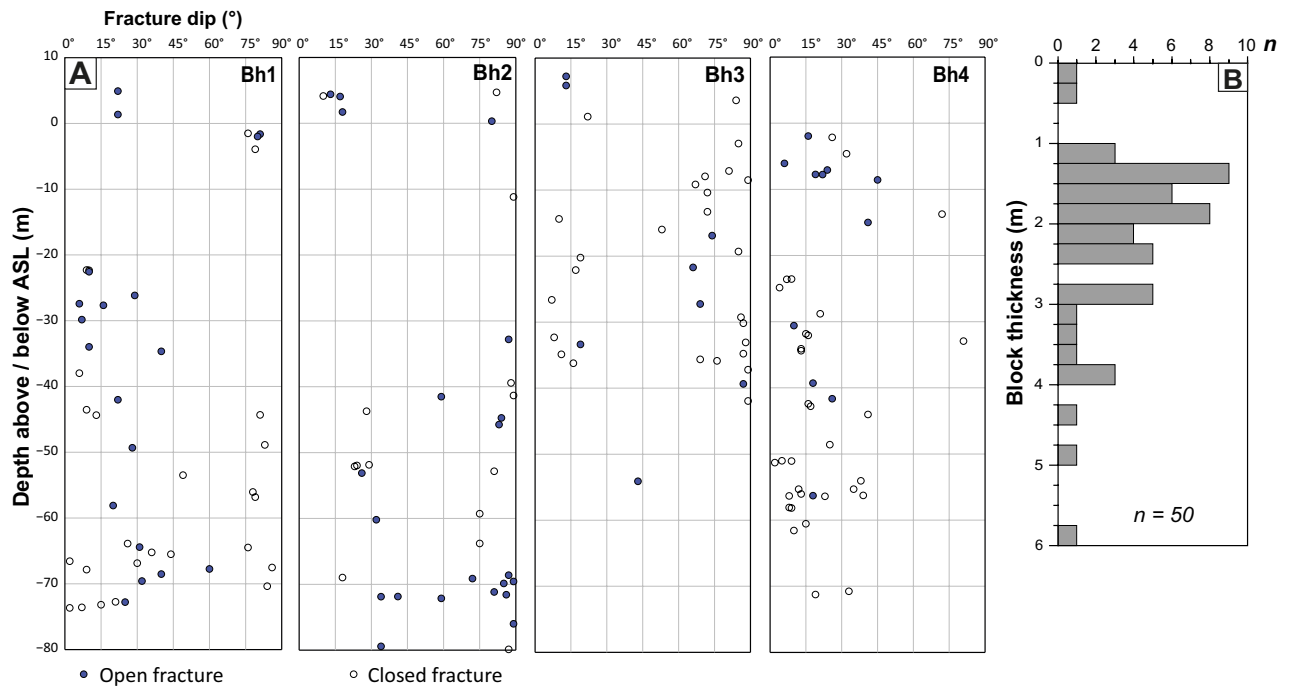
Figure 4-12. *Bodagrottorna. A. Fractures observed in boreholes (down hole video and radar) adjacent to Bodagrottorna, replotted from Carlsten and Strahle (2000). Depth versus fracture dip; open fractures highlighted. Clusters of steep fractures maybe the same fracture, due to undulating fractures. B. Histogram (bins 0.25 m) of thickness of blocks near surface, measured in the field. All blocks have abraded tops, so this measure is a proxy for the depth of the first subhorizontal fracture beneath the abraded surface.*

The Boda roche moutonnée contains a cave system which extends across an area of 150×100 m (Sjöberg 1994) (Figure 4-11D). The system comprises vertical passages 1–5 m wide, and 0.3–2 m high and up to 50 m long horizontal passages at three different levels (Sjöberg 1994). Passage width, and hence fracture displacement, decreases with depth, to a known depth of c. 10 m. Various geophysical methods, including ground penetrating radar (GPR) and gravity measurements, have shown that the cave system at Boda is limited to a depth of c. 5–15 m, and is a local feature (Wänstedt et al. 2000).

At Boda, the sizes of the fracture-bound blocks range mainly from 1–4 m (Figure 4-11C, B; 4-12B), although numerous blocks are larger (nominal B-axis: – 6–10 m). The height (z) of the surface blocks varies considerably: even adjacent blocks can vary in height between 2 and 4 m. Overall, the height of blocks with abraded tops (equivalent to the depth of the first subhorizontal fracture below the abraded surface) varies between 0.5–4 m, occasionally up to 6 m (Figure 4-12B). This is consistent with the vertical variation of the cave floor elevations, as shown in cave surveys (cave survey by A. Sidén 1980, shown in Sjöberg 1994) and the borehole observations of Carlsten and Stråhle (2000). This strongly suggests that there were no *continuous* sub-horizontal fractures present below the surface, but rather that subhorizontal fractures are short and occur at different depths.

On the partially freed blocks, abraded and fracture surfaces can be readily identified and distinguished, and aid in partial restoration of block movement. Hall et al. (2020) described an overall asymmetry of block movement, consistent with the ice-flow direction. Additional detailed analysis of block size and displacement is given here. As blocks are moved apart by fracture dilatation, minor tilting also occurred, which can be constrained by measuring the orientation of the abraded surfaces.

- In the N and NE, disruption is minor, with minor tilting (< 10°) of abraded surfaces, and limited (< 0.2 m) relative vertical displacement of blocks, with voids < 0.3 m wide and metres deep between blocks.

- On the NW (stoss) side, some large slab-shaped blocks show subhorizontal voids (presumably along previous gently inclined fractures), and were pushed beneath down-ice blocks, in a back-thrust-like arrangement (Figure 4-13B).

- On the highest part of the roche moutonnée, individual blocks with abraded tops were uplifted with respect to adjacent blocks and formed blunt stoss faces 0.3–1 m high in the up-ice direction (Figure 4-13C). Minor edge rounding (1–2 cm) is present locally.

- Between the two main cave entrances, a top layer of blocks has been removed, exposing sub-horizontal fracture surfaces (*FS* on Figure 4-13A, D, E). Some blocks remain resting on these fracture surfaces, but show displacement and may have overridden smaller blocks that now occur wedged below larger slabs (Figure 4-13E).

- On the SE or lee side, numerous blocks show substantial tilting and toppling, indicating an extensional ('pull') regime (Hall et al. 2020).
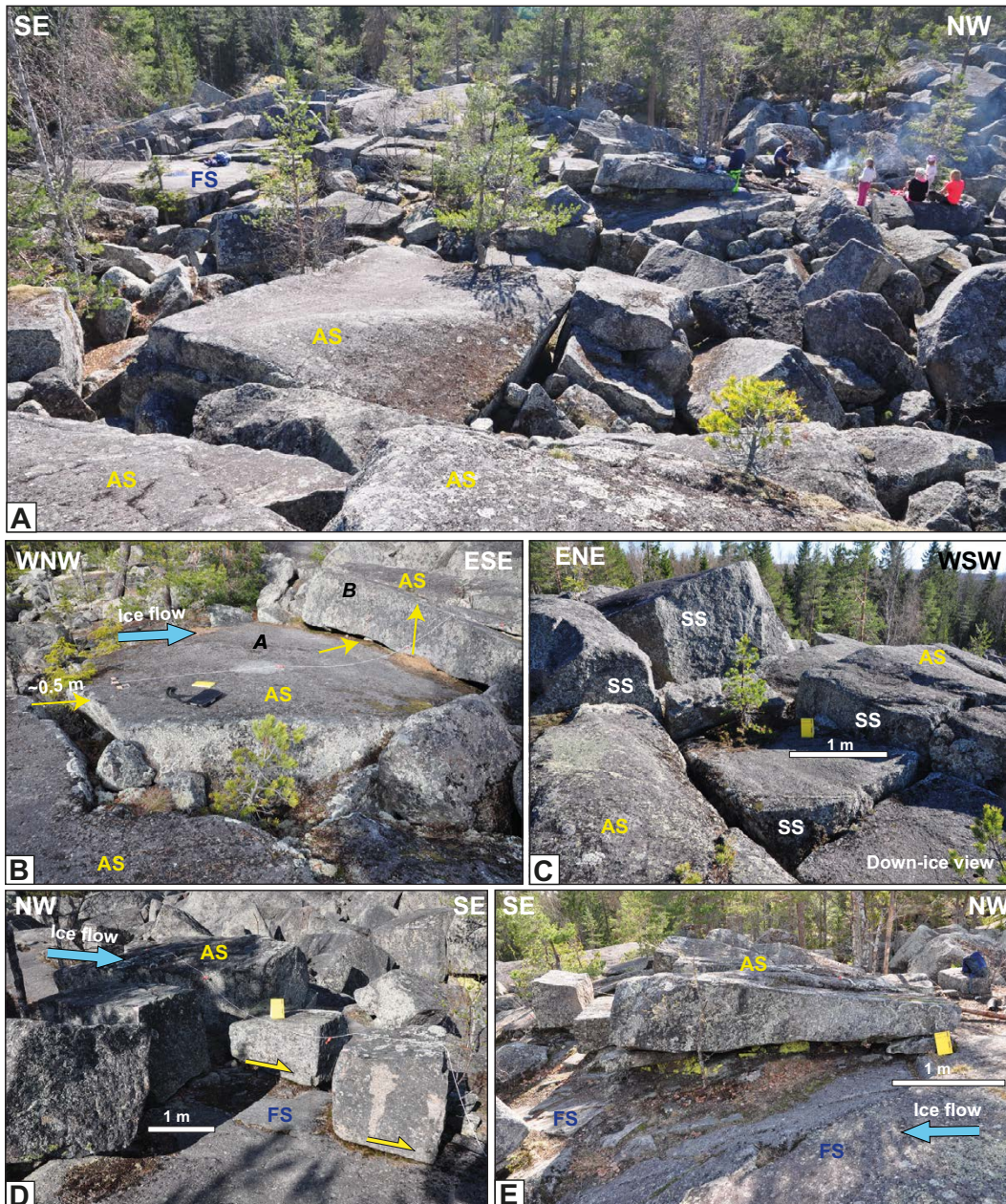
Figure 4-13. *Bodagrottorna roche moutonnée. A. overview. In foreground most surfaces are abraded (AS), in background is an exposed fracture plane (FS). B. Slab-shaped block, with void in up-ice direction. Down-ice the block A has shunted beneath an adjacent block B, by a form of back-thrusting. C. Blocks with abraded tops showing vertical relative displacement (0.3–1 m), now presenting blunt stosssides (SS); view ~ down-ice. Minor edge rounding occurs here. D. Centre of roche moutonnée. Exposed fracture plane (FS),with partially displaced and toppled blocks on top. E. Slab-shaped block with abraded top, resting on subhorizontal fracture plane, with smaller boulders wedged beneath.*

Interpretation Bodagrottorna

The bedrock hill has been disintegrated to a depth of c. 10–15 m. Fracture-bound blocks have moved along (short) subhorizontal fractures at several depths, creating voids to a maximum depth of 9 m (Carlsten and Stråhle 2000), linked together to form the cave system (also documented by Sjöberg 1994 and Mörner et al. 2000). Parts of the near-surface rock mass at Boda were uplifted, likely by hydraulic jacking. Jacking involved uplift up to c. 1 m along some subhorizontal fractures to allow for horizontal cave passages of that height. Boda shows the following asymmetries: (i) a general increase in disruption to the SE; (ii) near the stoss side, blocks are shunted SE-ward by back-thrusting, suggesting a contractional ('push') regime; (iii) on the flatter top of the hill, blocks show vertical uplift as well as translation: here some blocks have been removed to expose a subhorizontal fracture; (iv) on the SE or lee side, numerous blocks show tilting and toppling (see also Hall et al. 2020). The overall asymmetry, characterised by increasing disruption of the three zones, is consistent with the late-glaciation SSE ice-flow direction, as well as with the dispersion of nearby boulder spreads (Section 4.3.4). Overall, initial fracture dilation and disruption is interpreted as caused by hydraulic jacking, but the increase in disintegration towards the SE is likely caused by ice drag.

4.2.4   Grindstugan

South of Gimo, west of Lake Vällen (Figure 2-4D), is a small (15 m long; 5 m high), but steep and blunt roche moutonnée (Figure 4-14A) developed in coarse granitic gneiss. The hill stands isolated on the floor of the ~200 m wide and 10–15 m deep Olandsån valley. The large stoss side block remains *in situ* but the rest of the roche moutonnée has been disintegrated into large (B-axes: 2–6 m) blocks, with voids of 0.1–0.8 m wide in between. Some blocks on the lee-side appear to be 'missing'. Loose boulders, with B-axes 2–4 m, lie 50–80 m to the south (down-ice) of the disintegrated roche moutonnée. Boulder spreads are mapped 0.7–1.4 km to the north, but not in the immediate vicinity.

4.2.5   Pukberget

The Pukberget disintegrated roche moutonnée, c 1 km east of the hamlet of Domta, west of Uppsala (Figure 2-4), is a c. 250 m long ridge, developed in coarse granite gneiss, previously reported by Sjöberg (1994) and Mörner and Sjöberg (2018). The area is characterised by wide trenches in NNW-SSE and SW-NE directions, with rock hills rising 20–30 m above these, typically elongated and stream-lined along the NNW-SSE orientation. Sjöberg (1994) reports other small fracture caves nearby, and boulder spreads have been mapped by SGU within 1 km, but air photos suggest that most exposed bedrock surfaces of surrounding hills are intact. The Pukberget roche moutonnée, positioned down-ice from a wide trench, has similar elevation to other rock hills nearby, but is shorter and steeper, with a c. 20 m high, blunt stoss-side. A small esker extends from on its S flank.

In terms of boulder size, Pukberget roche moutonnée is arguably the most spectacular of all disrupted roches moutonnées, but dense forest cover prevents mapping using air photos. Blocks and boulders are large, typically 4–7 m across (Figure 4-14B). Summit blocks are tilted and separated by deep, 10–40 cm wide crevices along crossing fractures. Blocks have been removed elsewhere, locally leaving 6 m high rock towers (Figure 4-14B). Abraded surfaces are locally recognised; fracture surfaces with fracture coatings are ubiquitous. However, the different heights of the boulders and blocks shows that no continuous subhorizontal fractures existed at depth < 6 m. On the northern, stoss-side, the roche moutonnée is steep and blunt, but also shows incipient disintegration, with large voids and small rotations of blocks. On the SSE lee side, blocks lose coherence, become boulders and megaclasts and are dispersed: the entire rock hill has thus been affected by disintegration. In one locality, a well-rounded boulder (c. 0.4 m across) occurs in a subhorizontal void below a much larger block (Sjöberg 1994), suggesting vigorous water flow sometime during or after fracture dilation.

4.2.6   Trollberget

NE of Uppsala is the Trollberget disintegrated roche moutonnée (location Figure 2-4), measuring some 50×40 m, situated within a large (6–7 km²) boulder spread composed of large (B-axes: 1–4 m) boulders (Figure 4-14C, D). The western edge of the boulder spreads lies 1 km to the E; beyond this limit roches moutonnées remain intact (Lagerbäck et al. 2005). The size of the boulders is similar to that in the disintegrated roche moutonnée. The blocks in the disintegrated roche moutonnée are arranged in a domino-style arrangement, similar to back-tilted normal-fault blocks, requiring slip

Figure 4-14. Field photos of selected disintegrated roche moutonnées. A. Grindstugan: small partially ripped roche moutonnée; increasing disintegration down-ice. B. Pukberget: rock tower with disrupted blocks in back ground. Basal fractures occur at different levels. Height of view c. 6 m. C. Trollberget: Metre-sized blocks, in domino-style displacement. Top surfaces are abraded. D. Trollberget: Metre sized block with blunt stoss side facing up-ice. Note minor edge rounding.

at the base of the blocks. It is possible that this arrangement was relative stable during ice flow, leaving this part of the rock surface relative intact, whereas elsewhere the upper rock mass was completely ripped into a boulder spread. Blocks on the W and E flanks of the hill are tilted towards the flanks. One large (m sized) block has been tilted with the ice-flow, but appears to be 'stuck' by other blocks on its lee side: its steep sides would (c. 1 m²) would represent blunt stoss side to ice flow (Figure 4-14D). Minor edge rounding (1–2 cm) is present.

4.2.7 Himlingeborg

West of Flen, in Södermanland County, the terrain is dominated by WNW-ESE oriented ridges with 25–50 m relief and finger lakes in valleys developed parallel to fracture zones (Figure 4-15A, B). A distinctive feature of the area is the number of large glacial erratics, including mega-clasts (Figure 4-15A, B, C). Preliminary mapping suggests that mega-clasts are sourced from *in situ* rock kernels (grey granitic gneiss) with unusually wide fracture spacing delineating blocks with A-axis lengths 5–15 m. Spreads of large boulders, including mega-clasts, occur as trains and patches aligned with former NNW-SSE ice flow. Rock terrain in and adjacent to boulder spreads has high surface roughness (Figure 4-15D), with numerous sharp flank- and lee-side edges from which blocks have been lost. In this terrain, one partially disintegrated roche moutonnée occurs at Himlingeborg (Figure 4-15E).
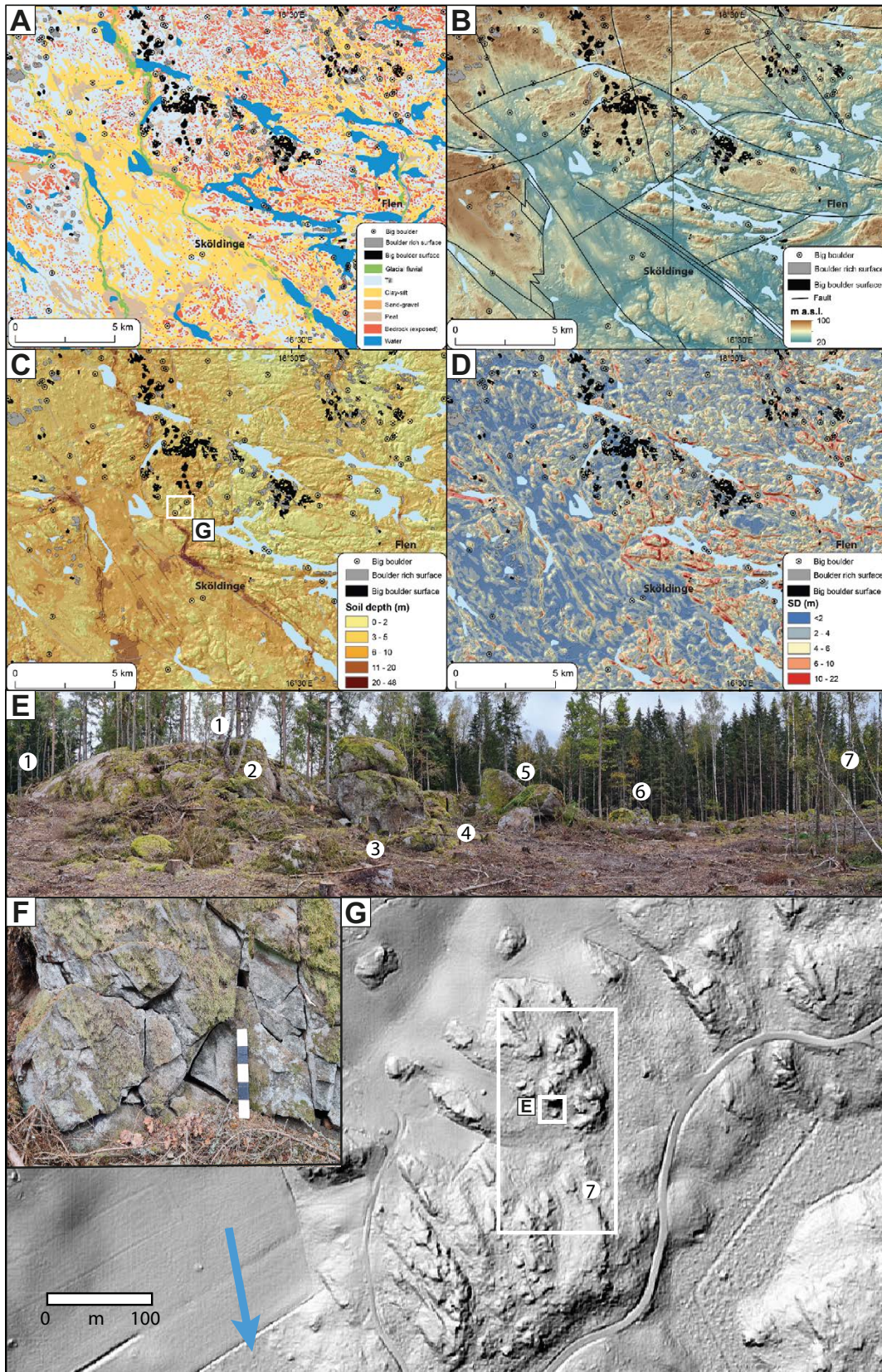
Figure 4-15. *Terrain around Flen and Sköldinge, Södermanland County. A. Quaternary sediment map after SGU data. B. Digital elevation map (from Lantmäteriet), with major fractures, boulder concentrations, and isolated big boulders based on SGU data. C. Soil depth, representing total Quaternary sediment thickness, based on SGU data. Box G refers to the location of the detailed DEM in G. D. Surface roughness (SD) derived from Lantmäteriet DEM. E. View across the former line of ice flow of the partially integrated roche moutonnée at Himlingeborg. Numbers explained in text. F. Detail of lower part of the rock face (at 2) showing development of new fractures and fracture dilation. G. Detailed DEM of the hill and its surroundings. The locations of the photo E) and mega-clast (at 7) indicated.*

Numbers refer to details on Figure 4-15E. The stoss side of this roche moutonnée comprises abraded surfaces (1). The lee-side of a large roche moutonnée shows fracture dilation and development of new fractures at its base (Figure 4-15F); one block has been rotated outward by 3–4 cm to the S. A pair of stacked blocks have moved 3 m to the south (3), possibly out of a socket (2). Residual *in situ* blocks, with dilated fractures remain up to 15 m from the lee face (5), possibly originating from sockets at (4). A boulder train extends to the south (6); a mega-clast with a 14 m a-axis (7) sourced from the lee-face stands 70 m to the SSE and marks the end of the boulder train sourced from the hill.

4.2.8   Damage patterns at low rock hills near Forsmark

A classification of damage patterns to roches moutonnées under glacial ripping has been made previously for Cambrian quartz sandstone terrain in NW Scotland (Hall et al. 2021a). The damage patterns were linked to the entry of overpressured meltwater from the ice sheet bed into fractures and to the balance of resisting and tractive forces across the roches moutonnées. In this sandstone, the fracture patterns are relatively simple, with long, continuous near-horizontal bedding planes and vertical fractures giving an orthogonal fracture pattern. Nonetheless, roches moutonnées and low-relief rock surfaces in the Forsmark area (Figure 4-16A, B) and more widely in eastern Sweden (Table 4-2) show similar types of damage, although the higher variability in fracture patterns and density (Section 4.1) need to be considered in interpretation.

Table 4-2. Types of damage to rock hills and low-relief rock surfaces in other parts of eastern Sweden. Grid references in SweRef 99.

Type of damage		Region	Locality	Northing	Easting	Figure
A	Minor damage. Precursor glacial form persists.	Skyttorp/Vattholma	Uppsala Krossen Quarry	6645251	656082	4-1; this report
			Ballast Quarry*	6662368	654856	4-20 in Hall et al. (2019a)
		Tämnaren	Karbo Quarry	6663691	618842	4-48; this report
		Vällen	Bladåker Quarry	6654699	682709	
			Pettbol	6658156	688822	5-14 in Lagerbäck et al. (2015)
		Iggesund	Viksbergen Quarry	6835002	607676	
			Bodberget Quarry	6840539	610589	
B	Extensive brecciation but no or little block movement	Skyttorp/Vattholma	Wild Rose*	6663554	654129	
		Tämnaren	Granlunda	6655106	627830	
			By	6660232	625832	
		Iggesund	Lelyckeberget Quarry	6834779	610462	
C	Lee side block loss	Skyttorp/Vattholma	Jälla excavation	6644536	651640	
			Gropdalen	6663614	654682	
		Tämnaren	By	6660341	625779	
		Vällen	Gropen	6654154	683687	
		Iggesund	Tönnebro	6770770	604990	4-48; this report
			Svagberget	6834180	605769	4-3; this report
D	Lee, flank and stoss side block loss	Skyttorp/Vattholma	Trollberget	6647936	652341	4-13; this report
			Heden	6664322	656470	
		Vällen	Grindstugan	6669900	679134	4-14; this report
			Rövargrottan	6667016	682693	4-9; this report
		Iggesund	Bodagrottorna	6837426	612719	4-11 and 4-14; this report
E	Rock sheet mobilised or removed	Skyttorp/Vattholma	Trollberget	6648470	652190	4-14; this report
		Tämnaren	Myggstenen	6660262	632571	
		Vällen	Åkersholm	6656470	684947	5-13; in Lagerbäck et al. (2015)
			Bladåker	6655028	682326	4-34C, D in this report
		Iggesund	Gryttjen	6851999	570780	4-25B; 4-34; this report
			Bodagrottorna	6837354	612512	4-11 and 4-14; this report

* Informal names.

Investigated low-relief rock surfaces on and around hills in the Forsmark area are shown in Figure 4-16B, and described in detail below.

Type A. Precursor forms with little or no damage, that retain roche moutonnée and whaleback forms with abraded tops and low cliffs along flanks and lee-sides (Figure 4-17A1–3). Examples include:

A1. Low-relief rock surface at the contact between meta-volcanic and amphibolite gneisses at Stora Asphällan. Stoss face showing smooth, abraded and striated surfaces (Figure 4-17A1).

A2. Road section at the informally named hill, Neon Roundabout (Hall et al. 2019a). Fractures are not dilated and lack sediment fill, except on the lee side where diamicton fills open vertical fractures. (Figure 4-17A2).

A3. DEM of Neon Roundabout showing the stoss and lee precursor form of the roche moutonnée (Figure 4-17A3).

Type B. Type B damage involves hydrofracturing, fracture dilation and fracture fills and /or brecciation, but with little block movement. Such damage was recorded in temporary excavations at Power Plant 3, the water drainage storage basin and the canal (Carlsson 1979), AFM001264 (Forssberg et al. 2007), AFM001265 (Petersson et al. 2007) and Drill Site 5 (Leijon 2005). Examples include:

B1. Cooling water canal section SE of Power Station Unit 3 with long dilated subhorizontal fractures but no disruption of the low-relief rock surface. (Figure 4-17B1).

B2. Dilated fractures with silt and sand sediment fills and extensive brecciation but no discernible movement at the rock surface (Figure 4-17B2).

B3. Fracture dilation and brecciation at the temporary excavation at Drill Site 5 (Figure B-2 from Forssberg et al. 2007). A former till layer was removed to expose the low-relief rock surface (Figure 4-17B3).

Type C. Type C damage involves displacement or loss of multiple blocks from lee-side steps. This pattern of damage is seen on Barrel Rock, an informally named hill SW of Unit 3, and Mt Megantic (Hall et al. 2019a).

C1. NE flank of Barrel Rock hill in amphibolite with widely spaced fractures; no fracture dilation (Figure 4-17C1).

C2. Onset of dilation of vertical fractures in mid-section, with diamicton infill (Figure 4-17C2).

C2. Lee-side separation, with pull-apart release of cuboidal blocks (Figure 4-17C3).

Type D. Extensive block loss from stoss, flank and lee sides: both examples from Mohägnaden (formerly termed Antenna View in Hall et al. 2019a); (Figure 4-17-D1, D2).

D1. Stoss-side ripping with extensive block loss has exposed a lower fracture surface (Figure 4-17D1).

D2. Flank cliff exposed after removal of blocks (Figure 4-17D2).

Type E. The disintegration and movement of surface rock sheets, leaving only small *in situ* outcrops, is seen at Gunnarsbo.

E1. Small remaining area of *in situ* rock with a striated surface within a boulder spread. Blocks have been lost from the lee-side cliff and from flanks (Figure 4-17E1).

E2. Separation of blocks along the lee-face (Figure 4-17E2).

E3. A former rock outcrop where all that remains is a scatter of blocks that can be fitted together to reconstruct part of the original rock surface (Figure 4-17E3).

Figure 4-16. A. Bedrock surface map at Forsmark showing the main areas with with damage from glacial ripping, indicated by yellow lines. Adapted from Figure 4-28 in Hall et al. (2019a). B. Classification of damage to roches moutonnées and other low-relief rock surfaces in the Forsmark area. Grey shading indicates abraded precursor surfaces. White surfaces indicate damage by block removal. Adapted from Hall et al. (2021).

The table in part B:

Type of damage	Distribution	Effects	Examples at Forsmark	Groundwater pressure and volume	Balance of resisting (R) and traction (T) forces
A	ice	Little damage. Precursor glacial form persists. Before deglaciation, abrasion operated widely	Neon Roundabout Lilla Sandgrund Stora Asphällan Wave Rock	Low	R > T
B	ice	Extensive brecciation but with no or little block movement	Canal excavations Reactor 3 excavations Test excavation AFM 001264	High across entire rock surface	R > T
C	ice	Lee side block loss	Barrel Rock Mt Megantic	High on lee face	R > T, except on lee face
D	ice	Lee, flank and stoss side block loss	Mohägnaden St Rangsons	High on all edges	R < T except across core of hill
E	ice	Rock sheet mobilised or removed	Tixelfjärden Gunnarsbo Fäskär	High across entire rock surface	R < T

Figure 4-17. Examples of roches moutonnées and low-relief rock surfaces with different patterns of damage (Types A to E in Figure 4-14) near Forsmark. B1: Figure 7-2. B in Carlsson and Christiansson (2007). Blue arrows show former ice flow direction. Photo G Hansson: Further explanation in text.

Similar types of damage are present in and adjacent to areas with extensive boulder spreads elsewhere in eastern Sweden (Table 4-2). Lack of damage in precursor forms (Type A) is often seen in quarries set in the flanks of large hills. Brecciation (Type B) is observed beneath low relief surfaces in temporary excavations (Lokrantz 2014) and quarries (Table 4-1) and in small roches moutonnées where vertical and horizontal fractures are dilated but block removal has been limited. Damage by lee-side block loss (Type C) is common and is well displayed at Himlingeborg where the removed blocks form a short (60 m), lee-side boulder train (Section 4.2.7). More extensive block loss (Type D) is recorded mainly for large roches moutonnées (Table 4-2). Wider rock sheet mobilisation and removal has occurred on large roches moutonnées (Trollberget, Myggstenen), small roches moutonnées (Åkersholm) and across low-relief rock surfaces (Gryttjen, Boda). Types of damage C–E are displayed on multiple small roches moutonnées that are damaged, or partially or wholly disintegrated within large areas

of boulder spreads at Skyttorp/Vattholma, lake Tämnaren, lake Vällen and Iggesund. The different types of damage to precursor glacial forms found at Forsmark and elsewhere occur in different rock types with different fracture patterns and on rock surfaces with different relief and roughness.

4.2.9 Disintegrated roches moutonnées: common characteristics

Disintegrated roches moutonnées have a set of common characteristics that may be summarised as:

1. Large roches moutonnées with steep and blunt stoss faces occur in massive, coarse-grained, granitic rocks with wide fracture spacing and consequently large block size.

2. In several disintegrated roches moutonnées the height (Z-axis) of the blocks varies strongly (Boda, Gillbergagryt, Pukberget): subhorizontal fractures occurred at different depths, but no continuous subhorizontal fractures occur. The original, irregular fracture network delineated a system of interlocking blocks.

3. Both vertical and inclined/subhorizontal fractures are widened by 0.1–5 m into voids and caves, involving horizontal and vertical displacement respectively.

4. Fracture dilation and disruption of the rock mass occurs at depth (typically < 10 m), including the development of caves, well below the ice-bed interface and the top row of blocks. At Rövargrottan, Boda, Pukberget, and Trollberget, the entire roche moutonnée is affected by disintegration whereas at Grindstugan, Gillbergagryt and Svagberget only part of the rock hill is affected.

5. Angular rock blocks, many still with abraded, striated surfaces, are rotated or displaced by 1–10 m.

6. Each partially disintegrated roche moutonnée shows an asymmetry in their pattern of disintegration of: (i) blocks displaced away from others consistent with local late-glacial ice-flow directions; (ii) an increase in disruption to major disintegration in a down-ice direction; (iii) a trail of loose boulders down-ice from the roches moutonnées (except at *Trollgrundet*, which is positioned within a large boulder spread).

7. The settings of the large disintegrated roches moutonnées differ: some are adjacent to mainly intact rock (Gillbergagryt) whilst others occur within boulder spreads (Boda, Trollgrundet, Forsmark). At Gillbergagryt, Pukberget, Rövargrottan, and Grindstugan, the partially disintegrated roches moutonnées occur on the sides or in shallow valleys.

8. At Forsmark, on low-relief rock surfaces that include small roches moutonnées, different patterns of damage occur that range from no damage and lee-side damage to complete surface disintegration. Similar damage patterns occur more widely in eastern Sweden.

4.3 Boulder spreads

4.3.1 Distribution at the landscape scale

The distribution of boulder concentrations at the landscape scale is studied using SGU data. In that mapping, any surface boulder concentration is mapped and, depending on the scale and particular dataset, may include periglacial block fields, slope deposits and moraine ridges. The general distribution of boulder concentrations in Sweden is uneven at the landscape scale (10–100 km) (Stendahl et al. 2009) (Figure 4-18). Few boulder concentrations have been mapped by SGU in the mountains of western Sweden; they are also of restricted extent across higher elevation terrain in Jämtland and in Västernorrland. In contrast, boulder concentrations extend intermittently for a S-N distance of ~1 000 km on the low ground of eastern Sweden. Seven main areas of high density can be identified (Figure 4-18).

In ground above 250 m a.s.l., boulder concentrations occur as periglacial blockfields on mountain summits and plateaux (Borgström 1999). In upland Areas D and G, above 250 m a.s.l. boulder-strewn ribbed and hummocky moraines occur mainly along valley floors and sides (Hättestrand 1997). Boulder-strewn ribbed moraines occur at Lake Rogen (Area F) (Lundqvist 1989, van Boeckel et al. 2022). In ground below 250 m a.s.l., periglacial blockfields are absent. Ribbed moraines occur in Gävleborg and into Uppland but are generally fragmented and modified forms (Hättestrand 1997). *Surface boulder concentrations* are the main boulder covers mapped in the lowlands of Sweden. The majority of these boulder concentrations are interpreted here as *boulder spreads* formed by glacial ripping.
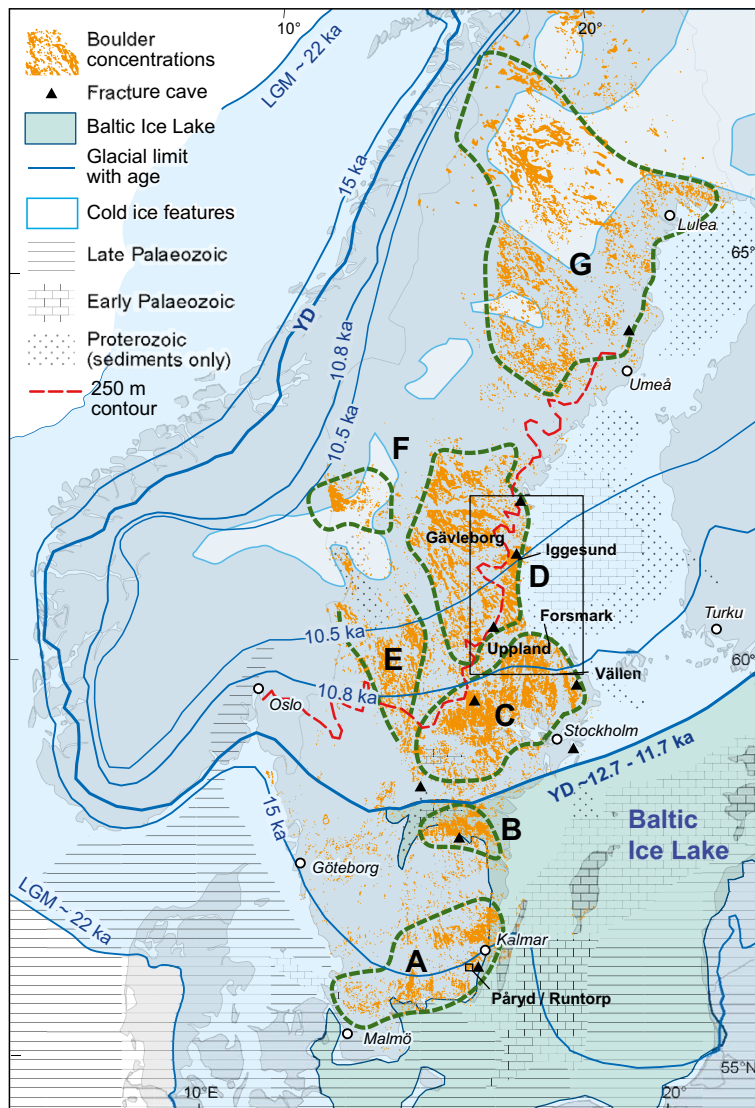
Figure 4-18. *Distribution of boulder concentrations in Sweden based on SGU Quaternary mapping data. A: southernmost Sweden; B: Östergötland; C: Uppland and Västmanland; D: Gävleborg and Västernorrland; E: Dalarna and Värmland; F: Lake Rogen and G: Norrbotten.*

Boulder spreads extend intermittently for a S-N distance of > 500 km on the low ground of eastern Sweden. Boulder spreads are of restricted extent in the lowlands of SW Sweden. The swaths in Landscapes A and B are in lowland terrain of similar topography and relief to adjacent areas. In Landscapes C (west), D and E boulder spreads remain widespread as the ground rises from the lowlands below 250 m a.s.l. to uplands and mountain plateaux. Boulder spreads occur indiscriminately across the Svecofennian gneiss of eastern Sweden and the Transcandinavian granite-porphyry belt, so these large-scale geological provinces have no bearing on the distribution. Boulder spreads occur above and below the marine limit (approximated by the 250 m a.s.l. contour; Figure 4-18). This suggests that boulder spreads were formed in both marine and terrestrial ice marginal settings.

In Landscapes A, B and C (Figure 4-18) boulder spreads occur as three W-E swaths that align with the retreating margin of the Fennoscandian Ice Sheet. Sediment sequences suggest that a phase of rapid retreat occurred during the warm Bølling-Allerød interval at 14.5–13.6 ka when ice retreated across the Kattegat (Hyttinen et al. 2021) and northward across SE Sweden (Avery et al. 2021). Landscapes C and D have some of the densest occurrence of boulder spreads in Sweden and lie within the Younger Dryas ice limit, and hence within the zone of rapid ice front retreat as the Fennoscandian Ice Sheet responded to early Holocene warming. In Landscape C, varve chronology indicates that ice margin retreat rates after 11.7 ka BP were high at 200–400 m yr^{-1} (Strömberg 1994). Later northward retreat into valleys in Landscapes D–G were also rapid at 660 m yr^{-1} (Stroeven et al. 2016). Boulder

spreads in SE Sweden show two gaps: between Landscapes A and B and B and C. The gap between B–C occurs just inside the Younger Dryas limit, and may be related to different glacio-hydrological conditions under slower retreat conditions. The gap between A–B is less easy to explain as there is no direct link with changing ice-sheet margin retreat rates. Overall, it appears that at the landscape scale, the densest occurrence of boulder spreads formed during phases of rapid ice retreat. However, rapid ice sheet retreat also occurred in some areas with few boulder spreads, such as around Trollhättan in SW Sweden (Hall et al. 2019b). Hence, whilst rapid melting and ice front retreat were likely important influences on the distribution of glacial ripping at the landscape scale, other factors were involved.

4.3.2 Distribution at the regional scale

Our examination of regional scale (1–10 km) boulder spread distribution focusses on Uppland. Here, the ice flowed southwards/SSE during the last glaciation under warm-based conditions (e.g. Sohlenius et al. 2004).

In the three different types of erosional terrain recognised earlier at the regional and local scales (Section 2.2 and Hall et al. 2019a), boulder spreads are uncommon in *ice-roughened terrain* and w*eakly streamlined terrain*. Boulder spreads are characteristic features of *glacially disrupted terrain* where they occur in association with markers for hydraulic jacking and fracture caves (Figure 1). In this terrain type, *in situ* bedrock with glacially abraded surfaces is typically not widely exposed. Rock surfaces and boulder spreads lack till cover except (i) in bedrock lows and (ii) on hummocks and ridges.

In Uppland, the boulder spreads occur in 2–10 km wide belts and patches (Figure 4-19) that lie broadly parallel to former SSE-directed ice flow during deglaciation (Hall et al. 2019a). Several belts of boulder spreads lie between the main esker systems of Uppland (Hall et al. 2020). For example, belts of boulder spreads are found south of lake Storfjärden and lake Tämnaren, and along the lake Vällen depression. These regional scale patterns are explored below. However, boulder spreads are also found alongside segments of the Uppsala, Rimbo and Börstil eskers.
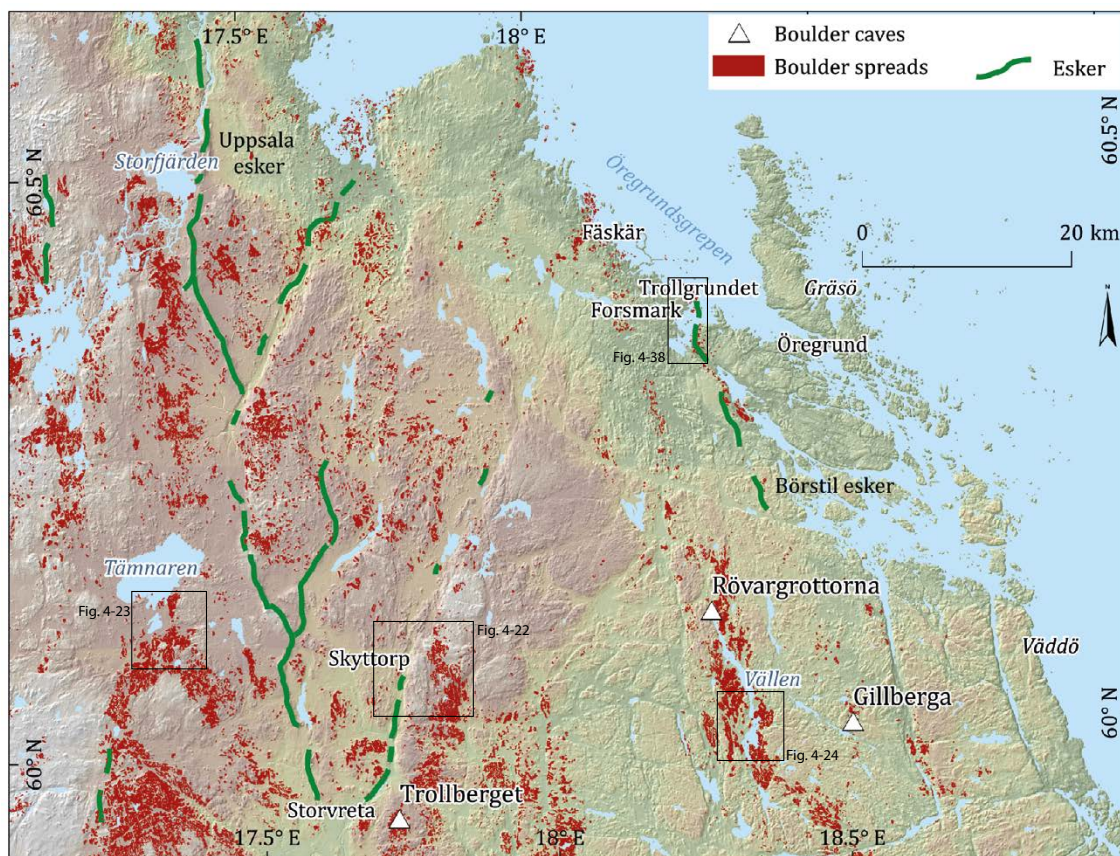
Figure 4-19. *Distribution of boulder spreads (after SGU data) and esker ridges in NE Uppland. Mapped eskers coincide with those mapped by Dewald et al. (2022). DEM from Lantmäteriet.*

We emphasise that although boulder spreads – and hence glacial ripping – was widespread in Uppland, there are still large swaths of the landscape that are free of boulder spreads and where glacial ripping did not occur. Boulder spreads are spatially limited, covering < 10–20 % of the investigated ice-sheet bed in Uppland (Figure 4-19).

We examine below the regional distribution of boulder spreads in Uppland in four case studies.

Forsmark: regional distribution of boulder spreads

The terrain around Forsmark includes each of the three types of erosional terrain outlined above (Section 2.2 and Hall et al. 2019a). Boulder spreads occur as two belts (Figure 4-20). The western belt, 1–2 km wide and c. 8 km long, stretches SSE, parallel to ice-flow direction. The ground surface here shows relatively high surface roughness compared to the N-S trending weakly streamlined belt to the east (Figure 4-20). The boulder spread belt cuts obliquely across lithological boundaries and steep regional deformation zones and the regional fracture zone orientation (which trend NW-SE – Figure 4-21). The eastern boulder spread belt occurs along the flanks of the Börstil esker, and shows a curved trajectory, from NNW-SSE to N-S (Figure 4-20). This boulder spread belt is c. 1.5 km wide and appears denser, with less rock outcrop, than the boulder spread belt to the west. Boulder spreads within these belts are described in detail in Section 4.3.4.
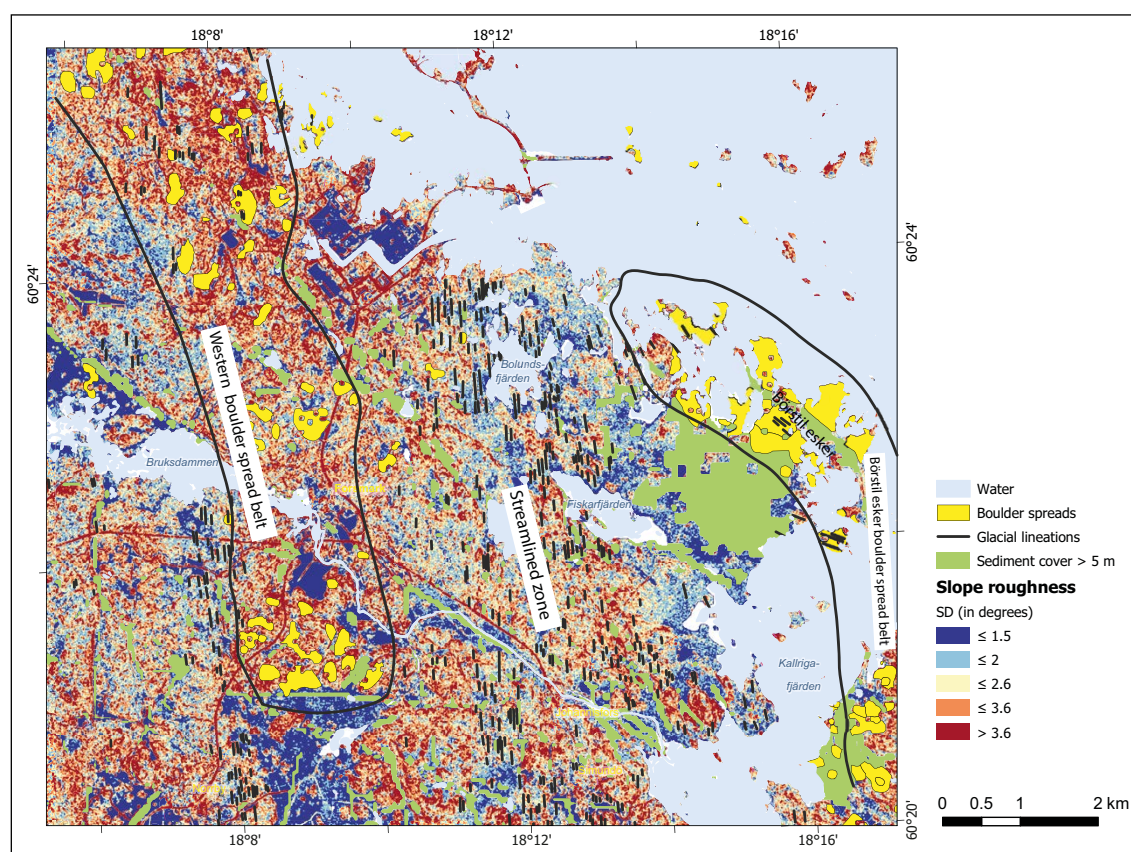
Figure 4-20. *Boulder spreads in the Forsmark area in relation to glacial lineations, mainly crags with till tails, sediment thickness and slope roughness. Map compiled from SGU data, with roughness map derived from Lantmäteriet elevation data.*
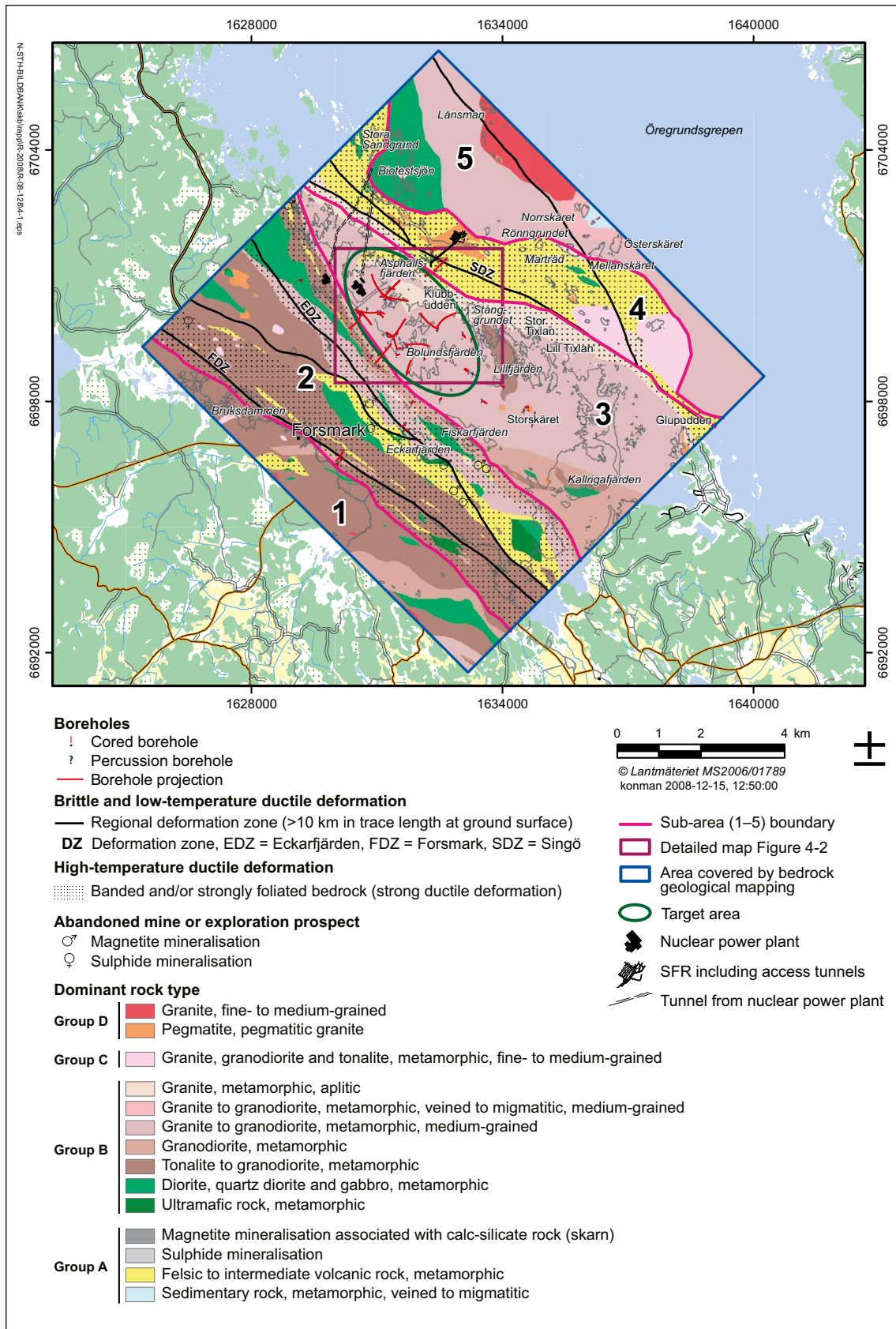
Figure 4-21. *Geology at Forsmark. Boulder spreads are marked in black. Modified from Figure 4.1 in SKB R-08-128 (Stephens et al. 2008).*

Skyttorp: regional distribution of boulder spreads

A similar tripartite terrain pattern is seen at Skyttorp (location on Figure 4-19), ~40 km SSW of Forsmark (Figure 4-22).

• The western low-lying area, characterised by extensive till cover in topographic lows, and including the Vattholma esker. In this zone, boulder spreads are rare.

• Moving east, there is a 2 km wide N-S tract of glacially roughened terrain, with extensive rock outcrops shaped as whalebacks and roches moutonnées and patchy, but locally thick, cover of sandy till (see Figure 4-20 in Hall et al. 2019a).

• Further east lies a 2 km wide belt of boulder spreads, with high surface roughness in DEMs. The boulder spreads have a sharp western boundary.

• Finally, on the eastern edge of the map area, glacially roughened terrain reappears, with till-covered depressions. Areas with boulder spreads become small.
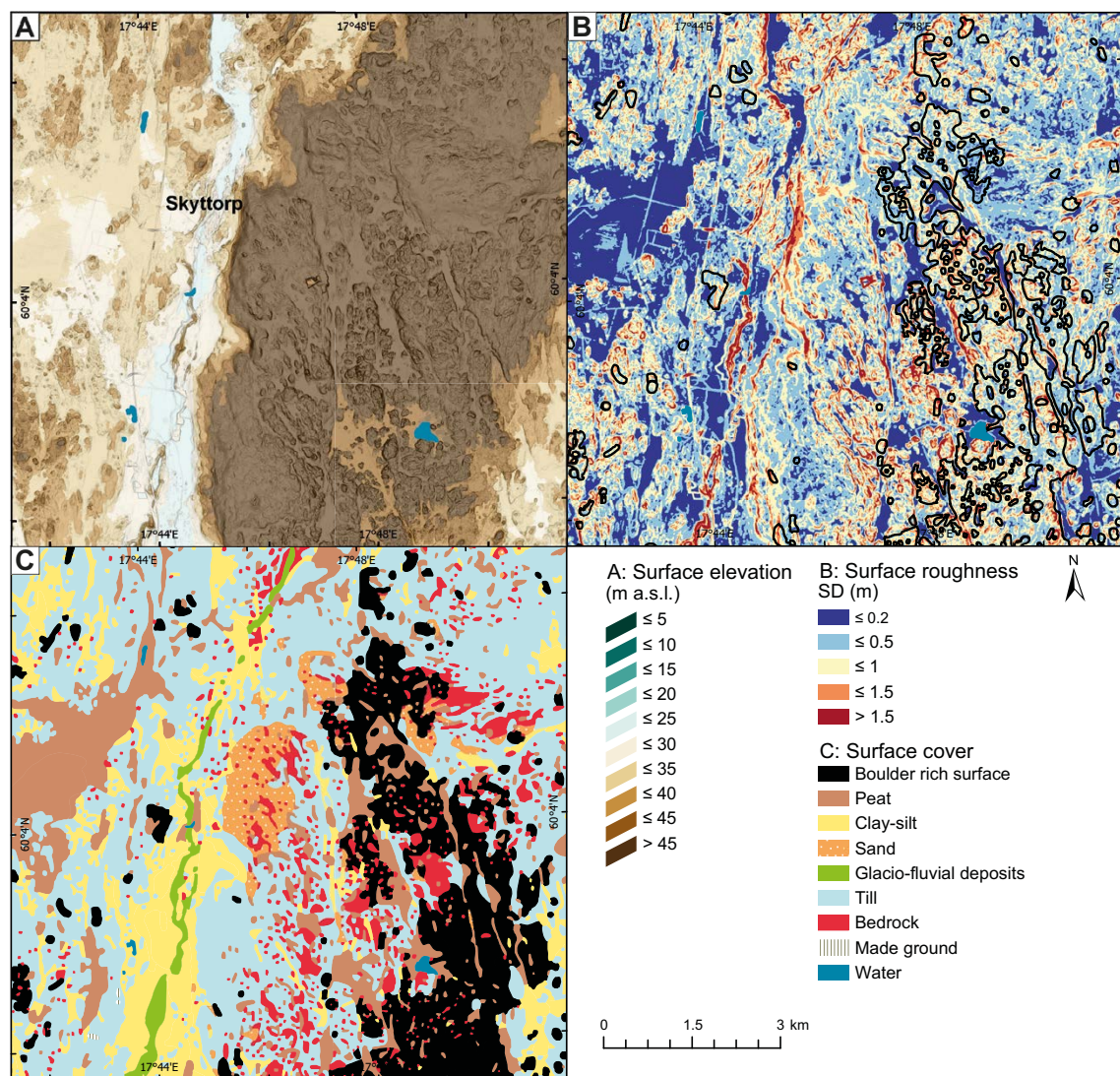
Figure 4-22. Skyttorp area. A. Elevation maps: DTM from Lantmäteriet; B. Roughness map derived from Lantmäteriet DTM; SD in m; window size of 20 × 20 m, outline of boulder rich surfaces added. C. Superficial geology map from SGU.

Tämnaren: regional distribution of boulder spreads

South of Lake Tämnaren (location on Figure 4-19) the three landscape types are similarly apparent in belts approximately parallel to N-S ice flow (Figure 4-23). Glacial erosion has exploited fractures oriented approximately N-S to produce weak streamlining in the bedrock.

- A western zone south of Sörsjön shows undamaged rock outcrops on small hills which are partly buried by thin (1–5 m) glacial and postglacial sediments. Remnants of ribbed moraine are seen in DEMs.

- An axial zone with boulder spreads extends south and then splits southward around a till-covered area. Patches with boulder spreads have sharp lateral boundaries and fluted surfaces.

- An eastern zone of typical glacially roughened terrain with common bedrock outcrops and patchy to extensive till, locally > 5 m in thickness and forming till tails.
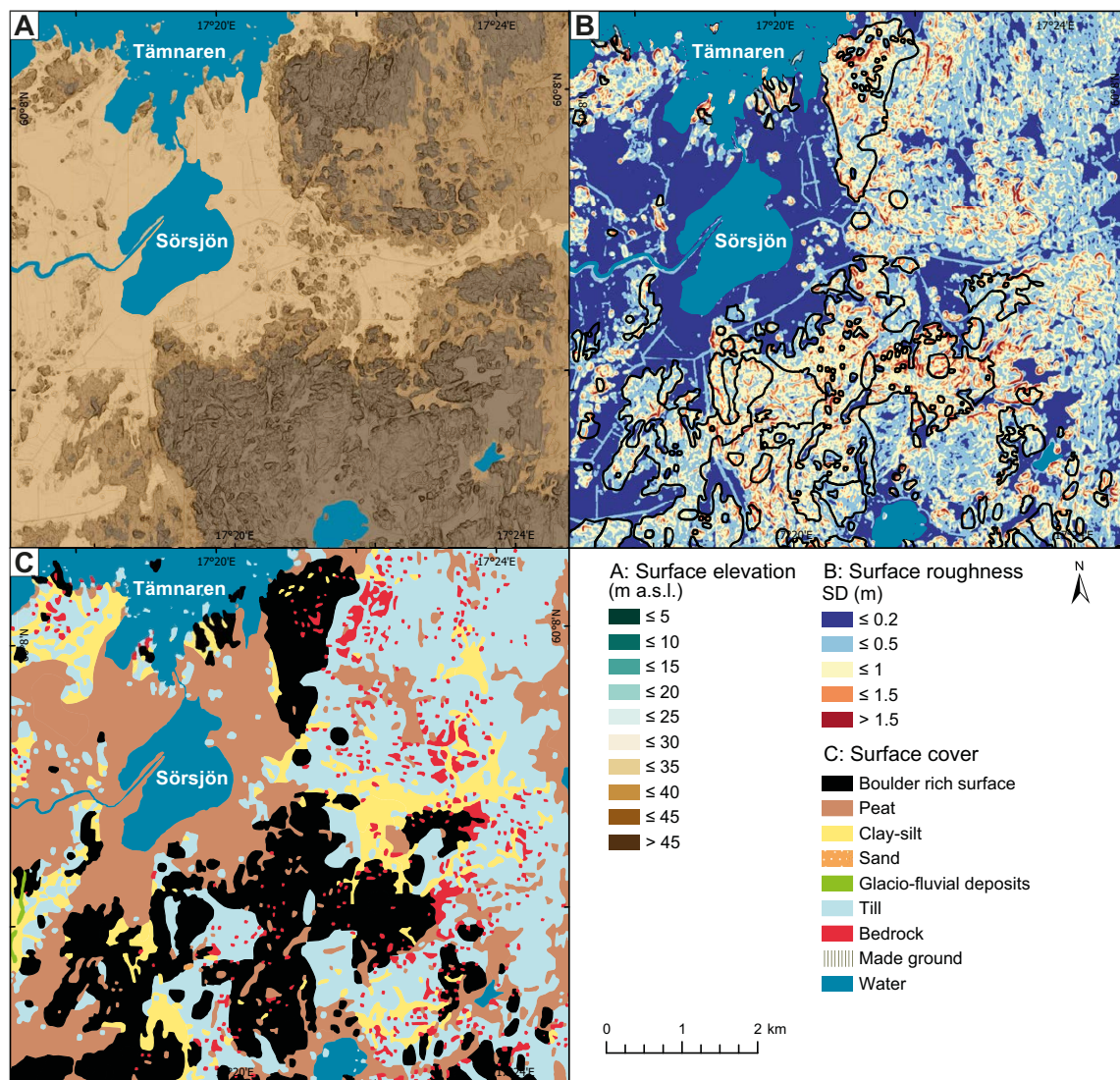
Figure 4-23. *Terrain south of Tämnåren. A. Elevation maps: DTM from Lantmäteriet; B. Roughness map derived from Lantmäteriet DTM; SD in m; window size of 20 × 20 m, outline of boulder rich surfaces added. C. Superficial geology map from SGU.*

Vällen: regional distribution of boulder spreads

Lake Vällen (location on Figure 2-4; 4-19) occupies a shallow (15–20 m) linear depression with a NNW-SSE orientation that follows one of the principal regional fracture sets (Figure 4-24A). A strong contrast exists between typical glacially roughened terrain found either side of the Vällen depression, and the disrupted terrain found directly flanking the lake basin (Lagerbäck et al. 2005). Boulder spread boundaries are sharp (Figure 4-24B). The area of boulder spreads has a high surface roughness compared to both the till-dominated terrain and some bedrock dominated terrain (Figure 4-24C), although some bedrock dominated terrain shows multiple sharp edges. Till is sparse within the area dominated by boulder spreads.
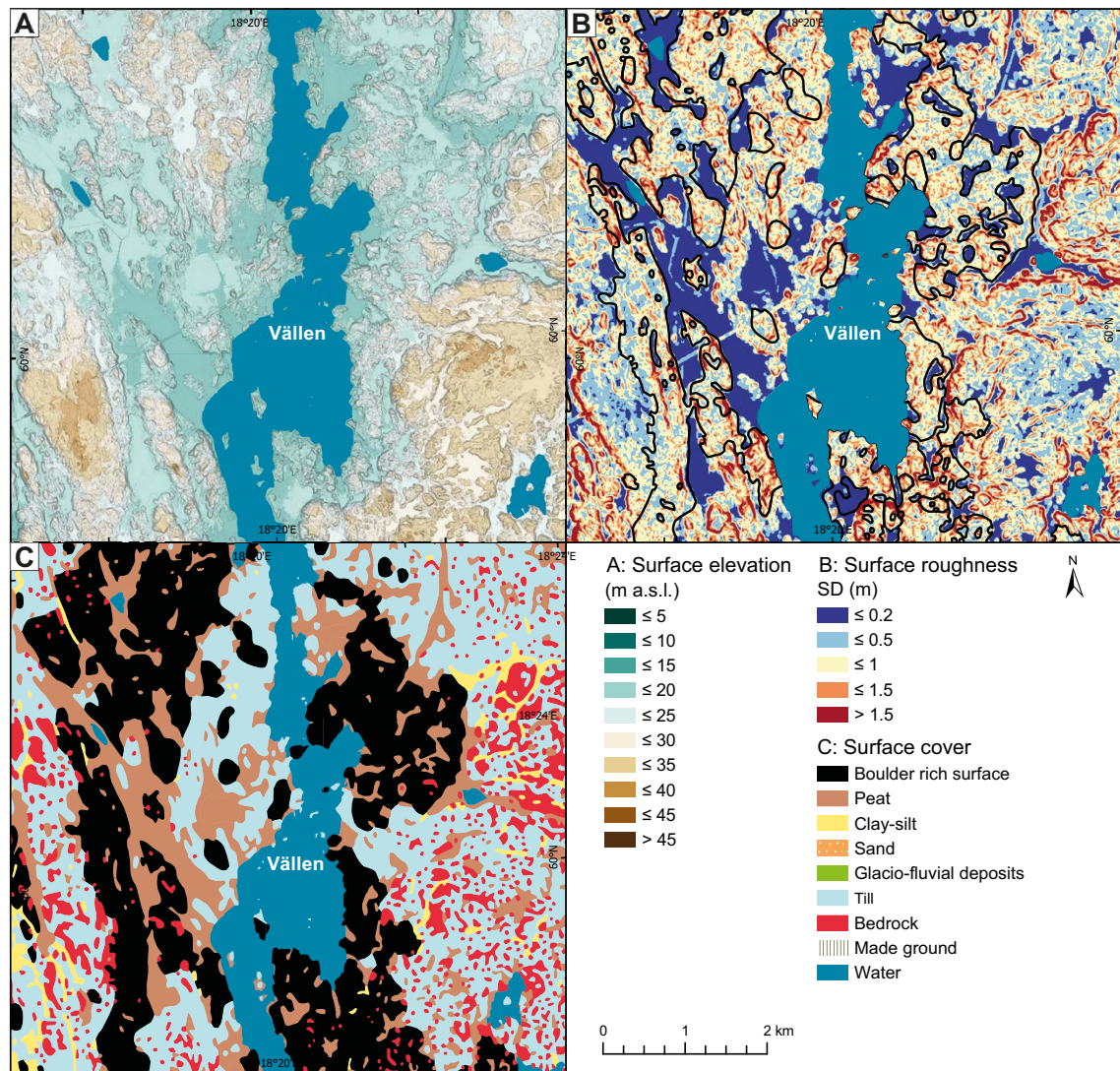
Figure 4-24. *Terrain at Vällen. A. Elevation maps: DTM from Lantmäteriet; B. Roughness map derived from Lantmäteriet DTM, SD in m; window size of 20 × 20 m, outline of boulder rich surfaces added. C. Superficial geology map from SGU.*

4.3.3 Interpretation of boulder spread distribution at the landscape and regional scales

The distributions of boulder spreads at the regional scale in Uppland, in part informed by the observations in the four case study areas, show a common set of characteristics: (i) large extent, covering many km², (ii) occurrence in discrete zones, commonly with sharp lateral boundaries. The discrete zones are mainly oriented N-S and parallel to former ice flow direction during deglaciation. However, not all boulder spreads occur as discrete linear zones: north of Skyttorp boulder spreads are more patchy, and south of Lake Tämnaren, the zones are discrete but not very linear. In some cases till cover is patchy or absent, elsewhere it is present.

In terms of the main spatial controls, the boulder spreads do not link closely to lithology at the the landscape and regional scales. Rock types in Uppland show little lithological variations: most rocks mainly very hard but variably fractured Svecofennian gneisses. Belts with boulder spreads are developed in different gneiss lithologies. Near Forsmark, boulder spread belts cut obliquely across lithological boundaries and steep deformation zones; equally in the same lithologies there are areas with and without boulder spreads (Figure 4-21), so neither lithology nor overall fracture zone orientation appear to control the distribution of boulder spreads. In the subdued topography of Uppland, boulder spreads are found on low, flat-topped fault blocks between fracture zones at Skyttorp (Figure 4-22) and lake Tämnaren (Figure 4-23). At lake Vällen, boulder spreads are extensive along the topographic depression in which the lake lies and along the western flank of the Olandsån valley (Figure 4-24) but are not extensively developed along the parallel valley of lake Gisslaren to the east. Hence, topographic controls on boulder spread distribution are not obvious at this scale. However, most studied partially disintegrated roche moutonnées (Section 4.2) are relatively high and blunt topographic features.

A number of boulder spreads belt occur adjacent to eskers, for instance along the Börstil esker. Many eskers are now recognised to be part of wider 'meltwater corridors', 100s to 1 000s of metres wide corridors characterised by an array of depositional or erosional glaciofluvial forms related to (seasonally) channelised flow subglacial meltwater flow (e.g. Lewington et al. 2020, Sharpe et al. 2021). Shallow tunnel valleys recognised in southern Sweden contain hummocks left after erosion (by subglacial meltwater) of pre-existing sediment (Peterson and Johnson 2018); at Lake Rogen, the establishment of meltwater corridors led to fluidization of sediments at the bed, dissection and modification of ribbed moraines and formation of murtoos and hummock corridors (van Boeckel et al. 2022). For boulder spreads adjacent to eskers, it is possible that these can be regarded as part of the wider meltwater corridor: this may well apply to the boulder spreads adjacent to the Börstil esker and in the Skyttorp area. Whether the linear belts of boulder spreads at Forsmark and Lake Vallen also constitute melt-water corridors is possible, but at present uncertain. The absence (or patchy occurrence) of till may be attributed to subglacial meltwater erosion, but could equally caused by original non-deposition. Hummocks do occur in the Forsmark area, but whether these are similar to the glaciofluvially formed hummocks of Peterson and Johnson (2018) would require more detailed sedimentological study. The Lake Vallen belt aligns with a strong N-S linear depression, but whether this was formed or deepened during late Weichselian meltwater activity is uncertain, as little or no glaciofluvial sediment was mapped by SGU.

Overall, the landscape and regional distribution of boulder spreads appears to be in part linked to melt-water corridors, but at present it is uncertain whether this link can explain all aspect of the distribution.

4.3.4 Detailed characteristics of boulder spreads

Boulder spreads occur widely in eastern Sweden (Figure 2-1). Most occur in dense forest (in part because other land use is not possible), hampering detailed mapping. We focussed detailed characteri-sation on a small number of boulder spreads that occur in clear-felled areas, e.g. Gunnarsbo boulder spread near Forsmark, Bladåker boulder spread near Vällen; Skogbo boulder spread; Gryttjen boulder spread ENE of Iggesund, and boulder spreads around the Börstil esker, east of Forsmark (Figure 2-4 for locations). Some boulder spreads previously documented by, for instance, Lagerbäck et al. (2005) are now overgrown.

On many boulders in most boulder spreads (e.g. Gunnarsbo, Bladåker), abraded bedrock surfaces with striae are readily recognised, and easily distinguished from planar, pre-existing fracture surfaces, which commonly still show fracture coatings, such as chlorite, epidote and iron staining. Such fracture surfaces appear somewhat more resistant to weathering. In granitic boulder fields, abraded rock surfaces are somewhat more difficult to demonstrate, likely due to superficial post-glacial weathering: striations were observed but more rarely. A series of aerial photos show the variation in boulder density, compared with an area without boulder spread at Stånggrundet, east of Forsmark (Figure 4-25). In five boulder spreads, boulders were digitised from air photos (see Methods, Section 3.3.3) and heat maps of the aerial boulder density can be constructed (Figure 4-26), demonstrating the high variability of aerial boulder density (Figure 4-27).
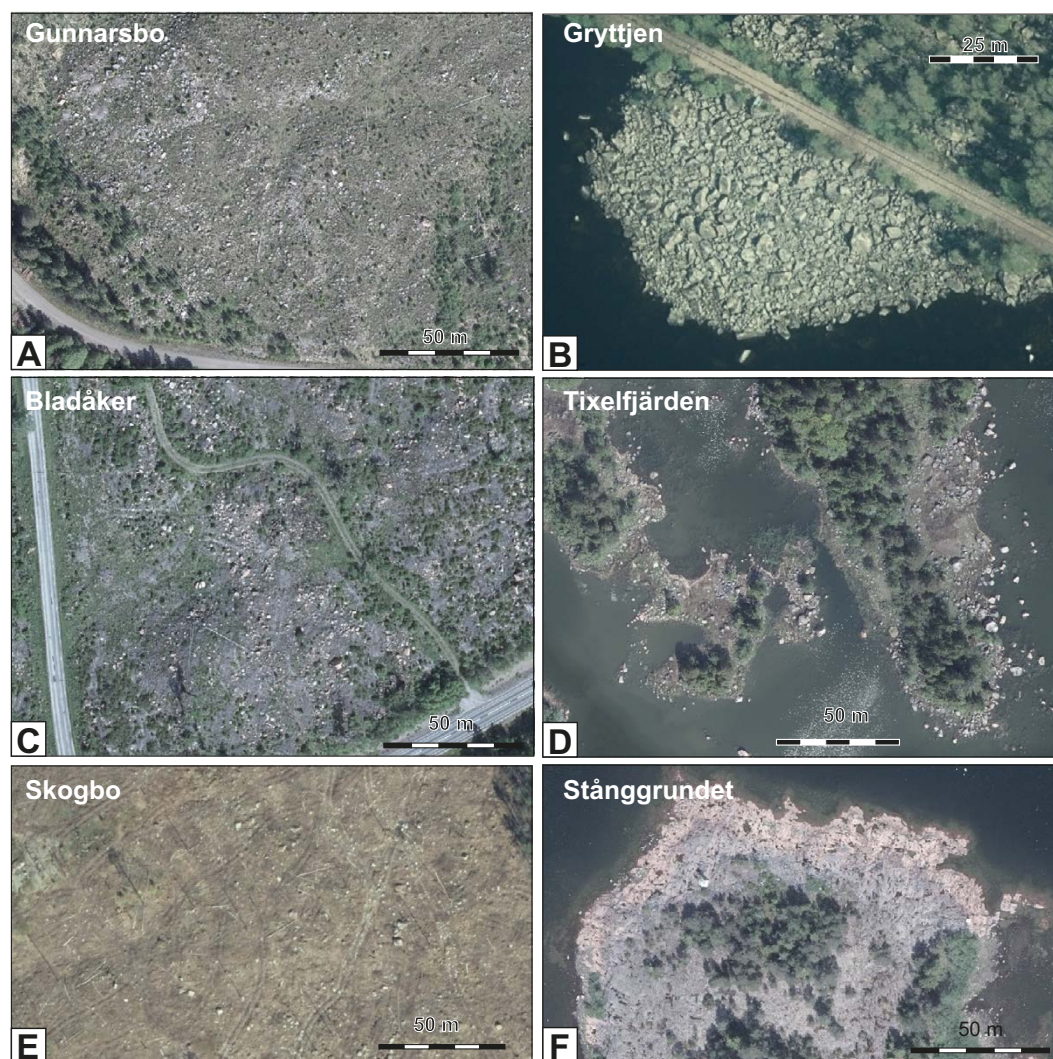
Figure 4-25. *Aerial photos from a selection of boulder spreads, showing variation in boulder density, compared with one area without boulder spread. Aerial photos downloaded from Lantmäteriet. A. Gunnarsbo, near Forsmark; B. Gryttjen, showing high boulder density with complete boulder cover; C. Bladåker, near Lake Vällen; D. Tixelfjärden, boulder spread emerging from Bothnian Gulf, near the Börstil esker; E. Skogbo, a low-density boulder spread; F. Stånggrundet, near Forsmark: an area of bare roches moutonnées without boulders.*
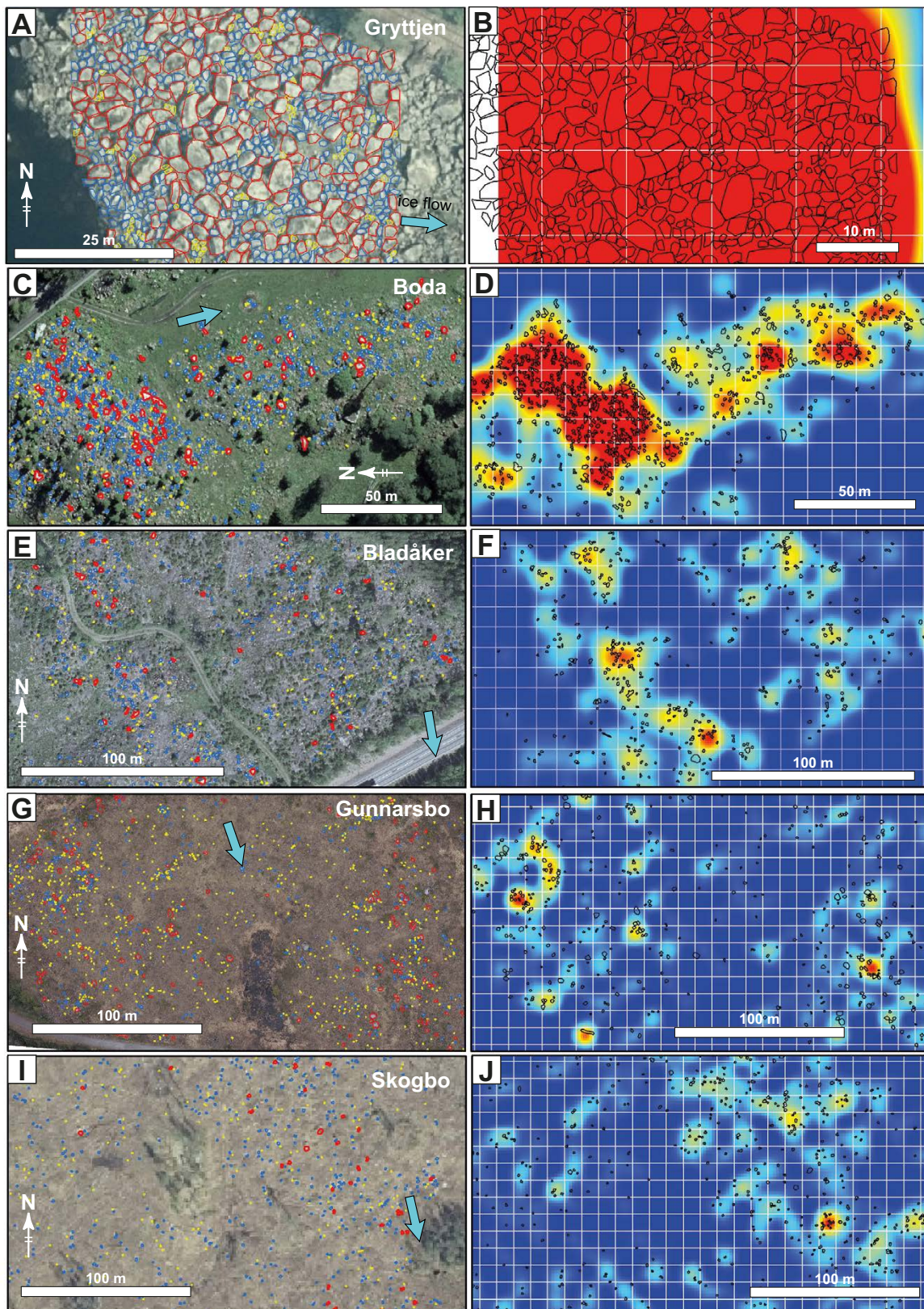
Figure 4-26. *Left panels: Aerial photos from a selection of boulder spreads, showing digitised boulders. Yellow < 0.65 m²; blue 0.65–2 m²; red > 2 m². Aerial photos downloaded from Lantmäteriet, except for Gunnarsbo. Right panels: heatmaps show boulder density, splined from 10 m fishnet grid. Blue = low; red = high. A–B: Gryttjen. C–D: Boulder spread south of Bodagrottorna. E–F: Bladåker, near Lake Vällen; G–H: Gunnarsbo, near Forsmark. I–J: Skogbo, a low-density boulder spread.*
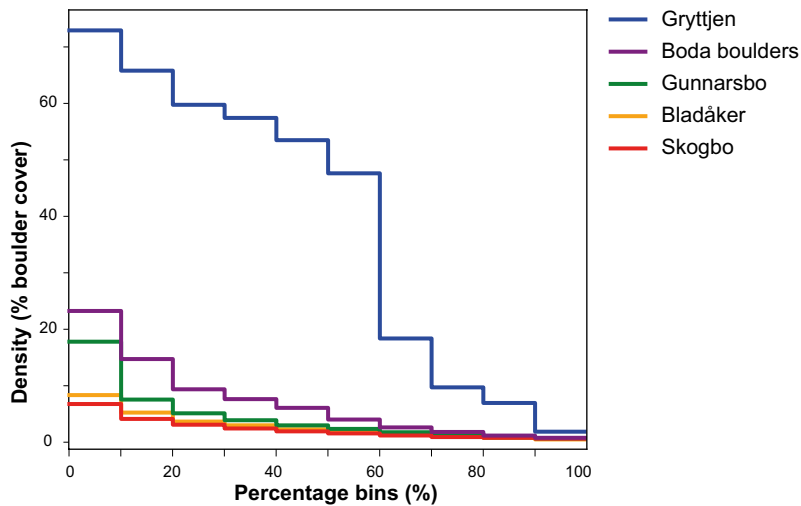
Figure 4-27. Bar chart showing boulder density (as % of total cover within 10 × 10 m squares) for five boulder spreads. Each bar is a bin representing 10 % of the analysed squares.

Gunnarsbo – Forsmark boulder spread

The Gunnarsbo boulder spread occupies c. 10 000 m^2 and is located c. 800 m SSW from the F3 Forsmark nuclear power plant (Figure 4-28A); it forms part of the boulder spread belt east of Forsmark (Section 4.3.2). Small, abraded rock outcrops occur within the boulder spread area. Linear terrain features in DEMs are subparallel to local fracture sets, indicating that the boulder spread is of shallow depth (Figure 4-28B). The Gunnarsbo boulder spread occurs over an outcrop of amphibolite gneiss that stretches NW-SE (based on SGU mapping augmented by our own field mapping), oblique to the regional late-glacial SSE-directed (Sohlenius et al. 2004) ice-flow direction (Figure 4-28). The surrounding rocks are felsic (granitic to tonalitic).

Low moraine ridges occur c. 750 m south of the Gunnarsbo boulder spread: these are typically 1–3 m high, with boulders 0.5–2 m across, and comprising a mix of amphibolite and granite gneiss boulders. A hummock ~6 m high composed of bouldery till overlain by openwork angular boulders occurs at the south-west corner of the Gunnarsbo boulder spread. Other till hummocks, with and without boulder spread covers, up to 5 m high and with transverse scarps on their south-eastern flanks, occur within and adjacent to the boulder spread area. Gouges north of the mega-block train have been interpreted as iceberg scour marks (Sohlenius et al. 2019), but at Gunnarsbo *in situ* bedrock occurs at shallow depth and the gouges could equally be the result of subglacial erosion.

A high resolution orthorectified photo-mosaic was acquired using an UAV (Figure 4-29; 4-30, 4-31), and the following observations were either made from digitising the georeferenced orthophoto, or using the georeferenced orthophoto as a base-map to acquire field data in a GIS on a portable, PC-Tablet, with in-built GPS. These data include (i) thickness (z), which can be used (together with the surface area obtained from polygons from digitised boulders) to calculate the approximate volume of the boulders; (ii) the orientation of striae on abraded surfaces; (iii) the orientation (dip azimuth and dip) of the amphibolite-gneiss foliation of the boulders.

The Gunnarsbo boulder spread is dominated by boulders of amphibolite (c. 95 %); the amphibolite varies from fairly fine grained (< 1 mm) and strongly sheared amphibolite, to coarse-grained (1–3 mm) and medium sheared amphibolite – the latter with a characteristic 'speckly' appearance. The azimuth and dip of the metamorphic foliation is readily measured (Figure 4-31, 4-32A, B, and see below). Granitic pegmatite veins are common in the amphibolite blocks, and range from 1–50 cm in width. Boulders of other lithologies are rare (5 %), and comprise a variety of felsic rocks, e.g. fine-grained granite; granitic augen gneiss, tonalitic gneiss; these are interpreted as normal erratics. Scattered bedrock outcrops and near *in situ* (partially disrupted) bedrock outcrops occur around and within the boulder spread.
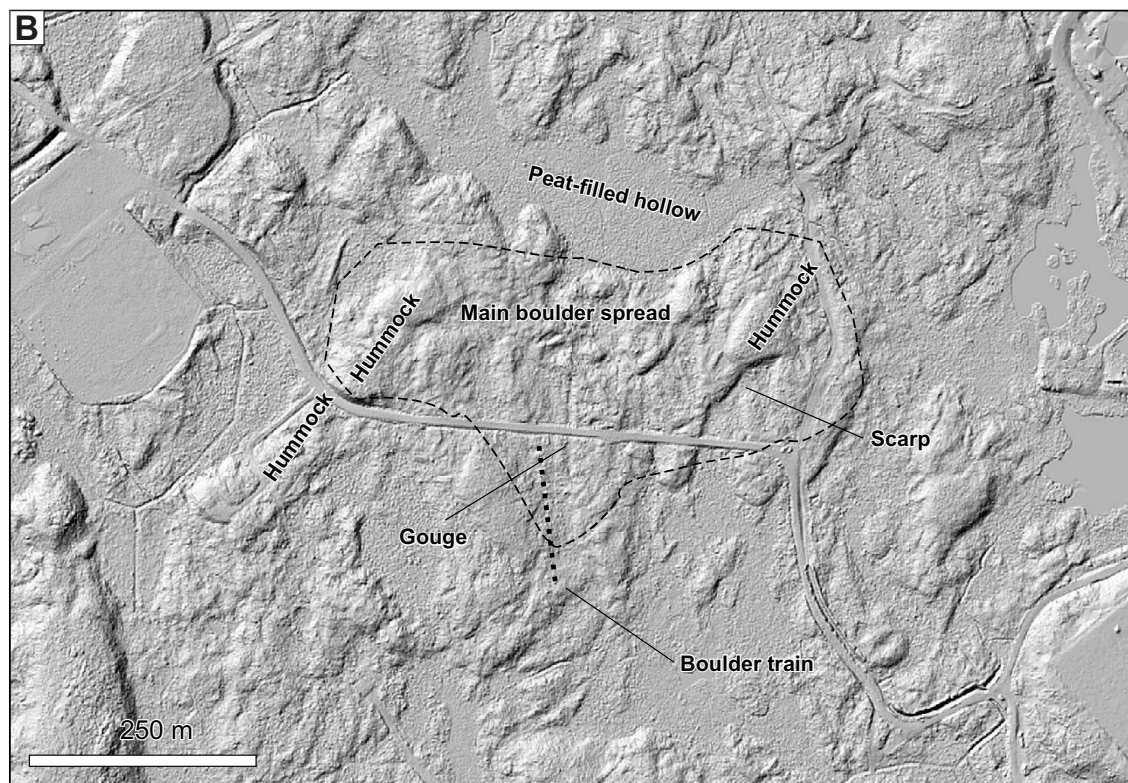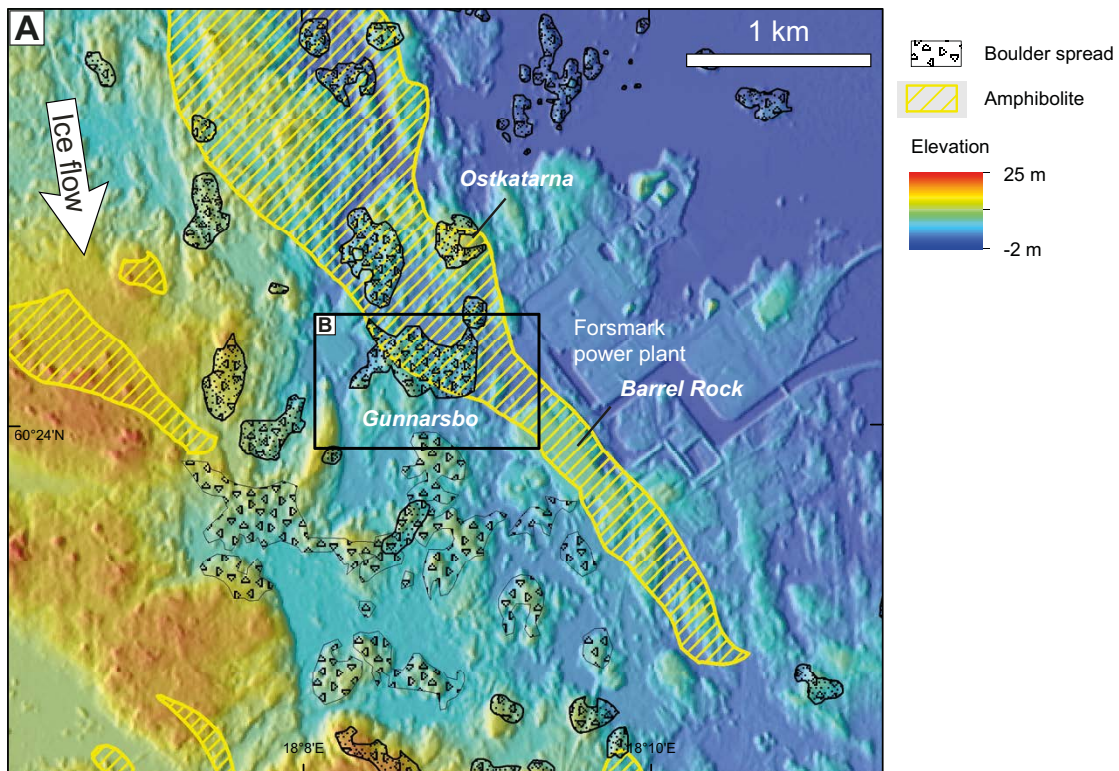
Figure 4-28. *A. Setting of Gunnarsbo boulder spread at Forsmark. Boulder spreads in the area around Forsmark, based on SGU mapping and, in southern part, after Sohlenius et al. (2019); amphibolite after SGU mapping and own work. B. Hill shade DTM view of Gunnarsbo boulder spread and immediate surroundings. DTM after Lantmäteriet.*
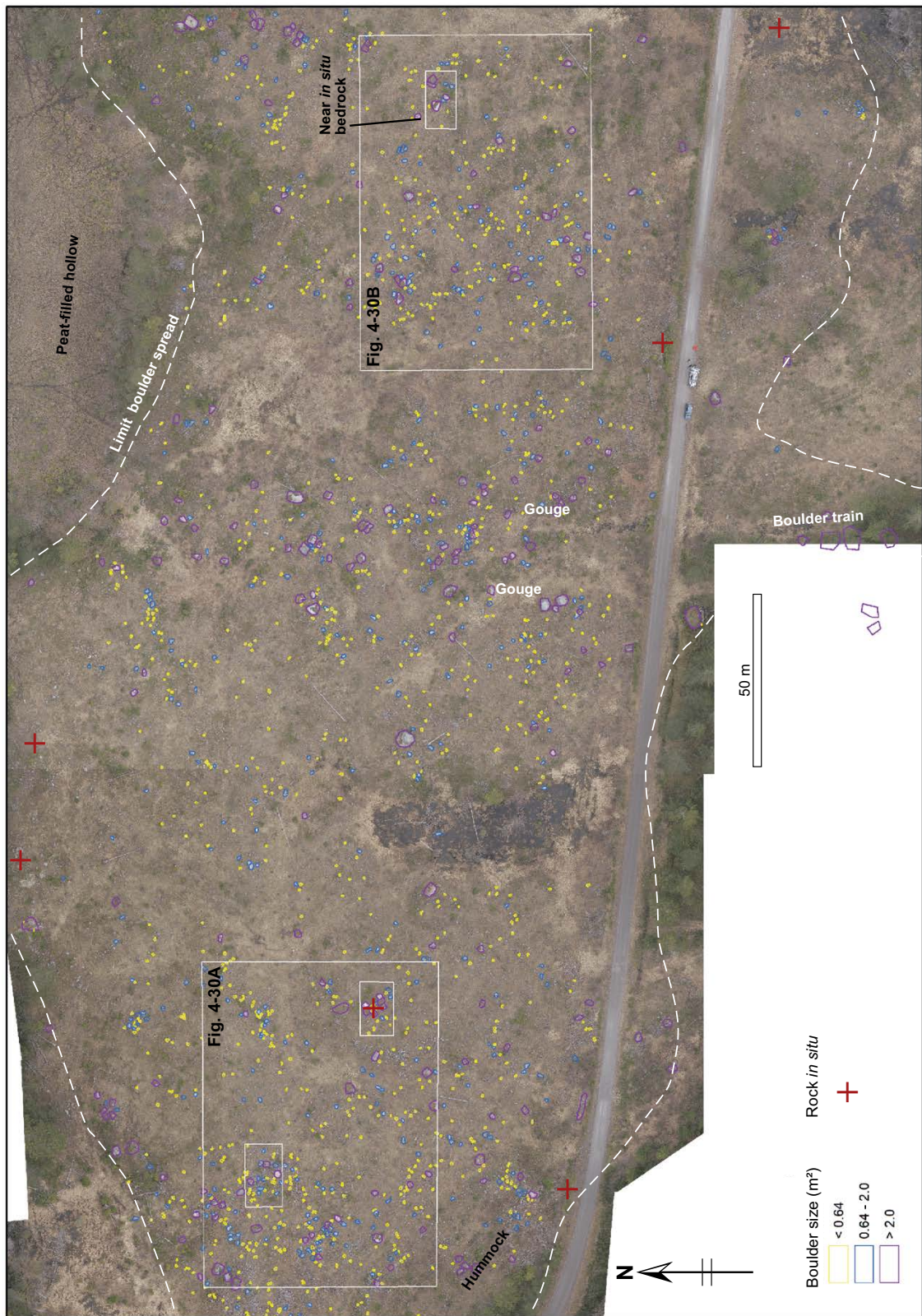
Figure 4-29. Orthophoto, obtained with UAV, of Gunnarsbo boulder spread near Forsmark. Boulders are digitised. Boxes indicate detailed zoom in Figures 4-30 and 4-31.
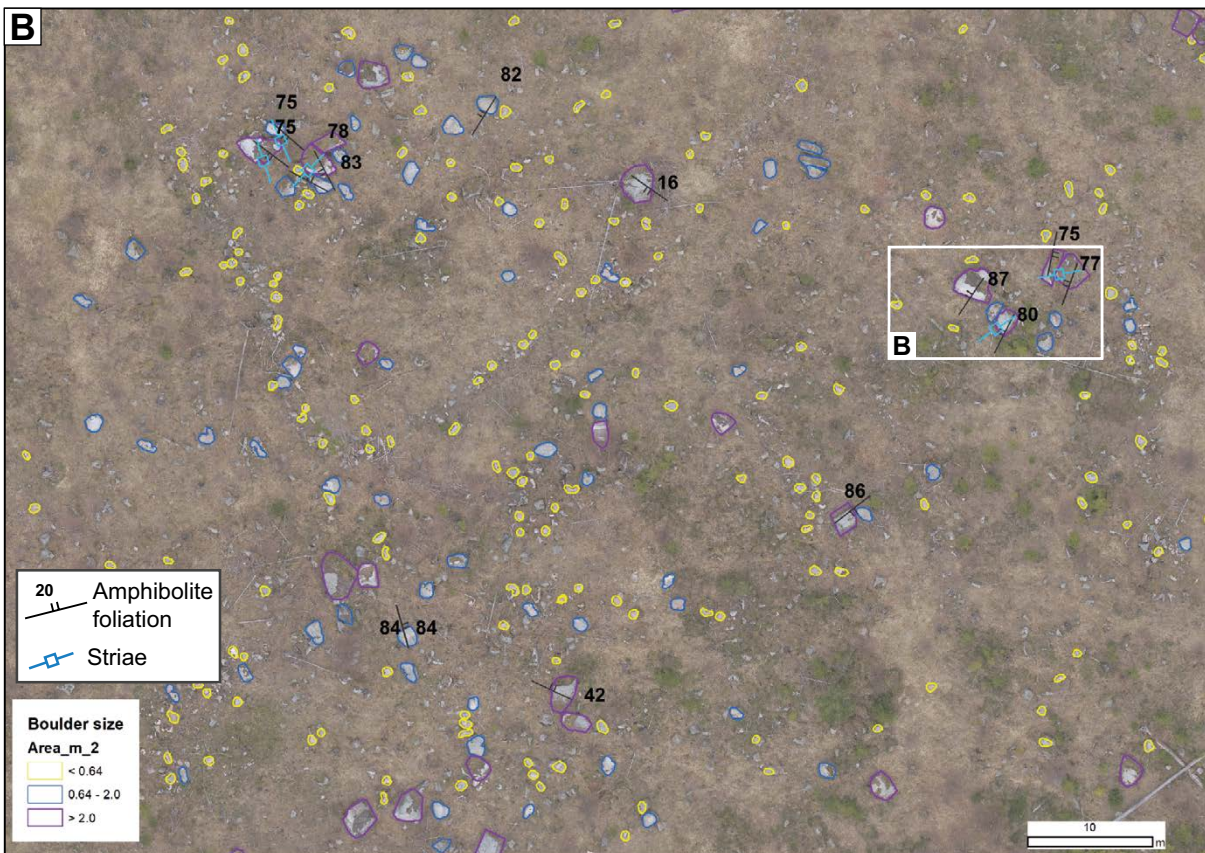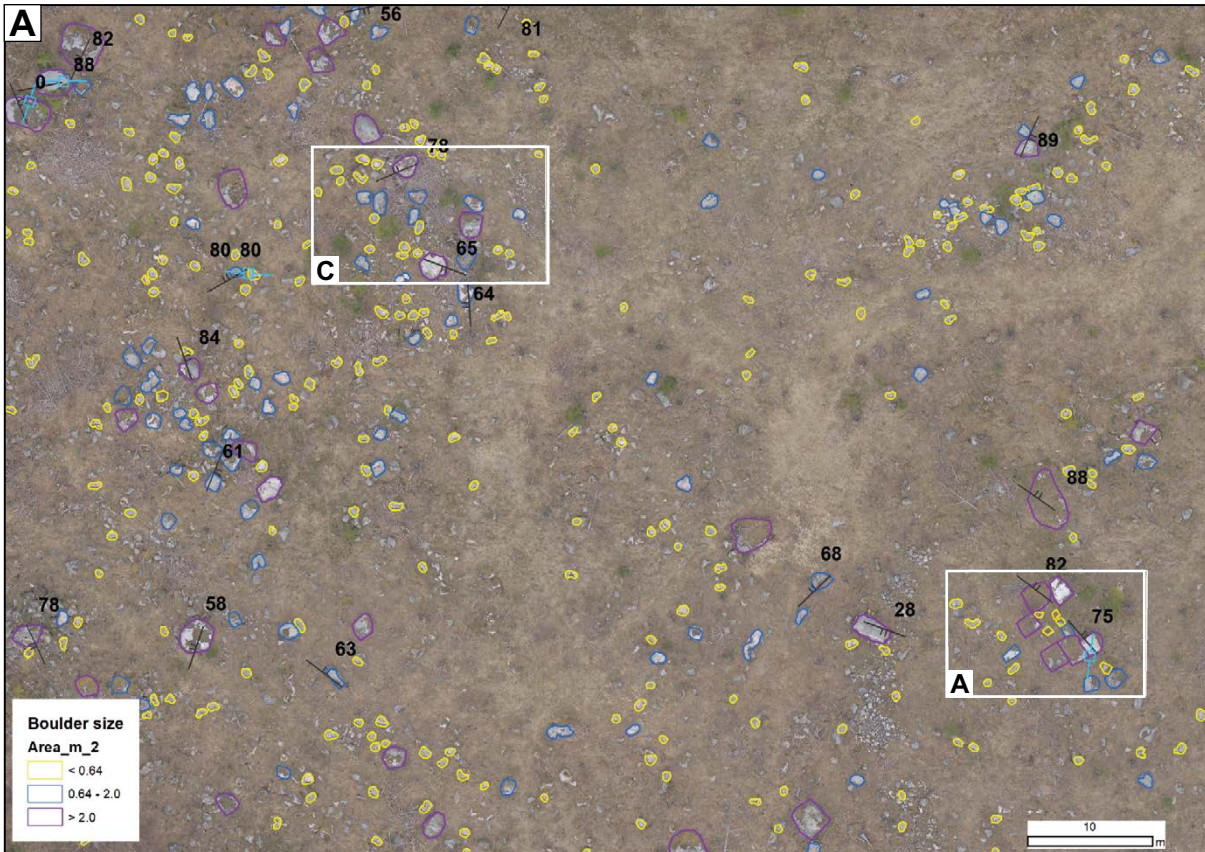
Figure 4-30. Detailed of Gunnarsbo boulder spread; orthophoto. Digitised boulders are separated by size (top surface area, in m²). Striae, measured on abraded surface of boulder, are shown and diverge from the regional SSE ice flow direction due to block rotation. Amphibolite foliation azimuth and dip are shown, and also diverge from the regional NNW-SSE trend. Boxes indicate detailed zoom ins in Figure 4-31
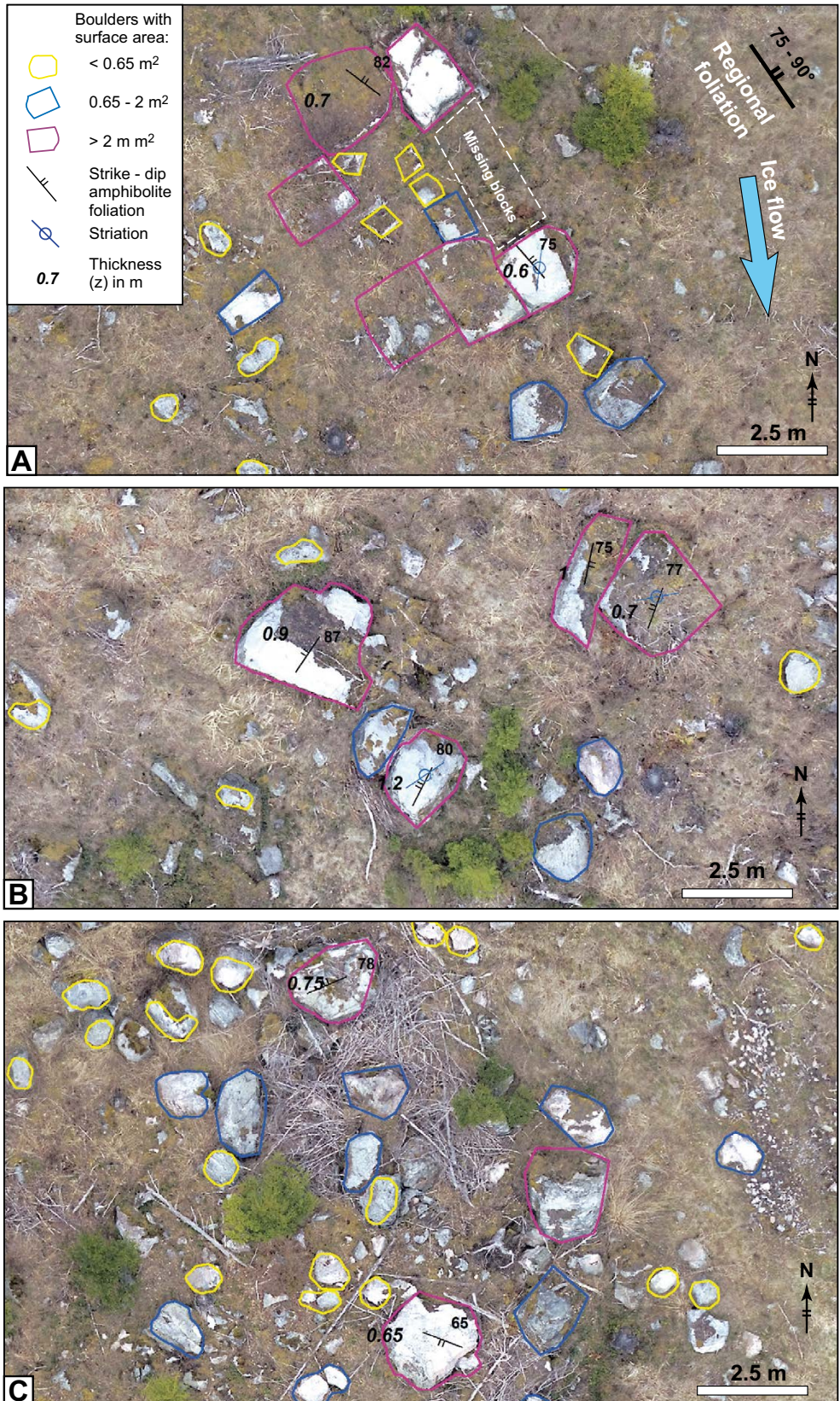
Figure 4-31. Details of orthophoto (obtained by UAV) of Gunnarsbo boulder spread. A. Near in situ cluster of blocks: blocks show no rotation, and only minor translation. Amphibolite foliation has same orientation as nearby in situ outcrops. Note missing block. B: Cluster of blocks with c. 90° rotations of amphibolite foliation and striae. C: Cluster of blocks with increasingly random orientations. Location shown in Figure 4-30.

Figure 4-32. *Gunnarsbo boulder spread, near Forsmark, field photos. A. Amphibolite boulder with abraded surface, striae, foliation traces and foliation plane indicated; abraded surface is right-way-up. B. Ditto, but abraded surface, striae and foliation trace has been rotated to steep orientation. C. Near in situ cluster of blocks: blocks show no rotation, and only minor translation. Note missing block. Location as in Figure 4-31A. D. Increasing rotation and displacement; two very different striae orientations on different blocks AS = abraded surface; FS = fractured surface. E. Increasing rotation and displacement, including toppling. F. Example of megaclast. Notebook is 20 cm long.*

The Gunnarsbo boulder spread comprises many boulders > 0.8 m across (B-axis), and some mega clasts 5–6 m across (Figure 4-29). Boulder density is < 25 % (Figure 4-27). The density heatmap (Figure 4-26G, H) shows patches of concentrated blocks that are nearby sources of intact bedrock.

Most boulders are subangular to angular. On most boulders, fracture surfaces with remnants of fracture coatings (e.g. chlorite, hematite, epidote) are still preserved; in many cases the formerly abraded surface with striations can also be recognised. Although some edge chipping has occurred, the overall edge rounding is thus minimal.

In some parts, clusters of blocks/boulders occur that can be 'fitted together' (Figure 4-31A, 4-32C). The orientation of the amphibolite foliation and the orientation of the striae on abraded surfaces show

only minor rotation (< 10–20°) compared to the regional ice flow and the amphibolite foliation on nearby *in situ* outcrops, such as 'Barrel Rock'. The top bedrock surface at the locality of Figure 4-31A, 4-32C) stands c. 1–2 m higher than of the surrounding boulder spread. Other clusters show more or less systematic rotations (Figure 4-31B, 4-32B), that is boulders appear all to be rotated c. 90°, and pairs of boulders can still be matched. Further transport is indicated by boulders with more random orientation, which includes rotation about horizontal axes, i.e. toppling (Figure 4-31C; 4-32E).

A train of amphibolite megaclasts (4–7 m across, similar to that shown in Figure 4-32F) extends from the boulder spread itself over the granite gneiss outcrop towards the SSE for c. 200 m (part is shown in Figure 4-29), suggesting longer transport distance for these larger boulders. Further, less dense boulder spreads lie to the south (Figure 4-28A; and Sohlenius et al. 2019).

Orientation analysis – Gunnarsbo

To assess transport and disruption, measurements were taken of the orientation of recognised abraded surfaces, any striations they carry, as well as the amphibolite foliation of the boulders. The orientation data (Figure 4-33) were compared to the orientations of striations and foliation on a nearby well-exposed, intact whaleback, 900 m to the SSE [N: 6700247 E: 673997]; informally termed 'Barrel Rock'), composed of amphibolite with similar character. In this outcrop, the high-grade ductile amphibolite foliation dips rather uniformly 225°/84° SW (dip azimuth/dip); i.e. a subvertical fabric striking NE-SW (135°-315°).
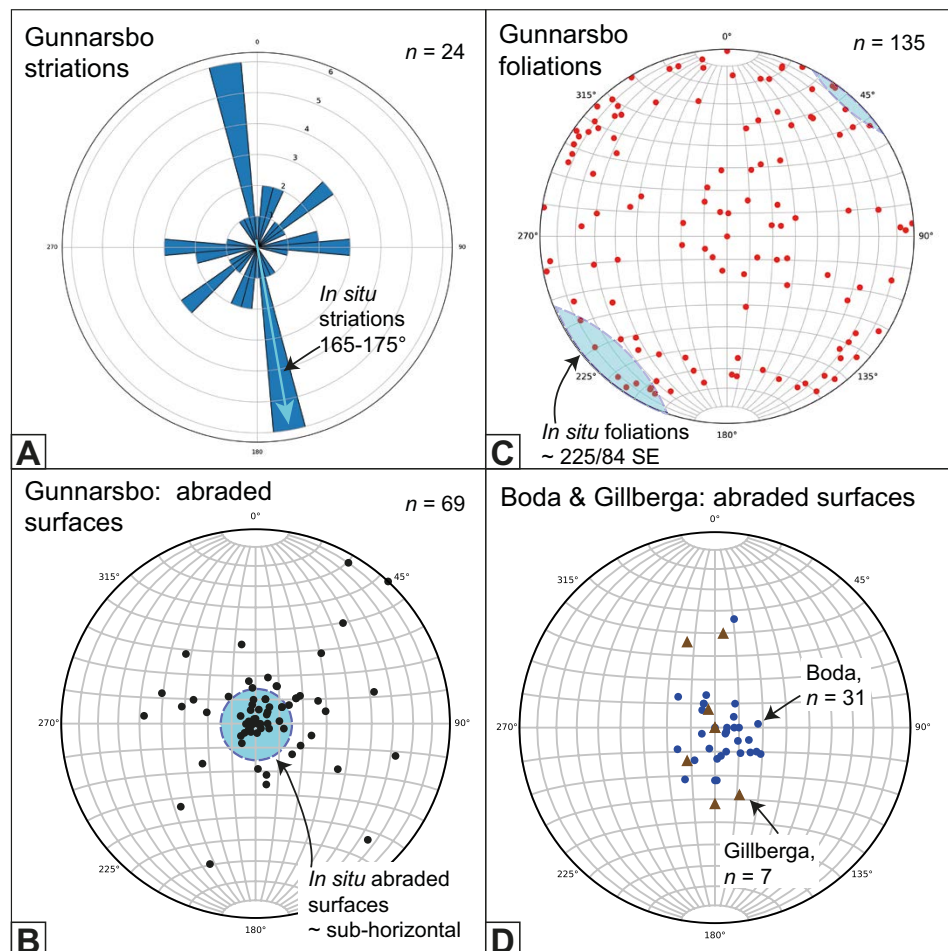
Figure 4-33. *Orientation data of Gunnarsbo boulders compared to in situ outcrop at 'Barrel Rock', and with blocks from disrupted roches moutonnées at Bodagrottorna and Gillbergagryt. A. Rose diagram of striations of boulders (dark blue – n = 24), with regional, in situ striations. B. Stereoplot with poles of abraded surfaces on boulders. Blue circle in centre is likely orientation of sub-horizontal and gently dipping abraded surfaces on in situ outcrops. C. Stereoplot with poles of amphibolite ductile foliations from boulders (red dots), compared with sub-vertical foliations of in situ amphibolite at 'Barrel Rock' (blue half circle). D. Stereoplot with poles of abraded surfaces on blocks from Bodagrottorna and Gillbergagryt. All stereoplots are lower hemisphere projection.*

Three dominant fracture sets occur: 1) subvertical with NW-SE strike; parallel to the ductile foliation; 2) subvertical with NE-SW strike; 3) a subhorizontal set; consistent with fracture mapping by Hermanson et al. (2003) on nearby sites. Glacial striae are oriented between 165–175° (consistent with Sohlenius et al. 2004), so that the glacial transport was c. 30° clockwise from the strike of the foliation.

Comparison between the orientations of the boulders with the *in situ* values (in blue on Figure 4-33) shows that surfaces with glacial striations have been rotated up to 90° (Figure 4-33A), but the number of observations is low (n=24). Abraded surfaces have been rotated up to about 50°, with very few abraded surfaces steeply dipping (Figure 4-33B). This likely reflects the difficulty of defining and recognising an abraded surface if the surface occurs on a steep or overhanging surface. Nevertheless, the rotations are substantially higher than the rotations of abraded surfaces from the disintegrated roches moutonnées at Boda and Gillbergagryt, see Figure 4-33D. Thus, although the striae and abraded surfaces do show rotations, the data is biased against rotations > 90°. In contrast, the gneiss foliations can be measured regardless of the rotation of the block, and show in essence a random distribution (n = 135; Figure 4-33C), demonstrating significant rotations of the boulders.

Gryttjen boulder spread

The Gryttjen boulder spread occurs as a small peninsula at c. 140 m a.s.l. in Lake Gryttjen, near Hybo, 40 km WNW of Iggesund (Figure 2-4A), on the floor and lower flanks of an east-west trending valley. Other boulder spreads extend along the lower flanks of the valley. This boulder spread with boulders of coarse augen gneiss is rather different from other boulder spreads in that all boulders touch each other (Figure 4-25B; 4-26A, B; 4-34A); it has the highest boulder density (approaching 70 %; Figure 4-27) and, in a sense, this boulder spread can be seen as transitional with a disintegrated rock surface. Boulders range in size < 1 to c. 6 m and are stacked, giving a thickness of the boulder spread > 6 m. All boulders are angular to very angular. Many boulders can be matched to each other, in that they share the same fracture surfaces, but have been moved 1–5 m with respect to each other. Abraded surfaces occur, commonly on top-surfaces, but locally rotated. Although no undisrupted bedrock was seen, it appears that the boulders are near *in situ*, with transport distances < 10 m.

A large, c. 20 m high moraine occurs c. 200 m down-ice (east) from the boulder spread. The moraine also comprises large boulders and megaclasts, set in a polymict matrix of smaller boulders, cobbles, gravel and sand, an observation showing on the one hand that some boulders were moved and deposited in the moraine, whilst on the other hand precluding that the Gryttjen boulder spread is a moraine itself.

Bladåker boulder spread

The Bladåker boulder spread is well exposed in a recently clear-felled area (Figure 4-34C, D), c. 1.5 km SE of the hamlet of Bladåker, along the Uppsala-Hallstavik road. It lies on the western edge of a much larger belt of boulder spreads on either side of Lake Vällen (Figure 2-4B). The boulder spread described by Lagerbäck et al. (2005) occurs 4 km farther east, but is now covered in young forest growth. The clear-felled area at Bladåker, measuring c. 200 × 200 m, comprises a series of low hills, with c. 8–10 m relative topography.

Boulders vary from < 0.8 m to 3–4 m, with a few larger megaclasts up to 6 m across; boulder density is overall < 10 % (Figure 4-26E, F; 4-27). The boulders are all of granite gneiss; no boulders of other lithologies were seen; boulders are subangular to angular. Fracture surfaces, recognisable by chlorite and/or epidote coatings, were widely observed, as well as abraded surfaces. Abraded surfaces on boulders have rotated 90° or more. Sets of closely-fitting blocks, typically forming small hills, suggest the local presence of disrupted but little-moved bedrock (Figure 4-34C, D).

On the south side (just north of the main road cut – see Figure 4-25C), the main hill (c. 23 m a.s.l.) is intact bedrock, with some boulders on top. This suggests that the existing topography is mainly derived from underlying bedrock, rather than of depositional origin. South and down-ice of the boulder spread there are sections showing poorly consolidated sandy, bouldery till overlain by large boulders (Figure 4-35).

Figure 4-34. *A, B. Gryttjen boulder spread. Near in situ, dense boulder spread. C, D. Bladåker boulder spread, granitic gneiss. Pronounced remnant relief of 5–8 m.*

Figure 4-35. *Section through immature, poorly consolidated sandy till with large boulders on top. 500 m SE of the Bladåker boulder spread. Sweref 99 TM N 6655065, E 682946. Persson (1985) describes similar localities in this area.*

Boulder spread near Bodagrottorna

Just south of the Bodagrottorna roche moutonnée there are two small boulder spreads (Figure 4-11B, 36A, B), which are elongated in a NNW-SSE direction and measure some 70 × 200 m. Most boulders measure 1–2 m (B-Axes), but a few are 4–5 m. All blocks are angular, and both abraded and coated fracture surfaces are seen (Figure 4-36C). On the northern side of the western boulder spread there is a stump of intact, *in situ* bedrock (Figure 4-11B), which is likely the remnant *in situ* bedrock hill from which the boulder spread originated. Boulder spread depth nearby is ≥ 1–3 m. The boulder density is < 30 % (Figure 4-26C) and shows a clear decrease in a SSE direction (Figure 4-11B), consistent with late glacial ice-flow direction, and consistent with a few megaclasts transported in a SSE direction from the Bodagrottorna roche moutonnée (Figure 4-11B). This boulder spread is in open, non-forested ground, and a clear lateral boundary can be seen on the ground (Figure 4-36B) and on the air photo (Figure 4-11B).

Skogbo boulder spread

The boulder spread near Skogbo, SE of Tierp (Figure 2-4A), is more dispersed than the other investigated boulder spreads (Figure 4-20E, 4-29D), with individual boulders locally tens of metres apart, and a density < 10 %. It was studied as it straddles a clear lithological boundary between amphibolite (down-ice) and felsic gneiss (up-ice). At Skogbo, boulder counts at measured distance from this lithological boundary show a clear trend (Figure 4-37): amphibolite boulders increase rapidly in abundance as ice moved from felsic gneiss over amphibolite. Nevertheless, felsic gneiss boulders remain present > 1.5 km from the nearest up-ice outcrop of felsic gneiss, so that individual boulders must have been transported by at least that distance. Shallow sections within the boulder spread show the occurrence of an immature rubble till, comprising sand, cobbles, gravel and boulders, which appears to underlie large parts of this boulder spread, although locally rock outcrops on low hills.
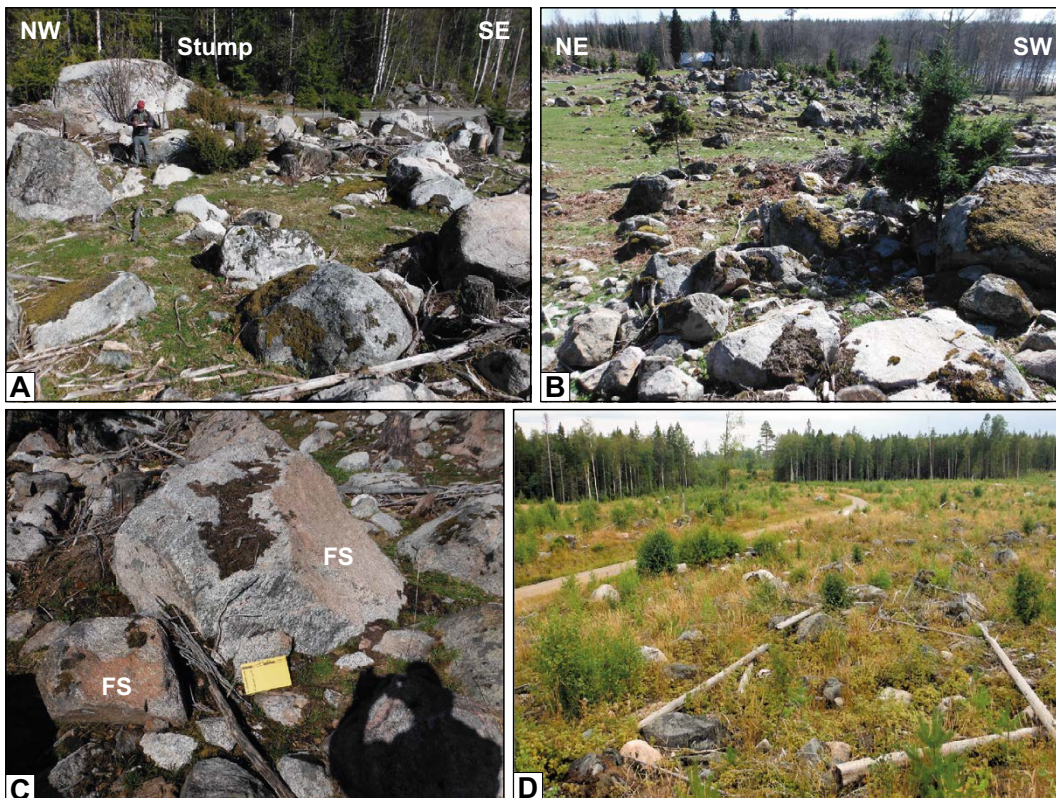
Figure 4-36. A, B, C. Boulder spread south of Bodagrottorna. A. View to NE; remnant in situ stump in the background. B. View SE (down-ice); lateral edge of boulder spread to left. C. Boulders with well-preserved fracture planes. D. Skogbo boulder spread, strongly dispersed, few large boulders.
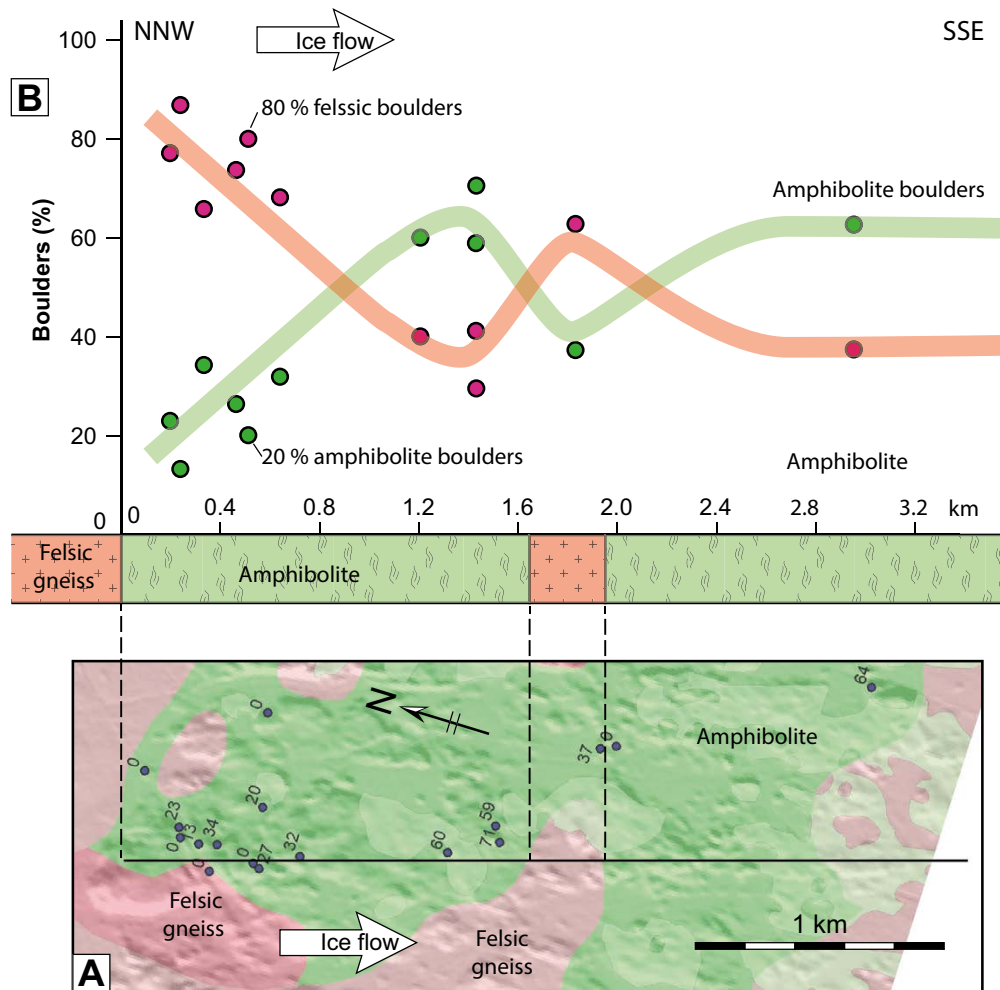
Figure 4-37. A: Geological map (after SGU mapping) of the boulder spread near Skogbo, SE of Tierp. The boulder spread crosses a clear lithological boundary of amphibolite and felsic gneiss. B. Diagram showing proportion of amphibolite/felsic gneiss boulders plotted against distance from lithological boundaries, shown at base.

Boulder spreads along the Börstil esker

Boulder spreads form a belt along the flanks of part of the Börstil esker, east of Forsmark (Section 4.3.2). This segment of the Börstil esker extends for 10 km from Trollgrundet in the north to Kallrigafjärden and from the southern shore of that fjärd to Vicklinge (Figure 4-38). It is typically a 3–4 m high and ~100 m wide ridge, esker sediments (sand and gravel) are ~5 m thick near Trollgrundet (Petrone et al. 2020). Boulder spreads occur on either side of the esker, for a combined width of 1–2 km (Figure 4-38, 4-39).

Where constrained, the boulder spread has a sharply-defined margin to terrain with undamaged, abraded rock surfaces. The boulder spread terrain has high surface roughness, compared to adjacent terrain (Figure 4-39C). The close spatial association of the boulder spreads with the esker suggest that the boulder spreads developed during the period of operation of the esker system.

Areas completely covered by boulders were identified at the islands of Lill-Tixlan and Stor-Tixlan (upper left in Figure 4-38). The boulder spreads are located close to bedrock exposures on the south-western slope of these islands, indicating that the boulder spreads have been transported a short distance from the original bedrock outcrops (Hedenström and Sohlenius 2008). The boulder spread at Kallriga comprises extensive covers of angular boulders, with occasional mega-blocks, and includes small bedrock outcrops. The density of boulders at Kallriga and Tixelfjärden appears to be highly variable, but is difficult to constrain, as some islands are densely forested, and it is not clear if boulders occur in deep water. Most boulders are in the 1–3 m range, with some megaclasts of c. 5 m across (Figure 4-40).
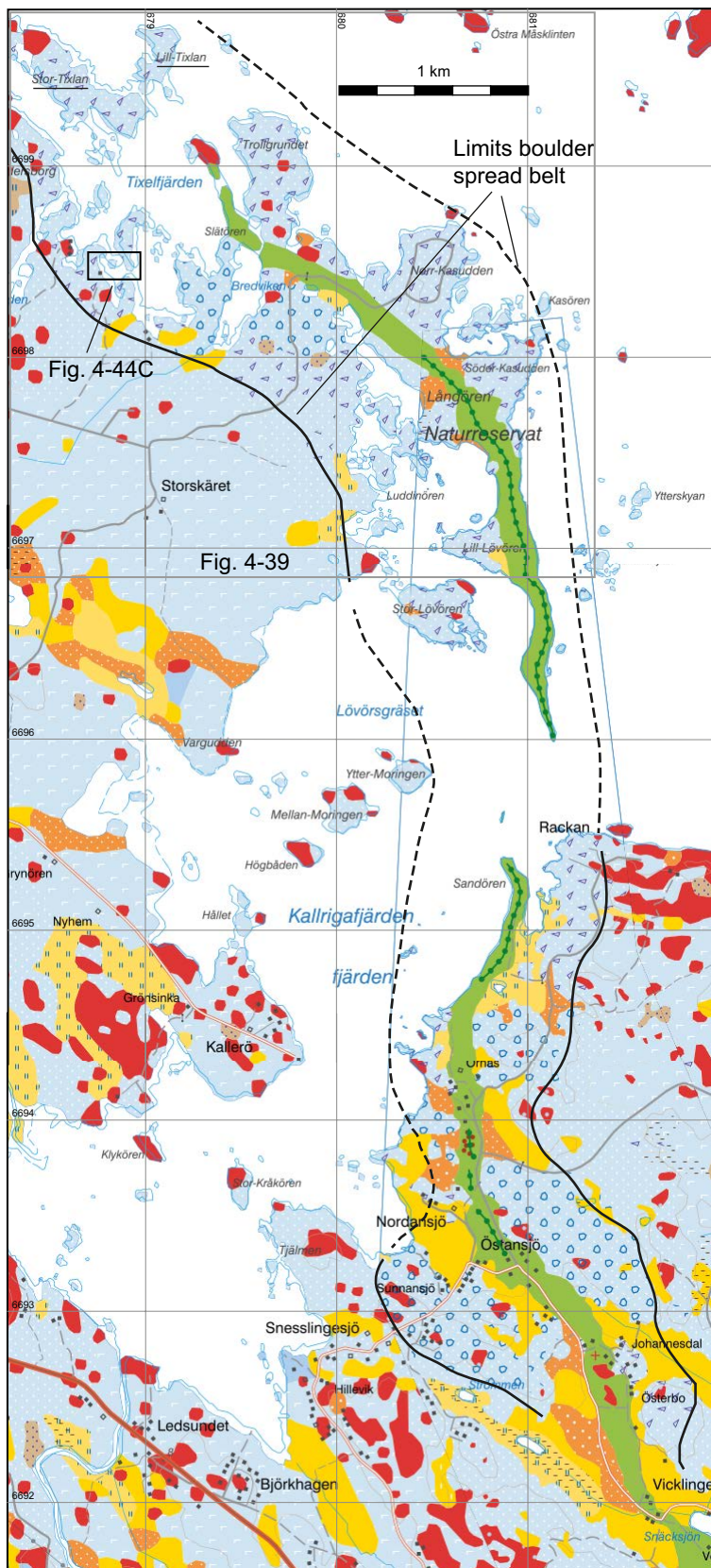
Figure 4-38. *SGU map extract for the northern section of the Börstil esker. The dashed lines indicate the boundaries of the interpreted meltwater corridor along the esker.*
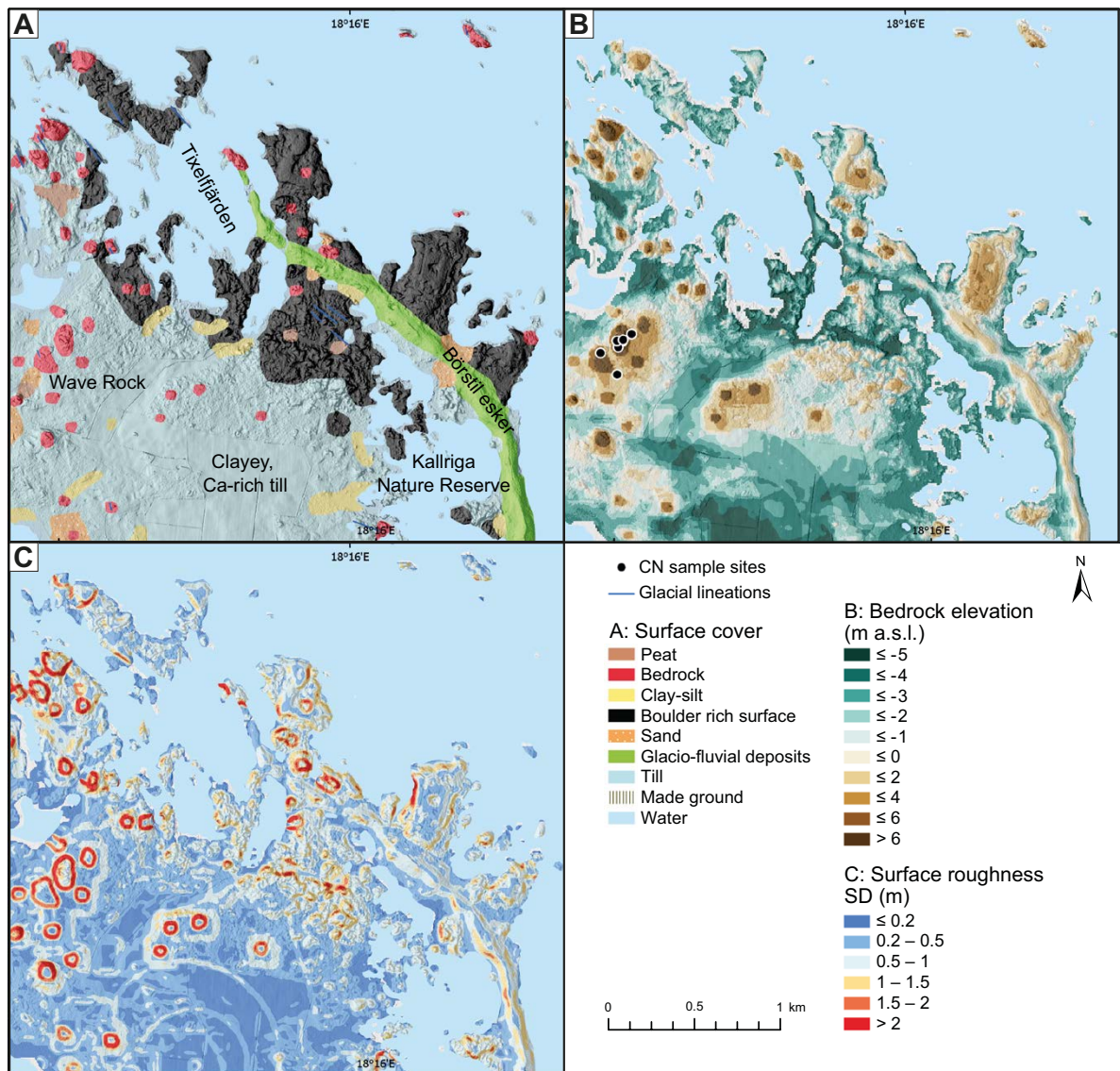
Figure 4-39. *The Börstil esker in the Kallriga Nature Reserve. A. Quaternary deposits from SGU data. B. Digital elevation model from Lantmäteriet data. C. Surface roughness model of the bedrock surface; SD in m; window size of 20 × 20 m. Circular edge effects derive from the thick till cover south of the Nature Reserve.*

At Örnäs, the esker deposits have flat upper surfaces, indicating truncation by erosion (Figure 4-40B). A 2 m-thick boulder spread with an area of 400 × 300 m overlies glaciofluvial gravel at Örnäs (N 6693324, E 681024). Boulder density is locally > 50 % and maximum boulder A-axis length is 8 m (Figure 4-40B). Several boulder spreads with similar areas occur on both sides of the esker separated by low ground with late- and post-glacial sediment cover (Figure 4-40C, D). Small roadside sections expose immature rubble till (for example at N 6694167, E 680864).

In the Börstil esker (boulder spread) corridor there are features that appear transitional appear between disrupted roches moutonnées and boulder spreads (Figure 4-41). At Österbo, south of Kallrigafjärden, quarrying of esker gravel has exposed a small roche moutonnée which shows dilated fractures and loss of rock blocks (Figure 4-41A, B). Around Tixelfjärden (Figure 4-39) there are a number small roches moutonnées in the shallow waters of Tixelfjärden which have been disrupted by hydraulic jacking and are partly or largely disintegrated, with missing lee-side blocks (Figure 4-41C–F). At an unnamed locality nearby (N 6698572, E 678757), roches moutonnées show pervasive lee-side disruption and boulder trains. Locally, a cluster of angular blocks is all that remains of a former small roche moutonnée (Figure 4-41C–F).

Interpretation

The relationships between the Börstil esker deposits and boulder spreads suggest that esker deposition occurred both prior and after boulder spread formation and boulder transport. Broadly speaking, they occur coevally, although the duration or timespan of neither esker deposition nor boulder spread formation is well constrained. The partial disintegration of the roches moutonnées around Tixelfjärden suggests that overpressured water was sourced from the esker system and extended outwards from an esker tunnel for distances of several hundred metres.

Boulder spread at Björklinge

Björklinge Quarry lies between at ~4 km distance from the Uppsala and Vattholma eskers. Air photos show boulder spreads in low relief terrain in the surroundings of the quarry (Figure 4-42A) with angular boulders of up to 4 m A-axis length (Figure 4-42B). In the NW corner of the corner of the quarry, the boulders rest on weakly-bedded till with sand interbeds (Figure 4-42C), immature rubble till (Figure 4-42D) and abraded rock surfaces (Figure 4-42E). Subhorizontal and vertical bedrock fractures are widely dilated to depths of 0.5–1.5 m below the rock surface, with fills of diamicton (Figure 4-4B, C).

Figure 4-40. A. Dense boulder spread of large boulders and megaclasts, near Tixelfjärden. B. General view of the boulder spread near or at Örnäs, at least 2 m thick with a step along its western and southern edges edge. The boulder spread extends south from a 350 m wide area of disrupted bedrock. Grassy area in the foreground comprises glaciofluvial sand and gravel. C. Small exposure at Örnäs on SE shore of Kallrigafjärden (60.33481 18.28099) showing boulder spread resting on glaciofluvial gravel. D. Excavation at Lindersvik at edge of Börstil esker: till/diamicton in foreground, sand and gravel in the background. Reproduced from Figure 4-4, Lagerbäck et al. (2005)
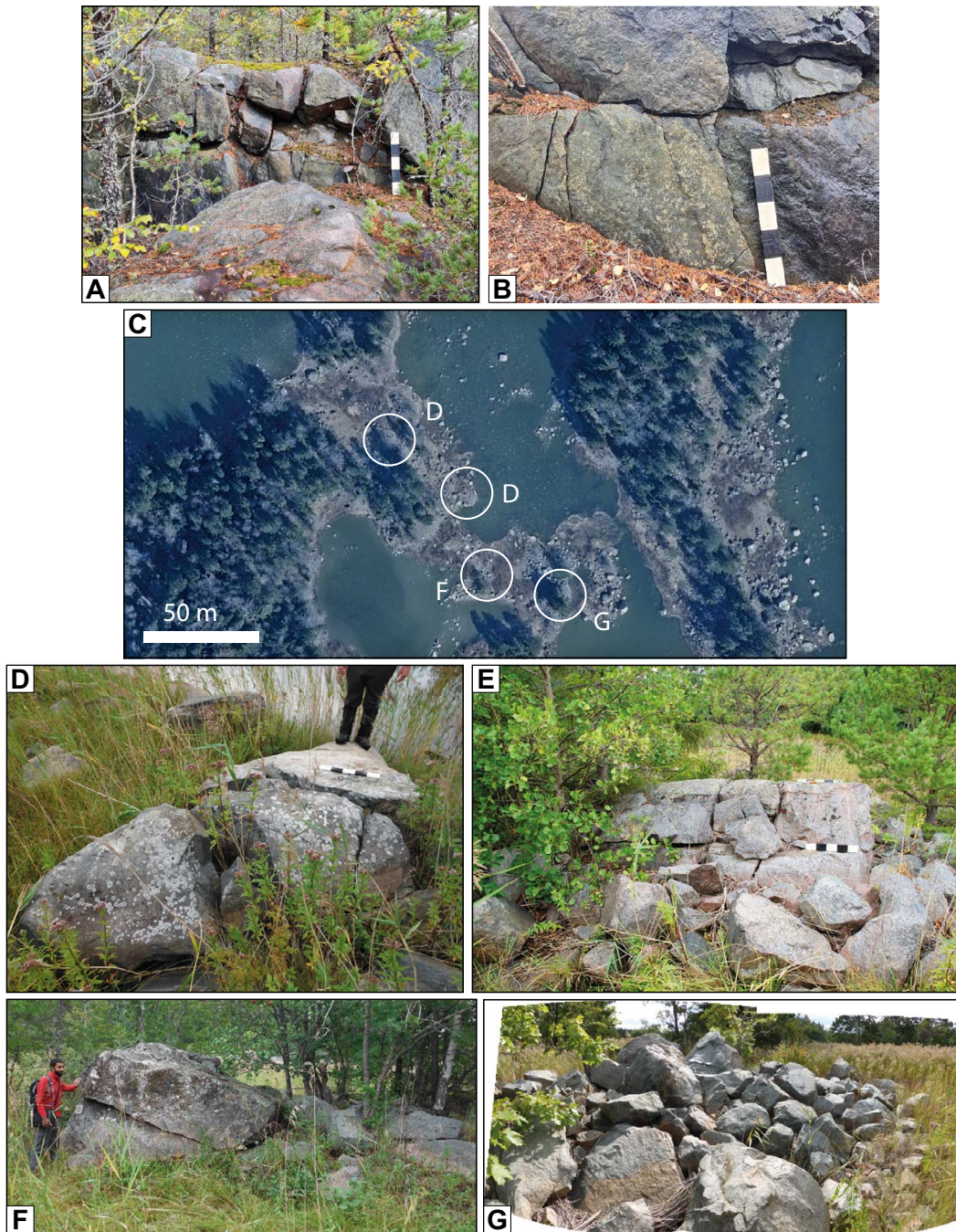
Figure 4-41. *Transitions between disrupted bedrock and boulder spreads: Tixelfjärden and Österbo. A, B. Dilated fractures in a small roche moutonnée formerly buried by esker gravel and now exposed after mining. Österbo [N6692590; E681423]. C. Air photo (Lantmäteriet) boulder spreads on-lying islands: circles refer to photo locations. D. Bedrock bump with abraded surface and dilated fractures broken into 4 blocks. E Bedrock bump with dilated fractures and missing lee-side blocks. F. Residual bedrock bump abraded top and missing flank blocks. Upper blocks moved 12 cm relative to lower block along subhorizontal fracture. G. Cluster of fitting blocks as remains of a former small roche moutonnée.*
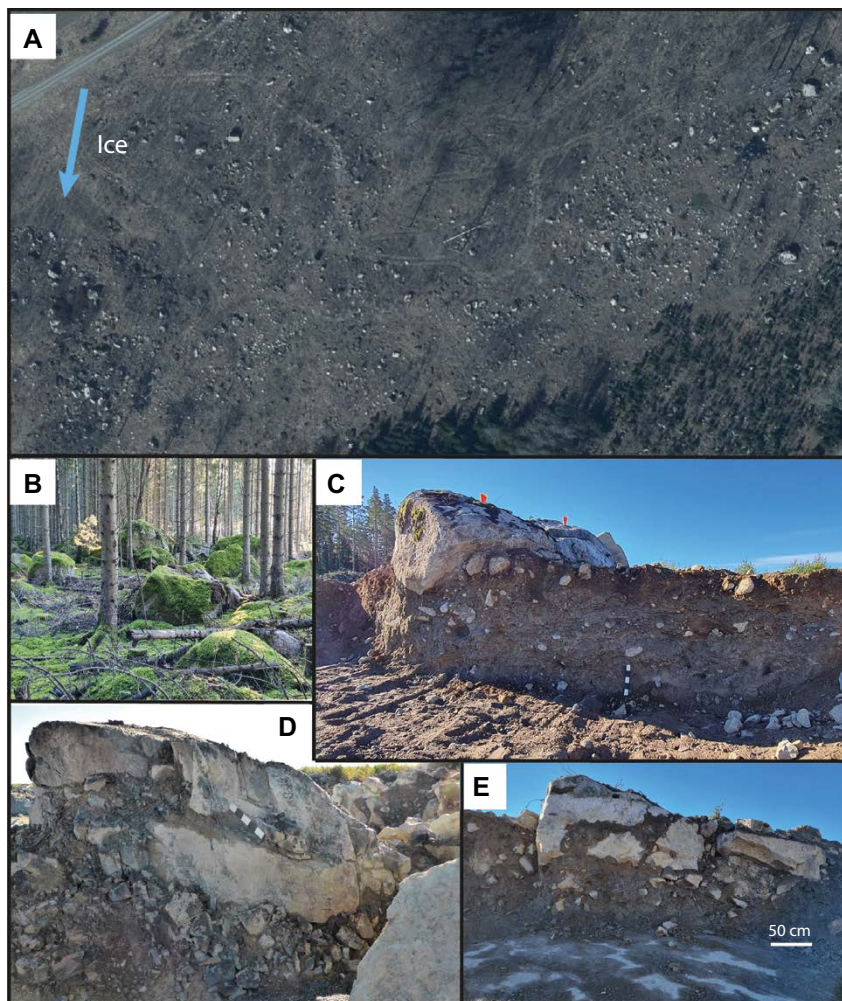
Figure 4-42. Boulder spreads and till facies at Björklinge Quarry, Uppland (N6654280, E647564). A. Boulder spreads on the SW edge of the quarry; air photo from Lantmäteriet after clear felling. Quarry sections C–E approximately 50 m NE of A. B. Boulder spread in forest on the NE edge of the quarry. C. Large boulder resting on layer of rubble till. D. Large boulder resting on rubble till with sandy silty matrix and an undisturbed abraded rock surface. E. Large boulder resting on subhorizontal, undulating beds of sandy slightly silty brown diamicton.

Boulder spread at Runtorp

At Runtorp, Kalmar, boulder spreads occur in an area of ribbed moraine set within a wide belt of hummocky moraine which, in turn, lies within Landscape A on Figure 4-18. Boulder densities are locally high (Figure 4-43A) and partly disintegrated roches moutonnées occur in forest north of the quarry.

Removal during quarrying of 0.5–1 m of till on the north edge of the quarry (Figure 4-43B) has exposed top surfaces of roches moutonnées showing dilated fractures and fracture fills of diamicton (2). A train of large subangular boulders at location (3) rest on a lower bed of gravel and sand overlain by 15 cm of rubble till (Figure 4-43C). The former soil surface is marked by the base of the zone of surface bleaching on the boulders (4). Beds of sand and gravel are deformed (5). A residual bedrock stump with fitting blocks shows dilated fractures (6). The ribbed moraine ridges are interpreted as formed in a subglacial position at some distance inside a land-based, retreating ice margin (Möller 2010). Deformation of earlier deposited sand and gravel deposits suggests high porewater pressures. The overlying boulder spreads were transported along with mobilised sediment for short distances at the glacier bed before deposition.
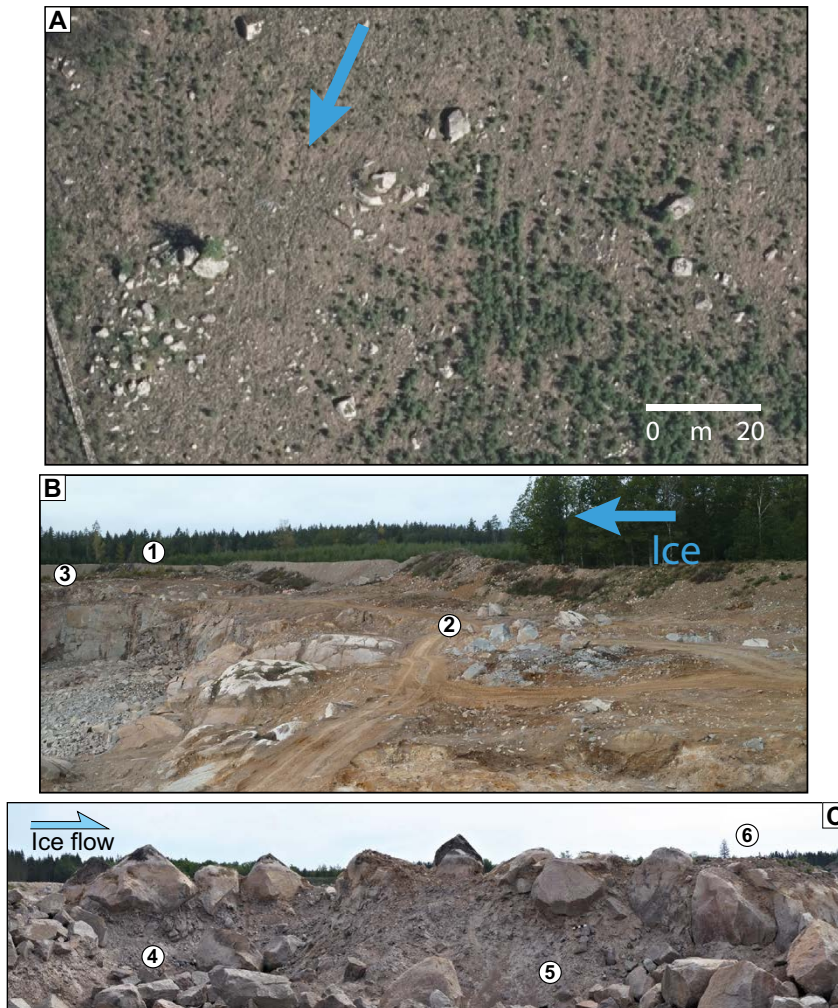
Figure 4-43. *Boulder spreads at Runtorp Quarry, Kalmar (N 6274411, E 560983). A. Boulder spreads on air photo from Lantmäteriet just W of Runtorp quarry. B. Looking W over a surface cleared of 0.5–1 m of till on the N edge of the quarry. (1). Location of Photo A. (2) Top surfaces of roches moutonnées showing dilated fractures and fracture fills of diamicton and partially disintegrated surface. (3) Location of photo C. C. Section in a train of large boulders. (4) Deformed gravel and sand overlain by rubble till and large angular boulders. Surface bleaching on boulders marks former soil surface prior to quarrying. (5) Deformed beds of sand and gravel. (6) Bedrock stump with dilated fractures. Dilated, sediment-filled fractures in same the quarry exposures shown in Figures 4-2E and F.*

4.3.5 Boulder dispersion and constraints on transport distance

The transport distance of the boulders in boulder spreads can be constrained by different lines of evidence. The range in boulder density from near complete cover at Gryttjen to the much more dispersed boulder spreads such as at Skogbo (Figure 4-26; 4-27) suggests that boulder transport is variable. At Gryttjen, boulders can still be matched and almost completely blanket the ground (Figure 4-26A): transport distance here is < 10 m. At Bodagrottorna, the boulder spread is attenuated in a SSE direction, with an original *in situ* stump at the northern end (Figure 4-11B; 4-26C). This suggests a transport distance of c. 200 m, but this should be regarded as a maximum, since the original bedrock outcrop would have extended further southward from the stump.

The Gunnarsbo boulder spread is dominated by amphibolite boulders and occur largely on the mapped occurrence of amphibolite bedrock. In the up-ice direction, this mapped occurrence extends for c. 3 km (Figure 4-28), which represents an absolute maximum transport distance. A c. 8 m deep peat-filled hollow c. 50 m up-ice from the boulder spread potentially makes a hill-hole pair like arrangement. However, the area between the hollow and the boulder spread shows very few boulders, suggesting that the peat-filled hollow is *not* the source the boulders, and also renders unlikely the possibility that

the source was further up-ice. The near *in situ* bedrock block cluster at Gunnarsbo (Figure 4-31A; 4-32C) suggests transport < 5 m (similar bedrock block cluster occurs at Tixelfjärden), whereas other clusters with larger rotations suggest more transport (tens of metres). The largest transport distance appears to be from megaclasts, a trail of which extends c. 200 m southward from the boulder spread (Figure 4-29). Altogether this suggests that the boulder spread largely covers its own source, with transport distances between 5–100 m, with a minority of (larger) boulders being transported further.

At Skogbo, a well-mapped lithological amphibolite/felsic gneiss contact constrains transport distances: this suggests transport distances of at least 1.5 km of some felsic gneiss boulders (Figure 4-30). However, Skogbo is the most dispersed boulder spread (< 10 % density), which suggests that less dispersed boulder spreads have a smaller transport distance, in the order of tens to hundreds of metres. This compares with till clast transport half-distance of ~3.5 km in this area (Lindén 1975), implying that relatively mature till was transported further than the boulder spreads and associated immature, poorly consolidated 'rubble' till.

4.3.6 Boulder spreads as stratigraphic units

Where sections are exposed, boulder spreads are typically between 1–2 boulders thick. In the Gryttjen boulder spread, the boulder spread is dense and comprises openwork, stacked boulders only, but this is arguably an exceptional case. In more dispersed boulder spreads, the boulders may be clustered or occur singly. The boulders may be (partially or wholly) embedded in immature rubble till. The different compositions and grain-size distribution of the boulder spread and associated rubble till may in part link to the block size in the rock hill or low-relief rock surface from which the boulders are sourced. In large roches moutonnées with wide fractures spacing, the rock blocks generated by jacking and disintegration are large and generate mega-boulder trains. (In some cases, e.g. Gunnarsbo and Boda, it appears the megaclasts travelled further than smaller boulders, possibly because the latter are impeded by being partially embedded in rubble till). On smaller hills with smaller rock block sizes, or where hydraulic jacking resulted in brecciation, disintegration generates bouldery rubble with small, angular clasts sourced from the most closely spaced fractures. Where existing till was mobilised with rock then rock boulders are locally encased in, or rest upon, diamicton, as at Björklinge and Runtorp (Figure 4-42; 4-43). However, the number of complete sections that show boulder spreads with immature till down to bedrock are limited, and more and different sedimentary associations are described in SGU regional reports (e.g. Persson 1985, Svantesson 1991, Möller 1993).

4.3.7 Morpho-stratigraphic relationships with other glacial deposits

In this section we consider the relationships between boulder spreads and till cover, eskers and moraines, which is relevant for establishing their relative timing of deposition. We focus on case studies near Forsmark and in Gävleborg.

Forsmark: relations with till

Till depths at Forsmark are variable (Figure 4-44). Three till areas have been mapped in the area SE of Forsmark, each with till with different characteristics (Hedenström and Sohlenius 2008). Till Area I is in weakly streamlined terrain where sandy till typically forms the upper till layer and till tails to hills. Parts of the target area show evidence of fracture dilation and rock brecciation below thin till (Leijon 2005). Boulder spreads are not widespread (Figure 4-44). Erratic boulder petrography indicates a transportation direction from north-west and an approximative transportation distance of 0.5–2 km (Bergman and Hedenström 2006). Till Area II comprises mainly clayey till, with rounded boulders: in places it comprises a very hard, thick (up to 5 m) calcareous till with a high content of Palaeozoic limestone in the gravel fraction (Bergman and Hedenström 2006, Hedenström and Sohlenius 2008)). Erratic boulder petrography of metamorphic boulders indicates transport from north-west over a distance of 3–8 km. This till occupies a large flat area south of the Börstil esker and is also found as a basal unit in excavations elsewhere (Albrecht 2005). Boulder spreads are not widespread in Till area II (Figure 4-44). Till Area III contains boulder spreads that flank the Börstil esker at the Kallriga Nature Reserve, described in some detail in Section 4.3.4. The frequency of bedrock outcrops is low within Till Area III; the petrographical composition of the boulders, dominated by metagranite, is similar to the local bedrock (Bergman and Hedenström 2006). No till unit is reported or observed to overlie the boulder spreads.

Till Area I includes several sites where temporary excavations revealed that till-covered rock surfaces are extensively hydro-fractured and dilated fractures are filled by water-lain sand and silt, described in Section 4.1.3. The till cover may have protected the rock surfaces from the effective application of tractive forces from sliding glacier ice, preventing further disintegration. In the western belt of boulder spreads at Forsmark (Figure 4-44), no till units are observed to overlie boulder spreads. However, residual till hummocks with boulder covers occur with the boulder spread at Gunnarsbo.

In summary, at Forsmark, the relationships between till covers and boulder spreads indicate that: (i) till tails and till cover were not widely removed from weakly streamlined terrain in Till Areas I and II during deglaciation, (ii) till was absent or removed in areas with boulder spreads, (iii) no younger till unit was deposited after the boulder spreads formed, and (iv) some areas of continuous stiff till cover do not show boulder spreads.

Gävleborg: relations with moraines

Near Forsmark, only some low, poorly defined low moraine ridges occur (Section 4.3.4) and relations with boulder spreads are difficult to established. Further north in Gävleborg county more moraines occur associated with boulder spreads. The eastern edge of Lake Örasjön, 9 km east of Ramsjö (Figure 2-2A), lies above the marine limit and shows a number of 5–7 m high hummocks and ridges at right angles to local ESE-directed ice flow (Figure 4-45A, B). The ridges here are short and irregular in shape, but show a distinct asymmetry, with a down-ice slope steeper than the up-ice slope. The ridges are largely or wholly constructed of sub-angular boulders 1–4 m across, with no sand and gravel fraction observed in the upper 2–3 m (no section was available for study). The ridges are mapped as moraines by SGU.
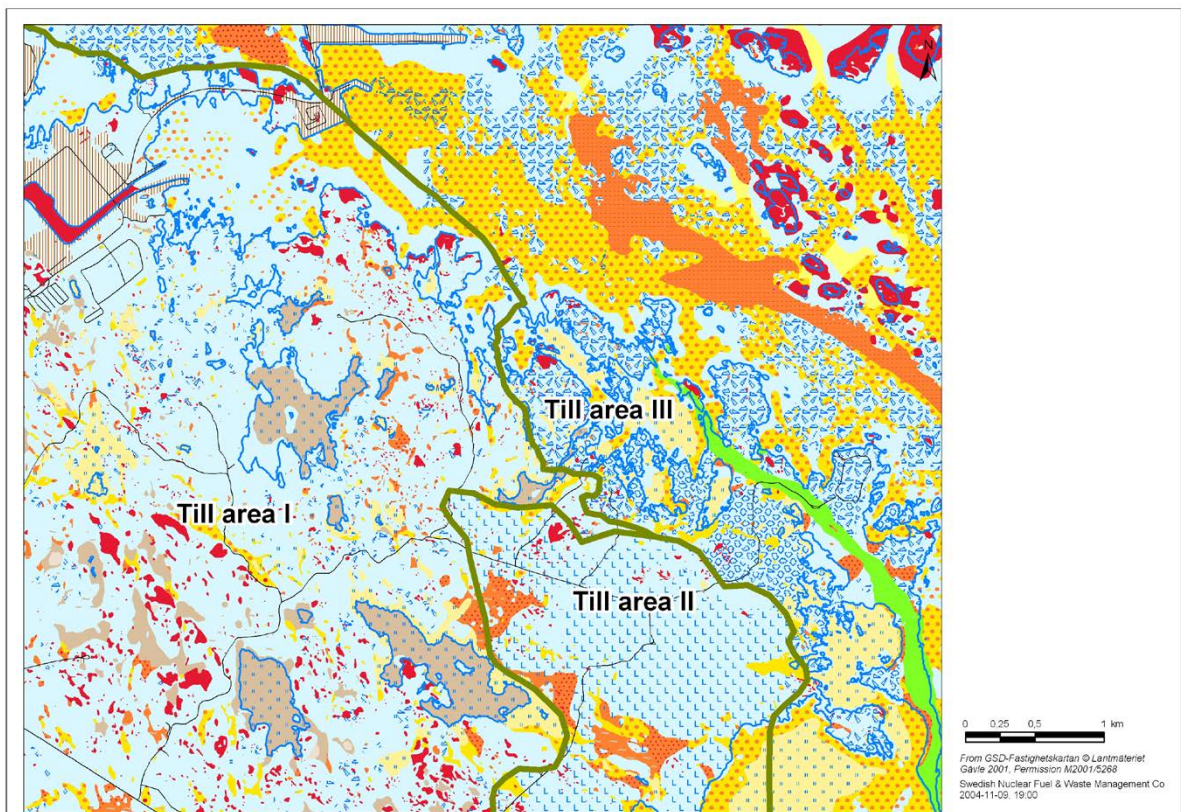
Figure 4-44. *Till areas between Forsmark and Kallrigafjarden, as mapped by Hedenström and Sohlenius (2008). Figure 5-13 in SKB R-08-04. Till area I has sandy till with a medium frequency of superficial boulders dominates. Till area II is dominated by Ca-rich clayey till. Till area III, flanking the Börstil esker, is characterised by a high frequency of large boulders.*
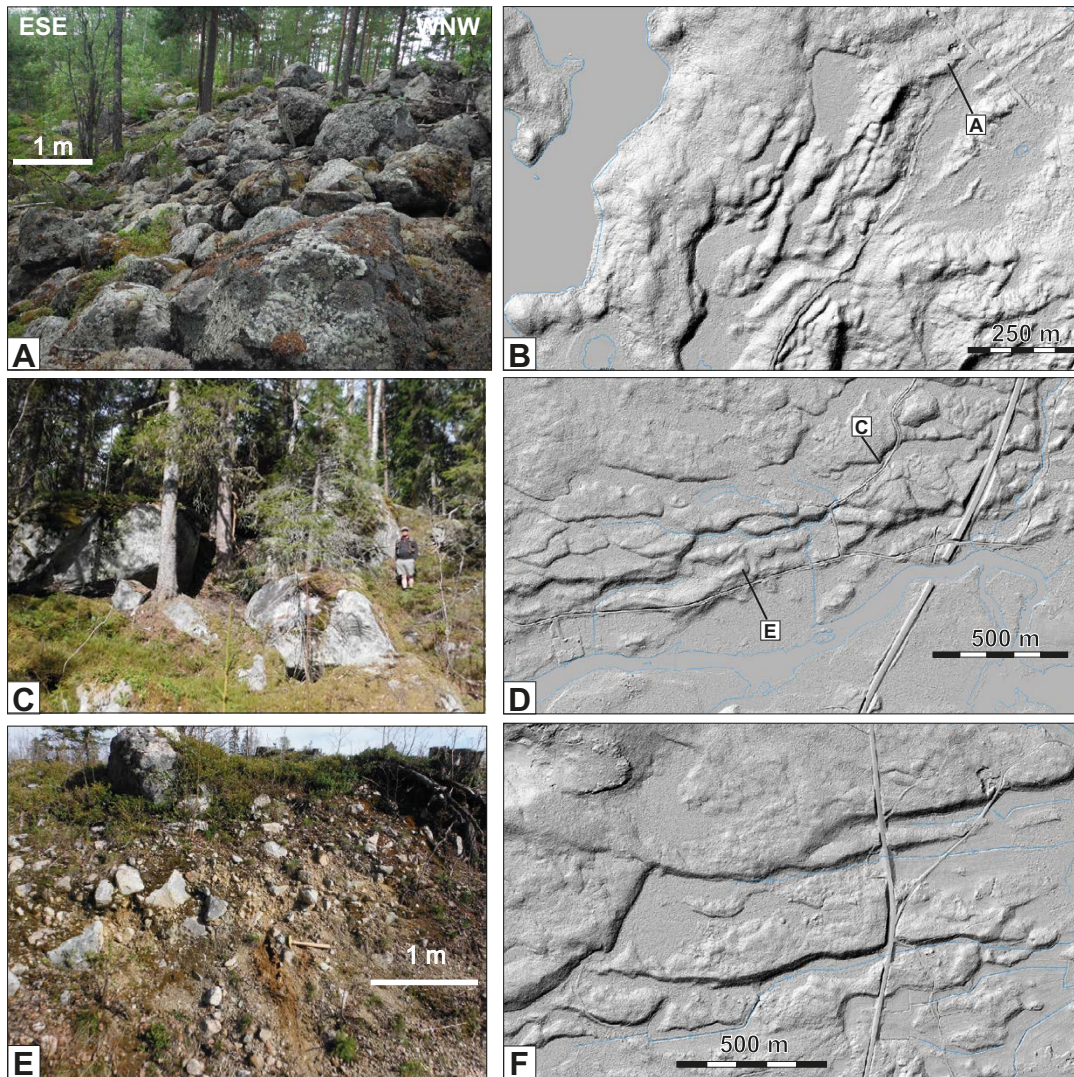
Figure 4-45. *Hill shaded relief maps and outcrop photos of moraines composed in part of large boulders. Location of photos indicated on the relief maps. A: Leeside of 5–6 m high moraine ridge, comprising metre-sized boulders; east of Lake Örasjön, 9 km east of Ramsjö. [E 543297; N 6892378]. B: Asymmetric moraine ridges; east of lake Örasjön. C: Moraine of boulders and mega clasts, up to 6 m high; west of Iggesund. [E 607090; N 6839192]. D: Asymmetric moraine ridges; west of Iggesund. E: Poorly sorted deposit of sand, gravel, cobbles and boulders, with larger boulder on top, in moraine ridge. [E: 606597; N 6838812]. F: Asymmetric moraine ridges; Rösånger, south of Iggesund. Hill shaded relief maps downloaded from Lantmäteriet.*

Three km WNW of Iggesund, a series of E-W and NE-SW trending ridges occur, north of a shallow valley. The ridges are 5–15 m high, and 0.1–2 km long, and typically 100–200 m wide (Figure 4-45D). The ridges are asymmetric, with a gently dipping stoss-side slope and a steeper lee-side frontal slope, like a transverse scarp (Figure 4-45D, F). Some sections of the scarps are developed on flanks, and scarps are locally curved. The ridges are in part covered by, and composed of, large boulders and megaclasts; the scarps are also normally composed of or draped by boulders (Figure 4-45C), but sporadic sections show that some ridges are mainly composed of poorly sorted deposit of sand, gravel and smaller boulders, with larger boulders concentrated at the top (Figure 4-45E). The ridges are mapped as moraines by SGU.

Six km S of Iggesund, near Sätra, a series of similar asymmetric E-W oriented moraine ridges occur that show boulders 1–4 m across that cover the surfaces or drape transverse scarps Figure 4-45D. Road cuts show that the cores of the moraine ridges are composed of sandy tills with small boulders.

At Bodarna, 800 m W of Bodagrottorna roche moutonnée, a small quarry occurs in the flank of a landform, characterised by a flat top and a curved, down-ice scarp comprising a c. 5 m high boulders pile (Figure 4-46A, B). The quarry has exposed a lower, stiff till with a sandy silt matrix and an upper, loose, bouldery rubble till with a sandy matrix (Figure 4-46C). Large angular boulders drape the scarp face. Large boulders (B-Axis 2–5 m) occur on top of the landform and drape the down-ice scarp.
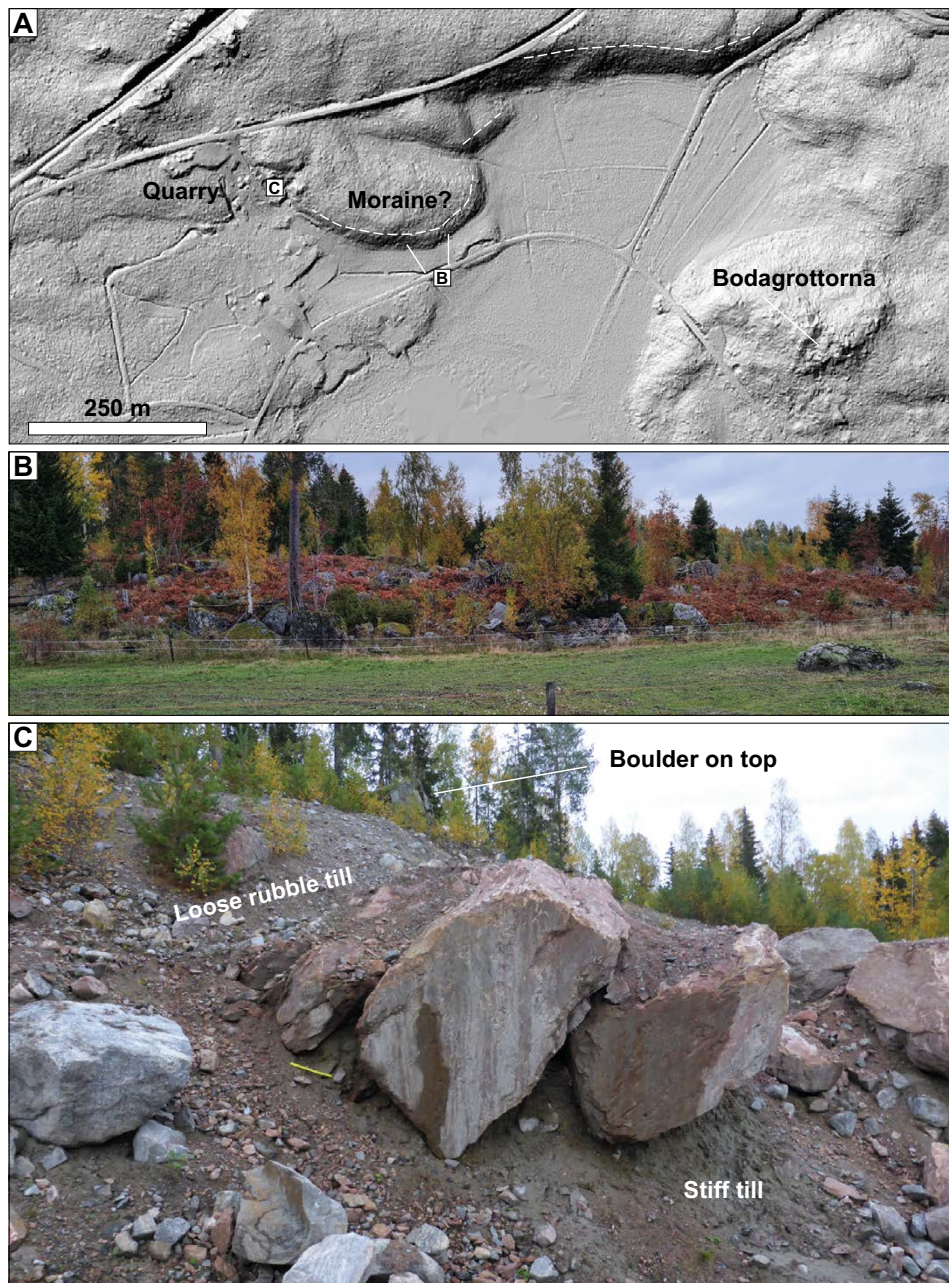
Figure 4-46. Bodarna Quarry, Iggesund. A. Overview of terrain (Lantmäteriet DTM), showing sharp down-ice scarps including the lee-side cliff of the Bodagrottorna roche moutonnee (0.75 km W). B. Up-ice view of boulder spread with fitting blocks indicating a bedrock core. C. Quarry cut with lower stiff till and an upper loose sandy till with a mix of angular and subrounded clasts up to boulder size. Large boulders occur on the surface and drape the steep slope.

The ridges near Iggesund and at Bodarna can be interpreted in different ways. (i) They are terminal (subaqueous) moraines and depositional features, with the frontal scarp comprising boulders and with boulders reworked on top and in front of the terminal moraine. (ii) The moraines were originally boulder-covered ribbed moraines, developed further up-ice with respect to the ice-margin, and the scarps are erosional features, formed by 'tear-away' of rock and till during glacial ripping. Similar ridges and traverse scarps are frequent to the west and south of Iggesund. In that case they may form part of a meltwater corridor: Vérité et al. (2022) noted associations of ribbed landforms, murtoos, hummocks and eskers in interpreted meltwater corridors in Finland and southern Sweden. Both scenarios require the reworking of large numbers of boulders from boulder spreads during deglaciation. Hence, whichever is the correct interpretation, the boulder spreads were formed as subglacial features.

Summary of relations to other deposits

Boulder spreads are commonly associated with rubble till, suggesting a common origin (Section 4.3.6). Both boulder spreads and rubble till are observed widely to overlie older deposits, including clay-rich and sandy tills, for example at Forsmark and at Bodarna (Section 4.3.7.1 and 4.3.7.1). However, younger till layers have not been observed overlying boulder spreads. Glaciofluvial sand and gravels are overlain by boulder spreads alongside the Börstil esker (Section 4.3.4.6), indicating deposition during operation of the esker system. However, the highest sections of the esker ridge likely representing the youngest esker deposits, rest on boulder spreads and lack boulder spread covers on the crest, suggesting the latest esker deposition occurred after boulder spread deposition. Ribbed moraines are overlain by boulder spreads. Terminal moraine ridges ridges and locally De Geer moraines (Svantesson, 1991) incorporate boulders reworked from boulder spreads. Altogether this suggests boulder spread deposition occurred subglacially, at various distances behind the ice margin, consistent with the limited transport distances (Section 4.3.5).

4.3.8 Summary characteristics of boulder spreads

The main characteristics of boulder spreads may be summarised as follows:

1. Boulder spreads extend for > 500 km along the length of eastern Sweden but are discontinuous and patchy. Individual boulder spreads vary in extent from 100 m^2 to > 50 km^2. In Uppland, boulder spreads occur in 2–10 km wide belts and patches that lie broadly parallel to former N-S ice flow.

2. Individual boulder spreads comprise many (n > 100–1 000) boulders and occasional mega-clasts. Boulder density varies from complete cover (> 60 % aerial extent; Gryttjen) to very dispersed (< 5 % aerial extent; Skogbo).

3. Boulders are angular to subangular, locally subrounded. Normally, > 95 % of boulders in a boulder field are of the same lithology. Typically, < 5 % of boulders are of different lithology; these represent normal glacial erratics with larger transport distances. Such erratics are more rounded, and also commonly smaller (< 1 m).

4. In many boulder spreads (e.g. Gunnarsbo, Bladåker), boulder facets with abraded surfaces with striae are readily recognised, and easily distinguished from planar fracture surfaces, which commonly still show fracture coatings, such as chlorite, epidote and iron staining. Non-horizontal attitudes of abraded surfaces with striations attest to rotation of blocks, which increases with increasing transport distance.

5. Within boulder spreads, undamaged rock outcrops are normally small in area. Many precursor roches moutonnées and whalebacks may be partially or wholly disintegrated within a single boulder spread (e.g. Bladåker, Gunnarsbo). Where seen in section below boulder spreads, the bedrock surface may show dilated fractures and disruption (Runtorp, Björklinge).

6. Boulder spreads occur as thin (1–4 m) sheets (Örnäs), and trains (Boda) often with sharp boundaries (Börstil, Bladåker).

7. Internal sedimentary properties vary from openwork, stacked boulder layers (Gryttjen) to spreads of isolated boulders (Skogbo) and boulder trains (Boda). Boulders seen at surface may be embedded in immature rubble till likely derived from disintegration of local bedrock (Bladåker) or in diamicton reworked from or representing earlier sediment (Björklinge, Runtorp).

8. Boulder spreads locally overlie older, subglacial clayey till. Some boulder spreads were deposited during the operation of esker systems but before the deposition of terminal moraines. This suggests subglacial deposition close to the ice margin, locally associated with subglacial meltwater corridors. Other boulder spreads, however, do not show a close association with eskers or other meltwater landforms.

4.4 Transitional cases between precursor forms, dilated fractures, disrupted bedrock and boulder spreads

The three features that provide evidence for glacial ripping (dilated fractures, disintegrated roches moutonnées and boulder spreads) have up to now been treated as separate features. However, if they are linked in the three-way process sequence of jacking, disintegration, and transport, (Hall et al. 2019a, 2020, Krabbendam et al. 2022) then some transitional cases should occur, at least locally. The Gryttjen boulder spread has very short transport distances and virtually no dispersion (Section 4.3.4), and can be seen as a transition between disrupted bedrock and a boulder spread. Four more transitional cases are described below.

4.4.1 Transitional case between open and dilated fractures – Lövstalöt

At Lövstalöt, 12 km N of Uppsala (Figure 4-19), low-relief rock surfaces are exposed in a rock quarry (granitic gneiss) adjacent to the Uppsala esker. SKB Quaternary maps indicate that the nearest boulder deposits lie 2 km to the east. The granite gneiss has extensive, low relief, abraded surfaces which remain unaffected by hydraulic jacking and disruption (Figure 4-47A). A section through a roche moutonnée buried by till shows that long, open, inclined and subhorizontal fractures delimit rock lenses and individual rock blocks (Figure 4-47B). A second section, further south (Figure 4-47C), shows a rock mass with similar fracture patterns where the upper 1–1.5 m of the rock mass shows dilated fractures above open fractures. This quarry exposes transitions between precursor low-relief rock surfaces shaped by abrasion and plucking only, and damaged rock surfaces that record the onset of hydraulic jacking in the shallow rock mass. The pattern of open fractures in the buried roche moutonnée suggests potential routeways for water entry and lines of decollement for block detachment and removal under subglacial traction.

4.4.2 Transition between fracture dilation and disrupted bedrock – Tönnebro

A transition between sediment-filled dilated fractures and disrupted bedrock was observed in a rock aggregate quarry in augen gneiss on the lee-side of a 20 m high hill, north of Tönnebro (location on Figure 2-2A). The gentle slope above the quarry shows a set of ribbed moraines with overlying boulder spreads; a large esker lies 0.8 km E. The section exposes sediment-filled, open, subhorizontal fractures that indicate jacking to a depth of 8 m. Although lack of safe access prevented detailed structural and sedimentological analysis, the following sedimentary units can be discerned (Figure 4-48A, B; top downward):

A. An uppermost unit that comprises large (> 0.5 m) boulders only, in essence part of the boulder spread found further east of and above the section;

B. A disrupted mass of bedrock with numerous open fractures, c. 3×8 m that appears to be uplifted and displaced towards the south-east by c. 2 m;

C. A middle unit comprising a boulder-rich diamicton (immature rubble till), mainly consisting of angular boulders in a poorly sorted matrix, and continuing below the mass of disrupted bedrock, possibly suggesting some form of till injection;

D. A lower unit of sorted sediment, bedded in its upper part and filling an open fracture at its base, and upwards and down-ice gradational with the overlying diamicton (Figure 4-48B). The sediment comprises sand and gravel, with minor subrounded cobbles, but no boulders, showing laminations at its top. This unit is interpreted as a deposit by water (or as a slurry), in a funnel-shape void. The top part of the unit shows deformation of the bedding/laminations indicating some movement of the diamicton after deposition of the sand and gravel.

The order of events and deposition at Tönnebro is here interpreted as follows: (1) hydraulic jacking opened up and brecciated the shallow rock mass, creating void space below the ice bed, (2) coeval with, or immediately followed by, deposition of sand and gravel (unit D). (3) Subsequently, the bedrock mass (unit B) and immature till (unit C) were translated a few metres to the SE (down-ice), deforming the sand and gravel below and forming part of the overlying ribbed moraine.
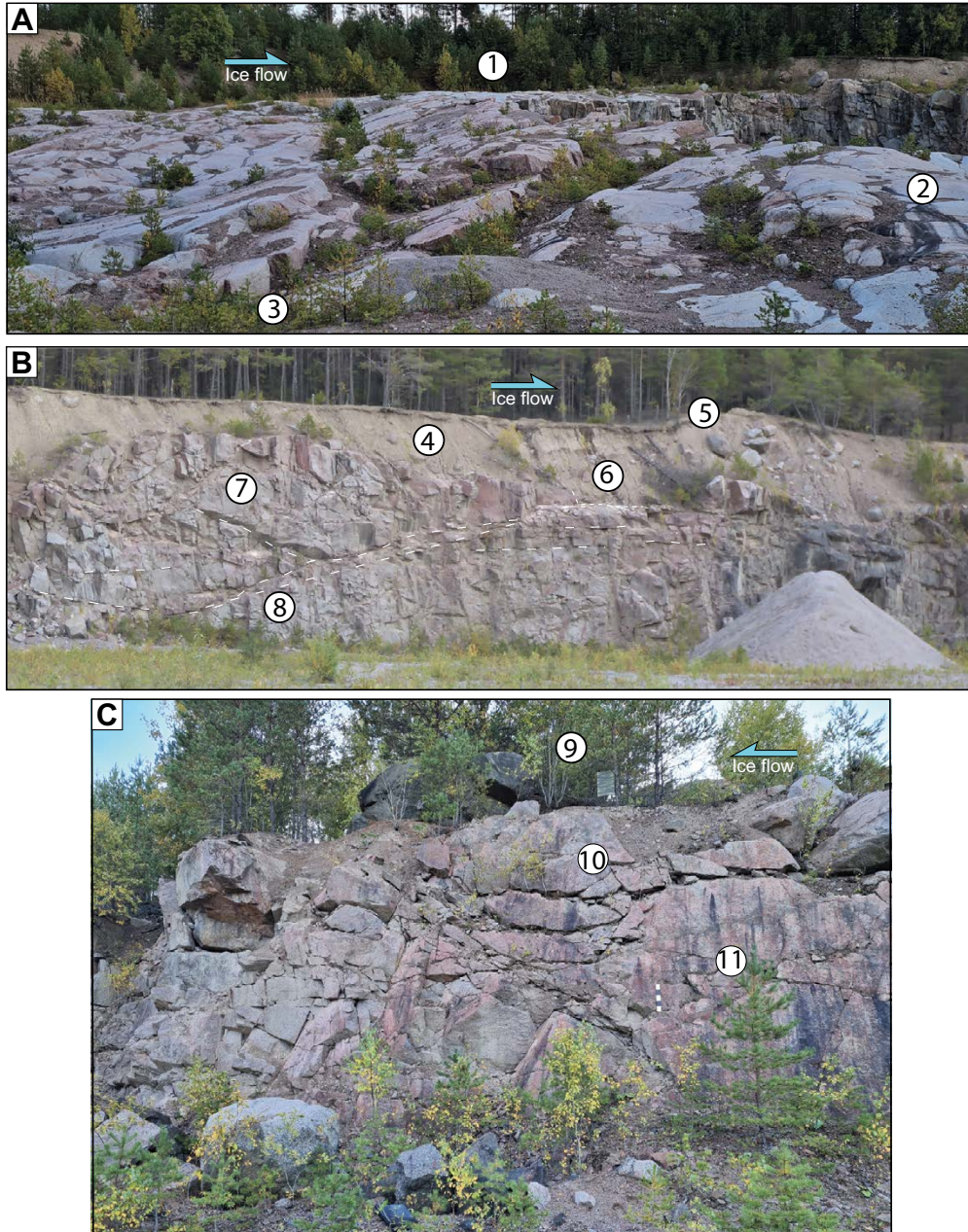
Figure 4-47. *Open and dilated fractures at Lövstalöt Quarry (location on Figure 4-19). A. Low-relief rock surface exposed after clearing of till cover in preparation for quarrying. (1) Low relief rock surface developed across vertical and inclined fractures. (2) Abraded rock surface. (3) Lee-side step. B. Quarry section, facing west. (4) Cover of sandy till. (5) Boulder cluster in till. (6) Fracture-bounded socket from which rock blocks have been removed. (7) Small roche moutonnée with open fractures. (8) Open subhorizontal and inclined fractures. C. Quarry section facing west. (9) Block moved during quarrying. (10) Dilated subhorizontal fractures. (11) Open fractures below.*
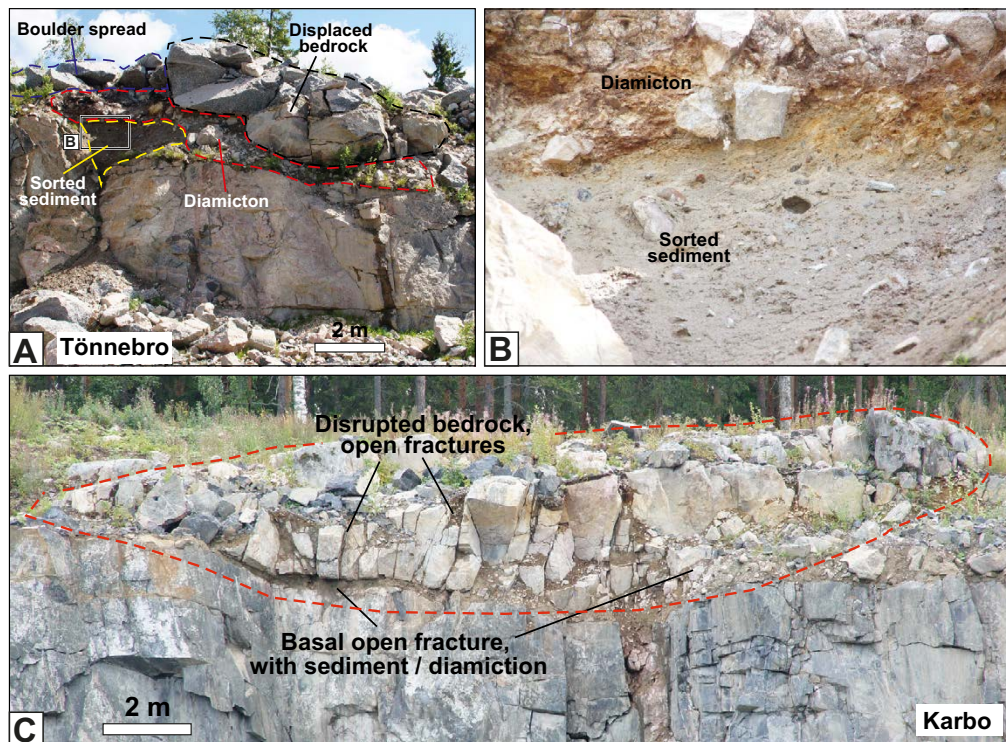
Figure 4-48. *Transitions between jacking and disintegration. A. Open fractures with void, filled with sorted sediment, overlain by diamicton, with mass of disrupted bedrock apparently moved to south. Boulder spread on top. Quarry in augen gneiss, north of Bergby/Tönnebro (location Figutre 2-2A) [N6770770; E604990]. B. Detail of sorted sediment, in A. C. Disrupted rock mass with open fractures, underlain by detachment filled with diamicton. Karbo quarry.*

4.4.3   Transitional case between dilated fractures and disintegrated bedrock – Karbo

At the Karbo quarry, NW of Uppsala (location Figure 2-2A), most fractures are tight or open, but not dilated, all the way to top-bedrock surface (Figure 4-1G). However, in one section, the upper 2–4 m of the rock mass shows a series of blocks, separated by subvertical dilated fractures (Figure 4-48C). This whole mass is separated from the lower, intact rock mass by a dilated subhorizontal fracture filled with diamicton, varying in thickness from c. 20–100 cm. Diamicton also appears to occur in some vertical fractures. The upper rock unit has lost most of its original rock mass strength (the strength of a rock mass including its fractures), and now in essence consists of loose blocks, separated by diamicton, along a detachment surface. This represents a transitional case between fracture dilation and disintegrated bedrock.

4.4.4   Transitional case between disrupted bedrock and boulder spread – Öskatarna (Forsmark)

A transition between disrupted bedrock and a boulder spread was observed at Öskatarna, just west of the Forsmark power plant (for location see Figure 4-28). Here, near *in situ* rocks, with clear abraded surfaces, have been brecciated and broken up into metre-sized blocks to a depth of ca. 1 m that have been displaced and rotated to varying degrees (Figure 4-49). Voids occur in between blocks, and blocks have been rotated 10–20° with respect to the *in situ* bedrock (Figure 4-34B, D). Block P and Q have the same orientation of amphibolite gneiss fabric, and the height of the abraded top surface is comparable, suggesting both these blocks are *in situ* That means that a large socket occurs between these two blocks: somehow a slab of rock (in one piece or as smaller blocks) of some $2.5 \times 3 \times 0.8$ m was removed from the rock surface, and transported elsewhere. Both intact bedrock and an incipient boulder spread thus occur here close together.
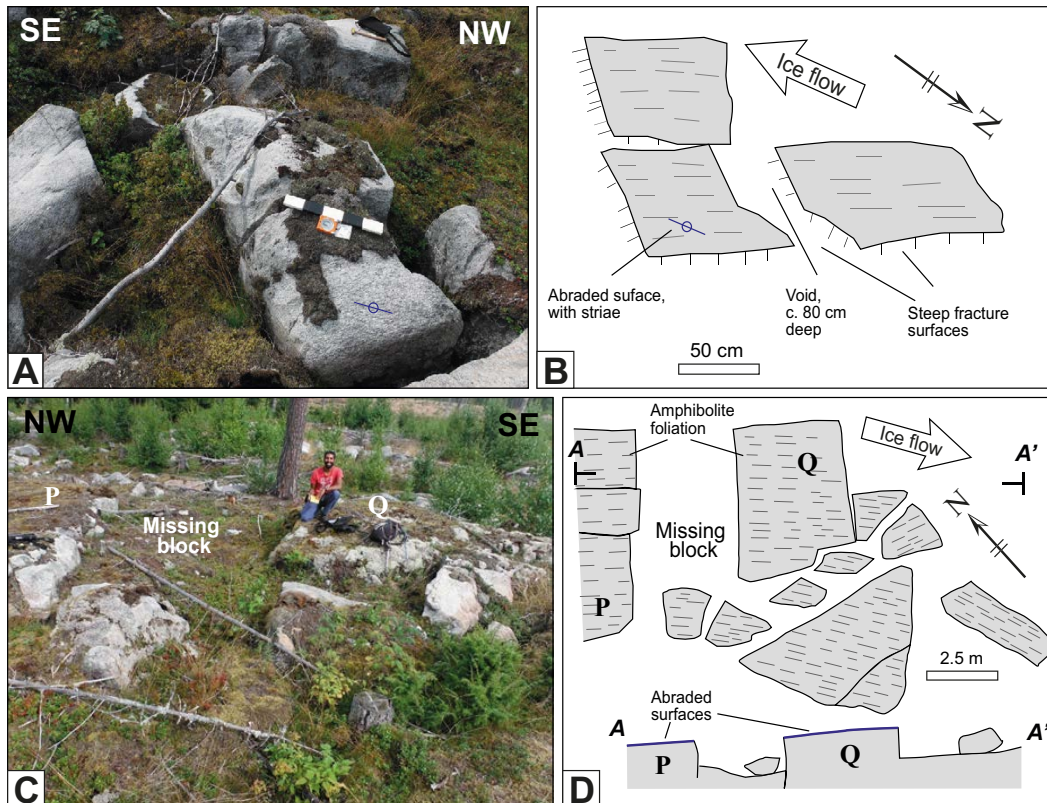
Figure 4-49. *Transitions between disintegration and transport, at Öskatarna, Forsmark. For location, see Figure 4-28.*

4.5 Boulder/block size comparison of fractured bedrock, roches moutonnées and boulder spreads

Block and boulder sizes were measured in quarries and excavation sections, and in disrupted roches moutonnées and boulder spreads, and are reported as nominal B-axes based on areal extent (Section 3). In quarries and sections most *in situ* block sizes are 0.4–1.2 m, although a substantial volume of rock (c. 20–40 %) comprises blocks with a nominal B-axis of 1.2–2 m (Figure 4-50). Only site SKB-006 shows larger blocks (2–3 m). These data are similar to those obtained by Jern (2004) for various quarries in southern Sweden, who obtained a typical block size of c. 0.5–1 m, with values > 2 m being rare.

Boulder size in boulder spreads ranges from 0.8 m (the cut-off – see Section 3) to 5 m, with Skogbo and Bladåker showing the smallest boulders (0.8–4 m), and the other boulder spreads also containing blocks 4–5 m. Even accounting for the fact that boulders and blocks with B-axis < 0.8 m were ignored in the analysis of the boulder spreads, it appears that boulder size in boulder spreads is slightly higher than block size in quarries and sections (Figure 4-50). It is possible that, as a rock mass with wide ranging fracture-bound block sizes is disintegrated, the smaller boulders and cobbles form an immature rubble till that commonly occur below boulder spreads. Some form of 'reverse sorting' (reverse or negative grading) may thus occur during boulder transport and deposition, since large boulders remain more exposed to transport by sliding ice than cobble-sized clasts.

The block size at the Bodagrottorna and Gillbergagryt roches moutonnées show a range of B-axes from 1–5 m, but with a number of very large blocks (B-axis c. 10 m). The large block size and hence wide fracture spacing at Bodagrottorna is consistent with borehole data from Carlsten and Stråhle (2000). Block sizes at other roches moutonnées were not measured, but Rövargrottan and Pukberget certainly contain blocks with B-Axis > 4–5 m.

The block size in the disrupted roches moutonnées is 2–3 times larger than typically found in quarries and excavations in basement terrain in Sweden. The large disintegrated roches moutonnées only occur in bedrock masses in which the largest block sizes (and hence fracture spacing) is much larger than average; this is further discussed in Section 7.4.
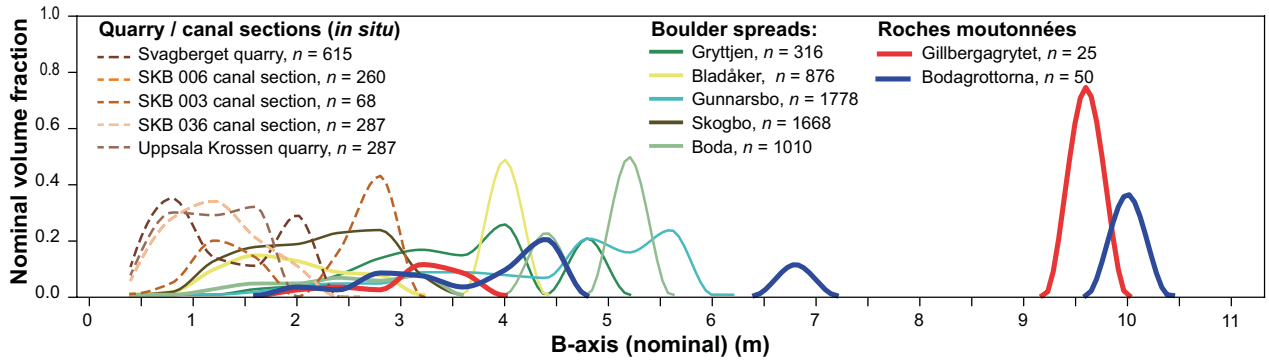
Figure 4-50. *Comparison of block size in quarries and excavation sections, boulder spreads and disrupted roches moutonnées (Bodagrottorna and Gillbergagryt). Nominal B-axis is based on areal extent, used as proxy for boulder/block size. Boulders and blocks with B-axis < 0.8 m were not measured in boulder spreads and roches moutonnées.*

5 The conceptual model of glacial ripping

Hall et al. (2019a, 2020) and Krabbendam et al. (2022a) proposed that the three types of features described above, namely (i) sediment-filled subhorizontal fractures, (ii) disrupted roches moutonnées and (iii) boulder spreads comprise a three-fold process sequence termed *glacial ripping*. First, we describe the conceptual model in detail (Section 5.1). As the conceptual model assumes glacial ripping occurred subglacially, lines of evidence for this are discussed in Section 5.2.

5.1 Conceptual model of glacial ripping

The conceptual model of glacial ripping is proposed (see also Hall et al. 2019a, 2020, Krabbendam et al. 2022a) to comprise a three-fold process sequence as follows (Figure 5-1):

Stage 1: Hydraulic Jacking and Dilation

Dilated and sediment-filled subhorizontal fractures occur in several places in eastern Sweden (Section 4.1.2) and indicate that hydrostatic pressures in fractures below the ice sheet bed were locally (and temporarily) sufficiently high to lift rock overburden and overriding ice, likely with temporary ice-bed separation. Overpressured subglacial groundwater locally penetrated the shallow rock mass and led to hydraulic jacking and dilation of pre-existing fractures (Carlsson 1979). Preserved dilated fractures indicate relatively widespread, shallow (up to 1–2 m) jacking in a variety of settings; deeper (2–13 m), dilation occurred mainly along open sub-horizontal fractures.

Hydraulic jacking was perhaps locally accompanied by propagation of subhorizontal fractures and formation of vertical fractures by hydraulic fracturing (Lönnqvist and Hökmark 2013): there is some evidence of actual hydraulic fracturing (Section 4.1.5). It is further possible that the action of jacking of subhorizontal or gently dipping fractures led to the development of new steeply dipping fractures above the lower jacked fracture by beam failure, thus further disrupting the upper rock mass (Krabbendam et al. 2021, and Section 6.2). On some large roches moutonnées and other low-relief rock surfaces, fracture dilation was pervasive, and led to brecciation of the near-surface rock mass. The resultant block breccia represents a form of mechanical weathering that affected parts of the shallow rock mass below the former glacier bed. Overpressured meltwater at the glacier bed likely also contributed to fluidisation and removal of till layers, explaining the lack of older till amongst the boulder spreads.
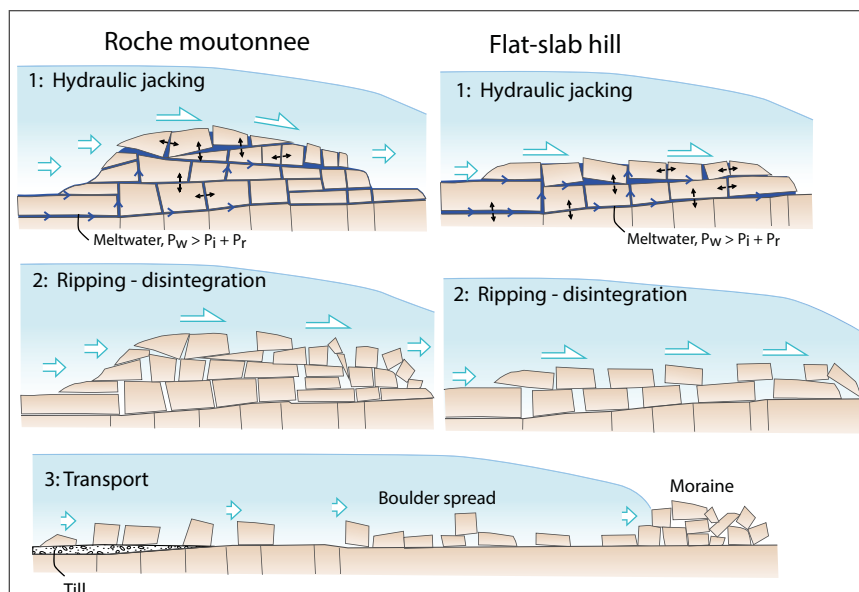
Figure 5-1. Conceptual model of glacial ripping involving three stages, shown for a blunt roches moutonnées and a flatter, slabby hill. After Hall et al. (2020) and Krabbendam et al. (2022b).

High water pressure events, temporarily exceeding ice overburden pressure (overpressure), were likely caused by processes similar to those that cause overpressures demonstrated beneath the ablation zone of the Greenland Ice Sheet (e.g. Das et al. 2008, Doyle et al. 2013, Andrews et al. 2014, Harper et al. 2016, 2019, Wright et al. 2018), discussed in more detail in Section 7.2. The extent, duration and volume of water at overpressure at the glacier bed varies strongly in time and space. At the regional scale in eastern Sweden, broad patterns of boulder spreads suggest this temporal and spatial variability links to differences in the availability of overpressured water at the base of the ice sheet (Section 4.3.1 and 4.3.2). On the local scale, subglacial meltwater ponding and routing, fracture patterns and till cover acted as significant controls on the volumes of meltwater that entered fractures in the shallow rock mass and caused hydraulic jacking, causing more local-scale variability (e.g. Section 4.2.8).

Stage 2: Glaciotectonic Disintegration and Ripping

Where hydraulic jacking and fracture dilation occurred, the static friction along these fractures was reduced and the overall rock mass strength of the shallow rock mass was lowered as blocks became separated along sub-horizontal fractures. Friction reduction may have been transient, operating during a high water-pressure event, or permanent, as fractures remained open due to slight block movement, rock chips or sediment fill, and remained filled with water. In addition, if hydraulic jacking was uneven (for instance because some horizontal fractures had higher initial aperture than others nearby or abut vertical fractures) this locally led to the creation of low, sharp steps or edges on the previously smooth, abraded surface. New rock steps allowed sliding ice to exert a higher shear or pushing force onto the bedrock blocks, in particular if these steps faced in the up-ice direction. Continuing ice traction from ice push and frictional drag exerted by the overriding ice then exceeded the friction along basal fractures, or exceeded the rock mass strength of a particular mechanically weakened bedrock hill or rock mass as a whole, resulting in disintegration. This stage of the process-sequence is a specific form of glacio-tectonics, as it involves brittle deformation (disintegration) of the ice bed (in this case hard bedrock) under ice drag. The disintegrated roches moutonnées represent this stage, but their further development into boulder spreads was aborted, for reasons discussed in Section 7.4.

It is difficult to determine in detail at which stage fracture dilation due to hydraulic jacking gives way to block translation by glaciotectonic disintegration by ice drag. On the one hand, dilation of 0.01–1 m along subhorizontal fractures is likely caused by hydraulic jacking. On the other hand, metre-scale lateral pull-apart of vertical fractures can be transitional to block movement involving ice drag.

Stage 3: Transport and deposition

Continuing traction by sliding ice transported and dispersed the fragmented blocks, creating boulder spreads that were emplaced on existing bedrock surfaces or till mantles, with typical transport distances ranging from a few metres to a few 100 m, rarely a few kilometres. Locally, boulder spreads were deposited on moraines. Some boulder spread deposition occurred broadly coeval with esker deposition. Smaller detritus (small boulders, cobbles and finer particles) from the original bedrock were either deposited as part of the immature rubble till found in many boulder spreads (e.g. at Skogbo, Björklinge, Runtorp) or may have been removed by subglacial meltwater. Limited rounding of boulders in boulder spreads indicates short distance transport, likely with deposition close to the retreating ice margin.

The above three-fold process-sequence represents in our view a plausible mechanism to explain i) sediment-filled subhorizontal fractures, ii) disintegrated roches moutonnées and fracture caves and iii) the boulder spreads in eastern Sweden. Observations on transitions between jacking and glaciotectonic disintegration or between disintegration and transport (Section 4.4) support the linking of the three features in a single process sequence.

The conceptual model as described above has a number of implications and required assumptions. Firstly, it assumes that hydraulic jacking, disintegration and transport occur subglacially. This is tested in Section 5.2. Secondly, it requires sufficient overpressured subglacial meltwater, at least locally and temporarily at the ice-sheet bed: this is discussed in Section 7.2. Thirdly, it assumes that if overpressured water occurs at the ice-bed that this water penetrates, at least locally, into fractures in the shallow rock mass, and increases the water pressure within the fractures. Water penetration is facilitated by the presence of open subhorizontal fractures, discussed in Section 7.3.

5.2 Glacial ripping in relation to the ice margin: subglacial or proglacial?

The conceptual model of glacial ripping assumes that hydraulic jacking, disintegration and dispersion in boulder spreads operated subglacially, but close to the retreating ice margin and hence only shortly before deglaciation. In contrast, Pusch et al. (1990) presented a model to explain hydraulic jacking as a proglacial process. Sjöberg (1994) and Mörner et al. (2000) similarly argue that disintegration of roches moutonnées could not have occurred subglacially, since the edges of the disintegrated blocks are not rounded, and striae have been cut by fractures.

Several lines of evidence indicate that hydraulic jacking, disintegration and dispersion in boulder spreads operated subglacially:

1. The occurrence of silt and sand, and locally diamicton, in the subhorizontal fractures suggest a subglacial origin, supported by high pre-consolidation loads of these sediments (Section 4.1).

2. Glaciotectonic disintegration of the roche moutonnées is asymmetric, with asymmetry consistent with local ice-flow direction during deglaciation (Section 4.2).

3. Where a transport direction for boulder spreads and trains could be established (Gunnarsbo and Bodagrottorna), it is consistent with local ice-flow direction during deglaciation (Section 4.3).

4. The boulder spreads show variable transport distances. Dispersion of the blocks, as well as the random rotation of the boulders in, for instance, the Gunnarsbo boulder spread suggest a certain amount of transport; however, the general survival of abraded and fracture surfaces, and angular shapes suggest limited transport. Limited transport can be explained if boulder spreads or disruption of bedrock occurred close to (within a few kilometres) the margin, and the margin retreated rapidly over the boulder spread or disrupted bedrock. Altogether this suggests boulder spreads were generated subglacially, but close to the ice margin (Section 4.3.5).

5. The spatial association of boulder spreads with segments of the Börstil esker (Section 4.3.4.6), the fluting of boulder spread surfaces near lake Tämnaren, and the recycling of boulders from boulder spreads into moraines indicates that the boulder spreads originated prior to final deglaciation (Section 4.3.7).

Concerning the purported lack of edge rounding that was used to argue for a proglacial origin (Sjöberg 1994, Mörner et al. 2000): there are a number of problems with this argument. Firstly, plucked faces, undoubtedly plucked subglacially, commonly also show sharp edges, in Sweden and elsewhere (e.g. Bradwell 2013, Krabbendam and Glasser 2011, Hall et al. 2019a, Alley et al. 2019, Glasser et al. 2020). Secondly, minor edge rounding does in fact occur in some of disintegrated roches moutonnées (Gillbergagryt, Bodagrottorna and Trollgrundet; Section 4.2). Thirdly, absence of significant edge rounding is plausible where the rock surface was protected from glacial abrasion by till cover (Section 4.1.3). Fourthly, hydraulic jacking along the Börstil esker occurred within an esker tunnel and the rock surface was then buried beneath sand and gravel (and protected from edge rounding) (Section 4.3.4).

Finally, if roches moutonnées were disintegrated subglacially, edge rounding may have been limited. In eastern Sweden there is now better data to constrain the rate of abrasion, and hence the rate of edge rounding. Terrestrial cosmogenic nuclide dating of samples collected in Uppland county estimates the total erosion of the tops of roches moutonnées, likely all achieved by abrasion, to be c. 1.6–3.5 m over the entire Weichselian period, involving two inferred stadial phases with ice coverage (Hall et al. 2019a). Ice sheet modelling of the Fennoscandian Ice Sheet suggests a total cumulative sliding distance of c. 3 000–5 000 km in the same area over the same time span (Näslund et al. 2003). This equates to an abrasion rate per kilometre of sliding ice of c. 0.3–1.1 mm km^{-1}. The retreat rate of the ice margin is similar to the modelled ice surface velocities (both in the order of 200–400 m yr^{-1}) (Strömberg 1989, Stroeven et al. 2016, Patton et al. 2017). Now consider a roche moutonnée that is disrupted subglacially at c. 10 km from the margin, creating some sharp edges. The maximum cumulative basal sliding distance after disintegration is c. 5 km, and the resultant abrasion is c. 1.5–5 mm, before the roche moutonnée emerges from the retreating ice margin, and abrasion stops. Even allowing for faster abrasion (or chipping) on sharp edges, such small abrasion would be barely discernible in the field. It is thus perfectly plausible for a roche moutonnée to disintegrate subglacially, but close (< 5–10 km) to the ice margin, showing minimal edge rounding.

Neither limited edge rounding, nor striae cut by fractures invalidate a subglacial origin. To satisfy the constraints of minimal edge rounding and asymmetry of disintegration, we conclude that the roches moutonnées were disintegrated and boulder spreads as described herein formed subglacially, but close to (< 5–10 km) the retreating margin, depending on the ice velocity.

Notwithstanding the above, it is likely that glacial ripping also occurred earlier during the Late Weichselian glaciation, further away from the margin, or even during earlier periods of ice coverage. The association with ribbed moraines, generally thought to form at considerable distance from the ice margin (Dunlop and Clark 2006), in the Iggesund area (Section 4.3.7) and at lake Rogen (van Boeckel et al. 2022), supports that notion. Survival of boulder spreads and other features that developed further away from the margin, and experienced longer duration of ice cover before deglaciation, would be facilitated if ice velocity was lower, which appears to have been the case in more inland locations, away from the Bothnian Sea (Patton et al. 2017). In the case of sustained ice sliding following glacial ripping it is likely that any boulder spreads developed far from the margin would have been subjected to additional dispersion and clast-size reduction, and transformed to till. That process would in essence degrade or obliterate the specific evidence for glacial ripping (the dispersed boulder spread at Skogbo is a good example of such degrading of evidence, see Section 4.3.4). In other words, while there is good evidence that glacial ripping occurred widely in east Sweden prior to final deglaciation, the possibility of glacial ripping earlier during the glacial cycle remains possible, but would be difficult to demonstrate.

6 Modelling and theoretical constraints

In this section we present three components of modelling:

(i) modelling of the maximum jacking depth of the shallow rock mass (Section 6.1),

(ii) modelling of the potential formation of new subvertical fractures by beam failure caused by hydraulic jacking along subhorizontal fractures (Section 6.2), and

(iii) modelling of the balance between ice drag forces exerted by the ice, and the resisting forces offered by an upstanding rock obstacle, to assess the physical plausibility of glaciotectonic disintegration of a rock mass with different fracture patterns (Section 6.3).

6.1 Overpressure and ice thickness – maximum jacking depth

If overpressure at the ice-bed was caused by the mechanisms observed below the ablation zone of the Greenland Ice Sheet (e.g. Das et al. 2008, Doyle et al. 2013, Andrews et al. 2014, Harper et al. 2016, 2019, Wright et al. 2018; discussed in detail Section 7.2), then the ice thickness h_i is an important constraint to the absolute magnitude of overpressure. The maximum jacking depth of fractures below the ice-bed interface is related to the maximum overpressure P_{omax}, which is given by:

$$P_{Omax} = P_{wmax} - P_i \text{ (in Pa)} \tag{6-1}$$

This is reached if the water column equals the thickness of the ice sheet h_i, and hence if $P_w = 1.1\,P_i$. This appears to be the theoretical maximum of over pressure, and is also broadly the maximum water pressure measured below the Greenland Ice Sheet (Das et al. 2008, Wright et al. 2016, Andrews et al. 2014).

If $P_{wmax} = 1.1\,P_i$, then:

$$P_{Omax} = \rho_w g h_i - \rho_i g h_i = g h_i \, (\rho_w - \rho_i) \text{ (in Pa)} \tag{6-2}$$

where h_i equals the thickness of the ice, ρ_i is the density of ice, ρ_w is the density of water, and g is the standard acceleration of gravity.

The maximum jacking depth D_{max} of a rock block with density ρ_r is then given by:

$$D_{max} = g h_i \, (\rho_w - \rho_i) / g \rho_r = h_i \, (\rho_w - \rho_i) / \rho_r \text{ (in m)} \tag{6-3}$$

Assuming rock density ρ_r of 2 800 kg/m³, then:

$$D_{max} = 0.032\,h_i \text{ (in m)} \tag{6-4}$$

As an example, with an ice thickness of 400 m, the maximum overpressure is c. 350 kPa ($\approx$ 35 m water head), and the maximum jacking depth is c. 12.5 m. (Figure 6-1).

Since most jacked subhorizontal fractures in Sweden occur at depths < 10 m and the deepest jacking recorded is 13–16 m (Leijon 2005), this suggests that jacking only required ice thickness < 400–500 m. Jacking to depths of < 5 m can occur with ice thickness of only 200–300 m.

These findings are consistent with our observations that the jacking and ripping occurred close to the ice margin (Section 5.2). Theoretically, the maximum jacking depth keeps increasing with increasing ice thickness. However, measured pressure fluctuations at the Greenland Ice Sheet (Wright et al. 2018, Harper et al. 2019) suggest that high-pressure events occur repeatedly during the melt season at 27–33 km from the terminus (with an ice thickness of 600–700 m), but are far less common further up the ice sheet (45 km from the terminus; 800 m ice thickness). Supraglacial lake drainage events are restricted to the ablation zone, as are moulins. It is likely that frequent, high magnitude water pressure fluctuations at the ice-bed are restricted to the ablation zone, especially its lowest parts (Claesson Liljedahl et al. 2016).
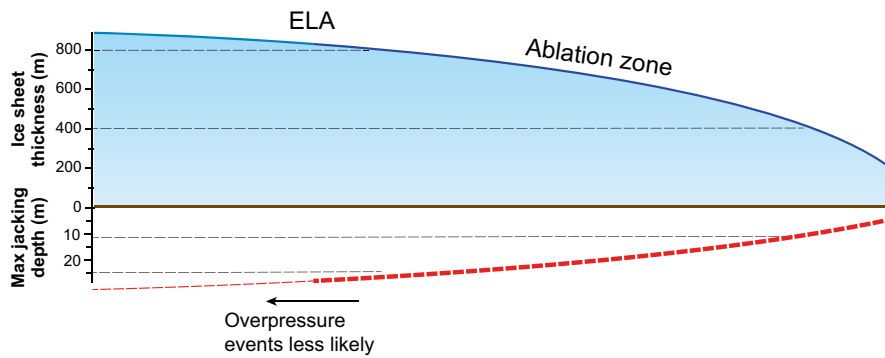
Figure 6-1. *Diagram showing maximum jacking depth as a function of ice thickness.*

It should be noted that hydraulic jacking of a fracture occurs when the water pressure within it exceeds the sum of the normal stress and tensile strength of the fracture (Hökmark and Lunnqvist 2014). Fracture tensile strength is close to zero for open fractures, but low tensile strengths of tight fractures up to 3 MPa is suggested by borehole hydraulic fracture tests (Stephansson and Ångman 1986). Tensile strengths in unfractured gneiss are much higher, e.g. in the order of 13.5–18.0 MPa (Glamheden et al. 2007). Hence, hydraulic jacking along existing fractures can occur when tensile strength is exceeded under hydraulic heads of c. 100–300 m beneath equivalent ice thicknesses but formation of new fractures (hydraulic fracturing *sensu stricto*) requires much greater water pressures.

6.2 Rock fracturing by subglacial hydraulic jacking: the role of beam failure

6.2.1 Introduction

The fracture analysis on the historic photos from the Forsmark excavations (Section 4.1) shows that:

a) dense networks of dilated fractures occur locally in the upper 1–10 m of bedrock,

b) in some sections, subvertical fracture density increases upwards in tandem with subhorizontal fracture density, in particular above open, jacked subhorizontal fractures,

c) conversely, some sections with non-dilated subhorizontal fractures do not show an upward increase in subvertical fracture density.

This suggests that hydraulic jacking and fracture dilation along subhorizontal fractures locally resulted in the generation of new subvertical fractures (Figure 4-5). Observations on the historic photos further show that the development of angular rock fragments in open sub-horizontal fractures at Forsmark is a common occurrence (Section 4.1.3). This implies that after a high-pressure jacking event, a fracture may remain 'jammed' open, leaving some void space. After a water pressure drop and increase in effective pressure, the rock slab above the fracture then functions mechanically like a beam. The modelling below tests if it is plausible that new subvertical fractures are generated by beam failure (see also Krabbendam et al. 2021).

6.2.2 Beam failure: model set-up

The modelling assumes that hydraulic jacking was driven by repeated water pressure fluctuations with a daily to seasonal frequency as measured at the base of the Greenland Ice Sheet (Section 7.2; Andrews et al. 2014, Claesson Liljedahl et al. 2016, Wright et al. 2016, Harper et al. 2019), and mainly resulted in dilation of subhorizontal fractures, which is consistent with the aperture measurements of Carlsson (1979). Relative water pressure is defined here as the fraction of overburden pressure P_w/P_i (where water pressure is P_w, and cryostatic pressure is P_i), following Wright et al. (2016); also termed the flotation factor (e.g. Shackleton et al. 2018). If the water pressure equals overburden pressure ($P_w/P_i = 1$), the ice is at (local) flotation, and the effective pressure (P_w–P_i) is zero.

Now consider a rectangular slab of rock at the base of an ice sheet, underlain by a transmissive sub-horizontal fracture (Figure 6-2A), that is jacked and uplifted by overpressured groundwater, by a few centimetres (Figure 6-2B).
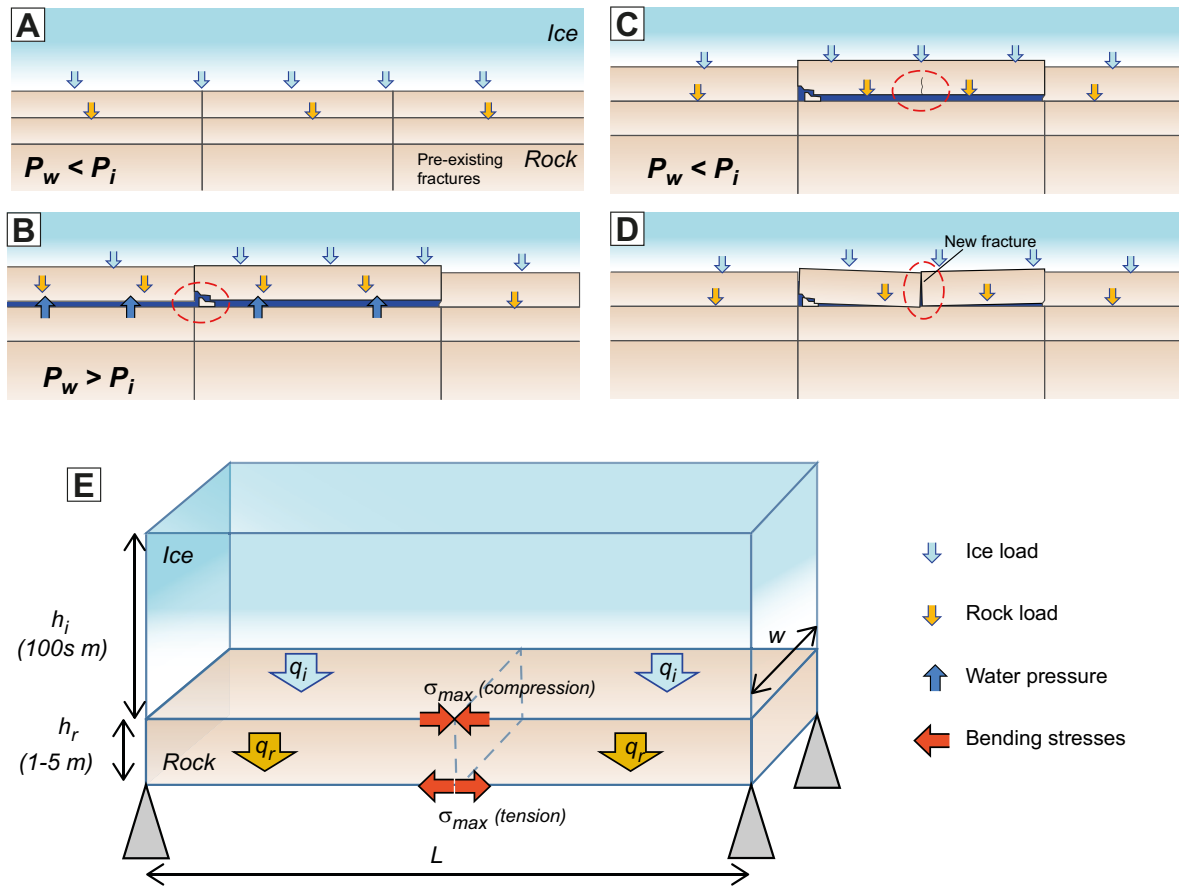
Figure 6-2. A. Conceptual model of rock overlying rock mass with orthogonal subhorizontal and subvertical fractures. B. Under overpressure events (Pw > Pi), rock slabs are lifted upwards. C. As pressure drops (Pw < Pi), the slabs are lowered again, but not in exactly same position. The imperfectly fitting slab functions as a beam. D. The beam may fail, forming a new fracture. E. Conceptual model of a rock slab as a beam, subjected to a distributed load of rock (q_r) and ice (q_i). Maximum stress σ_{max} is compressional at the top of the beam and tensional at its base. After Krabbendam et al. (2021).

As the water pressure drops, the slab will be lowered again (Figure 6-2C). Now consider that the slab will not be lowered back in its exact original place, but is 'hanging', supported at its ends, for instance by a broken rock fragment (circled in Figure 6-2B, C), such as observed in some of the test excavations near Forsmark (Section 4.1.3). The rock slab has now become a bridge or beam (Figure 6-2C). This beam is subjected to a bending stress, caused by the load provided by its own weight plus any load of the overlying ice. As the tensile strength of rock is much lower than its compressive strength, when the stresses are too high, the slab or beam may fail in a tensional manner near its base (Figure 6-2D), and a new subvertical fracture is formed.

This problem essentially equates to the structural engineering problem of a beam supported at both ends under a uniform distributed load (Figure 6-2E). The maximum stress σ_{max} that such a beam is subjected to is compressive at the top and tensional at the base and is given by:

$$\sigma_{max} = 0.5\, h_r\, q_{tot}\, L^2\, /\, 8I \qquad (6\text{-}5)$$

where h_r is the height of the beam, L the length of the beam, q_{tot} is the total load and I is the Area Moment of Inertia (Engineering ToolBox 2009). Since rock is much weaker in tension than in compression, any failure is likely to occur as a tensional fracture at the base of the beam. We use here the 'classic' or Euler–Bernoulli beam theory rather than the more involved Timoshenko–Ehrenfest beam theory. This simplification is justified as the elastic deflections before tensional failure are very small.

The Area Moment of Inertia I for a rectangular cross-section is (Engineering ToolBox 2008):

$$I = wh_r^3 / 12 \tag{6-6}$$

If we take a simple beam supported at both ends, the width of the beam is not relevant, and can be taken as $w = 1$. Combining Equations (6-8) and (6-9) gives:

$$\sigma_{max} = \frac{0.5\, h\, q_{tot}\, L^2\, 12}{8\, wh_r^3} = \frac{0.75\, q_{tot}\, L^2}{h_r^2} \tag{6-7}$$

The total load q_{tot} is the sum of the load of the overlying rock q_r and the ice q_i, minus the water pressure P_w at the base:

$$q_{tot} = q_r + q_i - P_w = gh_r\rho_r + gh_i\rho_i - P_w \tag{6-8}$$

where g is the gravity constant, h_i the thickness of the ice and ρ_i and ρ_r the density of ice and rock respectively.

It is convenient to express this in terms of relative water pressure (P_w/P_i), and Equation (6-11) is rewritten as:

$$q_{tot} = gh_r\rho_r + gh_i\rho_i\left(1 - \frac{P_w}{P_i}\right) \tag{6-9}$$

Combining Equations (6-11) and (6-12) gives the maximum stress at the base of a rock beam as a function of ice thickness, relative water pressure and the height and length of the beam:

$$\sigma_{max} = \frac{0.75\,[gh_r\rho_r + gh_i\rho_i\left(1 - \frac{P_w}{P_i}\right)]L^2}{h_r^2} \tag{6-10}$$

The maximum length of the beam can then be given as:

$$L = h_r\sqrt{[\sigma_{max}]/(0.75\,(gh_r\rho_r + gh_i\rho_i\left(1 - \frac{P_w}{P_i}\right))]} \tag{6-11}$$

The tensile yield strength of the felsic granodioritic gneiss at Forsmark is in the order of 10–15 MPa (Glamheden et al. 2007). (For comparison, the compressive strength of the same rocks is in the range of 150–250 MPa). These values are for intact rock without micro fractures or other flaws, so that the tensile strength of 10–15 MPa should be seen as a maximum. In nature, tensile strength is thus likely somewhat lower.

6.2.3 Modelling beam failure: results

The results are calculated for different scenarios: beam height $h_r = 1$ and 5 m; ice thickness $h_i = 200$, 400 and 600 m; relative water pressure P_w/P_i at 0.8 and 0.9 (this is the water pressure after the over-pressure event, as portrayed in Figure 6-2C, D). Tensile stresses increase exponentially with the length of the beam (Figure 6-3A). Failure is deemed plausible at 8 MPa and certain above 16 MPa. For instance (left hand blue line), a 1 m high beam, under 600 m of ice, with a relative water pressure of 0.8, will fail if longer than 3–4 m. Under a wide range of conditions, a 1 m high beam will fail if longer than 2 to 7 m. In contrast, a thick (5 m) beam, under relatively thin ice and high water pressure will not fail at less than 10 m length (black line).

The maximum length for different ice thickness and water pressures is plotted against beam height (Figure 6-3B), for a fixed tensile strength of 10 MPa. This shows that beams (i.e. rock slabs) have the tendency to fracture into short, stubby blocks with a length:height ratio between 4:1 and 3:1. This compares reasonably well with the block length:height ratios as seen in the Forsmark sections, which show ratios > 5:1 for sections without dilated fractures and < 5:1 for sections with (or above) dilated subhorizontal fractures (Figure 4-6). Overall, the results show that tensile beam failure during low water pressure events, following hydraulic jacking by a transient high water pressure event, is a plausible mechanism for the production of new vertical fractures in long rock slabs.
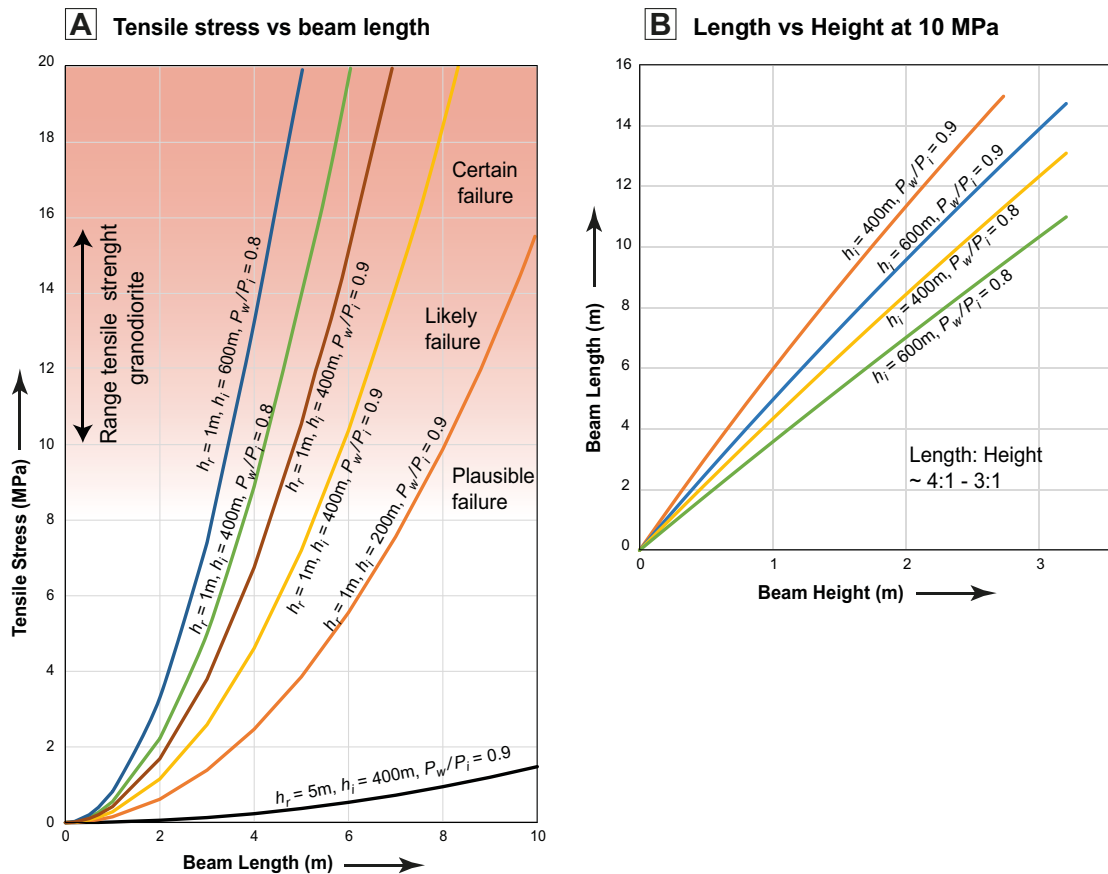
Figure 6-3. *A. Maximum tensile stress (MPa) at the base of a beam against length of bean (L in m) for different values of height or rock beam h_r, ice thicknesses h_i and relative water pressure P_w/P_i. Tensile failure is increasingly likely between 4 to 10 MPa, and certain for stresses > 10 MPa (red shading). B. Maximum length of beam against height of beam at a fixed breaking strength of 5 MPa for different values of ice thickness h_i and P_w/P_i. After Krabbendam et al. (2021).*

6.2.4 Implications of hydraulic jacking and beam failure

Hydraulic jacking followed by beam failure and the generation of new vertical fractures can thus contribute to the creation of a dense fracture network in the shallow bedrock. The generation of dilated, fracture networks in the shallow rock mass at Forsmark thus likely followed the following steps:

1. An overpressure event occurs at the ice-bed.

2. Water under high-pressure is squeezed into a pre-existing subhorizontal fracture. If water pressure exceeds overburden pressure, the fracture is jacked open (and may propagate), and the overlying rock slab is lifted upwards (together with the ice above it).

3. Locally, rock fragments may break off the roof or the sides of the dilated fracture. These rock fragments may then jam open the fracture after water pressure drops. Sediment, transported with the water, may be deposited in the dilated fracture, likely soon after peak pressure (e.g. Phillips et al. 2013).

4. As water pressure drops, the effective pressure and hence the load of overlying rock and ice increases, and horizontal fractures tend to close.

5. Now there are two possibilities:
   a. the overlying rock slab functions mechanically like a beam, the combined load of rock and ice breaks the rock slab by beam failure, and new subvertical fractures are generated,
   b. if sufficient sediment is available and deposited in the fracture, the sediment *may* take the load and becomes compressed, but beam failure may not occur.

6. Repetition of the above cycle, where it occurs, may result in either:

    a. an increasing number of subvertical fractures, resulting in a disrupted rock mass with small block size, contributing to brecciation as seen in Figure 4-2A, 4-3C; 4-5B,

    b. or – more rarely – very wide (> 10 cm) dilated fractures filled with laminated sediment, as has been observed occasionally at Forsmark (Figure 4-2B).

Beam failure modelling also implies it is not plausible that long slabs of rocks are jacked and lowered and remain intact. One exception is if the void space below the jacked slab is filled with sediment, so that the load overlying rock and ice distributed across a wider area of soft sediment. This scenario is only possible if sediment deposition occurred coevally with the jacking. Hydraulic jacking as such is not dependent on sediment availability. The combination of hydraulic jacking along long subhorizontal fractures and sufficient sediment availability may be rare and explain the rare observation of long dilated subhorizontal fractures with intact rock above at Forsmark (Figure 4-2B).

Hydraulic jacking followed by beam failure represents a form of mechanical weathering, operating subglacially. Hydrofracturing, for which there is local evidence (Section 4.1.5), has the same effect. The jacking and fracturing will lower the rock mass strength of the shallow bedrock, so that it is easier to erode, be it by plucking or by glacial ripping. The jacking and fracturing also greatly increases the hydraulic conductivity of the shallow rock mass.

Observational evidence for the origins of new fractures would be destroyed if glacial drag forces subsequently displaced rock blocks. Where drag forces were not applied directly to rock at the glacier bed, as beneath covers of till and glaciofluvial deposits, then new fractures may remain undisturbed, but this may be rare (Section 4.1.5). Beam failure as modelled can be predicted to produce fractured slabs, with underlying crushed chockstones, and minor downward displacement of blocks into former cavities that developed along hydraulically-jacked subhorizontal fractures.

6.3 Modelling drag and resisting forces

6.3.1 Introduction

Although overpressure and resulting fracture dilation appear a critical step for our process sequence, a second, major question is whether the resisting forces of a rock hill (of any size) are sufficiently lowered by hydraulic jacking so that the drag forces of the moving ice exceed them, thus leading to the glaciotectonic disintegration of the rock mass. At issue here is the balance between drag forces exerted by the ice versus the resisting forces of the surface rock mass, and the role of hydraulic jacking and rock mass disruption on this balance. To address these issues, in this section we attempt to model (see also Krabbendam et al. 2022b):

(i) the drag forces exerted by ice creeping and sliding past a range of rock obstacles (i.e. a rock bump or hill) of variable size and shape at the base of an ice sheet;

(ii) the resisting forces of rock mass obstacles, with varying internal fracture network configurations, and how these are affected by high water pressure events.

All scenarios are modelled as a function of glaciological variables such as water pressure, ice velocity and ice thickness. We then assess the force balance and assume that block movement, and hence glacial ripping, can occur if the ice drag forces exceed the resisting forces of the rock bump or hill. We are thus testing whether glacial ripping is a physically plausible process, and under what glaciological and geological conditions it may, or may not, operate at the base of an ice mass.

6.3.2 Modelling scenarios and model assumptions

The geometries of the ripped bedrock hills, their internal fracture networks, and the resultant glacial ripping in eastern Sweden are highly variable, and locally complex. We confine ourselves to model a number of simple scenarios, informed by natural examples, but including some end-member scenarios (Figure 6-4).

1. A blunt hemispherical obstacle of intact rock, without a basal fracture.

2. A blunt hemispherical obstacle with a continuous subhorizontal basal fracture.

These first two scenarios are perhaps unrealistic but serve as end-member scenarios.

3. A blunt hemispherical obstacle with a discontinuous basal fracture, formed by steps in the basal fracture system.

4. An elongate obstacle with subhorizontal fractures and a blunt stoss side, but a larger, flatter top.

5. A small rock step protruding above the surrounding rock surface, caused by the partial uplift of a rock block, as developed on the smooth surface of a larger rock hill or a low relief rock surface.

The development of whaleback and roche moutonnée forms occurred throughout the last and previous glaciations. Field evidence suggests that damage from glacial ripping was particularly effective below the ablation zone close to the retreating margin of the Fennoscandian, British and Laurentide ice sheets during deglaciation (Section 5.2, see also Hall et al. 2020, 2021a, Krabbendam et al. 2021, 2022b, Bukhari et al. 2021). Hence, we focus here on conditions beneath the Fennoscandian Ice Sheet at a late stage of its last deglaciation. Direct glaciological controls exerted by this palaeo-ice sheet are evidently not available, but the Greenland Ice Sheet is also in a state of retreat, so we use observations from its ablation zone, such as outcomes of the GAP and ICE projects in West Greenland (Claesson Liljedahl et al. 2016, Harper et al. 2019), as an analogue for the retreating Pleistocene ice sheets.

Relevant assumptions are as follows:

1. **Basal thermal regime**. The ice sheet was 'warm-based' with ice temperatures at the pressure melting point. A warm, sliding base in eastern Sweden, at least during deglaciation, is shown by the fact that rock hills are decorated with striae, showing that abrasion (and hence warm-based sliding) was active prior to glacial ripping (e.g. Sohlenius et al. 2014); ice-sheet modelling also suggest warm-based conditions close to the retreating margin (e.g. Näslund et al. 2003, Patton et al. 2016, 2017). Similarly, the basal temperature of Greenland Ice Sheet ablation zone is at the melting point (Macgregor et al. 2016), and ice motion shows a significant component (45–75 %) of basal sliding (Ryser et al. 2014).

2. We model ice as a viscous Newtonian medium, with a viscosity of $\eta = 1.3 \times 10^{11}$ Pa s, established experimentally by Byers and others (2012). Other theoretical studies applied the same simplifying approach (e.g. Nye 1970, Hallet 1979), but as it happens it is also realistic for temperate ice (Colbeck and Evans 1973, Chandler et al. 2008, Byers et al. 2012, Krabbendam 2016). In essence, we thus assume a basal layer of temperate ice, thicker than the highest rock obstacles. In Greenland, borehole temperature measurements show a 30–100 m thick basal layer of temperate ice at 20–50 km from the margin, whereas close to the margin the entire ice thickness is temperate (Lüthi et al. 2002, Ryser et al. 2014, Harrington et al. 2015, Harper et al. 2019).

3. **Ice sliding velocity**. Patton et al. (2017) modelled the maximum ice surface velocities during deglaciation of eastern Sweden at c. 200–400 m yr^{-1}. In the Greenland Ice Sheet ablation zone, basal sliding velocities are c. 50–75 % of the surface velocities (Ryser et al. 2014), so we assume c. 300 m yr^{-1} as the maximum realistic sliding velocity.

4. **Ice thickness**. Although the Fennoscandian Ice Sheet reached a maximum thickness of around 3 000 m during Last Glacial Maximum, with a thickness over the Forsmark site of ca. 2 900 m (Vidstrand et al. 2014), field evidence suggests that glacial ripping was particularly active just prior to deglaciation, hence with considerably lower ice thickness. In the lower ground in eastern Sweden, ice retreat was dominated by calving in the Baltic Sea or Yoldia Lake, with water depth up to 180 m (Section 2.3). The total ice thickness at the margin at Östhammar has been estimated as ~300 m (Persson 1988). We assume an ice thickness of 300 m or 600 m (see also Section 6.1).

5. **Basal water pressure fluctuations**. Evidence for hydraulic jacking includes dilated and sediment-filled fractures (see above). High water pressures, which may temporarily exceed overburden pressure (overpressure), have been measured or demonstrated at the base of the Greenland Ice Sheet ablation zone in two types of events: (i) large magnitude (in terms of volume) overpressure events caused by drainage of supraglacial lake drainage (Das et al. 2008, Doyle et al. 2013); (ii) small magnitude overpressure events occurring in 'weakly connected zones', without supraglacial lake drainage (Andrews et al. 2014, Harper et al. 2016, Wright et al. 2018, Harper et al. 2019). These documented overpressure events are discussed further in Section 7.2. Based on these studies we assume that pressure fluctuations between 80–105 % (or $P_w/P_i = 0.8 - 1.05$), around an average water pressure of c. 90–95 % are realistic for our models.

6. We assume that the fracture patterns of the bedrock are broadly orthogonal and comprise sub-horizontal and subvertical fractures. This broad geometry is common in basement rocks in Sweden (Section 4.1; Carlsson 1979, Krabbendam et al. 2021). However, we do model two different fracture patterns: (a) a scenario where all fractures are continuous in-plane, and (b) a scenario where sub-horizontal fractures occur at different levels ('stepped') but joined by subvertical fractures, via T-junctions, thus being discontinuous in a single plane (Scenario 3 in Figure 6-4).
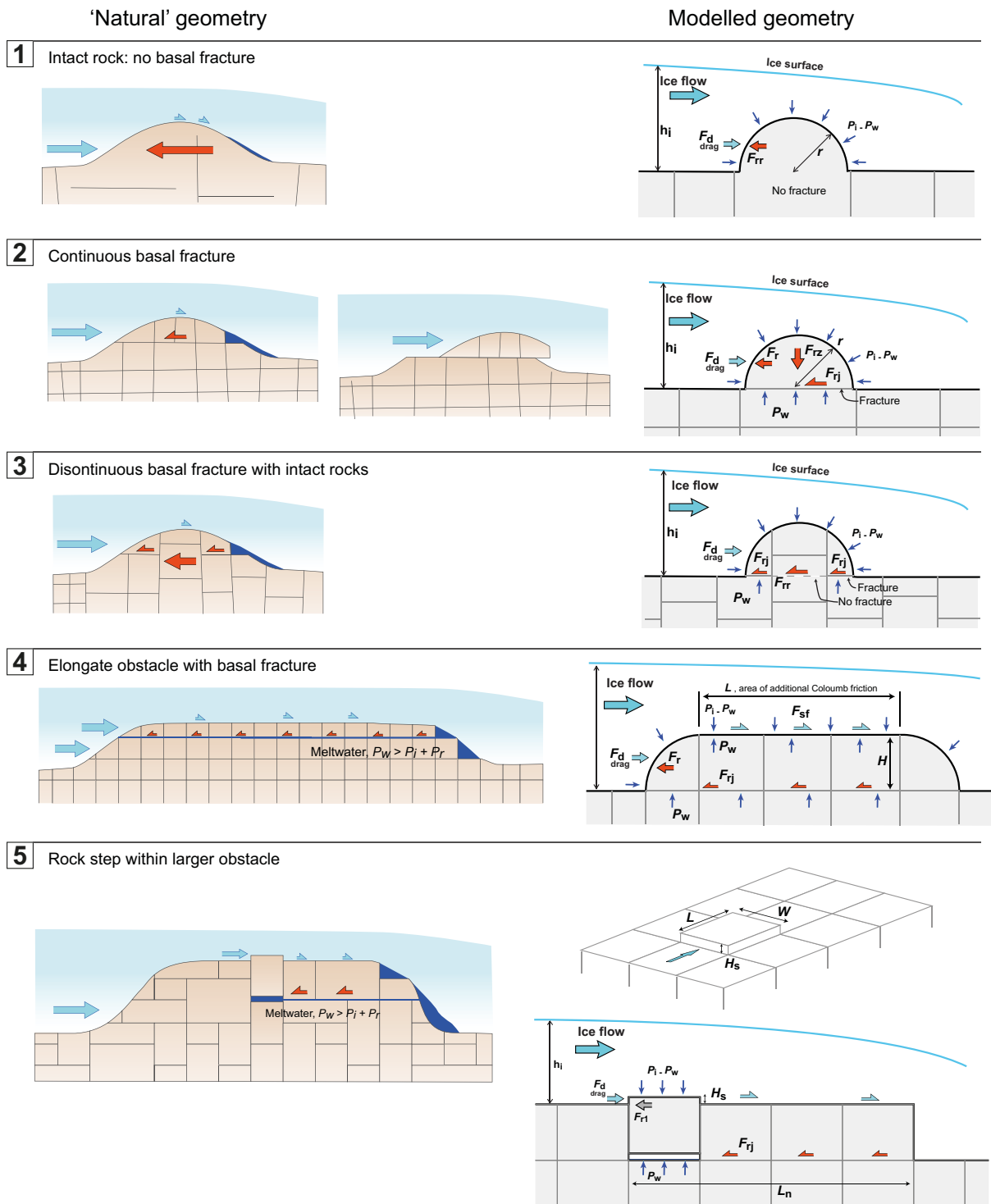
Figure 6-4. *Modelling scenarios 1–5: conceptual geometries; modelled geometries with some parameters indicated. After Krabbendam et al. (2022b).*

6.3.3 Modelling approach: defining drag and resisting forces

The basis of the modelling is the principle that if the drag force F_d exerted by ice flowing past a blunt obstacle exceeds the resisting forces F_r of that obstacle, then the obstacle moves or disintegrates:

$$F_d > F_{rx} \tag{6-12}$$

Drag forces for a hemispherical obstacle

Ice is modelled as a viscous Newtonian medium creeping at low velocities, valid for temperate ice (Hallet 1979, Byers et al. 2012). In this laminar flow regime with very low Reynolds number (Re <<1), also known as Stokes regime, the drag force F_d on a spherical particle has been obtained by solving for the Navier-Stokes equations (Stokes 1951, Loth 2008):

$$F_d = 6\pi\eta U r \tag{6-13}$$

where η is the viscosity of temperate ice, U the velocity of the medium and r the radius of a spherical particle. F_d is the sum of two contributions: (i) form drag, which arises from the pressure the fluid exerts on the cross-sectional area of the object perpendicular to the streamlines, and (ii) viscous friction (or: skin drag), which is caused by the tangential shear stress at the particle surface (Leith 1987). In a normal viscous medium, the creep velocity right at the contact is zero (non-slip boundary), and the tangential shear stress at the obstacle surface is substantial. This is evidently not the case for temperate ice, where sliding is known to occur with a thin film of water between the obstacle and the ice. Thus, for temperate ice creeping past an obstacle, the skin drag component maybe low. Consequently, some authors suggest $F_d = 4\,\pi\eta U r$ (e.g. Hallet 1979, Cohen et al. 2005). However, Byers et al. (2012) empirically confirmed that Equation (6-13) is broadly valid (with values of 5.5π; 6.9π and 7.5π) for temperate ice. As we also use the values of ice viscosity from the same experiments (see Section 6.3.2), we herein use Equation (6-13) as is. However, we cut the sphere in half to model a hemispherical obstacle (Figure 6-5) so that:

$$F_d = 3\pi\eta U r \tag{6-14}$$

Effects of regulation are ignored because our obstacles are very large compared to smaller debris particles, which diminishes the heat flow effect through the obstacle (see also Hallet 1979, Byers et al. 2012), and because there is likely to be excess flowing water in the system that evens out any temperature gradient (e.g. Krabbendam 2016).
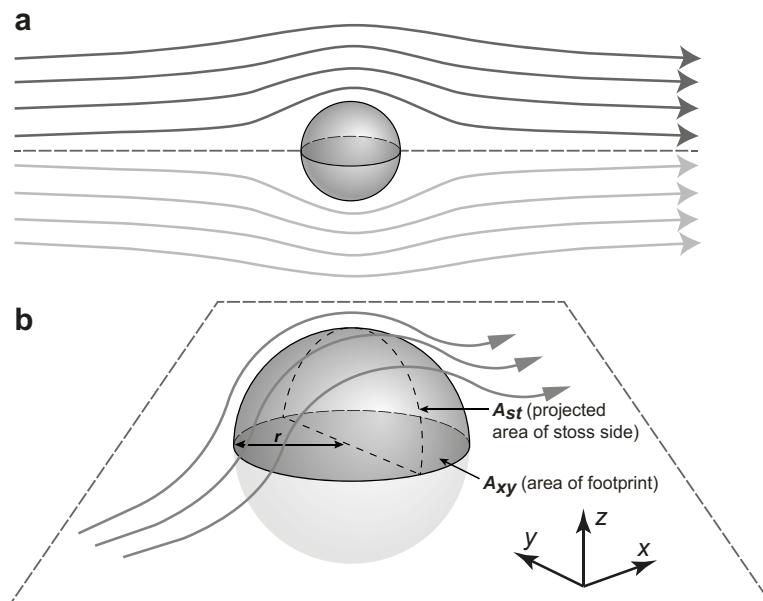
Figure 6-5. *Principle of applying Stokes Law for laminar flow around a sphere to a hemispherical obstacle. A. Laminar flow around a sphere. B. Hemispherical obstacle, in a half space, within a laminar flow field. Area of projected stoss side A_{st} and area of footprint of obstacle A_{xy} are indicated. Direction of ice flow = x. After Krabbendam et al. (2022b).*

Drag forces for a non-hemispherical, elongate obstacle

Drag forces for a non-hemispherical obstacle are more complicated as they depend on the shape of the object, which need to be quantified with a shape descriptor (e.g. Leith 1987, Ganser 1993, Bagheri and Bonadonna 2016, Dioguardi et al. 2018). These approaches all assume a non-slip boundary. As discussed above, slip does occur along the ice-rock boundary in temperate ice, so these approaches are not appropriate. To approximate the drag forces on an elongate obstacle, we model a geometry where we split the obstacle in (i) a blunt stoss side that faces ice flow, and (ii) a flat horizontal top surface parallel to ice flow. We assume that (i) the drag force at the stoss side is controlled by the viscous drag acting upon that stoss face (with surface A_{st}) and controlled by a form of Stokes law, and that (ii) the drag forces on the flat top surface area are controlled by the Coulomb friction law acting on the top surface (with surface A_{xy}). Coulomb friction along the flat top surface is then:

$$F_{sf} = \mu_{ir} \, F_{iz} \qquad\qquad (6\text{-}15)$$

where μ_{ir} is the friction coefficient on the ice-rock contact. Empirical and experimental studies (e.g. Cohen et al. 2005, Emerson and Rempel 2007) suggest a value of $\mu_{ir} = 0.05$. The normal force exerted by the overlying ice F_{iz} depends on the thickness and density of ice (cryostatic pressure P_i), the water pressure P_w, and the horizontal surface area A_{xy} over which it operates as follows:

$$F_{iz} = (P_i - P_w) \, A_{xy} \qquad\qquad (6\text{-}16)$$

The horizontal surface A_{xy} equates approximately with the surface area of the basal fracture of the rock obstacle. As we wish to explore the effects of relative overpressure, this can be rewritten as:

$$F_{iz} = g h_i \rho_i \left(1 - \frac{P_w}{P_i}\right) A_{xy} \qquad\qquad (6\text{-}17)$$

where g is the gravitational constant, h_i the ice thickness and ρ_i the density of ice. Total Coulomb friction along the top surface then becomes:

$$F_{sf} = \mu_{ir} \, g h_i \rho_i \left(1 - \frac{P_w}{P_i}\right) A_{xy} \qquad\qquad (6\text{-}18)$$

Note that Coulomb friction F_{sf} will approach zero if P_w approaches P_i; because a friction force cannot be negative, Equations (6-16) to (6-18) are not valid if $P_w > P_i$

The viscous drag F_{fd} acting on the blunt stoss side can be approximated by assuming that it is controlled by the square root of the vertical surface area that faces up-ice flow (the projected 'stoss-side surface area' A_{st}, which is half the surface area of a circle with radius r):

$$A_{st} = \frac{1}{2} \pi \, r^2 \text{ so that } r = \sqrt{2 A_{st}/\pi} \qquad\qquad (6\text{-}19)$$

The viscous drag component then becomes (Equation (6-14) combined with (6-19)):

$$F_{fd} = 3 \, \eta U \sqrt{2 A_{st}/\pi} \qquad\qquad (6\text{-}20)$$

The total drag forces of a non-hemispherical obstacle is then approximated as (Equation (6-18) and (6-20)):

$$F_d = 3 \, \eta U \sqrt{2 A_{st}/\pi} + \mu_{ir} g h_i \rho_i \left(1 - \frac{P_w}{P_i}\right) A_{xy} \qquad\qquad (6\text{-}21A)$$

For a rectangular cuboid-shaped obstacle, with width W, height H and length L this becomes:

$$F_d = 3 \, \eta U \sqrt{2HW/\pi} + \mu_{ir} g h_i \rho_i \left(1 - \frac{P_w}{P_i}\right) WL \qquad\qquad (6\text{-}21B)$$

Resisting forces for a hemispherical obstacle without fractures

If the rock obstacle is poorly fractured, for instance if the rock hill is smaller than the fracture spacing in the overall rock mass, or if no continuous subhorizontal fractures are present (Figure 6-4, Scenario 1), the resisting force of intact rock F_{rr} is controlled by the intact rock strength as follows:

$$F_{rr} = \tau_r A_r \tag{6-22}$$

where τ_r rock is the shear strength of intact rock, and A_r the surface area of the potential shear plane of the intact rock. Shear strength values for intact rock are rarely measured, compared to uniaxial compressive strength (UCS) and tensile strength. Singh et al. (2017) obtained shear strengths between c. 10–35 MPa for different gneisses. Shear strength is typically 20–30 % of UCS, and about twice the tensile strength. Rock mechanic tests on rocks near Forsmark yielded a range of 160–370 MPa for UCS and 10–18 MPa for tensile strength (Glamheden et al. 2007), suggesting a shear strength range of 20–60 MPa. We take a conservative value of ~ 20 MPa for τ_r, as in nature rocks may contain micro-structures, which lower the shear strength.

Resisting forces for a hemispherical obstacle with continuous basal fracture

If a rock hill contains fractures – as most do – its rock mass strength is lower than that of intact rock. We first consider the simple scenario of an obstacle with a single continuous subhorizontal fracture at its base (Figure 6-4, Scenario 2). In that case, the resisting force of the rock hill is controlled by the frictional force along a single fracture, defined as:

$$F_{rj} = \mu_{rr} F_{rz} \tag{6-23}$$

where μ_{rr} is rock-rock friction coefficient along the basal fracture, and F_{rz} the normal force acting vertically on the basal fracture. Rock-rock friction coefficient varies depending on rock type and fracture roughness; for natural fractures in gneissic rocks Ramana and Gogte (1989) report a range of 0.64–0.77; Glamheden et al. (2007) report a range of 0.48–0.77 (mean of 0.67), for rocks at Forsmark. We take a value of 0.7. We ignore fracture cohesion, since hydraulic jacking will have broken any such cohesion. The normal force F_{rz} has two components:

$$F_{rz} = F_{bz} + F_{iz} \tag{6-24}$$

where F_{bz} is the buoyant weight of the block and F_{iz} any force (weight) exerted by the overlying ice, as per Equation (6-17). The drag force exerted by ice flowing vertically downward due to basal melting is ignored: whilst significant for small (centimetre-sized) debris particles under conditions of vigorous basal melting (Cohen et al. 2005, Byers et al. 2012), it becomes very small for metre-sized obstacles (Krabbendam and Hall 2019).

The buoyant weight of the block F_{bz} is given by:

$$F_{bz} = V (\rho_r - \rho_w)g \tag{6-25}$$

where V is the volume of the block, ρ_r the density of rock, ρ_w the density of water. The total frictional resisting force along the fracture is then (Equations (6-24, 6-25, 6-17)):

$$F_{rj} = \mu_{rr} [V(\rho_r - \rho_w)g + gh_i\rho_i \left(1 - \frac{P_w}{P_i}\right) A_{xy}] \tag{6-26A}$$

For a hemispherical obstacle, as a direct function of r (with $V = 2/3 \, \pi \, r^3$ and $A_{xy} = \pi \, r^2$), this becomes:

$$F_{rj} = \mu_{rr} [\tfrac{2}{3}\pi \, r^3 (\rho_r - \rho_w)g + gh_i\rho_i \left(1 - \frac{P_w}{P_i}\right) \pi r^2] \tag{6-26B}$$

For a rectangular cuboid-shaped obstacle, with width W, height H and length L, this becomes:

$$F_{rj} = \mu_{rr} [H \, W \, L \, (\rho_r - \rho_w)g + gh_i\rho_i \left(1 - \frac{P_w}{P_i}\right) W \, L] \tag{6-26C}$$

Effect of variable transmissivity of basal fractures.

In the above, it is assumed that the water pressure within a basal fracture equalises instantaneously with any pressure fluctuation at the ice-bed contact, which only happens if the fracture is highly transmissive. This situation exists where fractures are open in the near-surface (Section 4.1). Fracture transmissivity, however, is highly variable in nature: low transmissive, tight fractures are common in basement rocks and imply that water pressure transients at the ice-bed may only penetrate a short depth below the bed or a short distance along the fracture (e.g. Neupane et al. 2020). Limited transmissivity dampens the effect of fluctuating water pressures at the bed in the fracture and hence lowers the peak water pressures within the fracture: water pressures in such fractures will stay close to the average water pressure at the ice bed (e.g. c. 90–95 % of P_i). A transmissivity factor T_j (1 for perfect transmissive fracture; 0 for completely tight, clogged fractures) can be introduced to model the effects of variable transmissivity along basal fractures, shown here for a hemispherical obstacle (3-15B).

$$F_{rj} = \mu_{rr} \left[\tfrac{2}{3}\pi\, r^3\,(\rho_r - \rho_w)g + gh_i\rho_i \left(1 - \tfrac{T_j P_w}{P_i}\right)\pi r^2\right] \tag{6-27}$$

Resisting Forces with discontinuous basal fracture and some intact rock

Fracture networks in the basement rocks of eastern Sweden (and elsewhere) are highly variable, and continuous subhorizontal fractures at the base of an obstacle are not necessarily ubiquitous: in various quarries and natural outcrops it was observed that subhorizontal fractures occur at different levels and hence discontinuous; in other sections subvertical fractures are dominant over subhorizontal fractures (Section 4.1; Krabbendam et al. 2021). This variability is modelled as a hemispherical obstacle where the base constitutes partly intact rock and partly a fracture (Figure 6-4, Scenario 3). (This is similar to the 'dovetail' construction of the coastal lighthouses designed by John Smeaton and the Stevenson's brothers in 18th century Britain (Bathurst 1999). Most of these are still standing). The total resisting force F_{rx} is then the resisting force of the fracture plus that of intact rock, proportional to the area occupied by the basal fracture A_j and intact rock A_r respectively:

$$A_{xy} = A_r + A_j \quad \text{and} \quad F_{rx} = F_{rr} + F_{rj} \tag{6-28}$$

Proportional by area this becomes:

$$F_{rx} = F_{rr}\,A_r + F_{rj}\,A_j = F_{rr}\,A_{xy}\,\frac{A_r}{A_{xy}} + F_{rj}A_{xy}\,\frac{A_j}{A_{xy}} \tag{6-29}$$

So that, using Equations (6-22) and (6-26):

$$F_{rx} = A_{xy}\,\tau_{rk}\,\frac{A_r}{A_{xy}} + \frac{A_j}{A_{xy}}\,\mu_{rr}\left[V(\rho_r - \rho_w)g + gh_i\rho_i\left(1 - \tfrac{P_w}{P_i}\right)A_{xy}\right] \tag{6-30A}$$

and for a hemispherical obstacle:

$$F_{rx} = \pi r^2 \tau_{rock}\,\frac{A_r}{A_{xy}} + \frac{A_j}{A_{xy}}\,\mu_{rr}\left[\tfrac{2}{3}\pi r^3\,(\rho_r - \rho_w)g + gh_i\rho_i\left(1 - \tfrac{P_w}{P_i}\right)\pi r^2\right] \tag{6-30B}$$

Testing plausibility at realistic glaciological conditions

For the different scenarios, both the drag and resisting forces are calculated. Lines where drag force equals resisting force are plotted for different obstacle radii against ice sliding velocity and relative water pressure.

$$F_d = F_{rx} \tag{6-31}$$

Above the line, $F_d > F_{rx}$ and the obstacle may be moved by the ice; below the line $F_d < F_{rx}$. Thus, for the example of an obstacle with a continuous basal fracture (Equation (6-26A)), one would expect the hemisphere to remain in place: if

$$3\pi\eta U r = \mu_{rr}\left[V(\rho_r - \rho_w)g + gh_i\rho_i\left(1 - \tfrac{P_w}{P_i}\right)A_{xy}\right] \tag{6-32}$$

And for a obstacle with a hemisphere shape (Equation (6-26B)):

$$3\pi\eta Ur = \mu_{rr}\left[\frac{2}{3}\pi\,r^3(\rho_r - \rho_w)g + gh_i\rho_i\left(1 - \frac{P_w}{P_i}\right)\pi\,r^2\right] \tag{6-33}$$

As function of sliding speed, F_d equals F_r if:

$$U = \mu_{rr}\frac{\left[\frac{2}{3}\pi\,r^3(\rho_r - \rho_w)g + gh_i\rho_i\left(1 - \frac{P_w}{P_i}\right)\pi\,r^2\right]}{3\pi\eta r} = \mu_{rr}g\frac{\left[\frac{2}{3}r^2(\rho_r - \rho_w) + h_i\rho_i\left(1 - \frac{P_w}{P_i}\right)r\right]}{3\eta} \tag{6-34}$$

On all graphs (Figures 6-6 to 6-11), boxes with plausible glaciological conditions are indicated. These are constrained as water pressure varying between 60 and 105 %, as measured beneath the Greenland Ice Sheet (Andrews et al. 2014, Wright et al. 2016, Claesson Liljedahl et al. 2016), and maximum sliding velocities of 300 m yr^{-1}.

6.3.4 Results

Different scenarios are calculated below and interpreted. Each interpretation leads to the constraints for the next scenario.

Scenario 1: hemispherical obstacle without fractures

In a hemispherical obstacle without a basal fracture (Figure 6-4, Scenario 1), the drag force F_d increases linearly as a function of sliding speed U (Equation (6-14)), whereas the resisting force F_r is constrained by the intact rock strength, independent of any glaciological parameter (Equation (6-22)). The resisting forces generally exceed the driving forces, even for very high sliding velocities (Figure 6-6). Small obstacles may fail at very high sliding velocities (> 1 700 m yr^{-1}), velocities that are not likely to occur on a hard-bedded ice sheet. There is no dependency on ice thickness.

This end-member scenario shows that rock hills without fractures are to all intents and purposes impossible to be disintegrated or moved by sliding ice. Such rock hills will be eroded by abrasion alone, and form smooth whalebacks, as opposed to roches moutonnées. The height of such monolithic hills is constrained by the fracture spacing of the bedrock, which is normally < 5–10 m. In nature, this scenario might thus apply to small whalebacks; larger hills are typically formed of several or many large rock blocks.
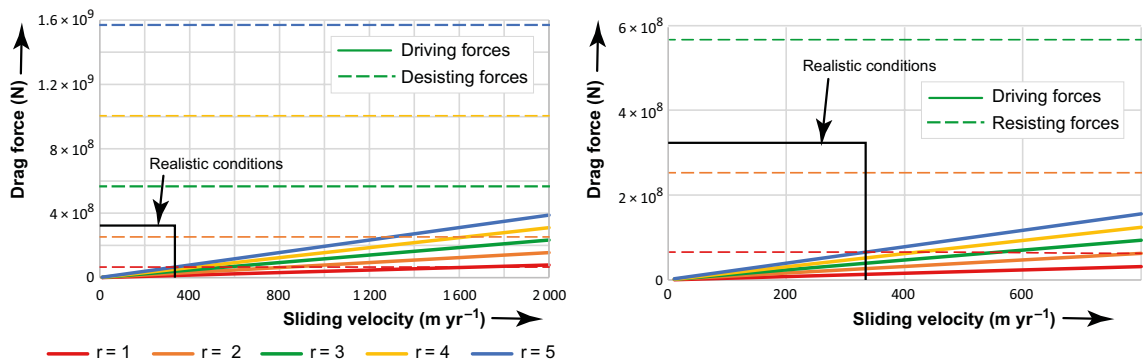
Figure 6-6. *Drag forces F_d (solid lines) and resisting forces F_r (dashed lines) as a function of sliding velocity U, for a hemispherical obstacle without basal fracture, for obstacles with radii 1–5 m. Intact rock strength τ_r is taken at ~ 20 MPa. After Krabbendam et al. (2022b).*

Scenario 2: hemisphere with continuous basal fracture

In a hemispherical obstacle with a continuous subhorizontal basal fracture, the resisting forces are controlled by the Coulomb rock-rock friction along the basal fracture (Equation (6-23, 6-26B)). They decrease linearly with relative water pressure P_w/P_i, and become zero just beyond the point of flotation ($P_w = P_i$), because of the buoyant weight (F_{bz}) of the hemisphere (Figures 6-6A, B, shown for ice thickness of 300 and 600 m). Drag force F_d increases linearly as a function of sliding speed U (Equation (6-14)), as in Scenario 1 (Figure 6-6). Lines of equal drag and resisting force as a function of sliding velocity and relative water pressure for this scenario are given by combining Equations (6-14) and (6-26):

$$3\pi \eta U r = \mu_{rr} \left[\tfrac{2}{3} \pi r^3 (\rho_r - \rho_w) g + g h_i \rho_i \left(1 - \tfrac{P_w}{P_i} \right) \pi r^2 \right] \tag{6-35}$$

$$U = \mu_{rr} \frac{\left[\tfrac{2}{3} \pi r^3 (\rho_r - \rho_w) g + g h_i \rho_i \left(1 - \tfrac{P_w}{P_i} \right) \pi r^2 \right]}{3\pi \eta r} \tag{6-36}$$

Interpretation of Scenario 2

The plots (Figure 6-7) show that under a very wide range of realistic conditions (boxes in graph), blunt, hemispherical obstacles with a continuous basal fracture can be removed by sliding ice. Small obstacles are considerably easier to move than large obstacles. Block removal can occur without overpressure: a small roche moutonnée ($r = 3$ m) can be removed at sliding speeds of 200 m yr^{-1}, with $P_w/P_i = 0.9$, which are fairly normal circumstances for ice sheets. Ice thickness has only a minor effect: a doubling of the ice thickness leads to somewhat higher resisting forces, but at higher water pressures this has little effect, and in the further modelling we only model with ice thickness of 300 m.
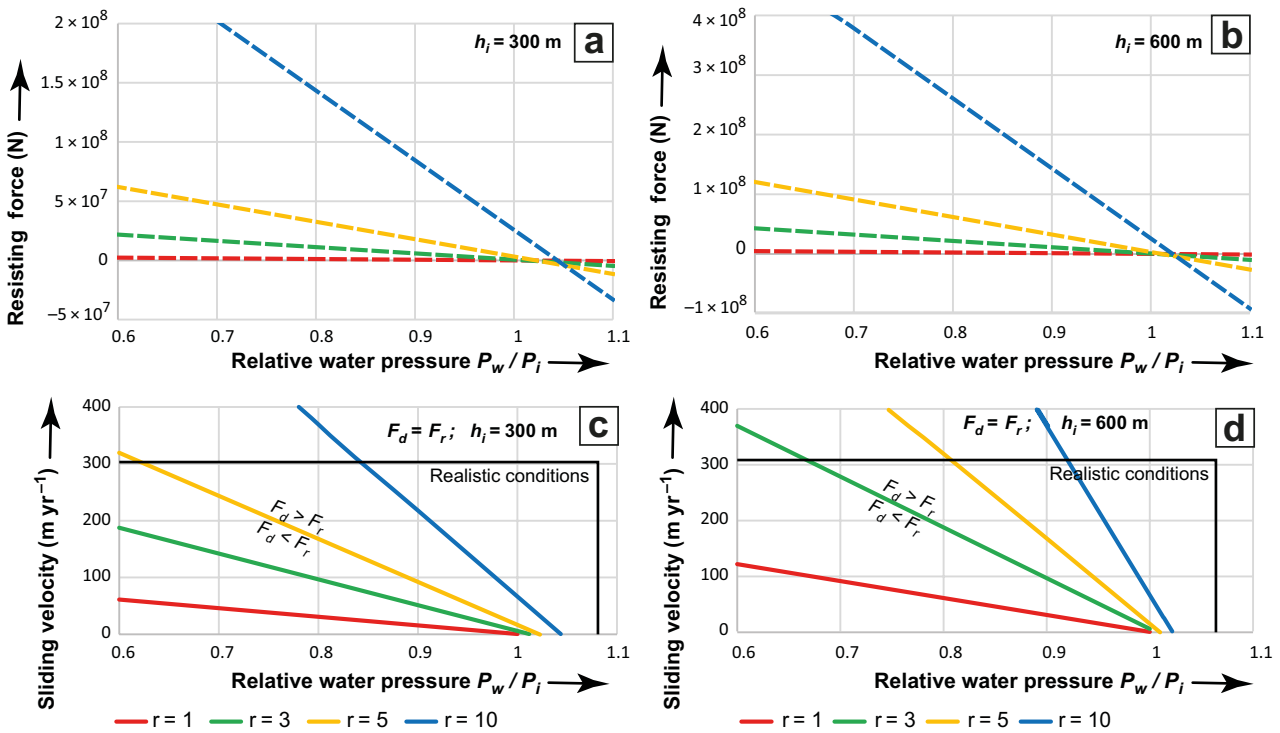
Figure 6-7. *A. Resisting forces (N) as a function of relative water pressure P_w/P_i, for hemispherical obstacles with radii 1 to 10 m; ice thickness 300 m. B. As A, but ice thickness 600 m. C. Lines of equal drag and resisting forces ($F_d = F_r$) as a function of sliding speed U and relative water pressure P_w/P_i, for hemispherical obstacles with radii 1 to 10 m. Above the lines, blocks can move, below the lines, blocks cannot move. Box indicates realistic conditions, e.g. water pressure variations between 60–105 %, and sliding speeds < 300 m yr^{-1}. D. As C., for ice thickness 600 m. After Krabbendam et al. (2022b).*

In the case of overpressure (e.g. $P_w/P_i = 1.05$, which has been observed beneath the Greenland Ice Sheet), all obstacles would be removed regardless of size. Given that the base of the ablation zone of Greenland Ice Sheet is rough (e.g. Lindbäck and Pettersson 2015, Cooper et al. 2019), and there is still a residual terrain roughness in eastern Sweden with a multitude of surviving roches moutonnées with heights of 5–20 m (Hall et al. 2019a), this scenario is not realistic as a general case. The critical assumption in this scenario, namely that of a perfectly continuous subhorizontal basal fracture in which P_w equalises perfectly with P_w at the ice-bed interface, is likely not realistic, and should be seen as an idealised end-member scenario.

Scenario 3a: hemisphere with part intact rock and part basal fracture

This scenario considers a rock hill with a discontinuous basal fracture, with part of the basal footprint comprising intact rock, the strength of which is controlled by the shear strength τ_{rk} of intact gneiss. We take a value of 20 MPa for this (Singh et al. 2017); weaker rocks will have lower values. Lines of equal driving and resisting force are then given by (combining Equation (6-14) and (6-30B)):

$$U = \frac{\pi r^2 \tau_{rk} \dfrac{A_r}{A_{xy}} + \dfrac{A_j}{A_{xy}} \mu_{rr} [\frac{2}{3}\pi r^3 (\rho_r - \rho_w)g + gh_i\rho_i \left(1 - \dfrac{P_w}{P_i}\right)\pi r^2]}{3\pi\eta r}$$

(6-37)

Interpretation of Scenario 3a

The graph (Figure 6-8A) plotting resisting force as a function of the proportion of intact rock vs basal fracture at the base of the hemisphere (for $P_w = P_i$, i.e. flotation) shows that even a very small proportion (5–10 %) of intact rock has a dramatic effect on the resisting forces. The points show the drag force exerted by ice sliding at 300 m yr^{-1} for the different radii, taken as a maximum. For large hemispheres ($r = 4$–5 m), blocks cannot move if < 10 % of the footprint is occupied by intact rock, for smaller blocks this can increase up to 15–20 %. On the graph (Figure 6-8B) showing sliding velocity vs relative water pressure for equal drag and resisting forces it is clear that larger (> 3 m) hemispheres in essence cannot be moved under realistic conditions (box) if intact rock occupies > 5 % of the footprint. Overall this shows that intact rock offers far more resistance that a continuous transmissive fracture. It also implies that a small step in the fracture, if facing up-ice, can effectively 'lock' an obstacle in place. A suitable fracture pattern with continuous sub-horizontal fractures would thus favour glacial ripping, whilst an unfavourable fracture pattern would strongly hinder glacial ripping.
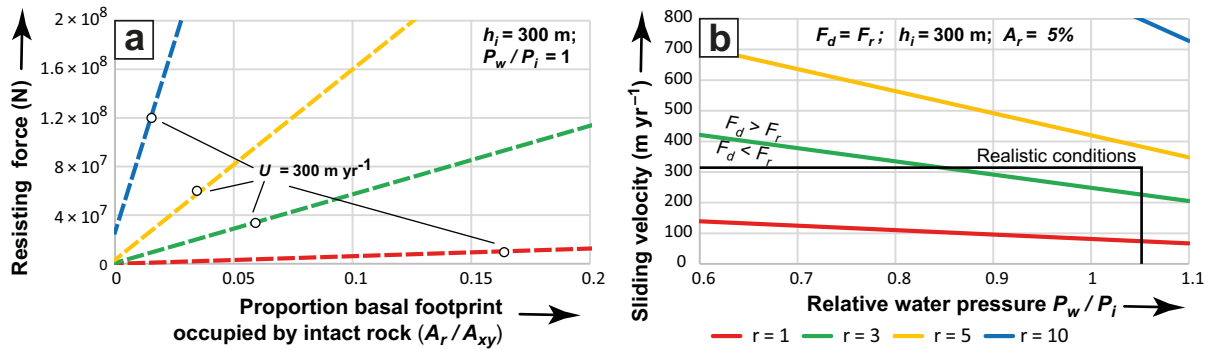
Figure 6-8. A. Resisting forces as a function of the proportion of basal footprint of hemisphere (radii 1–10 m) occupied by intact rock A_r/A_{xy}, for $P_w = P_i$ (flotation). Points are the maximum drag forces for sliding speeds of 300 m yr^{-1}. B. Lines of equal drag and resisting forces ($F_d = F_r$) as a function of sliding speed U and relative water pressure P_w/P_i, for hemispherical obstacles with radii 1 to 10 m. Above the lines, blocks can move, below the lines, blocks cannot move. Box indicates realistic conditions. After Krabbendam et al. (2022b).

Scenario 3b: hemisphere with low transmissivity basal fracture

In scenario 2 and 3A above it is assumed that if there is a fracture, then the water pressure in the fracture equalises rapidly with the water pressure at the ice bed. This will only happen if the fractures are open and highly transmissive (in the hydrological sense). In nature, fractures may have limited transmissivity. In that case the equalisation of water pressure between the ice bed and the fracture will be slow. The effects of limited fracture transmissivity can be assessed by introducing a transmissivity factor T_j; $T_j = 1$ for a perfect transmissive, open fracture in which the water pressure equalises instantaneously with the water pressure at the ice-bed contact outside the obstacle; $T_j = 0$ for completely tight, clogged fractures, that remains unconnected to the ice-bed. The actual value will vary from fracture to fracture, as will be discussed.

$$F_{rx} = \mu_{rr} \left[\tfrac{2}{3} \pi r^3 (\rho_r - \rho_w) g + g h_i \rho_i \left(1 - \tfrac{T_j P_w}{P_i} \right) \pi r^2 \right] \tag{6-38}$$

Interpretation Scenario 3b: hemisphere with low transmissivity basal fracture

From the graphs (Figure 6-9), it is evident that fracture transmissivity is an important factor. A lower transmissivity index would hamper hydraulic jacking, so that resisting forces of the rock hill are not lowered during a high water-pressure event. In the balance of drag and resisting forces, this implies that much higher sliding speeds would be required to mobilise roches moutonnées. With transmissivities below 0.6, mobilisation becomes unrealistic.

Scenario 4: Elongate obstacles with continuous basal fracture

For an elongate, flat-topped cuboid obstacle with a continuous basal fracture, the drag and resisting forces can be expressed in terms of length L, width W and height H of the obstacle. The drag force is calculated as a combination of form drag, acting on the stoss surface with surface area $H \cdot W$, and Coulomb friction acting on the flat top surface with surface area $L \cdot W$ and being dependent on the relative water pressure:

$$F_d = 3 \eta U \sqrt{2\, HW/\pi} + \mu_{ir} g h_i \rho_i \left(1 - \tfrac{P_w}{P_i} \right) LW \tag{6-39}$$

The resisting force is a function of the mass of the obstacle, with volume $H \cdot W \cdot L$, and the normal stress exerted by the ice acting on the top surface, with surface area $L \cdot W$.

$$F_{rj} = \mu_{rr} \left[HWL\, (\rho_r - \rho_w) g + g h_i \rho_i \left(1 - \tfrac{P_w}{P_i} \right) LW \right] \tag{6-40}$$
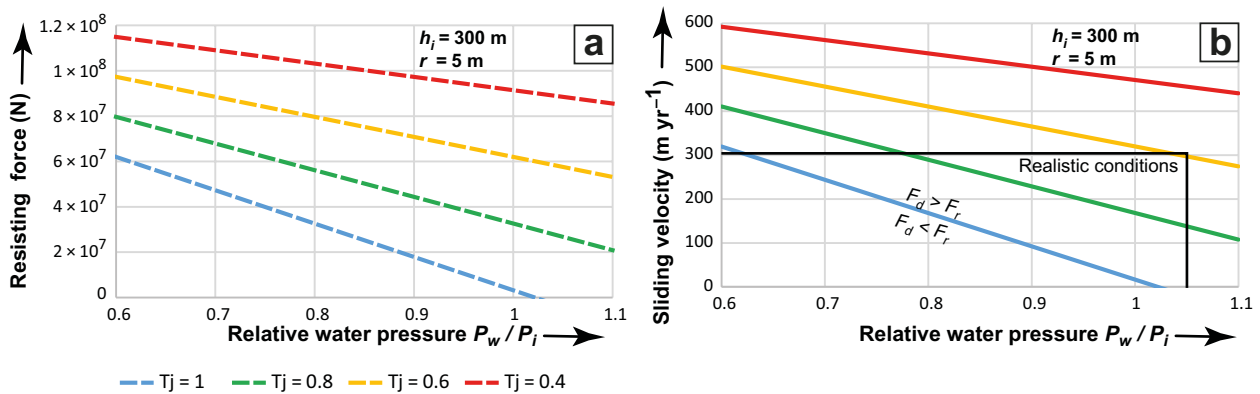
Figure 6-9. *Effect of limited transmissivity along basal fractures, ice thickness 300 m; hemispherical obstacle with r = 5. A. Resisting force in N versus relative water pressure, with transmissivity factor T_j varying between 0.4 and 1. B. Lines where drag forces equal resisting forces ($F_d = F_r$) as a function of sliding speed U and relative water pressure P_w/P_i, for hemispherical obstacles with 5 m radius, with transmissivity factor T_j between 0.4 and 1. Above the lines, blocks can move, below the lines, blocks cannot move. Box indicates realistic conditions. After Krabbendam et al. (2022b).*

The graph for an obstacle with fixed height (2 m), but variable length (Figure 6-10A), shows that whilst the drag force F_d depends somewhat on the length of the obstacle, this dependence is weak. This shows that most of the total drag force is provided by the viscous drag acting on the stoss side and thus dependent on the stoss surface area, but almost independent of the length of the obstacle, so that Coulomb friction on the top surface (which increases with increasing obstacle top surface area and hence length) only makes a minor contribution to the overall drag force. Figure 6-10B shows the effect of varying water pressure on the Coulumb friction on the top surface: overall the drag force decreases slightly with increasing water pressure.
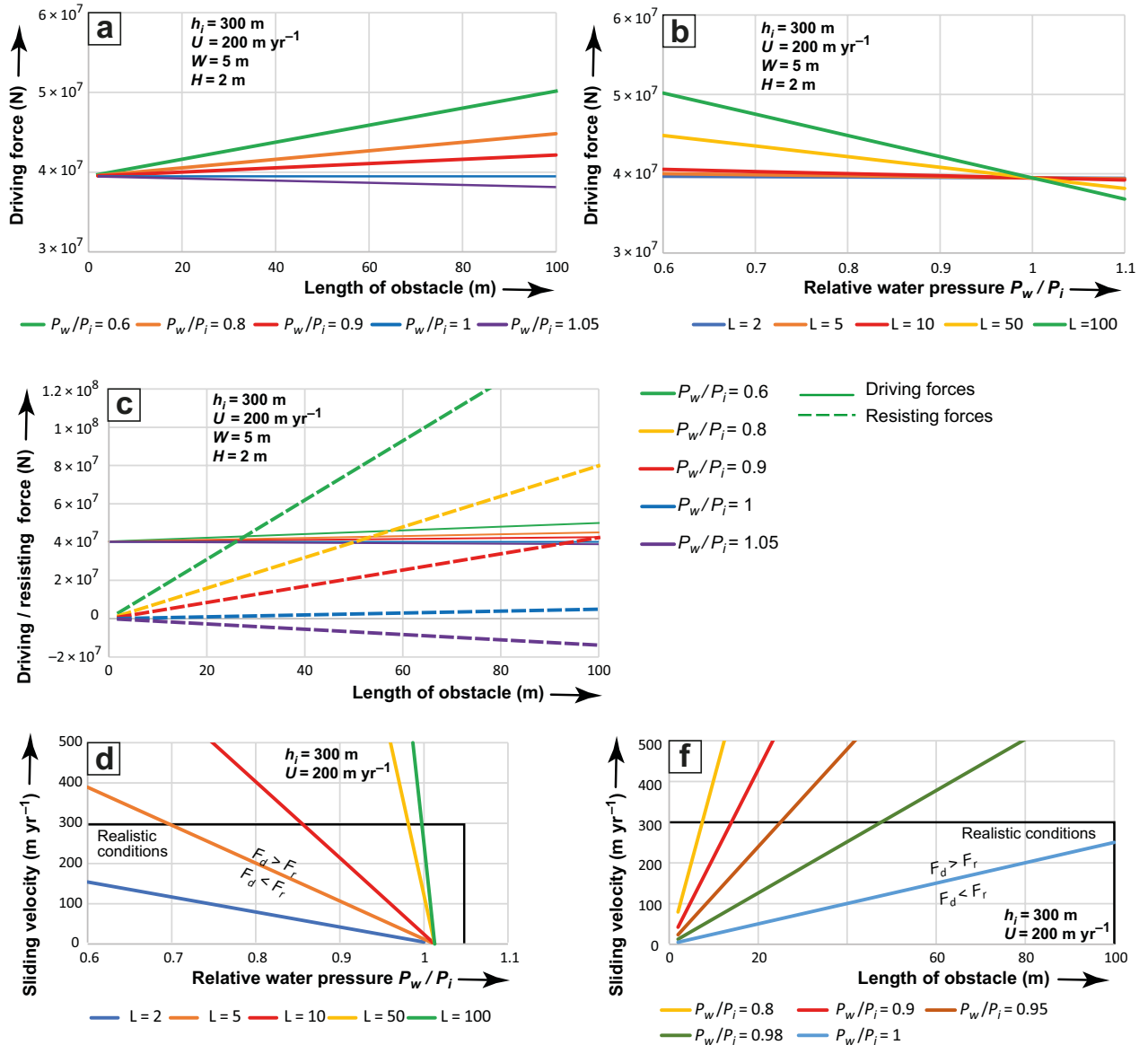
Figure 6-10. *A. Drag forces (N) as a function of length of an elongate obstacle, for different relative water pressure (with W = 5, H = 2 m, hi = 300 m; with sliding velocity U = 200 m yr^{-1}). B. Drag forces (N) as a function of relative water pressure, for obstacle with different length; other conditions same as A. C. Resisting forces (solid lines) and drag forces (dashed lines) as a function of length of a rectangular obstacle (W = 5, H = 2 m), for different relative water pressure P_w/P_i; ice thickness 300 m; ice sliding velocity 200 m yr^{-1}. D. Lines of equal drag and resisting forces ($F_d = F_r$) as a function of sliding speed U and relative water pressure P_w/P_i, for rectangular obstacles. Above the lines, blocks can move, below the lines, blocks cannot move. Box indicates realistic conditions. E. Lines of equal drag and resisting forces ($F_d = F_r$) as a function of sliding speed U and obstacle length, for different relative water pressure P_w/P_i (0.8–1.05). After Krabbendam et al. (2022b).*

Lines of equal resisting and drag forces as a function of sliding velocity become (Equation (6-21B) and (6-26C)):

$$U = \frac{\mu_{rr}\, HWL\, (\rho_r - \rho_w)g + \mu_{rr}\, gh_i\rho_i \left(1 - \frac{T_j\, P_w}{P_i}\right) LW - \mu_{ir}\, gh_i\rho_i \left(1 - \frac{P_w}{P_i}\right) LW}{3\eta\sqrt{2HW/\pi}}$$

(6-41)

For simplicity, we test an elongate rock hill with W = 5 m and H = 2 m, but with variable length, noticing that the width plays little role.

Drag forces are little affected by the length of the obstacle (Figure 6-10C), indicating that drag by Coulomb friction on the top surface has only minor influence compared to the viscous drag acting on the stoss face. The resisting forces, however, do increase linearly with the length of the obstacle: longer obstacles are more difficult to remove than shorter ones. Figures 6-10D and 6-10E show that, as water pressure in the fractures increases, increasingly long obstacles can be removed under constant ice velocity: at and just above flotation ($P_w = P_i$), very long obstacles can be removed at sliding velocities of 50–100 m yr^{-1}.

Interpretation Scenario 4

Long obstacles are more difficult to remove than short obstacles: removal requires high sliding velocities and high water pressures in basal fractures: at flotation ($P_w = P_i$), elongate obstacles up to 100 m can be removed at sliding velocities of 200 m yr^{-1}. All of this requires that the basal fracture is transmissive and continuous.

Scenario 5: Rock steps on a flat surface

In this scenario we look at a flat top surface of a longer rock hill or a low-relief rock surface. Over-pressure and hydraulic jacking can partially uplift a single block (Leijon 2005, Forssberg et al. 2007), so that a small rock step, with an up-ice facing stoss side, protrudes above the previously flat, abraded surface (Figure 4-2D; 6-4, Scenario 5). The drag force on that flat top surface, that previously only comprised Coulomb friction, now has an added component of viscous drag acting on the upstanding small rock step. The question is whether this drag force is sufficiently high to be able to disintegrate the top surface of that rock mass.

The drag force exerted on the top surface, with a rock step with height H_s is given by:

$$F_d = 3\,\eta U\sqrt{2H_sW/\pi} + \mu_{ir}gh_i\rho_i \left(1 - \frac{P_w}{P_i}\right) WL_n$$

(6-42)

where L_n is the total length of the row of blocks down-ice of the uplifted blocks. Since the rock mass is already opened up to allow hydraulic jacking, we assume a transmissivity of 1. The resisting forces of the row of blocks down-ice from the uplifted blocks is given by:

$$F_{rj} = \mu_{rr} \left[HWL_n (\rho_r - \rho_w)g + gh_i\rho_i \left(1 - \frac{P_w}{P_i}\right) WL_n\right]$$

(6-43)

Lines of equal resisting and drag forces as a function of sliding velocity become (Equation (6-42) and (6-43)):

$$U = \frac{\mu_{rr}\, HWL_n\, (\rho_r - \rho_w)g + (\mu_{rr} - \mu_{ir})\, g\, h_i\rho_i \left(1 - \frac{P_w}{P_i}\right) WL_n}{3\eta\sqrt{2HsW/\pi}}$$

(6-44)

Interpretation Scenario 5

The drag forces exerted on a flat surface rise very rapidly when a small (0.1 m high) rock step is created (Figure 6-11A). This relationship is proportional to the inverse of the square root of the height of the rock step. Clearly the drag forces exerted on a small step are significant. Interestingly, drag forces drop slightly with higher water pressures (Figure 6-11B), because Coulomb ice-rock friction acting on the top surface decreases with increasing water pressure. The lines of balanced drag and resisting forces (Figure 6-11D) show that a fairly long series of blocks with cumulative length of blocks of < 10 m, can be removed with sliding velocities < 200 m yr^{-1} when a rock step is introduced of 0.1–0.4 m height. Under overpressure ($P_w/P_i = 1.02$ as shown on Figure 6-11D), such block removal can occur at sliding velocities < 100 m yr^{-1}. The introduction of a rock step on the top of a hill or low-relief rock surface by hydraulic jacking thus radically increases the drag forces exerted on the top surface. Rock steps may thus assist in glaciotectonic disintegration of rock hills and low relief rock surfaces. However, block removal still requires a down-ice step to provide accommodation space.
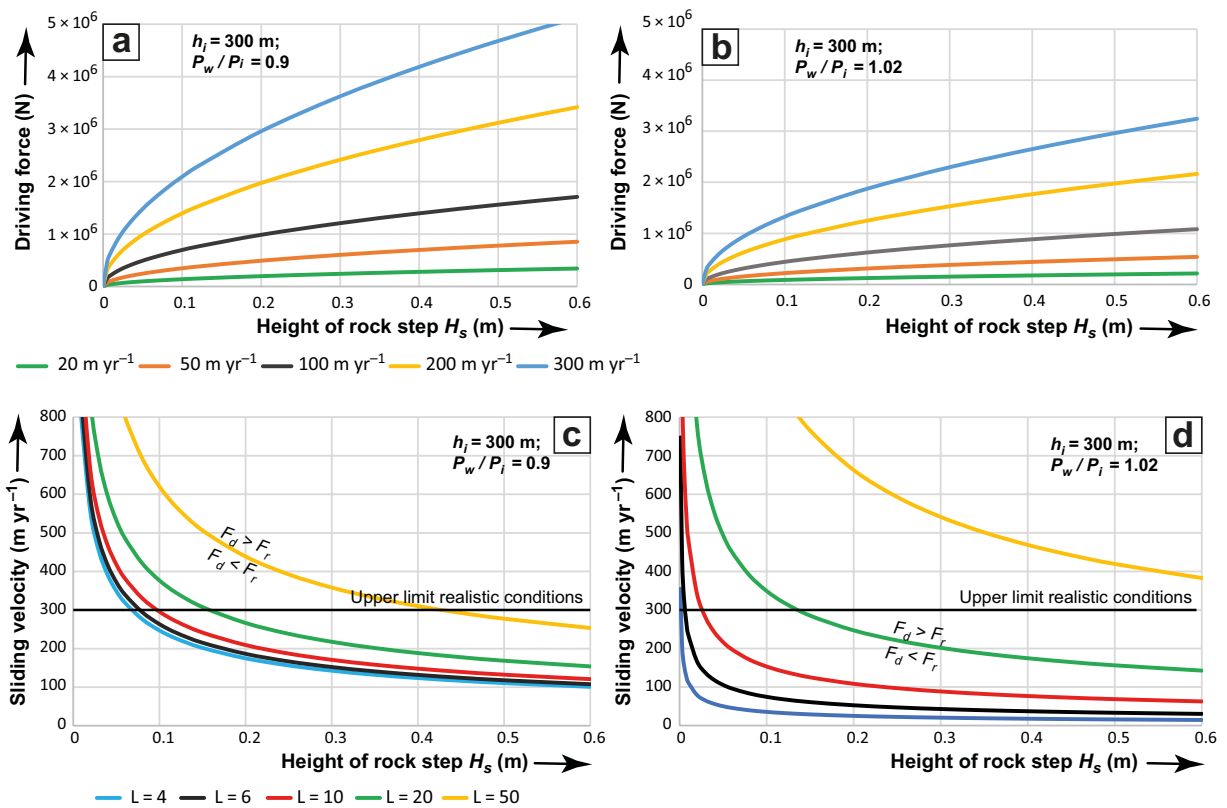
Figure 6-11. A. Drag forces (N) on a flat surface with a rock step, as a function of height of rock step Hs, for different ice velocities. Width and height of blocks are 5 and 2 m; ice thickness = 300 m, $P_w/P_i = 0.9$. B. as A., with $P_w/P_i = 1.02$ (2 % overpressure). C. Lines of equal drag and resisting forces ($F_d = F_r$) as a function of sliding velocity and height of rock step, for different cumulative length of blocks, $P_w/P_i = 0.9$. D. as C., with $P_w/P_i = 1.02$ (2 % overpressure). After Krabbendam et al. (2022b).

6.3.5 Modelling outcomes

The modelling shows the drag and resisting forces acting on rock hills of various sizes and shapes, and how the presence of water at overpressure in fractures can reduce resisting forces and lead to failure of the rock mass under continuous application of ice drag forces.

Ice drag forces increase linearly with ice sliding velocities, so fast-flowing ice can remove larger or more resistant rock hills than slow-moving ice. Ice drag forces also increase linearly with the radius of a hemispherical obstacle (equivalent to the square root of its stoss side area), so that high and blunt rock hills are more vulnerable to removal than low streamlined ones. Ice drag forces are also substantial on small upstanding up-ice facing steps.

Resisting forces are a function of the shape and size of the hill, the fracture pattern of the rock hill (in particular the presence of continuous shallow subhorizontal fractures) and the water pressure within the fractures. A rock hill without sub-horizontal fractures cannot be moved under plausible subglacial conditions. Such a rock hill is likely to be eroded by abrasion alone, forming whalebacks. However, ongoing erosion of surrounding fractured rock, for instance by further excavation of valleys may eventually expose a basal fracture.

In contrast, a small rock hill with a continuous, subhorizontal fracture is easily removed by sliding ice, at relatively low sliding velocities. If a 'perfect' smooth subhorizontal fracture is present, glacial ripping may in fact occur at water pressures below flotation. In the intermediate situation, even small areas of solid rock that interrupt the fracture ('rock bridge'), any irregularity like a small up-ice facing step in the subhorizontal fracture, or a very rough fracture surface) strongly increase the resisting forces, preventing rock removal.

Removal of larger and/or elongate rock hills requires water overpressure along the fractures. At and just above flotation ($P_w = P_i$), very long, low obstacles can be removed at sliding velocities of 50–100 m yr^{-1}, although in nature this likely requires quite smooth and long subhorizontal fracture planes. On the flat top surface of a large rock hill, uplift of blocks by hydraulic jacking may create a small rock step, as seen at Drill Site 5. If the rock step is oriented up-ice this dramatically increases the drag forces exerted on the top surface: modelled drag forces are sufficient to remove the brecciated rock surface, even if the hill as a whole is too resistant to be moved. Overall, high rock hills are thus more vulnerable because they (i) are subjected to higher drag forces, and (ii) have higher probability of having a subhorizontal fracture exposed to the ice bed to allow access for overpressured water to enter.

Glacial ripping is thus plausible under certain conditions, and it is physically plausible for sliding ice to remove or damage rock hills and low-relief rock surfaces, if the drag forces exerted by ice drag exceeds the resisting forces of the rock mass.

7 Discussion

7.1 General controls on glacial ripping

In this section, we first discuss the general controls on glacial ripping based on field observations and link those controls to the outcomes of the modelling in Section 6 to derive some general principles (Table 7-1). In Section 7.2, we will discuss the detailed controls on the spatial distribution of glacial ripping in eastern Sweden.

The general control of glacial ripping are those factors that lead to ice drag forces exceeding the resisting forces of the local rock mass. Glaciological factors that favour glacial ripping removal are: (1) water pressure fluctuations, in particular overpressure events, causing hydraulic jacking, and (2) moderate to fast sliding ice to provide the necessary ice drag forces causing further disintegration. The broad glaciological conditions necessary for glacial ripping are not unusual for the base of an ice sheet, but water pressure variations may be strongly localised (see Section 7.2). In broad terms, overpressure events are likely more common and significant in the ablation zone, providing a broad constraint as to where hydraulic jacking and hence glacial ripping most likely occurred. The modelling further suggests that general geological and topographic factors that favour glacial ripping include: (i) high, blunt stoss sides, so that ice drag forces can be exerted on the rock hills or rock bump; (ii) presence of continuous subhorizontal fractures; (iii) high fracture transmissivity, so that water pressure fluctuations at the ice-bed can penetrate into the rock mass and cause a decrease in the resisting forces of the rock hill.

Table 7-1. Overview of general controlling factors for glacial ripping.

Event	Favourable circumstances	Unfavourable circumstances
Water at the glacier bed	• Thawed bed • High meltwater flux • Deglaciation	• Frozen bed
Overpressure meltwater events	• Supgraglacial lake drainage events • Capacity of subglacial channels exceeded • Water trapped in weakly connected zones	• Low meltwater activity; meltwater at low pressure
Overpressured meltwater reaches bedrock	• Thin or patchy till	• Thick or extensive till
Overpressured meltwater enters fractures	• Open subhorizontal fractures that intersect the rock surface • High fracture density	• Tight fractures • Vertical fractures (inly) • Low fracture density
Ice drag forces exceed resisting forces	• Fast flowing ice • High, blunt obstacles • High fracture density • Advanced brecciation	• Slow flowing ice • Low streamlined obstacles • Low fracture density; interlocking blocks • Till cover

Field observations on partially disintegrated rock hills and boulder spreads indicate that ice drag forces locally exceeded the resisting forces of the local rock mass (Sections 4.2 and 4.3). In practice, and particularly in a terrain subjected to repeated glaciation (See section on Terrain Conditioning – Section 7.1.2), this implies that hydraulic jacking and hence overpressure events did occur and sufficiently lowered the resistant forces of rock hills for ripping to occur. Field evidence from eastern Sweden from dilated fractures and partially disintegrated rock masses confirms that sufficient volumes of overpressured water entered fractures over large areas at the glacier bed to cause hydraulic jacking. This also implies that fractures existed with sufficiently high transmissivity to allow hydraulic jacking. We have not however examined in detail in the field or modelled (i) the flow of water from the glacier bed and through existing fractures during overpressure events, or (ii) fracture propagation during those events.

7.1.1 Fracture characteristics

Fracture characteristics, particularly orientation, length and aperture, influence the rock mass strength but also the entry and movement of overpressured meltwater into the rock mass, and hence the likelihood of lowering the rock mass strength by hydraulic jacking (Section 4.1.6). Fracture characteristics controls the resistance of the rock mass to glacial drag forces and block removal. Fracture spacing controls the size of large rock blocks that indivually and collectively form keystones and kernels in large roches moutonnées. Fracture orientation and patterns influence the extent, position and angle of potential decollement surfaces and the distribution of interlocking blocks that tend to resist drag forces.

Horizontal and subhorizontal fractures are more hydraulically transmissive than vertical and subvertical fractures (Hökmark and Lönnqvist 2014). Vertical fractures on a smooth ice-bed are not likely to be jacked open, as there is no accommodation space for fracture dilation. Horizontally directed compressive tectonic stresses, as prevalent in eastern Sweden (e.g. Carlsson and Olsson 1981, Glamheden et al. 2007, Lund et al. 2009, Hökmark and Lönnqvist 2014) increase this effect: these stresses tend to open sub-horizontal fractures but keep subvertical fractures shut. Subhorizontal fractures can be jacked open as there is accommodation space (e.g. upward lift of rock and ice): thus for extensive hydraulic jacking to occur in a rock mass, subhorizontal fractures need to be present in the rock mass (Figure 7-1A). We note that in sedimentary rocks, gently dipping bedding planes can play the same role as subhorizontal fractures in basement rocks.

Wide vertical fracture zones have locally high permeability (Hall et al. 2022); whether these zones are more suceptioble to hydraulic jacking is not clear. Moreover, vertical fracture sets within a rock hill are not confined by the tectonic stress (the hill can expand laterally), and water may enter all or part of the hill from different directions (Figure 7-1A).

Topographic relief vs fracture density

To allow water entry and hydraulic jacking, fractures must be connected to the ice-bed, in other words, they must intersect the rock surface. Thus, given the same fracture density, a hilly terrain will have more subhorizontal fractures exposed to the ice bed, and hence is more vulnerable to hydraulic jacking than more topographically smooth terrain. Conversely, if local topographic relief is lower than the spacing of subhorizontal fractures, then less fractures will be connected to the ice-bed and hydraulic jacking is hampered: this may either happen with low fracture density, or with lower hills (Figure 7-1B). In reality, such hills will be low (more like rock bumps), would also experience limited plucking and are likely to develop smooth whaleback forms, eroded only by abrasion. Nevertheless, in low relief rock surfaces, horizontal fractures in the upper 1–3 m of the rock may connect to the rock surface in shallow depressions (e.g. Figures 4-1E) and individual, long subhorizontal or gently dipping fractures may rise from greater depths to intersect the ice bed (e.g. Figure 4-4). Thus, depending on the fracture density, a certain minimum relief is required to favour glacial ripping.

Combining relief and fracture pattern, a high hill with a dense fracture pattern, although rarely found in nature, would be very vulnerable to glacial ripping. Low hills with continuous subhorizontal fractures are also vulnerable. Under ideal circumstances of a rock hill with perfectly smooth basal fracture, glaciotectonic disintegration may occur at pressures below overburden pressures (Section 6.3), but such rock hills may be rare.

Conversely, low hills with few or no subhorizontal fractures retain very high resisting forces, regard-less of overpressure, and are resistant to glacial ripping. Various intermediate situations are possible, for instance a rock hill with discontinuous, stepped subhorizontal fractures. Depending on the particular fracture configuration, an overpressure event may, or may not, sufficiently lower the rock mass strength and lead to complete or partial glaciotectonic disintegration.
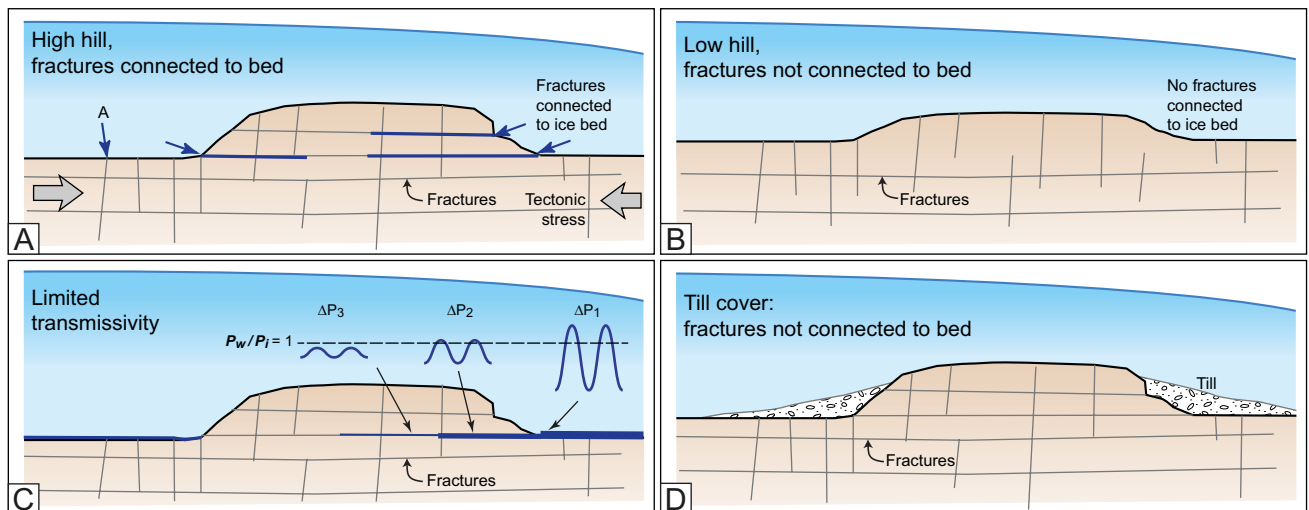
Figure 7-1. *Schematic diagram showing local controls on hydraulic jacking. A. Hill with subhorizontal fractures connected to the bed. Water can enter these fractures but may not be able to enter vertical fractures at A. B. Low hill: relief is lower than fracture density and: no fractures are connected to the bed. C. Attenuation of pressure fluctuations ΔP of the ice-bed, with increasing distance along a tight fracture. D. Till cover isolates the ice bed from the fractures; no direct connection between fractures and the bed.*

Hydraulic transmissivity of fractures

Even if subhorizontal fractures are present and intersect the ice-bed, the hydraulic transmissivity of the fractures needs to be sufficient for hydraulic jacking to happen. If fractures have low transmissivity, e.g. are tight with low aperture or wholly or partially sealed with mineral coatings, water pressure transients at the ice-bed will be attenuated, and water pressure within the fracture may not equalise rapidly enough to result in overpressure within the fracture (and no hydraulic jacking occurs), even if overpressure conditions occur temporarily occur at the ice-bed (Figure 7-1C). Whilst as a general rule, fracture transmissivity tends to be high in the uppermost bedrock and decreases with depth, many studies report a very high variability (4–5 orders of magnitude) in fracture transmissivity or overall conductivity in shallow (< 100 m) basement rocks in Sweden (e.g. Follin et al. 2007, Olofsson et al. 2007) and elsewhere (e.g. Stober and Bucher 2006, Neupane et al. 2020).

Studies in hydro-tunnels in Norway, with comparable overall water pressures and pressure transients, showed bimodal responses in boreholes to pressure fluctuations in the tunnel (Neupane et al. 2020). Some boreholes, presumably intersected by non-transmissive fractures, showed a delayed or virtually no response, whilst other boreholes showed a very rapid response to pressure transients, and are presumably intersected by highly transmissive fracture(s). The bimodality of the response observed by Neupane et al. (2020) likely relates to the 'cubic law', which states that fracture transmissivity is proportional to the cube of fracture aperture, and hence strongly non-linear (Witherspoon et al. 1980, Neuzil and Tracy 1981). A long-term increase in rock falls in hydrotunnels subjected to pressure transients suggests indirectly that fractures can incrementally increase their transmissivity under repeated pressure transients (Bråtveit et al. 2016). Translated to the subglacial setting discussed here, these studies imply that (i) the behaviour of fractures is broadly bimodal ('open' or 'tight') and (ii) it may be possible that fractures can be opened progressively due to repeated pressure transients. Whilst it is known that, below ice sheets such as the Greenland Ice Sheet, subglacial groundwater flows towards the margin even in crystalline rocks (e.g. Claesson Liljedahl et al. 2016, Harper et al. 2016), and that in eastern Sweden the extent of boulder spreads indicates that transmissive fractures at shallow depth did exist over wide areas, the spatial variability of fracture transmissivity remains poorly constrained.

7.1.2 Terrain conditioning

Eastern Sweden has been repeatedly glaciated during the Pleistocene, and its landscape has been sculpted and re-sculpted by subglacial erosion (e.g. Kleman et al. 2008). As such, the rock hills present in eastern Sweden are resistant to glacial drag forces, with medium to high rock mass strength. In contrast, landscapes not subjected to sustained glacial erosion commonly show small rock hills with low resistance, such as tors. In Europe, tors occur south of and outside the Pleistocene glacial limits, and in areas previously occupied by cold-based ice, characterised by minimal long-term glacial erosion (Hall and Phillips 2006, Hättestrand and Stroeven 2002, Darmody et al. 2008). They are absent in areas that have been (repeatedly) covered by warm-based Pleistocene ice sheets, and it can be surmised they were removed by glacial erosion during early Pleistocene ice sheet cover, together with vulnerable layers of regolith (e.g. Clark and Pollard 1998).

Tors can be regarded as blunt hills, and granite tors commonly possess long basal fractures. Modelling shows it is possible that such rock hills were removed by some form of glaciotectonic disintegration *without* overpressure (Scenario 2; Section 6.3.4). For instance, in the Cairngorms of Scotland remaining plinths and stumps of granite tors, suggest that tor superstructures were removed wholesale by (slow) moving ice (Hall and Phillips 2006).

However, once such vulnerable rock hills are removed from the landscape, more resistant rock hills cannot be removed by subglacial erosion without lowering their rock mass strength by hydraulic jacking and overpressure. The remaining high, blunt rock hills on the present ground surface in eastern Sweden are those with more complicated fracture patterns (e.g. with 'stepped' subhorizontal fractures), larger block size and higher rock mass strength. In other words, glacial ripping operating in areas that were previously glaciated requires the full three-stage process including overpressure (Hall et al. 2019a, 2020, Krabbendam et al. 2022a) to be effective.

7.1.3 Effects of till cover

The presence of till may have two effects. Firstly, till cover may attenuate or block the water pressure fluctuations at the ice-bed and effectively isolate any bedrock fractures from the pressure fluctuations at the ice-bed, thus hampering hydraulic jacking (Figure 7-1D). This dampening effect is controlled by Darcy's law and hence a function of both till thickness and till permeability, and thus more effective for more consolidated till. Secondly, a layer of actively deforming till (possibly overlying a layer of consolidated, non-deforming till, see Evans et al. 2006), will take up much of the drag forces exerted by the ice, and reduce the ice-drag forces exerted on the bedrock, hampering glaciotectonic disintegration. One would thus expect terrain with extensive till cover to be less susceptible to glacial ripping. We note however that the absence of till from large areas with boulder spreads suggests removal of till before or during phases of glacial ripping (Section 4.3.2).

7.1.4 Preservation of transient, intermediate features

Glacial ripping is seen as a three-stage process, ending with the deposition of boulder spreads. The preservation of dilated fractures as near Forsmark, partially roches moutonnées (e.g. Bodagrottorna, Gillberggrytta) as well as transitional stages in between (Section 4.4) shows that in some places the three-stage process was aborted or arrested. The two critical processes, hydraulic jacking and glaciotectonic disintegration, are controlled by different factors, and may thus not have been active at all times at every location.

As an example, ice drag is only effectively transferred onto the rock mass if there is an upstanding rock obstacle, be it the hill itself, or uplifted blocks on the top of that hill or steps on low-relief rock surfaces. The modelling shows that high, blunt rock obstacles and rock steps are much more susceptible to glaciotectonic disintegration than streamlined obstacles (Section 6.3.4). Glaciotectonic disintegration may thus not follow hydraulic jacking if the ice-bed remains very smooth, which may explain the survival of hydraulic jacking features at for instance Forsmark.

Arrested process stages in the ripping process sequence can be explained in different ways (Figure 7-1):

1. **Overpressure events end.** In the conceptual model of glacial ripping (Section 5; Figure 5-1), the process set is triggered by overpressured meltwater. When water pressure falls permanently below overpressure then hydraulic jacking is terminated.

2. **Overpressure events were limited in magnitude or repetition.** The occurrence of dilated fractures in quarries and sections but without brecciation or advanced disruption of the upper rock mass attests that this is fairly common (Figures 4-2; 4-3). Such rock masses were evidently subjected to overpressure events, but these were either too small in water volume or too short or infrequent to result in more advanced hydraulic disruption.

3. **Dilation of fractures by overpressure may be self-limiting**. Fracture dilation increases void space and increases the hydraulic conductivity of the shallow rock mass. If pressure fluctuations are small in magnitude with low volumes of water, then subsequent similar pressure fluctuations become progressively less effective (also discussed by Hökmark and Lönnqvist 2014). This may hamper disintegration in particular for rock masses comprising large blocks (wide fracture spacing), which need more void space to fully disintegrate than rock masses comprising smaller blocks. However, this effect is probably not important for large volume pressure fluctuations such as caused by supraglacial lake drainage events (See Section 7.3).

4. **Ice drag forces exerted onto bedrock were insufficient for disintegration**. What matters here is to what extent ice drag forces are exerted on the bedrock. The modelling shows that this requires blunt stoss sides or upstanding edges, exposed to sliding ice (Section 6.3). Glaciotectonic disintegration may not necessarily follow hydraulic jacking: (i) if the ice-bed remains smooth, which may explain the survival of hydraulic jacking features at for instance Forsmark and Svagberget, and (ii) where jacking occurred below till cover (Figure 4-5D; see Forssberg et al. 2007) so that ice movement was likely taken up by deforming till, and jacking did not increase the exposure of the bedrock to ice drag forces. Also, along segments of esker systems the bedrock surface was hydraulically jacked under overpressure but little or no glacial drag forces were applied subsequently to the disintegrated rock surfaces.

5. **Interlocking blocks hamper disintegration under drag forces.** As discussed in Section 7.3.2, rock hills with wide fracture spacing comprising interlocking blocks may still offer significant resistance to complete glaciotectonic disintegration, despite extensive hydraulic jacking and incipient disintegration. The fact that edge rounding is present, but minor (Section 4.2) suggests that such disintegrated roches moutonnées: (i) survived a few seasons under ice cover and experienced some abrasion; (ii) conversely did not disintegrate very far (< 10 km) from the retreating margin. Roches moutonnées with high rock mass strength may take several cycles of hydraulic jacking and partial disintegration to be completely destroyed, and thus have a higher preservation potential than a jacked and disintegrated rock mass with higher fracture density that may be destroyed in a single season.

6. **Glacial ripping was interrupted by deglaciation.** Any subglacial process below the ablation zone of a rapidly retreating ice sheet will be terminated when the ice stagnates, or the ice margin retreats across a site. We note here that the spatial extent of boulder spreads (100s of km^2) is much larger than that of partially disintegrated rock masses or the (known) occurrences of dilated fractures. This means that in most cases, glacial ripping progressed through to completion. Statistically it is then possible that, in a few cases, the process-sequence of glacial ripping was interrupted by final deglaciation, whether at the stage of hydraulic jacking, or at the stage of partial glaciotectonic disintegration.

7.2 Spatial controls on glacial ripping in eastern Sweden

The markers for glacial ripping – including dilated fractures, disrupted rock surfaces and boulder spreads – are unevenly distributed across eastern Sweden (Section 4.3) and occupy less than 10–20 % of the ice sheet bed in Uppland. In this section we discuss to what extent the general controls on glacial ripping (Section 7.1) constrain the spatial distribution of glacial ripping at different scales in eastern Sweden. We start with some broad observations derived mainly from Section 4.3.

7.2.1 Lithology

There are no strong lithology contrasts in eastern Sweden: almost all rocks are basement gneisses. At the landscape and regional scales, boulder spreads show no clear correlations with rock type (Section 4.3.1 and Section 4.3.2): boulder spreads involve both felsic gneisses and amphibolite, and commonly cross lithological boundaries. There is thus no strong control of lithology on glacial ripping in our satudy area. This is different to the settings of glacial ripping in NW Highlands, Ontario and at Lake Rogen (Hall et al. 2021a, Bukhari et al. 2021, van Boeckel et al. 2022), where sedimentary rocks appear much more susceptible to glacial ripping than adjacent basement gneisses, and lithology exerts a strong spatial control on glacial ripping.

7.2.2 Fracture patterns

Fracture patterns are highly variable across eastern Sweden: some areas are dominated by vertical fractures; in others long subhorizontal fractures occur (Section 4.1). In some areas, the fracture pattern is orthogonal, with continuous subhorizontal fractures, elsewhere, more stepped fractures occur. Whilst subhorizontal fractures are common in eastern Sweden, they are by no means ubiquitous (Section 4.1). Fracture density is also variable (Sections 4.1 and 4.5). The majority of boulders in boulder spreads are approximately cuboid, and have a typical boulder size of 1–4 m (Figure 4-50), which suggests that the parent rock mass of most boulder spreads contained a regular orthogonal fracture pattern with continuous subhorizontal fractures. Fracture density in eastern Sweden is relatively high compared to some other basement terrains, and certainly higher than in granite dominated terrains (compare Jern 2004, with Martel 2017).

At the regional scale, boulder spreads occur in different fracture domains and cross boundaries between domains and regional deformation zones (compare, for example, Figures 2-2 and 4-19). At the local scale around Forsmark, boulder spreads also lie across different fracture domains (Figure 4-1). Domain FFM002, however, shows strong local control on hydraulic jacking by long (Figure 4-7) and short (Figure 4-6) horizontal to gently-inclined fractures.

The critical fracture property for hydraulic jacking is the hydraulic transmissivity of the surface rock mass. This is strongly influenced by the number, spacing and aperture of subhorizontal fractures. Subhorizontal fractures, of clear importance to allow jacking and ripping, are widespread in some domains but not in others. In eastern Sweden, subhorizontal fractures occur on bedrock surfaces in three main situations as (i) widely-spaced (> 5 m vertical), long (> 10 m lateral), continuous fractures at depth that locally intersect the surface, (ii) closer-spaced (< 5 m), shorter (< 10 m), discontinuous, stepped fractures in hills and (iii) closely-spaced (< 1 m), short (< 5 m), discontinuous fractures at 1–2 m depth below rock surfaces with low topogreaphic relief. In eastern Sweden, hydraulic jacking by overpressured meltwater flowing along subhorizontal fractures opened fracture caves at depths of up to 13 m below the glacier bed, disrupted rock hills and led to disintegration of moderate to low relief surfaces over wide areas, promoting the formation of boulder spreads.

Also important for hydraulic transmissivity are the apertures of all fractures in the uppermost 1–2 m of the rock which also vary locally (Section 4.1). Hence, fracture patterns at the local scale are likely a significant control on the spatial distribution of glacial ripping. It is uncertain whether fracture patterns also exert a control at the larger, regional scale.

7.2.3 Topographic relief

The topographic relief in eastern Sweden is relatively subdued (< 30 m is typical). Within this range, some domains have low roughness and low relief (< 3 m), whereas other domains have higher roughness and medium relief (3–20 m) (Hall et al. 2019a). Boulder spreads occur, however, in different terrains (compare, for example, Figures 4-15 and 4-22) and cross boundaries between terrains (Figures 4-18 and 4-19). In lowland settings, boulder spreads are found on slightly elevated terrain (Tämnaren, Skyttorp, Vällen) but neighbouring areas of similar roughness and at similar elevation may lack boulder spreads.

At the local scale (0.1–1 km) and below, the main rock landforms are hills, surrounding low relief surfaces and trenches (Hall et al. 2019a). Hills are vulnerable to entry of overpressured water via long, open fractures. High and blunt rock hills are also subject to high glacial drag forces, so that

where rock mass strength is reduced by hydraulic jacking, disintegration of the hill may occur. Similar hill forms occur however inside and outside areas with boulder spreads, for example at Iggesund (Figure 4-11A), indicating that the presence of large hills is not, in itself, a control on the distribution of ripping. Boulder spreads occur on many low relief surfaces, for example at Forsmark (Figure 4-32) and Vällen (Figure 5-13 in Lagerbäck et al. 2005), where they occur in association with small, low and partially disintegrated roches moutonnées (Figure 4-2). Boulder spreads are not exposed along trench floors but may be concealed by sediment.

The exact relief and roughness in areas subjected to extensive glacial ripping (e.g. Gunnarsbo, Bladåker) is difficult to reconstruct, due to the wholesale desctruction of the original rock surfaces. We note that some low relief surfaces in eastern Sweden (e.g. Lilla Sandgrund, Lilla Asphällan, near Forsmark) have very few exposed subhorizontal fractures, and it may be that such surfaces were resistant to hydraulic jacking, even if overpressure events occurred at the ice-bed: the low-roughness and overall streamlining in these domains implies that ice-drag forces exerted on such (low) hills was small (Section 6.3.3). At the landscape and regional scales in lowland eastern Sweden, the topography of the ice-sheet bed does not have an obvious control over the distribution of glacial ripping but further systematic study of the spatial correlation between relief and glacial ripping is required.

7.2.4 Till cover

Boulder spreads generally occur in areas with no or thin or patchy till cover. Extensive till cover (a) attenuates water pressure fluctuations and (b) may hamper glaciotectonic disintegration as the ice-drag forces are taken up by deforming till (Section 7.1.3). In Uppland, some large areas of consolidated till, as in Till Area II east of Forsmark (Section 4.3.7), are devoid of signs of glacial ripping, which appears to suggest a spatial link. The survival of preserved jacked fractures in the canal cuts and in Drill Site 5 near Forsmark, and near Runtorp beneath till (Figure 4-2; Section 4.1.2) may be caused by deforming till preventing large ice-drag forces being exerted onto bedrock that has been jacked and partially brecciated. However, no systematic study was carried out as to the spatial correlation between till cover and glacial ripping.

7.2.5 Ice flow velocity

Moderate to fast ice flow developed at the base of much of the Fennoscandian Ice Sheet in the lowlands southern and eastern Sweden (e.g. Patton et al. 2017) with more or less continuous basal sliding over large areas throughout the Weichselian glaciation (e.g. Näslund et al. 2003). As such variations in ice flow velocity do not provide a distinctive spatial control for glacial ripping.

7.2.6 Subglacial meltwater at overpressure

In a repeatedly glaciated terrain, hydraulic jacking is a likely prerequisite for glacial ripping (Section 7.1.3). Hydraulic jacking of bedrock fractures requires entry of sufficient volumes of water at overpressure to allow fracture dilation. The availability of overpressured water and the repeat frequency of overpressure events may thus have a spatial component, which could provide a spatial control on hydraulic jacking and glacial ripping. If this spatial control is strong (i.e. stronger than other spatial controls) then the distribution of markers for overpressure could potentially provide a window on where subglacial meltwater reached overpressure at the base of the Fennoscandian Ice Sheet in eastern Sweden.

At the landscape scale, the absence of boulder spreads in Stockholm and Södermanland counties (between zones B and C on Figure 4-18; Section 4.3.2), may be related to diminished meltwater activity related to the cooling associated with the Younger Dryas, the ice limit of which occurs across that area. During the Younger Dryas, the ablation zone of the Fennoscandian Ice Sheet would become narrower and less active, with less meltwater production, thus possibly resulting in less and smaller overpressure events at the base. Conversely, the main occurrence of surface boulders is found in terrain where ice retreat was rapid and meltwater activity was vigorous, notably in terrain, including Uppland, that was deglaciated after the Younger Dryas.

At the regional and local (1–10 km) scales in Uppland, many boulder spreads occur in belts broadly parallel to former ice-flow directions with intervening tracts largely lacking these features (Section 4.3.1 and 4.3.2). The transport distances (1–100 m for boulder trains and < 1 km for boulder spreads) are too small for these elongate belts to be formed by glacial drag alone as mega-scale glacial boulder line-ations. Some boulder spread belts are spatially associated with eskers (Figure 4-19). On segments of the small Börstil esker, boulder spreads reach well-defined limits at distances of up to 1 km from the esker ridge (Figure 4-38). Boulder spreads rest locally on glaciofluvial sediment, indicating boulder transport and deposition during operation of the esker system (Figure 4-39).

Along the much larger Uppsala esker, dilated, sediment-filled fractures and small disrupted roches moutonnées occur within boulder spreads occur up to 4 km from the esker ridge at Björklinge (Figure 4-42), large boulders rest on esker sands and gravels (Murchison 1864) and large disrupted roches moutonnées occur along its trace, locally embedded in esker sand and gravel deposits (Hall and Krabbendam 2022). The presence of markers for hydraulic jacking along eskers suggest that overpressure developed transiently in the esker system. The distribution of disrupted rock surfaces and boulder spreads over distances of 0.4–4 km from esker ridges suggests that large volumes of overpressured water periodically escaped from esker systems.

Other elongate belts and patches of boulder spreads are not spatially associated with eskers or glaciofluvial sediments. For example, the boulder belt that extends along former ice flow from Forsmark towards Lake Vällen has only small, segmented eskers in its northern part and SGU Maps indicate that no glaciofluvial sediments are present around Lake Vällen to the S (Figure 4-19). At Iggesund, the boulder spreads cover > 50 km^2 (Hall et al. 2020) and the Boda fracture cave system lies 1.5 km E from the nearest esker. Yet the markers for groundwater overpressure show similar develop-ment in these locations as those found along esker systems. Hence, it is likely that large volumes of overpressured water were also available periodically in these locations. Why glaciofluvial sediment is absent in these locations is not clear.

Knowledge and understanding of subglacial hydrology are developing rapidly. Eskers are recognised as traces of dendritic subglacial channel systems (Boulton et al. 2007a) with lengths of many tens of km in eastern Sweden (e.g. Shackleton et al. 2018, Dewald et al. 2022) and on the floor of the Bothnian Sea (Greenwood et al. 2017). Recently, subglacial meltwater corridors with widths of several km have been interpreted beneath the former Laurentide and Fennoscandian ice sheets, with axial esker systems that acted as conduits (Lewington et al. 2020). The association of glaciofluvial landforms and sediments in these meltwater corridors suggest erosion and deposition by meltwater flowing in anastomosing, shallow channel systems (Sharpe et al. 2021). The meltwater corridors are interpreted as integral parts of the channelled subglacial hydrological system which developed during melting and ice retreat.

In Uppland, large volumes of subglacial meltwater flowed along esker channels and possibly other melt-water corridors. It is suggested these broad zones provided a certain spatial control on the distribution of glacial ripping, however other boulder spreads occur that are not closely adjacent to eskers (Figure 4-19).

7.2.7 Summary of spatial controls on glacial ripping in eastern Sweden

The spatial controls on glacial ripping in eastern Sweden can be summarised in terms of favourable and unfavourable circumstances (Table 7-1). Lithology (rock type) and ice velocity do not represent strong primary controls at the scales under consideration in east Sweden. Relief may present a local control, but this is linked to fracture density, and this combined effect has not been studied systemati-cally. Meltwater availability and activity appear to represent a significant control. The effects of till cover and variability in fracture patterns and fracture transmissivity may also present controls, which are as yet poorly constrained.

7.3 Causes of overpressure

The evidence of dilated subhorizontal fractures and open fractures filled with laminated sediment (Section 4.1) indicate that some form of subsurface jacking, and hence overpressure, must have occurred locally in eastern Sweden (see also Pusch 2005 in Leijon 2005). Fracture dilation opens

up the rock mass and lowers the rock mass strength, so overpressure is a critical first step in our process sequence, for most rock hills. Overpressure occurs if the local water pressure at the ice-bed exceeds the overburden pressure, which is the sum of the lithostatic pressure P_r (weight of overlying rock) plus the cryostatic pressure P_i (weight of overlying ice mass). Overpressure, or rather the resultant hydraulic jacking and/or fracturing or sediment injections, is also documented in Pleistocene subglacial tills (e.g. Larsen and Mangerud 1992, Rijsdijk et al. 1999, Phillips and Merritt 2008, van der Meer et al. 2009), with some studies reporting hydraulic jacking or fracturing of sedimentary bedrock (Phillips et al. 2013, Broughton 2018, Hall et al. 2021a).

How, and under what conditions and over what areas, might overpressure develop?

There has been much discussion about the maximum depth of possible overpressure below the planned Forsmark nuclear waste repository (Talbot 1990, 1999, 2014, Hökmark et al. 2010, Lönnqvist and Hökmark 2013, Hökmark and Lönnqvist 2014). Overpressure beneath or in front of an ice sheet at Forsmark has previously been attributed to different mechanisms.

1. A hydraulic gradient is imposed by a sloping ice sheet surface (e.g. Boulton et al. 1993, Lönnqvist and Hökmark 2013). During ice sheet thinning and retreat, residual 'pore' pressure in fractures may potentially exceed overburden pressure, but only if the rock has very low transmissivity. In a high transmissivity rock mass, the water pressure will equilibrate rapidly as the ice retreats (e.g. Lönnqvist and Hökmark 2013). However, this process is not thought important for the shallow hydro-jacking under consideration here, because the volumes of water involved are exceedingly small. Also, the repeat frequency is low: once the residual pore pressure is released, there is no reason for recurrence without readvance.

2. The same hydraulic gradient may lead to overpressure if ice retreats (or indeed advances) over permafrost, which would have a substantially lower transmissivity than a thawed rock mass (e.g. Piotrowski 1997, Lönnqvist and Hökmark 2013, Scheidegger and Bense 2014), in essence 'locking up' water deeper down. This is the scenario suggested by Talbot (1999) and modelled by Pusch et al. (1990), who envisaged that the jacking occurred pro-glacially, below a 20–30 m thick layer of permafrost. It is unknown, however, if such a layer of permafrost existed in the first place in eastern Sweden in the front of the Fennoscandian Ice Sheet and at the bottom of the Baltic Ice Lake. Also, if our three-fold process sequence is correct, then the jacking occurred subglacially, and not proglacially (Section 5.2).

Very different types of overpressure events have, however, recently been measured or documented at the ice bed in Greenland, and some smaller glaciers. These include (i) overpressure caused by drainage of supraglacial lake drainage (Das et al. 2008, Doyle et al. 2013), (ii) overpressure developed in 'weakly connected zones', without supraglacial lake drainage (Andrews et al. 2014, Harper et al. 2016, Wright et al. 2018, Harper et al. 2019) and (iii) pressure variations in subglacial channels (Boulton et al. 2007b).

7.3.1   Overpressure caused by supraglacial lake drainage events

Overpressure can be generated subglacially by rapid drainage of supraglacial lakes, as studied in the ablation zone of the Greenland Ice Sheet (e.g. Das et al. 2008, Doyle et al. 2013). Supraglacial lake drainage involves very rapid (hours) drainage of very large volumes of water (10^4 to 10^6 m^3) to the base of the ice sheet, with discharges in the order of 3.8×10^4 m s^{-1}. This resulted in rapid ice-surface uplift of 0.3–1.2 m over wide (several km^2) areas, reaching maximum uplift shortly after complete lake drainage, followed by slower (days) subsidence (Das et al. 2008, Doyle et al. 2013). Ice surface uplift of c. 1 m indicates ice-bed separation (Doyle et al. 2013), and hence overpressure conditions at the ice bed. Associated short duration acceleration of horizontal ice motion was also observed. Supraglacial lake drainage events thus can generate overpressure, involving large volumes of water and likely over substantial areas (> 6 km^2) of the ice bed; a kind of blister of water at the ice-bed is envisaged. The repeat frequency over any particular location, however, is low since supraglacial lakes take a year to refill, lakes are relatively widely spaced (Box and Ski 2007), drainage routes vary and not every lake drains in such dramatic fashion (e.g. Doyle et al. 2013).

The formation and filling of subglacial lakes may also result in overpressure events (whilst rapid drainage may propagate overpressure elsewhere in the subglacial channel system) as documented by Palmer et al. (2015) and Liang et al. (2022) in Greenland. Whilst subglacial lakes under the

Greenland Ice Sheet occur in areas of cold-based ice (and not be applicable to the general warm-based setting under discussion here), ice sheet models suggest that subglacial lakes were widespraed beneath the last FIS in eastern Sweden (Shackleton et al. 2018).

7.3.2 Overpressure in 'weakly connected zones'

Recent studies on the ablation zone of the western Geenland Ice Sheet have also measured *in situ* fluctuations in the basal water pressure, unrelated to supraglacial lake drainage (Andrews et al. 2014, Wright et al. 2018, Harper et al. 2019). Borehole pressure measurements were taken in hot-water drilled boreholes, which after insertion of pressure sensors were closed by ice-creep, isolating the pressure sensors from the ice surface. These studies suggest an extremely dynamic glacio-hydrological system with pronounced temporal and spatial variations in water pressures.

Andrews et al. (2014) measured pressures in boreholes and in moulins open to the ice surface, near the FOXX site (ice thickness 615–625 m). Pressures fluctuations in the FOXX moulins were large (50–150 m water head amplitude) and in-phase with the daily surface melting cycle, but the pressures were generally below overburden pressure (< 88–98 % of cryostatic pressure P_i), suggesting good connection with a subglacial channelized system. Water pressures in the FOXX boreholes show high frequency fluctuations in excess of overburden pressure (96 – 115 % of P_i), although the amplitudes of the fluctuations were lower (a few metres of water head). Water pressure fluctuations in boreholes at Issunguata Sermia, overlying a rough bedrock bed, also showed high frequency cycles in the melting season (85 – 105 % of P_i), with typical daily amplitude of 5–6 m water head (Harper et al. 2016, 2019, Wright et al. 2018). Overpressure events were short-lived (hours) but occurred repeatedly (10s of times) throughout the melting season; one borehole showed continuous overpressure between 102–115 % throughout the winter season. At both FOXX and Issunguata Sermia, water pressure fluctuations between closely spaced different boreholes were commonly out-of-phase (and at FOXX where also out-of-phase with moulin pressure fluctuations), indicating poor connectivity between borehole bases or with the channelized zones.

Thus, the boreholes appear to record pressure fluctuations in 'isolated' water patches on the bed that were poorly connected with each other and were not connected to the channelized drainage system (which is typically just below overpressure), in the so-called 'weakly connected zones' (Hoffman et al. 2016), related or similar to "distributed" drainage domains (e.g. Flowers 2015). The water pressure fluctuations in the weakly connected zones are not directly related to surface melt, but instead likely related to local increase and decrease in cavity volume (and hence to local ice sliding), whereby a localised decrease in cavity volume results in a localised pressure increase. Weakly connected zones are contrasted with the open channelized system with direct connections to moulins: the relative proportion of the weakly connected zones increases in autumn/winter and decreases in the melting summer (Hoffman et al. 2016). In the smaller and thinner Trapridge Glacier, Alaska, Murray and Clarke (1995) documented frequent overpressure events in both connected and unconnected boreholes. In these settings, water occupies cavities formed in the lee of bedrock bumps or of clasts in lodged till or the pores in the till itself (Hoffman et al. 2016, Harper et al. 2019); water volumes are low.

7.3.3 Overpressure in subglacial channels

In large ice sheets, the subglacial channel system is a large-scale system, as evidenced by mapped meltwater channel (eskers) in the Fennoscandian Ice Sheet (e.g. Dewald et al. 2022). The pressure in a subglacial channel is a function of water flow and its cross-section. Assuming the subglacial channel is in ice (a so-called R-channel), the cross-sectional area varies as a function of frictional melting by water flow, water pressure, and ice-creep closure rate (e.g. Röthlisberger 1972, Cutler 1998, Schoof 2010, Flowers 2015). However, water flow is commonly variable over a shorter time frame (hours, days) than subglacial channels can adjust their cross-sectional area. Meltwater inputs may thus temporarily exceed the capacity of subglacial channel and increases in water supply will lead to pressure increases (e.g. Schoof 2010, Cowton et al. 2013). In general, it is envisaged that a subglacial drainage system is inefficient in winter and spring, and opens up during summer (Schoof 2010, Cuffey and Paterson 2010). High water pressures are thus typical at the start of the melting season (e.g. Claesson Liljedahl et al. 2016, Harper et al. 2016), as meltwater supply overwhelms the drainage capacity of the channel system. However, Bartholomew et al. (2010) also infer high subglacial water pressures during very

high meltwater inputs, later in the melting season. Blockages by ice or sediment deposition may also lead pressure increases (Boulton et al. 2007b). Where lake drainage occurs and impinges or connects to a subglacial channel system, this system likely responds in a similar way to jökulhaup drainage, with a flood wave escaping channels and propagating as a thin, sheet-like tongue of overpressured water (Einarsson et al. 2017). If a subsequent lake drainage event intersects the same subglacial channel system, multiple overpressure events are possible during the same melting season. In short, pressure variations, including temporary overpressure events, are likely to occur within and immediately adjacent to subglacial meltwater channels.

In summary, pressure fluctuations are normal for the subglacial regime, and overpressure events occur frequently. Broadly speaking, high-volume events like the supraglacial lake drainage events (involving 1 000s of m^3 water), occur at lower frequency (typically once a season) but involve widespread and substantial (metre-scale) ice-bed separation. Conversely, low-volume events (involving a few m^3 water) can occur at high frequency (multiple events of a few m^3 during the melt season) but lead to minor (dm-scale) ice-bed separation (Andrews et al. 2014) except presumably in pre-existing cavities. At present it is difficult to judge which one of these types of events were mainly responsible for the hydraulic jacking and glacial ripping – possible all were. In eastern Sweden, some boulder spreads, and hence hydraulic jacking and glacial ripping, occurr adjacent to interpreted subglacial meltwater corridors that carried large volumes of water (Sections 4.3 and 7.2). However, glacial ripping also occurred outside such corridors, away from eskers. Further investigation is required to better understand water pressure variations beneath the former Fennoscandian Ice Sheet in eastern Sweden and the entry of pressurised water into the shallow bedrock.

7.4   Comparison with plucking (quarrying)

Glacial ripping studied here involved a form of block release and removal. Some authors regard any mechanism that removes any block from a bedrock hill as plucking (Benn and Evans 2010). However, most studies dealing with plucking document or model a scenario whereby fracture-bound blocks are removed *one after another* (or in small numbers) from the lee side, typically involving a lee-side cavity subjected to water pressure fluctuations (Iverson 1991, Sugden et al. 1992, 2019, Hallet 1996, Rea and Whalley 1996, Hooyer et al. 2012, Zoet et al. 2013, Anderson 2014). This mode of plucking can be described as "classic lee-side plucking", to distinguish it from block removal in other settings, or with other mechanisms. Classic lee-side plucking is similar to glacial ripping in that it also involves distinct steps of loosening, entrainment and transport of rock fragments (Röthlisberger and Iken 1981, Iverson 1991, Hallet 1996). Plucking is also known to be dependent on the fracture network of the rock mass (Dühnforth et al. 2001, Hooyer et al. 2012, Krabbendam and Glasser 2012, Iverson 2012). However, plucking is confined to rock steps, be they lee-side or lateral ones (Rea and Whalley 1996, Hooyer et al. 2012, Krabbendam and Bradwell 2011). The wide spacing of large boulders (erratics) in deglaciated low relief shield terrains where plucking has occurred suggests that (i) plucking events are relatively rare; (ii) only small numbers of blocks are released in each plucking event.

Thus, glacial ripping is different from classic lee-side plucking as follows:

(i)   glacial ripping can involve damage to the *internal* rock mass, with fracture dilation, block displacement and cave development many metres below the rock surface, affecting the rock mass well below the top layer of blocks;

(ii) glacial ripping involves a multitude of fracture-bound blocks ($n > 100$–1 000) at the same site in a single event (see also Lagerbäck et al. 2005), rather than the one-by-one block removal typical of plucking;

(iii) disintegration affects the stoss and upper surfaces of a roche moutonnée, as well as the lee-side: it may locally disintegrate and partially or wholly destroy entire bedrock hills.

Overall, glacial ripping is distinct from, and involves a much larger rock mass than, classic lee-side plucking. However, the ripping of entire rock sheets from the lee-side of hills, seen as Type C damage on partially disintegrated roches moutonnées (Figures 4-16 and 4-17 and Table 4-2), arguably represents a continuum with lee-side plucking.

7.5   Glaciotectonic deformation of bedrock in other settings

Glaciotectonics involves the deformation of the ice bed caused by glacier motion or loading, and can occur in either subglacial or proglacial settings; it does however encompass a wide range of materials, processes and end-products (Hart 1990, Aber et al. 2012, Lee et al. 2013). Most studies of glaciotectonics focus on subglacial till deformation (e.g. Boulton and Hindmarsh 1987, Benn and Evans 1996, Alley 2000, Evans et al. 2006) or on folding and thrusting of large, relative coherent rafts or sheets of (frozen) sediment or bedrock in ice-marginal or proglacial settings (e.g. Croot 1987, Ruszcyńska-Szenajch 1987, Hart 1990, Burke et al. 2009, Lee et al. 2013, Johnson et al. 2013, Evans et al. 2020). These processes differ from glacial ripping in setting, material and end-product.

However, a number of papers describe 'brecciation' or 'glaciotectonics' of subglacial bedrock, involving disintegration of the top few metres of bedrock (e.g. Harris 1991, Croot and Sims 1996, Hiemstra et al. 2007, Phillips and Auton 2008). In these sites (in Ireland, Scotland, and in Antarctica on pre-Quaternary tillite), immature rubble till of very local origin occurs above disrupted or disintegrated bedrock, but is in turn overlain by more mature till. Schroeder et al. (1986) describes 'ice-push caves' in Ordovician limestone below Montreal, Quebec, which show many similarities to the fracture caves in eastern Sweden. In the same limestone sequence, the Dummer 'moraine' in Ontario comprises large slabs (> 1 m thick; > 10 m long) set in a matrix of coarse immature rubble till (Schulmeister 1989) and has been interpreted as a 'debris factory' (Eyles and Doughty 2016). Hall et al. (2021a) also describe brecciated bedrock and rubble till in association with partially disintegrated roches moutonnées and boulder spreads in quartz sandstones in NW Scotland.

These processes are similar to the glaciotectonic disintegration of roches moutonnées described herein, except in that they: (i) involve relatively soft, and/or well stratified and densely fractured rocks such as mudstone, limestones or sandstone; (ii) produce immature rubble till instead of boulder spreads. These differences are likely related to the differences in protoliths. The lack of boulder spreads is likely caused by (i) weaker or more densely fractured sedimentary rock breaking up in smaller fragments in the first place; (ii) the softer rock fragments being readily crushed and progressively reworked and comminuted by shearing first into immature rubble till and then into mature till (Croot and Sims 1996). Thus, glacial ripping in weaker, well-bedded sedimentary bedrock may well be responsible for the widespread production of till. Of course, once a thick till layer is produced, this form of glacial ripping will stop, as the bedrock becomes mechanically isolated from the sliding ice above by a layer of deforming till (Evans et al. 2006, Alley et al. 2019; Section 7.3).

Localised examples of rock surfaces and small hills carrying features consistent with glacial ripping have also been reported from hard, crystalline rocks in North Wales (Glasser et al. 2020) and in Scotland on the islands of the Outer Hebrides (Hall et al. 2021b) and Shetland (Hall et al. 2021c).

7.6   Implications for glacial erosion depth in eastern Sweden and general 'erosion rules'

Recent results from cosmogenic nuclide inventories at Forsmark suggest the typical total depth of glacial erosion was 0.6–1.6 m (interquartile range) during the last, Late Weichselian glacial phase and 1.6–3.5 m (interquartile range) over the last 100 ka (Hall et al. 2019a, Heyman et al. 2019). However, most samples were taken from high points of abraded and undisrupted whalebacks and roches moutonnées, so these erosion depths are likely mainly caused by abrasion. Geomorphological evidence from depths of erosion of basement rocks below the sub-Cambrian unconformity suggests average values of 1.8–2.4 m of erosion (by any mechanism) per 100 ka glacial cycle, with ≥ 3 m in basins and trenches (Hall et al. 2019a).

In comparison, glacial ripping, as described here, has locally mobilised and removed 1–4 m of rock just prior to the Late Weichselian deglaciation. That is deeper erosion than achieved by abrasion over the entire Late Weichselian (Hall et al. 2019a). Thus, where it occurred (perhaps in about 10–20 % of the ice sheet bed), glacial ripping was the dominant erosion mechanism, whilst where it did not occur it made no contribution at all to the overall erosion depth. There is thus a strong spatial variability as to which mechanism of glacial erosion was dominant. The total glacial erosion in eastern Sweden should thus be seen as the result of a combination of abrasion, plucking and glacial ripping, operating with variable intensity in different locations.
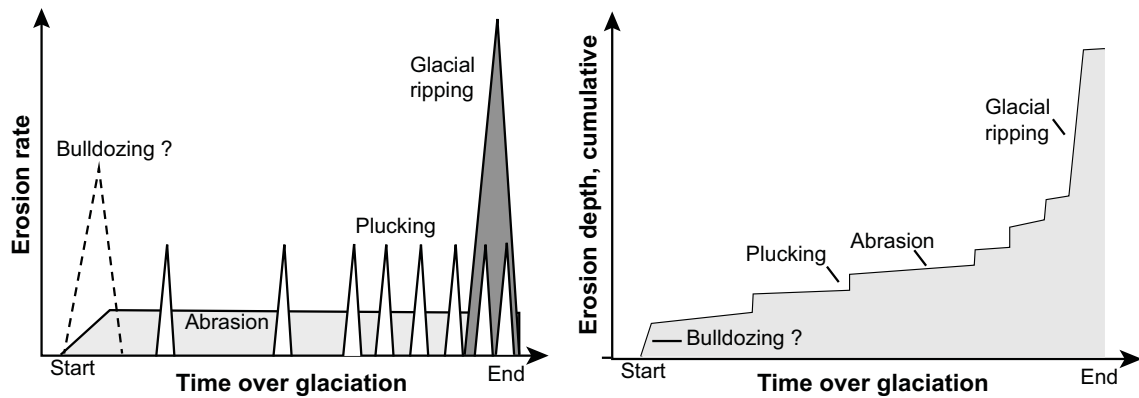
Figure 7-2. Conceptual evolution of erosion rate (left) and cumulative erosion depth (right) over a glacial cycle. The relative contribution of each erosion mechanism remains poorly constrained.

In terms of temporal variability, abrasion can be seen as a more-or-less constant process (so long as warm-based sliding occurs at the ice bed in the presence of basal debris); plucking is a more punctuated process possibly intensifying during deglacial phases, whereas glacial ripping appears as a distinct, intense 'pulse' of erosion, during final deglaciation (Figure 7-2). We note here that the field evidence presented here (limited edge rounding) strongly points to such a pulse of erosion during final deglaciation. However, it is possible glacial ripping occurred earlier in the glacial cycle, but its evidence was obliterated (Section 5.2).

Hydraulic jacking, disruption and partial disintegration operating at the end of a glaciation, also represent a phase of mechanical weathering, leaving a weakened rock mass as well as extensive boulder spreads. A potential next glaciation, or ice advance, would then likely cause an intensive phase of erosion ('bulldozing' in Figure 7-2), providing a large volume of broken rock for further till formation.

The cumulative erosion over a series of glaciations, integrated on the landscape-scale, is thus the result of different erosion processes, some of which scale with cumulative sliding distance (i.e. abrasion), whereas others more likely scale with the number of glaciations. Glacial ripping would represent a pulse of localised erosion at the end of a glacial cycle. Given that much loose material (boulder spreads but also glaciofluvial sediment and slope deposits in areas of higher relief) are left behind after a glaciation, a phase of 'bulldozing' (Winkler and Nesje 1999) or other debris entrainment at the glacier bed may be important at the start of a glacial cycle. Scaling of total subglacial erosion depth with cumulative sliding distance has been a first-order assumption in large-scale erosion modelling studies (Näslund et al. 2003, Egholm et al. 2009, MacGregor et al. 2009 – but see discussions by Iverson 2012 and Ugelvig et al. 2016). This first-order assumption needs to be refined in future erosion modelling.

7.7 Depth of hydraulic jacking and overpressure

The wealth of dilated fractures, many of which are sediment-filled, the disrupted bedrock, and the boulder spreads implies that subglacial overpressure was a fairly common occurrence across large parts of eastern Sweden. However, compared to the greater depths of possible overpressure at the site for the planned geological repository for spent nuclear fuel at Forsmark, discussed in previous studies (Talbot 1990, 1999, 2014, Hökmark et al. 2010, 2014, Lönnqvist and Hökmark 2013), the depths of jacked and disrupted bedrock indicate that overpressure sufficient to affect the rock mass strength focussed on the upper 1–10 m of the rock mass. Most damage by a glaciation to the rock mass is confined to the uppermost part. Since jacking and disruption substantially increase the conductivity of the uppermost rock mass, it may also function as a 'safety valve', dissipating overpressure before it affects deeper parts of the rock mass, a phenomenon also discussed in Hökmark et al. (2010) and Lönnqvist and Hökmark (2013). This leaky layer would of course only operate so long as it remained thawed.

7.8 Significance of glacial ripping for assessment of postglacial earthquake hazards

In eastern Sweden, the prevalent hypothesis has been that disintegrated roches moutonnées, fracture caves and associated boulder spreads provide evidence for large magnitude (> M7) earthquakes, caused by isostatic uplift during and after deglaciation (De Geer 1940, Mörner 1978, Sjöberg 1994, Mörner et al. 2000, Mörner 2017, Mörner and Sjöberg 2018).

The eartquakes were also seen to have disturbed glaciofluvial and glaciolacustrine deposits, and have been interpreted as paleo-tsunami depots. There are a number of problems with this overall paleo-seismic hypothesis:

1. An earthquake origin is difficult to reconcile with the systematic asymmetry of disintegration, and would not explain the removal of a large number of blocks, leaving exposed fracture surfaces as at Boda.

2. Earthquakes may have occurred in eastern Sweden during deglaciation and isostatic uplift, and disturbed varves (e.g. Mörner et al. 2000). However, the asymmetry of disintegration and transport of boulders strongly suggest a subglacial origin (Section 5.2), whilst varve deposition and subsequent disturbance by necessity occurred proglacially. There is therefore no demonstrable temporal link between varve disturbance and disintegration of roches moutonnées (cf. Mörner et al. 2000, Mörner 2017).

3. The mechanism by which a purported earthquake can disintegrate a massive bedrock hill remains unexplained. If this was physically plausible, earthquakes in other (non-glaciated) terrains should also produce such features. To our knowledge, there are no reports of disintegrated hills in high rock-mass strength rocks in low-relief landscapes in tectonically active regions.

4. Smith and Öhrling (2022) critically evaluated the evidence for paleo-tsunami deposition in east Sweden, including in the Iggesund area. They note that the sequences interpreted paleo-tsunami deposits by Mörner et al. (2000) (i) lack features that are nowadays are regarded as diagnostic for paleo-tsunami deposits, and (ii) cannot be reliably correlated to the established nearby varved sequences, so that the timing of deposition (and hence the interpreted seismic event) is in essence unconstrained.

An alternative methane venting hypothesis (Mörner 2017) suffers from the issue of methane sourcing: basement rocks are normally poor in hydrocarbons, in particular, if no source rocks are nearby, as is the case in eastern Sweden (e.g. Drake et al. 2019). This hypothesis equally cannot explain the systematic asymmetry of disintegration and formation of boulder spreads.

Glacial ripping represents an alternative, subglacial explanation for disintegrated roches moutonnées, fracture caves and boulder spreads, that does not involve seismic activity. Earthquakes caused by rapid isostatic uplift probably did occurr in eastern Sweden (e.g. Smith and Öhrling 2022), but they were not associated with the formation of fracture caves and disintegrated roches moutonnées, and these features cannot therefore be invoked to constrain the magnitude of any palaeoseismic event in Sweden.

8 Conclusions

We present evidence for glacial ripping as a locally effective, potent subglacial erosion mechanism. Bedrock with pre-existing, open subhorizontal fractures is hydraulically jacked and disrupted, disintegrated into boulders, which are subsequently transported, and deposited as spreads of large, angular boulders and mega-clasts. Geomorphological, structural and sedimentological evidence for this process-sequence in eastern Sweden comprises:

- subhorizontal fractures filled with water-lain silt and sand, and locally diamicton, that attest to hydraulic jacking in the top few metres of hard bedrock,

- disrupted roches moutonnées, some with fracture caves; and other disintegrated rock surfaces that show disruption of the shallow rock mass,

- 1–4 m thick boulder spreads of large, angular boulders, with subglacial transport distances ranging from tens of metres to a few kilometres.

The features occur together and transitions are recognised between hydraulic jacking, disruption, disintegration and transport. Our observations indicate that these landforms and sediments are genetically linked within a progressive three-stage process-sequence. Preserved dilated bedrock fractures, brecciated bedrock and disrupted roches moutonnées can be regarded as aborted stages in the overall process-sequence.

Hydraulic jacking and dilation of rock fractures is locally associated with the deposition of laminated sand and silt in fractures. Hydraulic jacking requires the development of groundwater overpressure below the former ice sheet bed. Strongly fluctuating water pressures, up to 110 % of overburden pressure, have been measured in the ablation zone at the bed of the Greenland Ice Sheet. Similar events are here suggested to be responsible for the hydraulic jacking below the retreating Fennoscandian Ice Sheet in eastern Sweden. Jacking and fracture dilation are interpreted to reduce the friction along basal fractures and lower the rock-mass strength. Continuing ice traction then results in disintegration of the rock mass into blocks and transport of boulders to form boulder spreads.

Various observations strongly suggest that jacking, disintegration and transport occurred subglacially. Consolidation loads on fracture fills suggest hydraulic jacking and infill occurred subglacially. Boulder spreads have locally been transported into moraines or are locally associated with esker deposits. However, transport distances for clasts within boulder spreads are short, indicating that the time available for boulder transport was brief and that glacial ripping occurred close to the retreating margin and prior to final deglaciation.

Where glacial ripping operated in eastern Sweden (affecting perhaps 10–20 % of the ice sheet bed), it resulted in the mobilisation and removal of 1–4 m of rock, mostly during the very last stages of the Late Weichselian glaciation. This is of the same order as the typical 0.6–1.6 m (interquartile range) depths of rock removed mainly by abrasion, as constrained by previous cosmogenic nuclide inventories from the Forsmark site and adjacent parts of Uppland. The inferred process sequence of glacial ripping appears to be, in the areas where it occurs, a highly effective process of glacial erosion.

Modelling shows that glacial ripping is a physically plausible under certain realistic conditions, but impossible under other, also realistic,conditions. Glaciological conditions that favour glacial ripping are moderate to fast flowing ice and the occurrence of hydraulic overpressure events at the ice-bed interface. Favourable geological conditions include the presence of transmissive and continuous near-surface subhorizontal fractures, which requires a minimum relief to be exposed to the ice bed.

The recognition of glacial ripping as an effective glacial erosion mechanism implies that (i) glacial ripping made a significant contribution to the cumulative integrated glacial erosion over eastern Sweden during the latest Weichselian glacial phase – the same may apply to other previously glaciated terrains; (ii) disintegrated roche moutonnees, fracture caves and boulder spreads cannot be used as evidence for high-magnitude earthquakes, as the features are formed subglacially by the action of water pressure and ice, not by seismic events; (iii) whilst some glacial erosion processes scale with cumulative sliding velocity (e.g. abrasion); glacial ripping more likely scales with the number of glacial cycles.

9   Acknowledgements

References

SKB's (Svensk Kärnbränslehantering AB) publications can be found at www.skb.com/publications.

Aber J S, Croot D G, Fenton M M, 2012. Glaciotectonic landforms and structures. Springer Science & Business Media. (Glaciology and Quaternary Geology 5)

Ahokangas E, Ojala A E K, Tuunainen A, Valkama M, Palmu J-P, Kajuutti K, Mäkinen J, 2021. The distribution of glacial meltwater routes and associated murtoo fields in Finland. Geomorphology 389, 107854.

Albrecht J, 2005. Forsmark site investigation: study of Quaternary sediments in connection with investigations of bedrock lineaments. SKB P-05-138, Svensk Kärnbränslehantering AB.

Alley R B, 2000. Continuity comes first: recent progress in understanding subglacial deformation. Geological Society, London, Special Publications 176, 171–179.

Alley R B, Cuffey K M, Zoet L K, 2019. Glacial erosion: status and outlook. Annals of Glaciology 60, 1–13.

Anderson R S, 2014. Evolution of lumpy glacial landscapes. Geology 42, 679–682.

Andrén T, Björck S, Andrén E, Conley D, Zillén L, Anjar J, 2011. The development of the Baltic Sea Basin during the last 130 ka. In Harff J, Björck S, Hoth P (eds). The Baltic sea basin. Berlin: Springer, 75–97.

Andrews L C, Catania G A, Hoffman M J, Gulley J D, Lüthi M P, Ryser C, Hawley R L, Neumann T A, 2014. Direct observations of evolving subglacial drainage beneath the Greenland Ice Sheet. Nature 514, 80–83.

Arnbom J-O, 2005. Dokumentation av berghällar och bergskärningar längs motorvägsbygget E4 mellan Uppsala och Mehedeby. SGU-rapport 2005:13, Geological Survey of Sweden. (In Swedish.)

Asch K, 2005. IGME 5000: 1:5 million international geological map of Europe and adjacent areas. Hannover: BGR.

Avery R S, Greenwood S L, Schenk F, Morén B M, Armstrong Mckay D I, Brunnberg L, Wohlfarth B, 2021. A 725-year integrated offshore terrestrial varve chronology for southeastern Sweden suggests rapid ice retreat~ 15 ka BP. Boreas 50, 477–496.

Bagheri G, Bonadonna C, 2016. On the drag of freely falling non-spherical particles. Powder Technology 301, 526–544.

Bartholomew I, Nienow P, Mair D, Hubbard A, King M A, Sole A. 2010. Seasonal evolution of subglacial drainage and acceleration in a Greenland outlet glacier. Nature Geoscience 3, 408–411.

Bathurst B, 1999. The lighthouse Stevensons: the extraordinary story of the building of the Scottish lighthouses by the ancestors of Robert Louis Stevenson. London: Harper Collins.

Benn D I, Evans D J, 1996. The interpretation and classification of subglacially-deformed materials. Quaternary Science Reviews 15, 23–52.

Benn D I, Evans D J, 2006. Subglacial megafloods: outrageous hypothesis or just outrageous. Glacier Science and Environmental Change 1, 42–50.

Benn D I, Evans D J A, 2010. Glaciers and glaciation. 2nd ed. London: Hodder Education.

Bergman T, Hedenström A, 2006. Forsmark site investigation. Petrographic analysis of gravel and boulders in the Forsmark candidate area. SKB P-06-87, Svensk Kärnbränslehantering AB.

Björklund A, 1990. Methane venting as a possible mechanism for glacial plucking and fragmentation of Precambrian crystalline bedrock. GFF 112, 329–331.

Borgström I, 1999. Basal ice temperatures during late Weichselian deglaciation: comparison of landform assemblages in west-central Sweden. Annals of Glaciology 28, 9–15.

Boulton G S, 1979. Processes of glacier erosion on different substrata. Journal of Glaciology 23, 15–38.

Boulton G S, Hindmarsh R C A, 1987. Sediment deformation beneath glaciers: rheology and geological consequences. Journal of Geophysical Research: Solid Earth 92, 9059–9082.

Boulton G S, Slot T, Blessing K, Glasbergen P, Leijnse T, van Gijssel K, 1993. Deep circulation of groundwater in overpressured subglacial aquifers and its geological consequences. Quaternary Science Reviews 12, 739–745.

Boulton G S, Hagdorn M, Maillot P B, Zatsepin S, 2007a. Drainage beneath ice sheets: groundwater–channel coupling, and the origin of esker systems from former ice sheets. Quaternary Science Reviews 28, 621–638.

Boulton G S, Lunn R, Vidstrand P, Zatsepin S, 2007b. Subglacial drainage by groundwater–channel coupling, and the origin of esker systems: part II – theory and simulation of a modern system. Quaternary Science Reviews 26, 1091–1105.

Box J E, Ski K, 2007. Remote sounding of Greenland supraglacial melt lakes: implications for subglacial hydraulics. Journal of Glaciology 53, 257–265

Bradwell T, 2013. Identifying palaeo-ice-stream tributaries on hard beds: Mapping glacial bedforms and erosion zones in NW Scotland. Geomorphology 201, 397–414.

Bråtveit K, Bruland A, Brevik O, 2016. Rock falls in selected Norwegian hydropower tunnels subjected to hydropeaking. Tunnelling and Underground space technology 52, 202–207.

Bretz J H, 1969. The Lake Missoula floods and the channeled scabland. The Journal of Geology 77, 505–543.

Brojerdi F S, Zhang F, Juhlin C, Malehmir A, Lehtimäki T, Mattsson H, Curtis P, 2014. High resolution seismic imaging at the planned tunnel entrance to the Forsmark repository for spent nuclear fuel, central Sweden. Near Surface Geophysics 12, 709–720.

Broughton P L, 2018. Subglacial blowouts in western Canada: insights into extreme meltwater pressures and hydrofracturing. Boreas 47, 326–346.

Bukhari S, Eyles N, Sookhan S, Mulligan R, Paulen R, Krabbendam M, Putkinen N, 2021. Regional subglacial quarrying and abrasion below a paleo ice stream crossing the Shield-Paleozoic boundary of central Canada: the importance of substrate control. Boreas 50, 781–805.

Burke H, Phillips E, Lee J R, Wilkinson I P, 2009. Imbricate thrust stack model for the formation of glaciotectonic rafts: an example from the Middle Pleistocene of north Norfolk, UK. Boreas 38, 620–637.

Byers J, Cohen D, Iverson N R, 2012. Subglacial clast/bed contact forces. Journal of Glaciology 58, 89–98.

Bödvarsson R, Lund B, Roberts R, Slunga R, 2006. Earthquake activity in Sweden. Study in connection with a proposed nuclear waste repository in Forsmark or Oskarshamn. SKB R-06-67, Svensk Kärnbränslehantering AB.

Carlsson A, 1979. Characteristic Features of a Superficial Rock Mass in Southern Sweden. Striae 11, 1–79.

Carlsson A, Olsson T, 1976. Joint fillings at Forsmark, Uppland, Sweden: A discussion. Geologiska Föreningen i Stockholm Förhandlingar 98, 75–77.

Carlsson A, Olsson T, 1978. Joint apertures in a pre-Cambrian crystalline rock mass in Sweden. Bulletin of the International Association of Engineering 18, 127–130.

Carlsson A, Olsson T, 1982a. Rock bursting phenomena in a superficial rock mass in southern central Sweden. Rock Mechanics 15, 99–110.

Carlsson A, Olsson T, 1982b. High rock stresses as a consequence of glaciation. Nature 298, 739–742.

Carlsson A, Christiansson R, 1987. Geology and tectonics at Forsmark, Sweden. Report SV-UB-1987-42, Swedish State Power Board.

Carlsson A, Christiansson R, 2007. Construction experiences from underground works at Forsmark. Compilation report. SKB R-07-10, Svensk Kärnbränslehantering AB.

Carlsten S, Stråhle A, 2000. Borehole radar and BIPS investigations in boreholes at the Boda area. SKB TR-01-02, Svensk Kärnbränslehantering AB.

Chamberlin T C, 1888. The rock-scorings of the great ice invasions. US Geological Survey Annual Report 7, 155–248.

Chandler D, Hubbard B, Hubbard A, Murray T, Rippin D, 2008. Optimising ice flow law parameters using borehole deformation measurements and numerical modelling. Geophysical Research Letters 35, L12502.

Cheng Y, Zhang Y, 2020. Experimental study of fracture propagation: The application in energy mining. Energies 13, 1411.

Claesson Liljedahl L, Munier R, Sandstroem B, Drake H, Tullborg E-L, 2011. Assessment of fractures classified as non-mineralised in the Sicada database. SKB R-11-02, Svensk Kärnbränslehantering AB.

Claesson Liljedahl L, Kontula A, Harper J, Näslund J-O, Selroos J-O, Pitkänen P, Puigdomenech I, Hobbs M, Follin S, Hirschorn S, Jansson P, Kennell L, Marcos N, Ruskeeniemi T, Tullborg E-L, Vidstrand P, 2016. The Greenland Analogue Project: Final report. SKB TR-14-13, Svensk Kärnbränslehantering AB.

Clark P U, Pollard D, 1998. Origin of the middle Pleistocene transition by ice sheet erosion of regolith. Paleoceanography 13, 1–9.

Cohen D, Iverson N R, Hooyer T, Fischer U, Jackson M, Moore P L, 2005. Debris-bed friction of hard-bedded glaciers. Journal of Geophysical Research: Earth Surface 110, F02007.

Colbeck S C, Evans R, 1973. A flow law for temperate glacier ice. Journal of Glaciology 12, 71–86.

Cooper M A, Jordan T M, Schroeder D M, Siegert M J, Williams C N, Bamber J L, 2019. Subglacial roughness of the Greenland Ice Sheet: relationship with contemporary ice velocity and geology. The Cryosphere 13, 3093–3115.

Cowton T, Nienow P, Sole A, Wadham J, Lis G, Bartholomew I, Mair D, Chandler D, 2013. Evolution of drainage system morphology at a land-terminating Greenlandic outlet glacier. Journal of Geophysical Research: Earth Surface 118, 29–41.

Croot D G, 1987. Glacio-tectonic structures: a mesoscale model of thin-skinned thrust sheets? Journal of Structural Geology 9, 797–808.

Croot D G, Sims P, 1996. Early stages of till genesis: an example from Fanore, County Clare, Ireland. Boreas 25, 37–46.

Cuffey K, Patterson W, 2010. The physics of glaciers. Burlington, MA: Elsevier.

Cutler P M, 1998. Modelling the evolution of subglacial tunnels due to varying water input. Journal of Glaciology 44, 485–497.

Curtis P, Markstroem I, Petersson J, Triumf C-A, Isaksson H, Mattsson H, 2011. Site investigation SFR. Bedrock geology. SKB R-10-49, Svensk Kärnbränslehantering AB.

Darmody R G, Thorn C E, Seppälä M, Campbell S W, Li Y K, Harbor J, 2008. Age and weathering status of granite tors in Arctic Finland (~ 68° N). Geomorphology 94, 10–23.

Das S B, Joughin I, Behn M D, Howat I M, King M A, Lizarralde D, Bhatia M P, 2008. Fracture propagation to the base of the Greenland Ice Sheet during supraglacial lake drainage. Science 320, 778–781.

De Geer G, 1940. Geochronologia Suecica Principles. Kungliga Svenska Vetenskaps Akademiens Handlingar 18, 1–360.

Dewald N, Lewington E L, Livingstone S J, Clark C D, Storrar R D, 2021. Distribution, characteristics and formation of esker enlargements. Geomorphology 392, 107919.

Dewald N, Livingstone S J, Clark C D, 2022. Subglacial meltwater routes of the Fennoscandian Ice Sheet. Journal of Maps. doi:10.1080/17445647.2022.2071648

Dioguardi F, Mele D, Dellino P, 2018. A new one-equation model of fluid drag for irregularly shaped particles valid over a wide range of Reynolds number. Journal of Geophysical Research: Solid Earth 123, 144–156.

Doyle S H, Hubbard A L, Dow C F, Jones G A, Fitzpatrick A, Gusmeroli A, Kulessa B, Lindback K, Pettersson R, Box J E, 2013. Ice tectonic deformation during the rapid in situ drainage of a supraglacial lake on the Greenland Ice Sheet. The Cryosphere 7, 129–140.

Drake H, Roberts N M W, Heim C, Whitehouse M J, Siljeström S, Kooijman E, Broman C, Ivarsson M, Åström M E, 2019. Timing and origin of natural gas accumulation in the Siljan impact structure, Sweden. Nature Communications 10, 1–14.

Dühnforth M, Anderson R S, Ward D, Stock G M, 2010. Bedrock fracture control of glacial erosion processes and rates. Geology 38, 423–426.

Dunlop P, Clark C D, 2006. The morphological characteristics of ribbed moraine. Quaternary Science Reviews 25, 1668–1691.

Egholm D L, Nielsen S B, Pedersen V K, Lesemann J-E, 2009. Glacial effects limiting mountain height. Nature 460, 884–887.

Einarsson B, Jóhannesson T, Thorsteinsson T, Gaidos E, Zwinger T, 2017. Subglacial flood path development during a rapidly rising jökulhlaup from the western Skaftá cauldron, Vatnajökull, Iceland. Journal of Glaciology 63, 670–682.

Ekman M, 1988. Gaussian curvature of postglacial rebound and the discovery of caves created by major earthquakes in Fennoscandia. Geophysica 24, 47–56.

Emerson L F, Rempel A W, 2007. Thresholds in the sliding resistance of simulated basal ice. The Cryosphere 1, 11–19.

EngineeringToolBox, 2008. Area moment of inertia – Typical cross sections I. Available at: https://www.engineeringtoolbox.com/area-moment-inertia-d_1328.html [accessed 07 December 2020].

EngineeringToolBox, 2009. Beams – Supported at both ends – Continuous and point loads. Available at: https://www.engineeringtoolbox.com/beam-stress-deflection-d_1312.html [accessed 07 December 2020].

Evans D J A, Phillips E R, Hiemstra J F, Auton C A, 2006. Subglacial till: formation, sedimentary characteristics and classification. Earth-Science Reviews 78, 115–176.

Evans D J A, Atkinson N, Phillips E R, 2020. Glacial geomorphology of the Neutral Hills Uplands, southeast Alberta, Canada: The process-form imprints of dynamic ice streams and surging ice lobes. Geomorphology 350, 106910.

Eyles N, Doughty M, 2016. Glacially-streamlined hard and soft beds of the paleo-Ontario ice stream in Southern Ontario and New York state. Sedimentary Geology 338, 51–71.

Fabel D, Stroeven A P, Harbor J, Kleman J, Elmore D, Fink D, 2002. Landscape preservation under Fennoscandian ice sheets determined from in situ produced ^{10}Be and ^{26}Al. Earth and Planetary Science Letters 201, 397–406.

Flowers G E, 2015. Modelling water flow under glaciers and ice sheets. Proceedings of the Royal Society A: Mathematical, Physical and Engineering Sciences 471, 20140907.

Follin S, Leven J, Hartley L, Jackson P, Joyce S, Roberts D, Swift B, 2007. Hydrogeological characterisation and modelling of deformation zones and fracture domains, Forsmark modelling stage 2.2. SKB R-07-48, Svensk Kärnbränslehantering AB.

Forssberg O, Mærsk Hansen L, Koyi S, Vestgård J, Öhman J, Petersson J, Albrecht J, Hedenström A, Gustavsson J, 2007. Forsmark site Investigation. Detailed fracture and bedrock mapping, quaternary investigations and GPR measurements at excavated outcrop AFM001264. SKB P-05-269, Svensk Kärnbränslehantering AB.

Ganser G H, 1993. A rational approach to drag prediction of spherical and nonspherical particles. Powder Technology 77, 143–152.

Glamheden R, Fredriksson A, Roeshoff K, Karlsson J, Hakami H, Christiansson R, 2007.
Rock mechanics Forsmark. Site descriptive modelling Forsmark stage 2.2. SKB TR-07-31, Svensk
Kärnbränslehantering AB.

Glasser N F, Warren C R, 1990. Medium scale landforms of glacial erosion in south Greenland;
process and form. Geografiska Annaler: Series A, Physical Geography 72, 211–215.

Glasser N F, Roman M, Holt T O, Žebre M, Patton H, Hubbard A L, 2020. Modification of
bedrock surfaces by glacial abrasion and quarrying: Evidence from North Wales. Geomorphology
365, 107283.

Goodfellow B W, Stroeven A P, Martel S J, Heyman J, Rossi M, Caffee M W, 2019. Exploring
alternative models for the formation of conspicuously flat basement surfaces in southern Sweden.
SKB TR-19-22, Svensk Kärnbränslehantering AB.

Greenwood S L, O'Regan M, Swärd H, Flodén T, Ananyev R, Chernykh D, Jakobsson M, 2015.
Multiple re-advances of a Lake Vättern outlet glacier during Fennoscandian Ice Sheet retreat, south-
central Sweden. Boreas 44, 619–637.

Greenwood S L, Clason C C, Nyberg J, Jakobsson M, Holmlund P, 2017. The Bothnian Sea ice
stream: early Holocene retreat dynamics of the south-central Fennoscandian Ice Sheet. Boreas 46,
346–362.

Grigull S, Peterson G, Nyberg J, Öhrling C, 2019. Phanerozoic faulting of Precambrian basement
in Uppland. SKB R-19-22, Svensk Kärnbränslehantering AB.

Hall A M, Krabbendam M, 2022. A fresh perspective on Swedish fracture caves. Grottan 57, 4–8.

Hall A M, Phillips W M, 2006. Glacial modification of granite tors in the Cairngorms, Scotland.
Journal of Quaternary Science 21, 811–830.

Hall A M, Hansom J D, Jarvis J, 2008. Patterns and rates of erosion produced by high energy wave
processes on hard rock headlands: The Grind of the Navir, Shetland, Scotland. Marine Geology 248,
28–46.

**Hall A M, Ebert K, Goodfellow B W, Hättestrand C, Heyman J, Krabbendam M, Moon S,
Stroeven A P, 2019a.** Past and future impact of glacial erosion in Forsmark and Uppland.
SKB TR-19-07, Svensk Kärnbränslehantering AB.

Hall A M, Krabbendam M, van Boeckel M, Ebert K, Hättestrand C, Heyman J, 2019b. The
sub-Cambrian unconformity in Västergötland, Sweden: Reference Surface for Glacial Erosion of
Basement, Technical Report. SKB TR-19-21, Svensk Kärnbränslehantering AB.

**Hall A M, Krabbendam M, van Boeckel M, Goodfellow B W, Hättestrand C, Heyman J,
Palamakumbura R, Stroeven A P, Näslund J-O, 2020.** Glacial ripping: geomorphological evidence
from Sweden for a new process of glacial erosion. Geografiska Annaler: Series A, Physical Geography
112, 333–353.

Hall A M, Mathers H, Krabbendam M, 2021a. Glacial ripping in sedimentary rocks: Loch Eriboll,
NW Scotland. Geosciences 11, 232.

Hall A M, Ballantyne C K, Hansom J D, 2021b. The Outer Hebrides and St Kilda. In Ballantyne C K,
Gordon J E (eds.). Landscapes and Landforms of Scotland. Cham: Springer International Publishing,
169–191.

Hall A M, Hansom J D, Gordon J E, 2021c. Shetland. In Ballantyne C K, Gordon J E (eds.).
Landscapes and Landforms of Scotland. Cham: Springer International Publishing, 135–150.

Hall A M, Krabbendam M, van Boeckel M, 2022. Glacial erosion in the Öregrund archipelago
– potential for headward erosion towards Forsmark in future glaciations? SKB TR-22-08, Svensk
Kärnbränslehantering AB.

Hallet B, 1979. A theoretical model of glacial abrasion. Journal of Glaciology 23, 39–50.

Hallet B, 1996. Glacial quarrying: a simple theoretical model. Annals of Glaciology 22, 1–8.

Hallet, B. 2011. Glacial erosion assessment. NWMO DGR-TR-2011-18, Nuclear Waste Management Organization, Canada.

Harper J, Hubbard A, Ruskeeniemi T, Claesson Liljedahl L, Kontula A, Bougamont M, Brown J, Dirkson A, Dow C, Doyle S, Drake H, Engström J, Fitzpatrick A, Follin S, Frape S, Graly J, Hansson K, Harrington J, Henkemans E, Hirschorn S, Hobbs M, Humphrey N, Jansson P, Johnson J, Jones G, Kinnbom P, Kennell L, Klint K E S, Liimatainen J, Lindbäck K, Meierbachtol T, Pere T, Pettersson R, Tullborg E-L, van As D, 2016. The Greenland Analogue Project: Data and processes. SKB R-14-13, Svensk Kärnbränslehantering AB.

Harper J T, Meierbachtol T, Humphrey N F, 2019. Greenland ICE Project. Final report. SKB R-18-06, Svensk Kärnbränslehantering AB.

Harrington J A, Humphrey N F, Harper J T, 2015. Temperature distribution and thermal anomalies along a flowline of the Greenland ice sheet. Annals of Glaciology 56, 98–104.

Harris C, 1991. Glacially deformed bedrock at Wylfa Head, Anglesey, North Wales. Geological Society, London, Engineering Geology Special Publications 7, 135–142.

Hart J K, 1990. Proglacial glaciotectonic deformation and the origin of the Cromer Ridge push moraine complex, North Norfolk, England. Boreas 19, 165–180.

Hedenström A, Risberg J, 2003. Shore displacement in northern Uppland during the last 6500 calendar years. SKB TR-03-17, Svensk Kärnbränslehantering AB.

Hedenström A, Sohlenius G, 2008. Description of the regolith at Forsmark. Site descriptive modelling .SDM-Site Forsmark. SKB R-08-04, Svensk Kärnbränslehantering AB.

Helmens K F, Katrantsiotis C, Kuosmanen N, Luoto T P, Salonen J S, Väliranta M, 2020. Prolonged interglacial warmth during the Last Glacial in northern Europe. Boreas 50, 331–350.

Hermanson J, Hansen L, Vestgård J, Leiner P, 2003. Forsmark site investigation. Detailed fracture mapping of the outcrops Klubbudden, AFM001098 and Drill Site 4, AFM001097. SKB P-03-115, Svensk Kärnbränslehantering AB.

Hermansson T, Stephens M B, Page L M, 2008. ^{40}Ar/^{39}Ar hornblende geochronology from the Forsmark area in central Sweden: constraints on late Svecofennian cooling, ductile deformation and exhumation. Precambrian Research 167, 303–315.

Heyman J, Goodfellow B W, Stroeven A P, Hall A M, Caffee M, Hättestrand C, Ebert K, Näslund J-O, Hippe K, Martel S, Moon S, Perron J T, Stuart F M, 2019. Erosion of low-relief basement by the Fennoscandian ice sheet based on bedrock ^{10}Be and ^{26}Al. INQUA 2019 O-1070.

Hiemstra J F, Evans D J, Cofaigh C Ó, 2007. The role of glacitectonic rafting and comminution in the production of subglacial tills: examples from southwest Ireland and Antarctica. Boreas 36, 386–399.

Hoffman M J, Andrews L C, Price S F, Catania G A, Neumann T A, Lüthi M P, Gulley J, Ryser C, Hawley R L, Morriss B, 2016. Greenland subglacial drainage evolution regulated by weakly connected regions of the bed. Nature Communications 7, 1–12.

Hooyer T S, Cohen D, Iverson N R, 2012. Control of glacial quarrying by bedrock joints. Geomorphology 153–154, 91–101.

Huigen Y, Andriessen P, 2004. Thermal effects of Caledonian foreland basin formation, based on fission track analyses applied on basement rocks in central Sweden. Physics and Chemistry of the Earth, parts A/B/C 29, 683–694.

Hyttinen O, Quintana Krupinski N, Bennike O, Wacker L, Filipsson H L, Obrochta S, Jensen J B, Lougheed B, Ryabchuk D, Passchier S, 2021. Deglaciation dynamics of the Fennoscandian Ice Sheet in the Kattegat, the gateway between the North Sea and the Baltic Sea Basin. Boreas 50, 351–368.

Hättestrand C, 1997. Ribbed moraines in Sweden – distribution pattern and palaeoglaciological implications. Sedimentary Geology 111, 41–56.

Hättestrand C, Stroeven A P, 2002. A relict landscape in the centre of Fennoscandian glaciation: Geomorphological evidence of minimal Quaternary glacial erosion. Geomorphology 44, 127–143.

Hökmark H, Lönnqvist M, 2014. Reply to comment by Christopher Talbot on "Approach to estimating the maximum depth for glacially induced hydraulic jacking in fractured crystalline rock at Forsmark, Sweden". Journal of Geophysical Research: Earth Surface 119, 955–959.

Hökmark H, Lönnqvist M, Fälth B, 2010. THM-issues in repository rock. Thermal, mechanical, thermo-mechanical and hydro-mechanical evolution of the rock at the Forsmark and Laxemar sites. SKB TR-10-23, Svensk Kärnbränslehantering AB.

Iverson N R, 1991. Potential effects of subglacial water-pressure fluctuations on quarrying. Journal of Glaciology 37, 27–36.

Iverson N R, 2012. A theory of glacial quarrying for landscape evolution models. Geology 40, 679–682.

Iverson N, Person M, 2012. Glacier-bed geomorphic processes and hydrologic conditions relevant to nuclear waste disposal. Geofluids 12, 38–57.

Jansen J D, Codilean A T, Stroeven A P, Fabel D, Hättestrand C, Kleman J, Harbor J M, Heyman J, Kubik P W, Xu S, 2014. Inner gorges cut by subglacial meltwater during Fennoscandian ice sheet decay. Nature Communications 5, 1–7.

Jern M, 2004. Determination of the in situ block size distribution in fractured rock, an approach for comparing in-situ rock with rock sieve analysis. Rock Mechanics and Rock Engineering37, 391–401.

Johansson M, Migon P, Olvmo M, 2001. Development of joint-controlled rock basins in Bohus granite, SW Sweden. Geomorphology 40, 145–161.

Johansson P-O, 2008. Description of surface hydrology and near-surface hydrogeology at Forsmark. Site descriptive modelling SDM. Site Forsmark. SKB R-08-08, Svensk Kärnbränslehantering AB.

Johnson M D, Benediktsson Í Ö, Björklund L, 2013. The Ledsjö end moraine—a subaquatic push moraine composed of glaciomarine clay in central Sweden. Proceedings of the Geologists' Association 124, 738-752.

Juhlin C, Stephens M B, 2006. Gently dipping fracture zones in Paleoproterozoic metagranite, Sweden: Evidence from reflection seismic and cored borehole data and implications for the disposal of nuclear waste. Journal of Geophysical Research: Solid Earth 111, B09302.

Kleman J, Hättestrand C, 1999. Frozen-bed Fennoscandian and Laurentide ice sheets during the Last Glacial Maximum. Nature 402, 63–66.

Kleman J, Stroeven A P, Lundqvist J, 2008. Patterns of Quaternary ice sheet erosion and deposition in Fennoscandia and a theoretical framework for explanation. Geomorphology 97, 73–90.

Koppes M N, Montgomery D R, 2009. The relative efficacy of fluvial and glacial erosion over modern to orogenic timescales. Nature Geoscience 2, 644–647.

Krabbendam M, 2016. Sliding of temperate basal ice on a rough, hard bed: creep mechanisms, pressure melting, and implications for ice streaming. The Cryosphere 10, 1915–1932.

Krabbendam M, Bradwell T, 2011. Lateral plucking as a mechanism for elongate erosional glacial bedforms: explaining megagrooves in Britain and Canada. Earth Surface Processes and Landforms 36, 1335–1349.

Krabbendam M, Bradwell T, 2014 Quaternary evolution of glaciated gneiss terrains: pre-glacial weathering vs. glacial erosion. Quaternary Science Reviews 95, 20–42.

Krabbendam M, Glasser N, 2011. Glacial erosion and bedrock properties in NW Scotland: Abrasion and plucking, hardness and joint spacing. Geomorphology 130, 374–383.

Krabbendam M, Hall A, 2019. Subglacial block removal – A preliminary analysis of driving and resisting forces under different glaciological scenarios. SKB TR-19-18, Svensk Kärnbränslehantering AB.

Krabbendam M, Palamakumbura R, Arnhardt C, Hall A, 2021. Rock fracturing by subglacial hydraulic jacking in basement rocks, eastern Sweden: the role of beam failure. GFF 143, 390–405.

Krabbendam M, Hall A M, Palamakumbura R N, Finlayson A, 2022a. Glaciotectonic disintegration of roches moutonnées in east Sweden: a transient phase during glacial ripping. Geografiska Annaler: Series A, Physical Geography 104, 35–56.

Krabbendam M, Dioguardi F, Arnhardt C, Robertson S, Hall A M, 2022b. Drag forces at the ice-sheet bed and resistance of hard-rock obstacles: the physics of glacial ripping. Journal of Glaciology. doi:10.1017/jog.2022.49

Krzaczek M, Nitka M, Kozicki J, Tejchman J, 2020. Simulations of hydro-fracking in rock mass at meso-scale using fully coupled DEM/CFD approach. Acta Geotechnica 15, 297–324.

Lagerbäck R, 1990. Late Quaternary faulting and-paleoseismicity in northern Fennoscandia, with particular reference to the Lansjärv area, northern Sweden. Geologiska Föreningen i Stockholm Förhandlingar 112, 333–354.

Lagerbäck R, Sundh M, Svedlund J-O, Johansson H, 2005. Searching for evidence of late- or postglacial faulting in the Forsmark region. Results from 2002–2004. SKB R-05-51, Svensk Kärnbränslehantering AB.

Lane E W, 1947. Report of the subcommittee on sediment terminology. Eos, Transactions American Geophysical Union 28, 936–938.

Larsen E, Mangerud J, 1992. Subglacially formed clastic dikes. Uppsala: Geological Survey of Sweden, 163-170. (Ser. Ca 81)

Larson S A, Tullborg E, Cederbom C, Stiberg J, 1999. Sveconorwegian and Caledonian foreland basins in the Baltic Shield revealed by fission-track thermochronology. Terra Nova 11, 210–215.

Lee J R, Phillips E, Booth S J, Rose J, Jordan H M, Pawley S M, Warren M, Lawley R S, 2013. A polyphase glacitectonic model for ice-marginal retreat and terminal moraine development: the Middle Pleistocene British Ice Sheet, northern Norfolk, UK. Proceedings of the Geologists' Association 124, 753–777.

Leguy G R, Asay-Davis X S, Lipscomb W H, 2014. Parameterization of basal friction near grounding lines in a one-dimensional ice sheet model. The Cryosphere 8, 1239–1259.

Leijon B, 2005. Forsmark site investigation. Investigations of superficial fracturing and block displacements at drill site 5. SKB P-05-199, Svensk Kärnbränslehantering AB.

Leith D, 1987. Drag on nonspherical objects. Aerosol Science and Technology 6, 153–161.

Lewington E L M, Livingstone S J, Clark C D, Sole A J, Storrar R D, 2020. A model for interaction between conduits and surrounding hydraulically connected distributed drainage based on geomorphological evidence from Keewatin, Canada. The Cryosphere 14, 2949–2976.

Liang Q, Xiao W, Howat I, Cheng X, Hui F, Chen Z, Jiang M, Zheng L, 2022. Filling and drainage of a subglacial lake beneath the Flade Isblink ice cap, northeast Greenland. The Cryosphere 16, 2671–2681.

Lidmar-Bergström K, 1993. Denudation surfaces and tectonics in the southernmost part of the Baltic Shield. Precambrian Research 64, 337–345.

Lindbäck K, Pettersson R, 2015. Spectral roughness and glacial erosion of a land-terminating section of the Greenland Ice Sheet. Geomorphology 238, 149–159.

Lindén A, 1975. Till petrographical studies in an Archaean bedrock area in southern central Sweden. Striae 1, 3–57.

Lokrantz H, 2004. Sedimentfyllda sprickor i berggrunden, Rångsta, norr om Uppsala. Rapport 2004:17, Geological Survey of Sweden.

Loth E, 2008. Drag of non-spherical solid particles of regular and irregular shape. Powder Technology 182, 342–353.

Lund B, Schmidt P, Hieronymus C, 2009. Stress evolution and fault stability during the Weichselian glacial cycle. SKB TR-09-15, Svensk Kärnbränslehantering AB.

Lundqvist J, 1987. Glaciodynamics of the Younger Dryas Marginal zone in Scandinavia: implications of a revised glaciation model. Geografiska Annaler: Series A, Physical Geography 69, 305–319.

Lundqvist J, 1989. Rogen (ribbed) moraine – identification and possible origin. Sedimentary Geology 62, 281–292.

Lundqvist J, 1999. Periodical sedimentation in Scandinavian eskers. GFF 121, 175–181.

Lüthi M, Funk M, Iken A, Gogineni S, Truffer M, 2002. Mechanisms of fast flow in Jakobshavn Isbræ, West Greenland: Part III. Measurements of ice deformation, temperature and cross-borehole conductivity in boreholes to the bedrock. Journal of Glaciology 48, 369–385.

Löfgren M, Sidborn M, 2016. Quantitative mapping and statistical evaluation of fracture minerals in the granitic bedrock at Forsmark, Sweden. Mineralogy and Petrology 110, 663–680.

Lönnqvist M, Hökmark H, 2013. Approach to estimating the maximum depth for glacially induced hydraulic jacking in fractured crystalline rock at Forsmark, Sweden. Journal of Geophysical Research: Earth Surface 118, 1777–1791.

MacGregor K R, Anderson R S, Waddington E D, 2009. Numerical modeling of glacial erosion and headwall processes in alpine valleys. Geomorphology 103, 189–204.

MacGregor J A, Fahnestock M A, Catania G A, Aschwanden A, Clow G D, Colgan W T, Gogineni S P, Morlighem M, Nowicki S M J, Paden J D, Price S F, Seroussi H, 2016. A synthesis of the basal thermal state of the Greenland Ice Sheet. Journal of Geophysical Research: Earth Surface 121, 1328–1350.

Martel S J, 2017. Progress in understanding sheeting joints over the past two centuries. Journal of Structural Geology 94, 68–86.

Mattila J, Ojala A, Ruskeeniemi T, Palmu J-P, Aaltonen I, Käpyaho A, Lindberg A, Sutinen R, 2019. Evidence of multiple slip events on postglacial faults in northern Fennoscandia. Quaternary Science Reviews 215, 242–252.

Mikko H, Smith C A, Lund B, Ask M V, Munier R, 2015. LiDAR-derived inventory of post-glacial fault scarps in Sweden. GFF 137, 334–338.

Min K-B, Stephansson O, 2011. The DFN-DEM approach applied to investigate the effects of stress on mechanical and hydraulic rock mass properties at Forsmark, Sweden. Tunnel and Underground Space 21, 117–127.

Moon S, Perron J T, Martel S J, Goodfellow B W, Mas Ivars D, Hall A, Heyman J, Munier R, Näslund J O, Simeonov A, 2020. Present-day stress field influences bedrock fracture openness deep into the subsurface. Geophysical Research Letters 47, e2020GL090581.

Morrow D W, 1982. Descriptive field classification of sedimentary and diagenetic breccia fabrics in carbonate rocks. Bulletin of Canadian Petroleum Geology 30, 227–229.

Murchison R I, 1846. On the superficial detritus of Sweden, and on the probable causes which have affected the surface of the rocks in the central and southern portions of that kingdom. Quarterly Journal of the Geological Society 2, 349–381.

Murray, T, Clarke, G K, 1995. Black-box modeling of the subglacial water system. Journal of Geophysical Research: Solid Earth 100, 10231–10245.

Möller H, 1993. Beskrivning till Jordartskartan Uppsala NV. Uppsala: Geological Survey of Sweden. (Ser. Ae113)

Möller P, 2010. Melt-out till and ribbed moraine formation, a case study from south Sweden. Sedimentary Geology 232, 161–180.

Mörner N-A, 1978. Faulting, fracturing, and seismicity as functions of glacio-isostasy in Fennoscandia. Geology 6, 41–45.

Mörner N-A, 2017. Methane hydrate in crystalline bedrock and explosive methane venting tectonics. Earth-Science Reviews 169, 202–212.

Mörner N-A, Sjöberg R, 2018. Merging the concepts of pseudokarst and paleoseismicity in Sweden: A unified theory on the formation of fractures, fracture caves, and angular block heaps. International Journal of Speleology 47, 393–405.

Mörner N-A, Tröften P E, Sjöberg R, Grant D, Dawson S, Bronge C, Kvamsdal O, Sidén A, 2000. Deglacial paleoseismicity in Sweden: the 9663 BP Iggesund event. Quaternary Science Reviews 19, 1461–1468.

Neupane B, Panthi K K, Vereide K, 2020. Effect of power plant operation on pore pressure in jointed rock mass of an unlined hydropower tunnel: an experimental study. Rock Mechanics and Rock Engineering 53, 3073-3092.

Neuzil C, Tracy J V, 1981. Flow through fractures. Water Resources Research 17, 191–199.

Nielsen A T, Schovsbo N H, 2011. The Lower Cambrian of Scandinavia: depositional environment, sequence stratigraphy and palaeogeography. Earth-Science Reviews 107, 207–310.

Niven E B, Deutsch C V, 2010. Relating different measures of fracture intensity. CCG Annual Report-Paper 103.

Nordgulen Ø, Saintot A, 2008. Forsmark site investigation. The character and kinematics of deformation zones (ductile shear zones, fault zones and fracture zones) at Forsmark – report from phase 3. SKB P-07-111, Svensk Kärnbränslehantering AB.

Nye J F, 1970. Glacier sliding without cavitation in a linear viscous approximation. Proceedings of the Royal Society of London. A. Mathematical and Physical Sciences, 315, 381–403.

Näslund J-O, Rodhe L, Fastook J L, Holmlund P, 2003. New ways of studying ice sheet flow directions and glacial erosion by computer modelling – examples from Fennoscandia. Quaternary Science Reviews 22, 245–258.

Ó Cofaigh C, Dowdeswell J A, King E C, Anderson J B, Clark C D, Evans D J, Evans J, Hindmarsh R C, Larter R D, Stokes C R, 2010. Comment on Shaw J., Pugin, A. and Young, R. (2008):"A meltwater origin for Antarctic shelf bedforms with special attention to megalineations", Geomorphology 102, 364–375. Geomorphology 117, 195.

Olofsson I, Simeonov A, Stephens M, Follin S, Nilsson A-C, Roeshoff K, Lindberg U, Lanaro F, Fredriksson A, Persson L, 2007. Site descriptive modelling Forsmark, stage 2.2. A fracture domain concept as a basis for the statistical modelling of fractures and minor deformation zones, and inter-disciplinary coordination. SKB R-07-15, Svensk Kärnbränslehantering AB.

Olvmo M, Johansson M, 2002. The significance of rock structure, lithology and pre-glacial deep weathering for the shape of intermediate-scale glacial erosional landforms. Earth Surface Processes and Landforms 27 251–268.

Palamakumbura R, Krabbendam M, Whitbread K, Arnhardt C, 2020. Data acquisition by digitizing 2-D fracture networks and topographic lineaments in geographic information systems: further development and applications. Solid Earth 11, 1731–1746.

Palmer S, McMillan M, Morlighem M, 2015. Subglacial lake drainage detected beneath the Greenland ice sheet. Nature Communications 9, 8408.

Patton H, Hubbard A, Andreassen K, Winsborrow M, Stroeven A P, 2016. The build-up, con-figuration, and dynamical sensitivity of the Eurasian ice-sheet complex to Late Weichselian climatic and oceanic forcing. Quaternary Science Reviews 153, 97–121.

Patton H, Hubbard A, Andreassen K, Auriac A, Whitehouse P L, Stroeven A P, Shackleton C, Winsborrow M, Heyman J, Hall A M, 2017. Deglaciation of the Eurasian ice sheet complex. Quaternary Science Reviews 169, 148–172.

Persson C, 1985. Beskrivning till jordartskartan Östhammar NO. Rapport Ae 73, Geological Survey of Sweden. (In Swedish.)

Persson C, 1988. Beskrivning till jordartskartan Östhammar SO. Rapport Ae 90, Geological Survey of Sweden. (In Swedish.)

Peterson G, Johnson M D, 2018. Hummock corridors in the south-central sector of the Fenno-scandian ice sheet, morphometry and pattern. Earth Surface Processes and Landforms 43, 919–929.

Petersson J, Skogsmo G, Vestgård J, Albrecht J, Hedenström A, Gustavsson J, 2007. Bedrock mapping and magnetic susceptibility measurements, Quaternary investigations and GPR measurements in trench AFM001265. Forsmark site investigation. SKB P-06-136, Svensk Kärnbränslehantering AB.

Petrone J, Sohlenius G, Ising J, 2020. Baseline Forsmark – Depth and stratigraphy of regolith. SKB R-17-07, Svensk Kärnbränslehantering AB.

Philip A L, 1990. Ice-pushed boulders on the shores of Gotland, Sweden. Journal of Coastal Research 6, 661–676.

Phillips E, Auton C, 2008. Microtextural analysis of a glacially 'deformed' bedrock: implications for inheritance of preferred clast orientations in diamictons. Journal of Quaternary Science 23, 229–240.

Phillips E, Merritt J, 2008. Evidence for multiphase water-escape during rafting of shelly marine sediments at Clava, Inverness-shire, NE Scotland. Quaternary Science Reviews 27, 988–1011.

Phillips E, Everest J, Reeves H, 2013. Micromorphological evidence for subglacial multiphase sedimentation and deformation during overpressurized fluid flow associated with hydrofracturing. Boreas 42, 395–427.

Piotrowski J A, 1997. Subglacial groundwater flow during the last glaciation in northwestern Germany. Sedimentary Geology 111, 217–224.

Pusch R, Börgesson L, Knutsson S, 1990. Origin of silty fracture fillings in crystalline bedrock. Geologiska Föreningen i Stockholm Förhandlingar 112, 209–213.

Ramana Y V, Gogte B S, 1989. Dependence of coefficient of sliding friction in rocks on lithology and mineral characteristics. Engineering Geology 26, 271–279.

Rastas J, Seppälä M, 1981. Rock jointing and abrasion forms on roches moutonnées, SW Finland. Annals of Glaciology 2, 159–163.

Rea B R, Evans D J A, 1996. Landscapes of aerial scouring in NW Scotland. Scottish Geographical Magazine 112, 47–50.

Rea B R, Whalley W B, 1996. The role of bedrock topography, structure, ice dynamics and preglacial weathering in controlling subglacial erosion beneath a high-latitude, maritime ice field. Annals of Glaciology 22 121–125.

Rijsdijk K F, Owen G, Warren W P, McCarroll D, van der Meer J J, 1999. Clastic dykes in over-consolidated tills: evidence for subglacial hydrofracturing at Killiney Bay, eastern Ireland. Sedimentary Geology 129, 111–126.

Roberts D H, Long A J, 2005. Streamlined bedrock terrain and fast ice flow, Jakobshavns Isbrae, West Greenland: implications for ice stream and ice sheet dynamics. Boreas 34, 25–42.

Robertsson A-M, 2004. Forsmark Site Investigation: Microfossil Analyses of Till and Sediment Samples from Forsmark, Northern Uppland. SKB P-04-110, Svensk Kärnbränslehantering AB.

Ruszcyńska-Szenajch H, 1987. The origin of glacial rafts: detachment, transport, deposition. Boreas 16, 101–112.

Ryser C, Lüthi M P, Andrews L C, Hoffman M J, Catania G A, Hawley R L, Neumann T A, Kristensen S S, 2014. Sustained high basal motion of the Greenland ice sheet revealed by borehole deformation. Journal of Glaciology 60, 647–660.

Röthlisberger H, 1972. Water pressure in intra-and subglacial channels. Journal of Glaciology 11, 177–203.

Röthlisberger H, Iken A, 1981. Plucking as an effect of water-pressure variations at the glacier bed. Annals of Glaciology 2, 57–62.

Sandegren R, Asklund B, Westergård A H, 1939. Beskrivning till kartbadet Gävle. Rapport Aa 178, Geological Survey of Sweden. (In Swedish.)

Sandström B, Tullborg E, Smellie J, MacKenzie A, Suksi J, 2008. Fracture mineralogy of the Forsmark site. SKB R-08-102, Svensk Kärnbränslehantering AB.

Sandström B, Tullborg E-L, Larson S Å, Page L, 2009. Brittle tectonothermal evolution in the Forsmark area, central Fennoscandian Shield, recorded by paragenesis, orientation and $^{40}Ar/^{39}Ar$ geochronology of fracture minerals. Tectonophysics 478, 158–174.

Sandström B, Annersten H, Tullborg E-L, 2010. Fracture-related hydrothermal alteration of metagranitic rock and associated changes in mineralogy, geochemistry and degree of oxidation: a case study at Forsmark, central Sweden. International Journal of Earth Sciences 99, 1–25.

Scheidegger J, Bense V, 2014. Impacts of glacially recharged groundwater flow systems on talik evolution. Journal of Geophysical Research: Earth Surface 119, 758–778.

Schoof C, 2010. Ice-sheet acceleration driven by melt supply variability. Nature 468, 803–806.

Schroeder J, Beaupré M, Cloutier M, 1986. Ice-push caves in platform limestones of the Montréal area. Canadian Journal of Earth Sciences 23, 1842–1851.

Selroos J-O, Follin S, 2014. Overview of hydrogeological site-descriptive modeling conducted for the proposed high-level nuclear waste repository site at Forsmark, Sweden. Hydrogeology Journal 22, 295–298.

Shackleton C, Patton H, Hubbard A, Winsborrow M, Kingslake J, Esteves M, Andreassen K, Greenwood S L, 2018. Subglacial water storage and drainage beneath the Fennoscandian and Barents Sea ice sheets. Quaternary Science Reviews 201, 13–28.

Sharpe D R, Shaw J, 1989. Erosion of bedrock by subglacial meltwater, Cantley, Quebec. Geological Society of America Bulletin 101, 1011–1020.

Sharpe D, Lesemann J, Knight R, Kjarsgaard B, 2021. Regional stagnation of the western Keewatin ice sheet and the significance of meltwater corridors and eskers, northern Canada. Canadian Journal of Earth Sciences, 58, 1005–1026.

Shaw J, 2010. In defence of the meltwater (megaflood) hypothesis for the formation of subglacial bedform fields. Journal of Quaternary Science 25, 249–260.

Shulmeister J, 1989. A conceptual model for the deposition of the Dummer Moraine, southern Ontario. Geomorphology 2, 385–392.

Singh P K, Tripathy A, Kainthola A, Mahanta B, Singh V, Singh T N, 2017. Indirect estimation of compressive and shear strength from simple index tests. Engineering with Computers 33, 1–11.

Singhal B B S, Gupta R P, 2010. Applied hydrogeology of fractured rocks. Springer Science & Business Media.

Sjöberg R, 1986. Caves indicating neotectonic activity in Sweden. Geografiska Annaler: Series A, Physical Geography 68, 393–398.

Sjöberg R, 1994. Bedrock caves and fractured rock surfaces in Sweden. Occurrence and origin. PhD Thesis. Stockholm University.

SKB, 2010. Climate and climate-related issues for the safety assessment SR-Site. SKB TR-10-49, Svensk Kärnbränslehantering AB.

SKB, 2013. Site description of the SFR area at Forsmark at completion of the site investigation phase. SDM-PSU Forsmark. SKB TR-11-04, Svensk Kärnbränslehantering AB.

SKB, 2020. Post-closure safety for the final repository for spent nuclear fuel at Forsmark – Climate and climate-related issues, PSAR version. SKB TR-20-12, Svensk Kärnbränslehantering AB.

Smith C A, Öhrling C, 2022. Assessing the validity of proposed paleo-tsunami deposits in Sweden. Quaternary Science Reviews 298, 107849.

Sohlenius G, Hedenström A, Rudmark L, 2004. Forsmark site investigation. Mapping of unconsolidated Quaternary deposits 2002–2003. Map description. SKB R-04-39, Svensk Kärnbränslehantering AB.

Sohlenius G, Strömgren M, Hartz F, 2013. Depth and stratigraphy of regolith at Forsmark. SR-PSU Biosphere. SKB R-13-22, Svensk Kärnbränslehantering AB.

Sohlenius G, Wilin L, Hedenström A, Karlsson C, 2019. Quaternary deposits in the drainage area of Gunnarsboträsket in Forsmark. Stratigraphical and surficial distribution of Quaternary deposits. SKB P-19-15, Svensk Kärnbränslehantering AB.

Stendahl J, Lundin L, Nilsson T, 2009. The stone and boulder content of Swedish forest soils. Catena 77, 285-291.

Stephansson O, Ericsson B, 1975. Pre-Holocene joint fillings at Forsmark, Uppland, Sweden. Geologiska Föreningen i Stockholm Förhandlingar 97, 91–95.

Stephansson O, Ångman P, 1986. Hydraulic fracturing stress measurements at Forsmark and Stidsvig, Sweden. Bull. Geol. Soc. Finland 58, 307–333.

Stephens M B, 2010. Forsmark site investigation. Bedrock geology – overview and excursion guide. SKB R-10-04, Svensk Kärnbränslehantering AB.

Stephens M B, Bergman T, Isaksson H, Petersson J, 2008. Bedrock geology Forsmark. Modelling stage 2.3. Description of the bedrock geological map at the ground surface. SKB R-08-128, Svensk Kärnbränslehantering AB.

Stober I, Bucher K, 2007. Hydraulic properties of the crystalline basement. Hydrogeology Journal 15, 213–224.

Stokes G G, 1951. On the effect of the inertial friction of fluids on the motions of pendulums. Transactions of the Cambridge Philosophcial Soceity 9, 1851.

Stroeven A P, Hättestrand C, Kleman J, Heyman J, Fabel D, Fredin O, Goodfellow B W, Harbor J M, Jansen J D, Olsen L, 2016. Deglaciation of Fennoscandia. Quaternary Science Reviews 147, 91–121.

Strömberg B O, 1989. Late Weichselian deglaciation and clay varve chronology in east-central Sweden. Uppsala: Geological Survey of Sweden. (Ser. Ca 73)

Strömberg B O, 1994. Younger Dryas deglaciation at Mt. Billingen, and clay varve dating of the Younger Dryas/Preboreal transition. Boreas 23, 177–193.

Sugden D E, Glasser N, Clapperton C M, 1992. Evolution of large roches moutonnées. Geografiska Annaler: Series A, Physical Geography 74, 253–264.

Sugden D E, Hall A M, Phillips W M, Stewart M, 2019. Plucking enhanced beneath ice sheet margins: evidence from the Grampian Mountains, Scotland. Geografiska Annaler: Series A, Physical Geography 101, 34–44.

Sund M, Ericsson B, 2015. Beskrivning till jordartskartorna 13H Gävle NV, NO, SV och SO. Uppsala: Geological Survey of Sweden. (Ser. K 513–516)

Svantesson S-I, 1991. Description to the Quaternary map Enköping NO. Uppsala: Geological Survey of Sweden. (Ser. Ae 110)

Söderlund P, Hermansson T, Page L M, Stephens M B, 2009. Biotite and muscovite ^{40}Ar–^{39}Ar geochronological constraints on the post-Svecofennian tectonothermal evolution, Forsmark site, central Sweden. International Journal of Earth Sciences 98, 1835–1851.

Talbot C, 1990. Problems posed to a bedrock radwaste repository by gently dipping fracture zones. Geologiska Föreningen i Stockholm Förhandlingar 112, 355–359.

Talbot C J, 1999. Ice ages and nuclear waste isolation. Engineering Geology 52, 177–192.

Talbot C J, 2014. Comment on "Approach to estimating the maximum depth for glacially induced hydraulic jacking in fractured crystalline rock at Forsmark, Sweden" by M. Lönnqvist and H. Hökmark. Journal of Geophysical Research: Earth Surface 119, 951–954.

Terry J, Goff J, 2014. Megaclasts: proposed revised nomenclature at the coarse end of the Udden-Wentworth grain-size scale for sedimentary particles. Journal of Sedimentary Research 84, 192–197.

Tirén S A, Beckholmen M, 1989. Block faulting in southeastern Sweden interpreted from digital terrain models. Geologiska Föreningen i Stockholm Förhandlingar 111, 171–179.

Tsai V C, Rice J R, 2012. Modeling turbulent hydraulic fracture near a free surface. Journal of Applied Mechanics 79, 031003.

Ugelvig S V, Egholm D L, Iverson N R, 2016. Glacial landscape evolution by subglacial quarrying: A multiscale computational approach. Journal of Geophysical Research: Earth Surface 121, 2042–2068.

van Boeckel M, van Boeckel T, Hall A M. 2022. Late erosion pulse triggered by rapid melt in the cold-based interior of the last Fennoscandian Ice Sheet, an example from Rogen. Earth Surface Processes and Landforms 47, 3376–3394.

van der Meer J J, Kjær K H, Krüger J, Rabassa J, Kilfeather A, 2009. Under pressure: clastic dykes in glacial settings. Quaternary Science Reviews 28, 708–720.

Vérité J, Ravier É, Bourgeois O, Bessin P, Livingstone S J, Clark C D, Pochat S, Mourgues R, 2022. Formation of murtoos by repeated flooding of ribbed bedforms along subglacial meltwater corridors. Geomorphology 408, 108248.

Vidstrand P, Follin S, Selroos J-O, Näslund J-O, 2014. Groundwater flow modeling of periods with periglacial and glacial climate conditions for the safety assessment of the proposed high-level nuclear waste repository site at Forsmark, Sweden. Hydrogeology Journal 22, 1251–1267.

Viola G, Venvik Ganerød G, Wahlgren C H, 2009. Unraveling 1.5 Ga of brittle deformation history in the Laxemar-Simpevarp area, southeast Sweden: A contribution to the Swedish site investigation study for the disposal of highly radioactive nuclear waste. Tectonics 28, TC5007.

Winkler S, Nesje A, 1999. Moraine Formation at an Advancing Temperate Glacier: Brigsdalsbreen, Western Norway. Geografiska Annaler: Series A, Physical Geography 81, 17–30.

Witherspoon P A, Wang J S, Iwai K, Gale J E, 1980. Validity of cubic law for fluid flow in a deformable rock fracture. Water resources research 16, 1016–1024.

Wright P J, Harper J T, Humphrey N F, Meierbachtol T W, 2016. Measured basal water pressure variability of the western Greenland Ice Sheet: Implications for hydraulic potential. Journal of Geophysical Research: Earth Surface 121, 1134–1147.

Wänstedt S, 2000. Geophysical and geological investigations of the Boda area. SKB R-00-23, Svensk Kärnbränslehantering AB.

Zoet L, Alley R B, Anandakrishnan S, Christianson K, 2013. Accelerated subglacial erosion in response to stick-slip motion. Geology 41, 159–162.

Öhrling C, Peterson G, Mikko H, 2018. Detailed geomorphological analysis of LiDAR derived elevation data, Forsmark. SKB R-18-10, Svensk Kärnbränslehantering AB.

SKB is responsible for managing spent nuclear fuel and radioactive waste produced by the Swedish nuclear power plants such that man and the environment are protected in the near and distant future.

skb.se